Abstract

STOVER, TRACY EUGENE, JR. Optimization of Fast Critical Experiments to Reduce Nuclear Data Uncertainties in Support of a Fast Burner Reactor Design Concept. (Under the direction of Paul J. Turinsky).

An optimization technique has been developed to select optimized experimental design specifications to produce data specifically designed to be assimilated to optimize a given reactor concept. Data from the optimized experiment is assimilated to generate posteriori uncertainties on the reactor concept's core attributes from which the design responses are computed. The reactor concept is then optimized with the new data to realize cost savings by reducing margin. The optimization problem iterates until an optimal experiment is found to maximize the savings.

A new generation of innovative nuclear reactor designs, in particular fast neutron spectrum recycle reactors, are being considered for the application of closing the nuclear fuel cycle in the future. Safe and economical design of these reactors will require uncertainty reduction in basic nuclear data which are input to the reactor design. These data uncertainty propagate to design responses which in turn require the reactor designer to incorporate additional safety margin into the design, which often increases the cost of the reactor. Therefore basic nuclear data needs to be improved and this is accomplished through experimentation.

Considering the high cost of nuclear experiments, it is desired to have an optimized experiment which will provide the data needed for uncertainty reduction such that a reactor design concept can meet its target accuracies or to allow savings to be realized by reducing the margin required due to uncertainty propagated from basic nuclear data. However, this

optimization is coupled to the reactor design itself because with improved data the reactor concept can be re-optimized itself. It is thus desired to find the experiment that gives the best optimized reactor design.

Methods are first established to model both the reactor concept and the experiment and to efficiently propagate the basic nuclear data uncertainty through these models to outputs. The representativity of the experiment to the design concept is quantitatively determined. A technique is then established to assimilate this data and produce posteriori uncertainties on key attributes and responses of the design concept. Several experiment perturbations based on engineering judgment are used to demonstrate these methods and also serve as an initial generation of the optimization problem.

Finally, an optimization technique is developed which will simultaneously arrive at an optimized experiment to produce an optimized reactor design. Solution of this problem is made possible by the use of the simulated annealing algorithm for solution of optimization problems. The optimization examined in this work is based on maximizing the reactor cost savings associated with the modified design made possible by using the design margin gained through reduced basic nuclear data uncertainties. Cost values for experiment design specifications and reactor design specifications are established and used to compute a total savings by comparing the posteriori reactor cost to the a priori cost plus the cost of the experiment. The optimized solution arrives at a maximized cost savings.

Optimization of Fast Critical Experiments to Reduce Nuclear Data Uncertainties in Support of a Fast Burner Reactor Design Concept

by
Tracy E. Stover, Jr.

A dissertation submitted to the Graduate Faculty of
North Carolina State University
in partial fulfillment of the
requirements of the Degree of
Doctor of Philosophy

Nuclear Engineering

Raleigh, North Carolina

2011

APPROVED BY:

_____	_____
Dr. Ralph C. Smith	Dr. Dmitriy Y. Anistratov
_____	_____
Dr. Hany S. Abdel-Khalik	Dr. Paul J. Turinsky Advisory Committee Chair

Dedication

I can do all things through Christ which strengthens me.

(Philippians 4:13, NKJV)

I dedicate this dissertation to my loving wife Maria who supports me in all my endeavors, to my parents who without their support I would never have gotten this far, and to my aunt who has always encouraged me.

Biography

Tracy Eugene Stover, Jr. was born in Fairlea, West Virginia on December 1, 1983 to Tracy and Gay Stover of Smoot, West Virginia. He received elementary and secondary education at Smoot Jr. High and Elementary School. He graduated as salutatorian from Greenbrier West High School of Charmco, West Virginia in 2002.

Tracy attended Murray State University of Murray, Kentucky as a major in the area of Engineering Physics. In the summer of 2004 he received the Summer Undergraduate Research Fellowship at the National Institute of Standards and Technology in Gaithersburg, Maryland. After receiving his B.S. from Murray State in May of 2005 he enrolled at North Carolina State University for graduate studies in Nuclear Engineering under the direction of Dr. Paul J. Turinsky. In December 2007 he received his M.S. in nuclear engineering with a project that quantified cross-section induced uncertainties on back-end fuel cycle metrics. In summer of 2008 Tracy worked at the Idaho National Laboratory under the direction of Dr. Samuel Bays where he studied and modeled benchmark fast critical experiments and began data assimilation studies that served as a basis for this work. While at NC State, Tracy has been primary author on three papers, and co-author on an additional five. He also served two years as president of the Nuclear Engineering chapter of the Graduate Student Association, and one year as secretary/treasurer.

Before completing his Ph.D., Tracy spent 6 months as a research engineer at NC State and joined Westinghouse Electric Company, LLC in July 2009 as a core design engineer. He returned to school in January 2010 and is currently still employed by Westinghouse.

Acknowledgements

This work has been funded by the U.S. Department of Energy under the Nuclear Energy Research Initiative Grant Number DE-FC07-06ID14746.

Assistance is acknowledged to the following individuals and organizations:

Dr. Samuel Bays

Dr. David Nigg

Dr. Matthew Jessee

Dr. Masood Iqbal

Dr. Won-Sik Yang

Mr. Ross Hays

Mr. Jason Elkins

Mr. Shuang Du

Idaho National Laboratory

Argonne National Laboratory

Westinghouse Electric Company, LLC

Table of Contents

List of Tables

List of Figures

Nomenclature

ABTR – Advanced Burner Test Reactor

ANL – Argonne National Laboratory

BOC – Beginning of cycle

BOL – Beginning of life

DU – Depleted uranium

EOC – End of cycle

EOL – End of life

ESM – Efficient Subspace Method

FPY – Fission Product Yield

MWD/MT – Megawatt days per metric ton

INL – Idaho National Laboratory

LWR – Light water reactor

MOC – Middle of cycle

SA – Simulated Annealing

SNF – Spent Nuclear Fuel, also refers to Spent Nuclear Fuel sample drawer for ZPPR

TRU – Transuranics, also refers to transuranics sample drawer for ZPPR

ZPPR – Zero Power Physics Reactor

1. INTRODUCTION

1.1. Motivation and Scope for Research

All nuclear reactor designs rely on basic nuclear data, which are obtained by evaluating experimental data from differential and integral experiments designed to provide information about basic nuclear data and reactor operation, e.g. determining reaction cross sections. In the U.S. between the 1950s and the 1990s, many reactor physics and criticality integral experiments were performed. The integral experiments most crucial to this particular study were performed on the fast critical Zero Power Reactor, ZPR, and the Zero Power Plutonium (or Physics) Reactor, ZPPR, at Argonne National Laboratory – West, which is now Idaho National Laboratory. The ZPPR and the smaller ZPR were split-table reactors which housed a grid of drawers that were filled with fuel, reflector, blanket, and structural materials in various geometries and compositions for various experiments [1]. These experiments were conducted to provide information on the physics of Generation IV type fast reactors. Interest in fast reactor and closed fuel cycle analysis began to decline in the 1980s and virtually ended in the early 1990s reflecting the political climate of the times.

Today there is renewed interest in Generation IV type fast reactors, especially with the continuing buildup of high level nuclear waste and the difficulties associated with interring spent fuel. This study focuses on the Advanced Burner Test Reactor, ABTR, proposed by Argonne National Lab in 2006 [2]. This reactor is a possible means of demonstrating the closing of the fuel cycle by burning off plutonium and minor actinides from spent light water reactor fuel, thus reducing the burden on a geologic repository. This

reactor, like all others, relies on established basic nuclear data, namely isotopic reaction cross sections, to compute the necessary neutronics design calculations. These data, established by experiments like those conducted on ZPPR, include uncertainty derived from various sources during the experiment and in evaluation. Uncertainties for these cross sections are often included with the basic data in the form of a covariance matrix containing variance and covariance information for different isotopes and reactions. Design calculations must therefore include uncertainty of key reactor operating parameters that result from the uncertainty in these basic data.

Related to uncertainty analysis is another aspect of the nuclear data that is increasingly becoming of interest as well – representativity, which is a quantitative measure of how similar the sensitivity profiles for a parameter are between two different reactors [3]. An experiment might be performed very well and the information obtained from it may be very accurate, but if that experiment does not reasonably represent the physics of the design being considered the information obtained from it may not be applicable to said design. To examine this portion of the problem, the representativity factor has been developed as a means to measure whether integral parameters in an experiment are sensitive to similar basic data, i.e. representative, of a given design [4]. In contrast to accuracy, an experiment and a design may have a large uncertainty on a given parameter, but if that parameter is sensitive to the same basic data by similar magnitudes, then the representativity will be high despite inaccuracy. A good design is therefore one which draws upon data from an accurate experiment that is representative of the design being considered.

However, it is not sufficient merely to have a representative experiment with very accurate results. Those results must be realistically incorporated into the overall knowledge base to be used to reduce the uncertainty and required margin on key reactor operating parameters. In this work, adaptive simulation will be used to make this incorporation. Adaptive simulation utilizes both experimental data and a priori values of nuclear data and associated uncertainties to obtain posteriori values and uncertainties. In this work a computational, subspace-based data assimilation technique is employed [5]-[11]. This approach solves a generalized minimization problem [11] that has been appropriately regularized to treat its ill-posed nature [12]. The solution that results is the optimal perturbation to be applied to the input nuclear data which, when propagated through the analysis model, comes as close as possible to obtaining the desired results, the improved agreement between measured and predicted observables. The solution to this problem used in this work will not only be constrained to the space spanned by the a priori input cross section covariance information, but also factor in experimental errors, i.e. counting statistics, fission product yield uncertainty, etc.

Given a method to measure the representativity of an experiment to a design and a method to assimilate the data from an experiment into design calculations, a methodology will be developed in this work to optimize the experiment for the desired uncertainty reduction to reduce required design margins. Considering the high cost of nuclear experiments, especially those concerned with advanced reactor designs, the benefit of performing an experiment must outweigh the cost. In practical terms the monetary savings realized by reducing design margins must outweigh the cost of the experiment which

produces the data to reduce those margins. Initially, numerous core attributes and design responses of a reactor design, ABTR, were examined for potential posteriori uncertainty reduction using representative experiments, i.e. variations of ZPPR. The benefit of the experiment can be determined by examining whether the posteriori values fall within the desired safety criteria [13] and operating margin [14] when considering uncertainty as opposed to their a priori values. A subset of ABTR design responses and their associated core attributes were selected for optimization of the ABTR design. The responses were assigned a monetary value developed in this work. ZPPR experiment design specifications were also assigned a monetary value. This information was then incorporated in a two-level optimization problem in which ZPPR design specifications are varied to produce experimental results that are assimilated into posteriori uncertainty data for an ABTR design. The ABTR design specifications are then varied to produce an optimized design, in terms of monetary savings. The price of the experiment is compared with the cost savings on the ABTR design and iterations performed to reach an optimal combination of experiment and reactor design, i.e. optimized the net savings defined as ABTR cost savings minus ZPPR experimental cost. Finally, a discussion will be presented on the cost of experiments versus the economic worth of margin, and the feasibility of some of the experiments simulated in this work.

1.2. Literature Review

This section briefly reviews literature available on nuclear data needs that in part motivate this work and familiarizes the reader with some of the available mathematical tools

that will be used. Discussion of the reactors examined in this work, including a summary of the ZPPR program history, will be deferred to subsequent sections.

1.2.1. Nuclear Data Needs

The previous section indicated that a principle motivation for this work was the need for reduction in the uncertainty on basic nuclear data so as to benefit reactor designers who must allow additional safety margin due to uncertainty on design responses induced by these nuclear data uncertainties. Both recent and historic research has been done explicitly on the topic of nuclear data needs for the design of Generation-IV type reactors.

As early as 1968 work was being done to analyze the sensitivity of fast reactor designs to deficiencies in basic nuclear data. At that time Greebler identified deficiencies in sodium cross sections and the Pu-239 fission yield as the main sources of uncertainties yielding 1 to 4 % uncertainties on reactivity coefficients [60]. He also quantified uncertainties in terms of mills per kWh installed capacity. Salvatores and Palmiotti made an extensive study in 1985 about uncertainty and target accuracy needs for the liquid metal fast breeder reactor initiative of those days [61]. They examined the critical mass which was determined to need integral experiments to improve data, burnup dependent core reactivity changes which had a 16% uncertainty, reactivity control issues (control rod worth and reactivity coefficients) which had a range of 3 to 10% uncertainty, fission uncertainties of 5%, capture uncertainties of up to 20%, sodium void worth which had a 10% uncertainty, and secondary sodium activation which had an overwhelming 50% uncertainty. They determined

that with the current deficient data that an unacceptable 25% bias would need to be applied on reactivity parameters of fast reactors.

Interest in fast reactors revived in the 2000s with the intention of closing the nuclear fuel cycle. In turn nuclear data needs for fast reactors again came into question and produced some recent work. Some of these recent works focus particularly on a certain aspect of nuclear data uncertainty. For example D'Angelo and Rowlands examine exclusively the uncertainty in delayed neutron data for major actinides, which is important for reactivity control of cores that are heavily loaded with actinides [57]. Williams examines the uncertainty and sensitivity of eigenvalue difference responses, i.e. how uncertainties will propagate to reactivity coefficients which are key core attributes for designing a reactor that will operate safely [58]. Elkins [34] and Stover [35] examine more global affects of nuclear data uncertainty propagation by evaluating the effects on fuel cycle performance and waste management parameters. Konomura and Ichimiya have taken a different path and investigate the materials needs of fast reactors, which are removed from basic data but still depend on the effects calculated by using cross sections [62]. They identify concerns with in-service repair and inspection and in finding sodium resistant materials. However, it is a series of works by Aliberiti, Salvatores, Palmiotti, and others that provides the most in-depth modern research in references [4], [14], [63], [64], and [65]. Aliberti most completely addresses the sensitivity and uncertainty effects on typical Generation-IV systems and suggests target accuracies that will be needed for future systems. The short paper referenced is an abbreviated version of a much longer and more extensive report coordinated by Salvatores. In the long report the target accuracy of nuclear data required for new and innovative nuclear

systems is addressed extensively. The team of investigators that compiled this report carefully lays out in detail the nuclear data needs for various innovative systems such that the design margins and reactor responses will be acceptable with regard to the safe and economic operation of these Generation-IV type systems. While the full details of these works are too lengthy to include here, it was the conclusion that for most Generation-IV reactor types to operate safely and economically, the nuclear data would have to be improved to give accuracies of ±0.5% on reactivity, ±3% on power peaking factor, ±300 pcm on burnup calculations, ±5% on transmutation rates, and ±10% on reactivity coefficients including void worth. Several of these references made use of the representativity factor to evaluate how representative experiments were to the systems being considered and [64] went as far as to suggest a data assimilation technique similar to the one that is employed in this work.

This work intends to respond to these nuclear data needs by developing a method for optimized experiment design to meet the target uncertainties on key reactor design responses. Experiment optimization has been applied extensively in other fields such as aerodynamics and aviation, semiconductors and electronics, chemical engineering, mechanical design, and mineral processing [44]-[50]. However, a survey of integral nuclear experiments, for reference any of the more than 500 ZPPR program reports, shows nuclear experiments are often performed for a very targeted evaluation rather than optimized for a subsequent process or design. For example, common ZPPR experiments were criticality tests and reaction rate sampling. These types of experiments were important to the understanding of generalized fast reactor physics, however some even specifically designed to study the design of a particular commercial reactor design or process, e.g. the Clinch River reactor mock-up.

1.2.2. Uncertainty Propagation Techniques

The first tool required for this work is an efficient uncertainty propagation technique. Cross section a priori covariance data is propagated through the ABTR models and through ZPPR experiment variations to selected observables and core attributes. The experimental data is then used to generate posteriori covariance data on the ABTR attributes and responses.

The field of uncertainty and sensitivity analysis is rich with methods and literature. The three most common methods are stochastic sampling, general perturbation theory using adjoint functions, and forward deterministic methods. Stochastic methods require a number of random samples that exceeds the number of input uncertainty parameters being sampled [30]. This method is impractical for this work since there are many input uncertainty parameters. Adjoint methods are used for linear systems when there are only a few output responses of interest and very large amounts of input parameters that must be perturbed since an adjoint function is required for each output parameter [31]. This method is marginally practical for this work because there are also many output responses. The forward deterministic methods, such as the "propagation of errors" method [32], are most useful when there are many output responses and only a few input parameters to perturb as this method perturbs input and runs the model in a forward calculation.

In the case of reactor design, often the number input parameters and output responses that must be perturbed and analyzed, respectively are both very large. In the case of large input and output data streams, the above methods are effective but hardly efficient; however there is an alternative option. The Efficient Subspace Method (ESM) can reduce the number

of forward simulations by recognizing the more important contributors to uncertainty, allowing the less important contributors to be ignored and thus reduce the number of forward simulations required to propagate the uncertainty information [5][8][9][33]. Since this work involves large input and moderate output streams, ESM was chosen. ESM works particularly well when there is strong correlation among the nuclear data uncertainties and some of the responses are insensitive to components of the nuclear data uncertainties. For the application of interest, these two attributes exist. A final requirement of ESM, which will be discussed in more detail in Chapter 3, is that the core simulator responses behave linearly with respect to the nuclear data. It is shown that this is the case within the range of input parameters as defined by their uncertainties, so that ESM is applicable.

1.2.3. Data Assimilation Techniques

The goal of performing an experiment is to provide useful information to advance the field of knowledge of a subject. In particular the experiments simulated in this work are intended to provide improved basic nuclear data with which a reactor design may be optimized by reducing design margins. Therefore a technique is required that will permit the assimilation of the new experimental data into the current data to improve its quality.

Tarantola [66] presents in a very general fashion a direct computation method to assimilate responses to modify an a priori set of parameters, in this case a covariance matrix, into a posteriori set of parameters. Within the context of our usage, the results of his presentation are consistent with a Bayesian approach. His formulation shows that the posteriori covariance information is a matrix product involving the a priori covariance

information, the experimental uncertainties and a linear operator that maps between the experiment space and the covariance data space, i.e. sensitivities of the experiment to the desired covariance data. This serves as the starting point for the assimilation, but Tarantola's formulation assumes a well-conditioned problem. For the problem of interest in this work, the data assimilation problem is actually ill-conditioned.

Tikhonov generalized the Bayesian approach [12]. By introducing a regularization parameter, the weight given to improving agreement of prediction with experiment, i.e. the mismatch term, relative to allowed deviation from the a priori parameter values, i.e. the regularization term, can be selected. The value of this term is then selected to minimize the mismatch term while minimizing the regularization term. Ideally this regularization parameter must be as close to 1 as possible since the farther from unity this value is, the more different the problem actually being solved is from the problem that is desired to be solved, that being the Bayesian approach to achieve maximum likelihood.

In his work, Jessee applied Taratonla's described assimilation technique with Tikhonov's regularization technique to a multi-physics core simulator [11]. In that work, nuclear reaction cross sections were adjusted based on measured values of reactor responses in a technique known as adaptive simulation. The cross sections were adjusted, within their a priori uncertainty space, so that the simulated core yielded responses closer to actual measured data. Jessee took his formulation to the point that measured data along with a priori covariances could be used to compute posteriori covariances. This technique was adapted for use in this work the difference being that now the source of the experimental data

and the reactor whose response uncertainties are being determined for are no longer one and the same.

1.2.4. Experiment Optimization

Experiment optimization is an effort to maximize the effectiveness of the data obtained from an experiment toward the solution of a particular problem. This practice is often applied in fields of study where experiments can be both complex and expensive. Therefore a good experiment that yields the desired results toward the solution of a problem is of importance. This can be seen in such highly competitive fields as mining and ore processing [47], chemistry [48], and electronics [45]. It is also of high importance where experimentation is often not only expensive but time consuming and complicated such as mechanical designs [46], medicine [49], and robotics [50]. Of the papers reviewed, perhaps the one that best shows a potential application for the nuclear industry is the one by Zheng [44]. His work was to optimize a wind tunnel experiment. Like the nuclear industry, aeronautical experiments can be very expensive and time consuming to both develop and to implement. They also involve complicated fluid dynamics problems, often based on empirical relationships, which require great care in studying, much like the study of the nuclear physics that go into reactor design. One trait common to these optimizations is that these are directed experiments meant to provide specific data for a specified design. Many of the more than 500 ZPPR program technical reports indicate that these experiments were intended to provide general knowledge about fast reactor physics, with fewer cases being experimental mock-ups. Therefore, in a time concerned with the high cost of nuclear

technology, it only makes sense to apply this practice of experiment optimization to nuclear designs.

As indicated in the discussion of the scope of this work, an original optimization problem will be developed to determine the optimal experiment that yields an optimal ABTR design. One method to optimize the design is by use of factorial design [72]. In factorial design, two or more factors, i.e. design specifications, are varied in all possible combinations. This exhaustive search not only requires discrete values for each of the factors but requires, for k factors, 2^{k-1} experiments to be analyzed. Since the choices available for both the ABTR and the ZPPR design specifications optimization are very numerous (e.g. loading patterns) and oftentimes continuous (e.g. enrichments), an exhaustive search of all options is computationally demanding and therefore possible but infeasible. Note simulated annealing also cannot treat continuous variables. This is addressed in Section 3.6.4. Randomly choosing the design specifications will not approach a truly optimized solution. Experienced engineering judgment adds a degree of informed decision making to design specification choice and indeed this is how the initial generation of ZPPR experiment perturbations was developed. As will be shown, these ZPPR perturbations based on choice of test drawer fuel composition, detector number and position, and loading pattern did yield reasonably good results for posteriori uncertainties reductions in ABTR design responses. These "hand optimized" choices were based largely on the concept of exposing ABTR type fuel forms and loading patterns to the ZPPR flux spectrum which, as will be shown, strongly resembled the predicted irradiation conditions of the ABTR. However, once the formal optimization

problem for this work was developed, it became necessary to apply a proven, logical, mathematical technique for the solution of the optimization problem.

An entire field of research is devoted solely to advancing the knowledge of optimization algorithms so even a generalized discussion of the various techniques is beyond the scope of this work. As such only the technique applied in this work is discussed.

The simulated annealing algorithm method for solving optimization problems is employed in this work. Simulated annealing was chosen primarily for its ease of implementation and for its extensive application in nuclear industry optimization problems, such as fuel management, that are very much similar to the type of optimization problem encountered in this work. In metallurgy, annealing is the process of cooling a hot material at a specified rate so as to achieve a desired crystalline structure by getting all the particles to arrange in a low energy state. Simulated annealing is a optimization algorithm for solving combinatorial problem which uses a Boltzman machine to progressively narrow the range of accepted solutions. This is analogous to the Boltzman probability distribution which characterizes the probability of being at a stated energy at a given temperature for a solid that is in thermal equilibrium, and this is used to determine the cooling schedule for the physical annealing process [51].

A very readable text on this subject is that by van Laarhoven [51] which contains discussion on the original method development by Metropolis and Kirkpatrick and subsequent advances. The algorithm begins with a large range of values of the objective function, values less than the previous generation are always accepted and values greater than the previous generation are accepted with a probability defined by a Boltzman distribution

based on the change in the objective function value and the annealing temperature. This prevents the solution for being trapped in local minima. After a number of acceptances, the system is "cooled", that is the probability of acceptance of an inferior solution decreases. The process continues asymptotically approaching a solution in the neighborhood of the global minima.

This process was applied to the field of in-core nuclear fuel management by Kropaczek [52] in 1990. The in-core fuel management problem, with 10^{50} or more possible combinations of fuel assembly placement and enrichment, is ideal for this application because the search field is very large and fraught with local minima. The design of the ZPPR experiment is analogous to this with multiple choices for sample drawer loading, and instrumentation location and quantity available. Since Kropaczek, the nuclear industry has applied this process to improve economics and fuel utilization. Ye [56] applied the method to core control utilizing very detailed penalty functions to augment the objective function, and a cooling schedule based on the distribution of accepted values rather than just a scalar constant between 0.5 and 0.99 [51]. He also applied a limit to the maximum number of trials per generation as well as the number of acceptances. Moore used the method for fuel loading pattern optimization for boiling water reactors [53]. This problem included hard constraints which resulted in an immediate rejection of the trial solution. Du applied this optimization engine in the out-of-core fuel cycle economics code OCEON [55]. He added to his method an initial "temperature" based on the standard deviation of the objective function values from a survey generation, here after referred to as the 0^{th} generation of the annealing process. Most recently Hays [54] has parallelized the method for use in the FORMOSA-B fuel

management code. In addition to running the algorithm in parallel, he added the constraint on the cooling schedule to make the cooling adjustment a minimum value or the value determined from the distribution of the acceptance, whichever is larger. If the system is cooled too quickly trapping in a local minima can occur. So as can be seen the simulated annealing algorithm is a common choice for solving large combinatorial problems with certain attributes.

1.3. ZPPR Program History

The ZPPR fast reactor experimental program ran from 1963 to 1990 at what was once Argonne National Lab – West but is now Idaho National Lab. It consisted of four actual reactors: ZPR-3, ZPR-6, ZPR-9 and ZPPR, all of which are split table designs as indicated in Figure 1.1. ZPR-3 seems to be the least applicable to this work and is not possible to be restarted for future work as it has been fully decommissioned and is on display at the Experimental Breeder Reactor No. 1 Museum just east of Arco, ID. ZPR-3 was a "table top reactor", i.e. the entire apparatus is about the size of a small sport utility vehicle, with a 30 x 30 matrix of 1 inch drawers. It was typically uranium fueled and graphite moderated, although assemblies 48 through 57 were plutonium fueled and are occasionally referenced as early plutonium benchmarks. ZPR-6 and ZPR-9 were essentially of the same design. They were 45 x 45 matrices of 2.2 inch drawers (~8 ft square matrix) housed in an apparatus about 12 feet in height. ZPR-9 improved on ZPR-6's sampling capabilities by adding sample traverse tubes and a more controllable axial sampling device that spanned the axial length of both halves. ZPR 6 and ZPR 9 hosted a wide variety of experiments that drifted away from first generation graphite moderation to sodium moderation using metal sodium clad in non-

reactive material. These also experimented with various fuel isotopes including both plutonium and uranium and various fuel forms including both metal and oxide fuels. An analysis of ZPR 6 Assembly 7a has been previously performed as a starting point for this work [7]. ZPR 6 and 9 are fully decommissioned but the physical apparatuses are still housed at INL. ZPPR was the largest and most versatile of the reactors having a maximum of 77 x 77 2.2 inch drawers (~14 ft square matrix), however, they assumed circular cores so the lower corners, which are 10x10 solid blocks, are not available for use (Figure 1.2). ZPPR is currently in standby mode, which means it is fully unloaded but still mechanically operable from its original control room. INL's current plan is to decommission this reactor whenever funding is available. Costs for decommissioning are estimated at $5 million. The estimated cost to refurbish the control room, bring in new expertise, and restart the ZPPR program is $60 million, not including annual operating and maintenance costs [15]. A general reference for all ZPR and ZPPR experiments can be found in Reference [1]. Plate compositions are given in many of the ZPPR technical reports but are clearly tabulated in Reference [17].

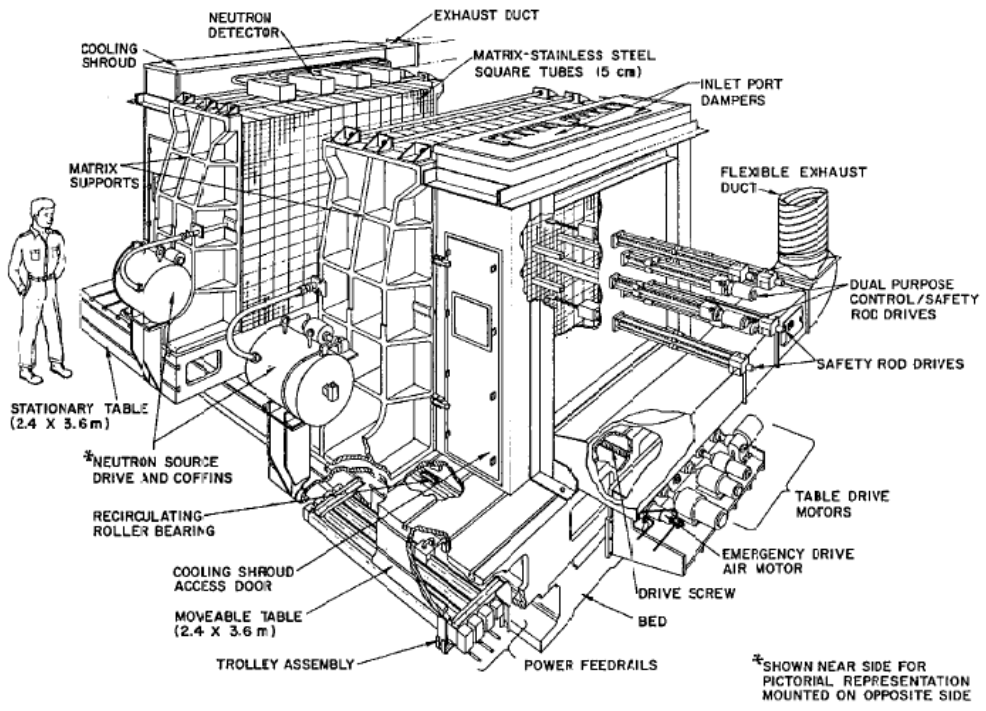

Figure 1.1 : Cartoon schematic for ZPR-6 and ZPR-9.

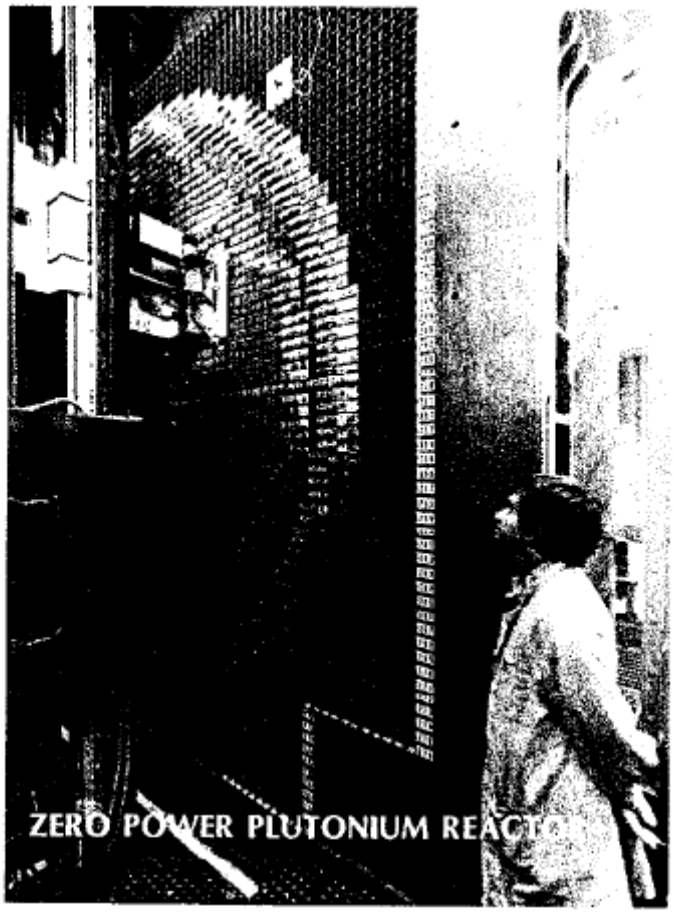

Figure 1.2 : Photograph of ZPPR while being loaded.

1.3.1. Experimental Capabilities

This and subsequent subsections refer to a selection of general information about the ZPR and ZPPR programs. This information was obtained from the ZPR Technical Memoranda Series, which is a collection of 500 documents detailing the ZPR and ZPPR programs from 1963 to 1991. Due to the large volume of information, specific memos are only referenced when it is pertinent to the topic being discussed.

First it should be noted that the drawers for ZPR-6, -9 and ZPPR are all the same size and fully interchangeable with each other and with any of the plates. A drawer or tray is filled with a combination of several plates that together form a composition for a given region of the core, e.g. high enriched inner core or a depleted uranium blanket (Figure 1.3). The plates are short enough to be able to be arranged in such a manner as to give radial instrumentation or sample gaps as small as 0.5 inch. The plates exacting widths allow only a few millimeters axial spacing however. Special empty steel cans are used to replace sodium cans in voiding experiments and there are enough available to void about 1200 liters worth of sodium cans from an experiment. Reactivity was measured by finely calibrated control rods and later by power feedback calculations. Neutron spectra were typically taken by proton-recoil detectors which took up an entire drawer. Single drawer worth was measured prior to neutron spectra measurements. For the whole program neutron detectors were placed in thin lead shields to reduce gamma interference with the measurements. In the early 1980s high energy neutron detectors were developed for testing in the ZPPR. These used thicker energy filters to stop low energy neutrons and gammas, so the detectors could focus on the spectrum greater than 1 MeV. That is all the information on detector shielding or energy filters contained in the technical memos.

Irradiation experiment sampling was conducted one of three ways – by foils, axial sample changer typically near the core center, and radial transverse tube just behind the mid-plane of the stationary half. If the sample can fit in a 2 x 2 x 2 inch box, a 0.5 inch diameter tube or can be wedged in between the plates, it can be irradiated. The 2 in. cubic box usually contained a 2 x 2 x 1 inch sample plate or was otherwise filled with thin stainless steel plates.

Fission chambers were usually placed in the axial changer or traverse tube, but later ZPPR assemblies had several specific drawers that consistently housed fission detectors. Finally, and perhaps most importantly for advanced designs, the drawer cross sectional area is such that most hexagonal fuel assemblies can be approximated well with a 2 x 2 or 3 x 3 block of drawers. To further facilitate experiments simulating assemblies with fuel pins rather than plates, a number of pin cell calandria drawers were constructed. These were drawer sized cells that had 16 evenly spaced fuel pins surrounded by appropriate amounts of sodium and structural material which, combined in 2 x 2 or 3 x 3 groups, simulated a fast reactor fuel assembly.

Figure 1.3 : A fully loaded ZPPR drawer.

1.3.2. Measurement Techniques

As mentioned in the previous section, measurements of reactivity were taken either by means of a finely calibrated control rod or by power feedback calculations which used inverse kinetics. Reactivity parameters such as void worth were measured by reactivity changes and a known delayed neutron fraction. Proton-recoil neutron detectors were used for neutron flux spectrum measurement. Other integral parameters such as power peaking factor or power density were determined by back end calculations using other measured information.

Reaction rates from irradiated samples as well as the fuel itself were of key importance. Fissile and fertile uranium and plutonium samples were loaded into fission chambers and irradiated. Small samples of uranium and structural material were irradiated as well. Button sized foils of uranium and plutonium as well as more rare materials such as americium were also irradiated. Irradiated samples were counted over time after being irradiated. Fission reactions were calculated by the decay of the prominent fission product Mo-99 into Tc-99 with a half life of 65.94 hours. Capture reactions were calculated by counting the decay of capture daughter products such as U-239 from U-238 capture. This introduces three sources of error: 1) counting statistics uncertainty of $1/\sqrt{\#\ of\ counts}$, 2) fission product yield uncertainty, and 3) decay constant yield uncertainty, in addition to sample isotope purity, density, and dimensions.

Other than an occasional discussion of mass uncertainties on plates, foils and samples, there is little or no other information, especially about cost, in the ZPR and ZPPR

Technical Memos. The following comes mainly from discussions with Dr. Samuel Bays of INL and from a single material science paper from the 1970s where one of the companies that produced the foils discussed manufacturing techniques [16]. The cylindrical samples were indicated to have been made in-house, either at INL or ANL. The foils' manufacture appears to have been contracted to chemical companies, like the ones who created the plates, e.g. DOW Chemical. The one paper on foil manufacture indicated that the foils had to be made very precisely and up to 40% were rejected for impurities or manufacturing problems – no indication of cost. The uranium samples could be handled openly and the plutonium samples were made in glove boxes. Discussion with Dr. Bays yielded a little more information on the plates and the small samples. The plutonium plates are incredibly valuable, especially today as are the enriched uranium plates. The others, he indicated, could be reproduced if more were needed, especially the sodium and steel plates. INL can and does make its own minor actinide samples and is currently producing on an as-needed basis, which is briefly address in the next section. These are small cylindrical samples however, created on a laboratory basis, nothing on the scale of producing hundreds of plates.

There were typically five experiments performed on every ZPR and ZPPR assembly. These were criticality, Doppler reactivity, void worth, small sample worth, and reaction rates and ratios. Criticality was measured directly as indicated above. Small sample Doppler reactivity experiments, usually with natural uranium oxide and plutonium oxide samples, were performed by placing a heated sample in various locations along the traverse tube. Core wide Doppler reactivity experiments involved shutting off the cooling fans and allowing the core to heat up a few degrees while critical. Void worth was measured both by

small sodium samples and by voiding portions of the core in radial increments. Small samples were measured in the axial sample changer or in the traverse tube and the worth accounted for by the fine control rod. Reaction rates were taken by irradiating foils at various locations, by traversing uranium and plutonium fission chambers, and by small spherical double-foil counters placed in either the axial sample changer or specially made gaps in the plates. Locations of these counters and especially of the foils are well documented for most experiments. Later in the program, methods were reported for converting the point-wise foil and fission chamber measurements to cell-averaged values which one would get from a computational model. Documentation is better for the ZPPR experiments than the ZPR ones. Neutron spectra were reported for only select reactors and assemblies. Less common experiments, such as the use of pin calendria rather than fuel plates, were also conducted but these are often specific to a given reactor and assembly.

1.3.3. History of Minor Actinide Analysis

Difficulty in producing and handling pure minor actinides has been a hindrance in doing research with these matrerials up until modern times. With the exception of the occasional Am-241 sample in ZPPR, that program has almost no information. Further information is sparse on minor actinide irradiation up until modern times. One special experiment conducted on the ZEBRA 21 reactor was cited in a ZPPR report. This experiment irradiated Am-241 and Am-243 samples to determine production rates of Cm-242, Am-242m, and Cm-244 [18]. A long term irradiation study on minor actinide samples was recently completed at INL [19]. Other than this, little information was found on minor

actinide irradiation in fast critical facilities in the USA. Therefore the minor actinide reaction rates calculations rely on very little a priori cross section information.

1.4. ABTR Concept

The following discussion comes mostly from the ABTR pre-conceptual design report [2]. The ABTR is a small, prototype scale fast flux power reactor rated at 250 MW. It consists of 199 hexagonal fuel assemblies of which 78 are reflectors, 48 are shielding, 10 are control, and 3 are material test, i.e. inert. The remaining 60 are divided between 3 fuel regions – inner core, outer core and middle core. When the ABTR first starts up, the 54 inner and outer core assemblies are composed of a Pu-U-Zr alloy fuel in which the plutonium content is weapons grade. The 6 middle core assemblies are composed of SNF acquired from used LWR fuel that is also alloyed with uranium and zirconium. After each planned cycle of 4 to 6 months, fuel from the ABTR is recycled and mixed with more incoming SNF from LWRs. This recycled fuel is added into ABTR in greater and greater quantities, slowly replacing the high enrichment weapons grade plutonium fuel until the reactor reaches an equilibrium flow. Equilibrium is reached when the reactor's own recycled spent fuel and incoming supplies of LWR SNF are unchanged from cycle to cycle and sufficient to sustain repetitive cycle lengths.

The ABTR represents one of many Generation IV reactor concepts designed to close the fuel cycle, employ advanced methods and technology, and reduce the amounts of high level waste that must be disposed of. ABTR also reflects a shift in energy policy from its predecessor designs of the 1970s and 1980s in that this reactor is designed to burn rather than breed. There is no U-238 blanket present with which to generate Pu-239. Instead the reactor

uses a hard neutron spectrum to fission many threshold-reaction isotopes such as neptunium, americium and curium. ABTR creates usable power while simultaneously destroying long lived isotopes that limit waste disposal. Combined with the use of passive safety systems, modern materials, and other advanced concepts, ABTR is the model of the current trend in Generation-IV concepts in the USA.

1.5. Establishing a Language for this Work

The optimization problem developed in this work, and indeed the whole body of this paper, will apply a specific set of terms to describe specific pieces of information. This terminology seeks to provide a common, specific language for discussion in this work. The special terms are as follows:

For the ZPPR Experiment

1. ZPPR Design Specifications: items that define the experimental setup and are the decision variables
2. ZPPR Observables: the instrument readings that are used for adaption
3. ZPPR Experiment Cost: function of the ZPPR Design Specifications and associated with multiple experiments

For the ABTR Reactor

1. ABTR Design Specifications: items that define the design of the reactor
2. ABTR Core Attributes: Items that the design responses are dependent upon and for which uncertainties can be determined from the uncertainties in the parameters

3. ABTR Design Responses: responses that have limits whose uncertainty distributions can be determined from the ABTR Core Attributes uncertainty distributions and the ABTR Design Specifications
4. ABTR Design Limits: values that the ABTR Design Responses should not exceed for a stated probability
5. ABTR Reactor Cost: Function of the Design Specifications
6. ABTR Design Spec Range: allowed combinations of ABTR Design Specifications that do not violate any of the limits and is a function of ABTR Core Attributes uncertainties
7. ABTR Optimum Design Specs: that combination of ABTR Design Specifications constrained to be within the ABTR Design Spec Range that minimizes the ABTR Reactor Cost
8. ABTR Reactor Cost Savings: Difference between the ABTR Reactor Cost using ABTR Optimum Design Specifications for a priori minus posteriori ABTR Optimum Design Specs

Optimization Problem Terms

1. Parameters: input data, i.e. cross-sections, used in modeling both ZPPR and ABTR that are adapted and who's a priori and posteriori uncertainties are known or can be determined
2. Cost Objective Function: difference of ABTR Reactor Cost Objective Savings and ZPPR Experiment Cost

To summarize the relationship: Design specs produce some set of design attributes calculated from a set of parameters and the attributes produce some set of design responses which must be within the bounds of a set of design limits.

Note that since the ZPPR Experiments Cost and the ABTR Optimum Design Specifications using the posteriori ABTR Core Attributes Uncertainties are functions of the ZPPR Design Specifications, the Cost Objective Function can be maximized by selection of the ZPPR Design Specifications.

Outline for this Work

In Chapter 2 the selection of the ZPPR experiment design is discussed as are the choice of observables, attributes, and responses. Chapter 3 discusses the methodologies employed and developed in this work. Chapter 4 reviews the modeling of the ZPPR experiment and ABTR reactor design concept. Chapter 5 presents the numerical results of this study. Chapter 6 will discuss experiment feasibility and Chapter 7 the conclusions and recommendations for future work. Appendices A and B present supporting analyses to show applicability of the uncertainty propagation methods. Appendix C shows graphically all of the ZPPR perturbations examined in the optimization demonstration. Appendix D presents additional numerical results.

2. EXPERIMENT SELECTION AND KEY OBSERVABLES

2.1. Experiment Selection

2.1.1. Experiments Considered

For a ZPPR experiment to be considered as a potential for use in this study it had to meet several criteria. The first and foremost criterion is that similar irradiation conditions must exist within the experiment that would be found in the ABTR. That is, while the absolute magnitudes will be orders of magnitude different, the normalized neutron flux spectra of both ABTR and the chosen experiment must be very close in energy distribution, preferably both in the central core location and at some point in the outer core region. Furthermore, it is desired that the chosen experiment have similar material properties as ATBR, for instance ABTR has only metal fuel elements so it would be desired that an experiment have no oxide fuels or oxide blanket material in it.

In reviewing the ZPR and ZPPR experiments, including the ZPR-6 Assembly 7 model created by Dr. Masood Iqbal at NC State in 2007 [7], there were potentially six experiments that may be useful, two of which appear very applicable to the ABTR design. These are ZPR-6 Assembly 7, ZPR-9 Assembly 27, ZPPR-3, ZPPR-6, ZPPR-10 Assemblies A and B, and ZPPR-15, the latter two being the ones most applicable. Each is briefly discussed and a neutron flux spectrum provided when available in the reports. Spectra were collapsed to fit to a specified 15-group structure that is used throughout this work (Table 2.1). While ZPR-6 and early ZPPR experiments routinely recorded, tabulated, and plotted flux spectra this practice nearly ceased with all ZPR-9 assemblies and most ZPPR assemblies

later than No. 3. The experimenters seem to have fallen into the routine of reporting only the typical measurements and their analysis and moving rapidly on to the next assembly. Also, only ZPR-6, Assemblies 6A and 7 and ZPPR Assemblies 2, 3, 9, 20 and 21 have been extensively studied and documented and included in the NEA's Benchmark Collections [20][21]. The others have had mostly basic analyses and report the raw measurements; therefore, most of the information available comes from the ZPR Technical Memos series.

The ZPR-6 Assembly 7 core is discussed first since it has been studied extensively at NC State [7]. This is a uniform core of plutonium metal and depleted U_3O_8 fuel surrounded by a DU blanket [22]. This core has the same composition as the ZPPR 2 inner core and so these two have almost identical inner core spectra [23]. Calculated ZPR-6 Assembly 7 15-group spectra and ZPPR 2's reported spectra are compared with the ABTR start-up core spectra in Figure 2.1, labeled ZPR6-7, ZPPR2, and ABTRneq respectively. Assembly 7 also had a modified version which replaced the typical plutonium in the central core with plutonium with a high Pu-240 content, (increase from 11 a/o to 24 a/o) to simulate the recycle of LWR fuel. This version is also included in Figure 2.1, labeled ZPR6-7H240 [17].

ZPR-9 Assembly 27 is a smaller core which is an engineering mock-up of the Fast Test Reactor, FTR [24]. The design includes many ABTR-type assembly mockups (shim rods, fuel tests, control rods, etc.) and the core goes through 4 loadings, each of which are documented, to simulate EOC, two MOC burnup steps, and a BOL core. The compositions also included the higher Pu-240 content to simulate LWR recycle. There are several drawbacks to this model. First, there is almost no documentation beyond the memo specifying loadings and the three memos which reported only select measurements. Second,

the core has complicated axial and radial heterogeneities which would be very difficult to model. Third, while similar to ABTR, the core's volume is smaller since it was modeled on ZPR type machine. A central flux spectrum was not found for this core, but there is one for the BOL version of FTR, which this assembly was supposed to simulate. This spectrum is presented in Figure 2.2, labeled FTR.

The ZPPR-3 reactor is a two-region core, outer zone having fuel spikes, and is almost identical to ZPPR-2, except that ZPPR-3 had 19 2 x 2 control/test assembly positions mocked-up in the core [25]. Its geometry is also similar to ABTR and ZPPR 10. While no spectra were to be found it is likely similar to ZPPR 10. Core compositions are related to ZPR-6 Assembly 7 and ZPPR-2. ZPPR-6 is another two-region core that was based on hexagonal geometry, in this case the compositions of the Clinch River Breeder Reactor [26]. It also models variations of the 19 2 x 2 drawer control rod assemblies. Unfortunately, it is also one reactor for which documentation is sparse.

ZPPR-10 configurations A and B are larger 57 x 57 drawer cores. These have a uniform plutonium loading and with a pseudo-two region structure [27]. "Pseudo" terminology is used because uniformly placed fuel "spikes", replacing U_3O_8 with plutonium, were used to achieve criticality. The geometry closely resembles ABTR in that it includes a thick reflector and has 19 mockup control/test assemblies in the inner core, just as the reference ABTR core. No tabulated flux spectra were found for this model. ZPPR 10 configurations C and D were much larger and part of the U.S.-Japan JUPITER-I Program. The size makes them inapplicable to the ABTR but may indicate an ability to model/study larger cores.

Finally, ZPPR-15 is the core most applicable to ABTR, and as such was the core selected to be modified for adapting the input cross section data for ABTR. Since this is the experiment that will be used and modified throughout this work, discussion of its properties warrants a separate section, which follows.

Table 2.1 : 15-Group energy structure used in this work.

Group	Upper Energy (eV)	Lower Energy (eV)
1	1.4190E+07	6.0650E+06
2	6.0650E+06	2.2310E+06
3	2.2310E+06	1.3530E+06
4	1.3530E+06	4.9790E+05
5	4.9790E+05	1.8320E+05
6	1.8320E+05	6.7380E+04
7	6.7380E+04	2.4790E+04
8	2.4790E+04	9.1190E+03
9	9.1190E+03	2.0350E+03
10	2.0350E+03	4.5400E+02
11	4.5400E+02	2.2600E+01
12	2.2600E+01	3.9940E+00
13	3.9940E+00	5.4050E-01
14	5.4050E-01	4.1400E-01
15	4.1400E-01	0.0000E+00

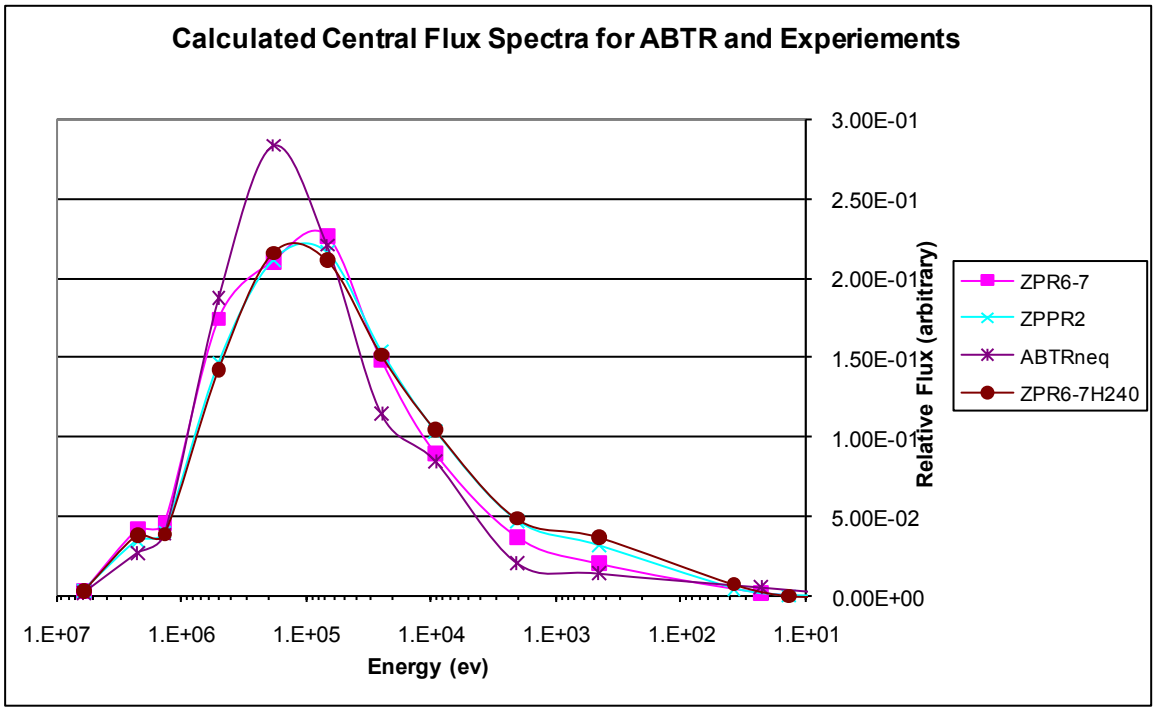

Figure 2.1 : ZPR-6 and ZPPR 2 flux spectra compared to ABTR.

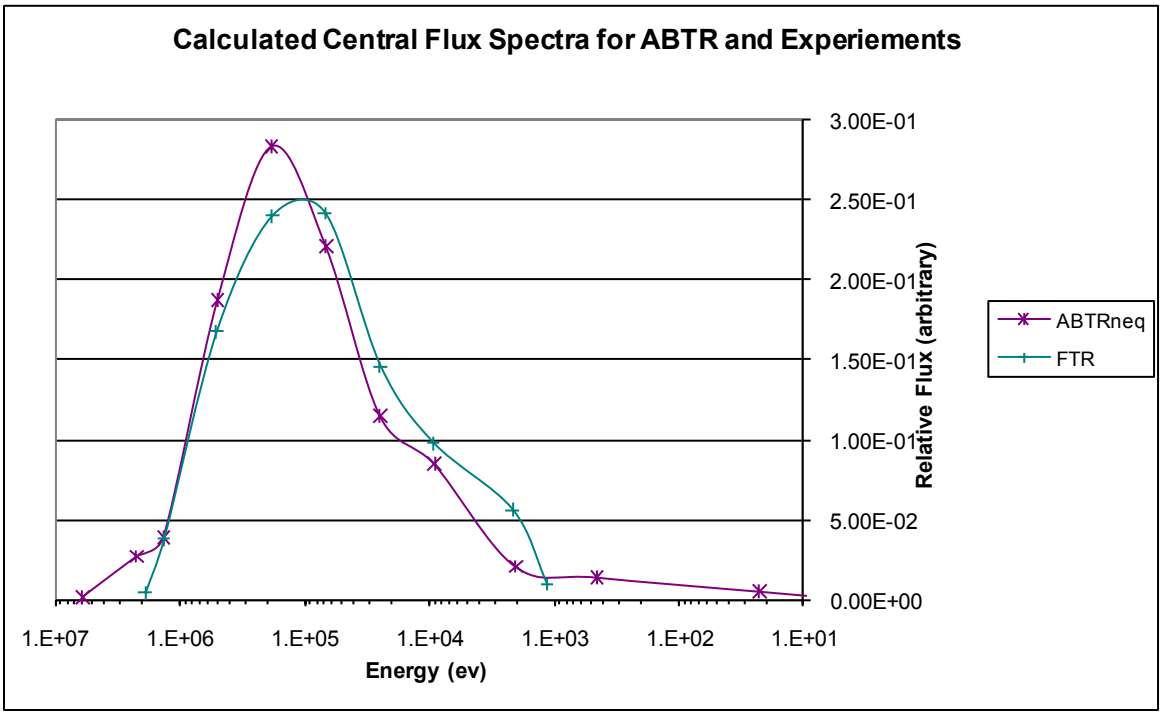

Figure 2.2 : FTR or ZPR-9 flux spectrum compared to ABTR.

2.1.2. Applicability of ZPPR 15-B

ZPPR-15 is a true two-zone core surrounded by a thin blanket and thick reflector [28]. Further this is an all-metal core; the typical U_3O_8 was replaced by DU metal plates. Also, thin plates of zirconium were added along the fuel plates to give the neutronics of alloying fuel in the mixture U-Pu-Zr. The one drawback is that this core has no mockup control or test assemblies, but these could be simulated by test material in a model. Note in Figure 2.3 that the center and edge neutron spectra of this core, labeled Z15, are very close to the ABTR start-up core [18][29]. This is probably due to the metal fuel and addition of the zirconium. Another benefit of ZPPR 15 is that the various configurations represent clean and expected compositions for both BOL and EOC cores, which make it even more promising. Finally, ZPPR-15B has been cited in other work as being used to adjust data for sodium fast reactor calculations [4].

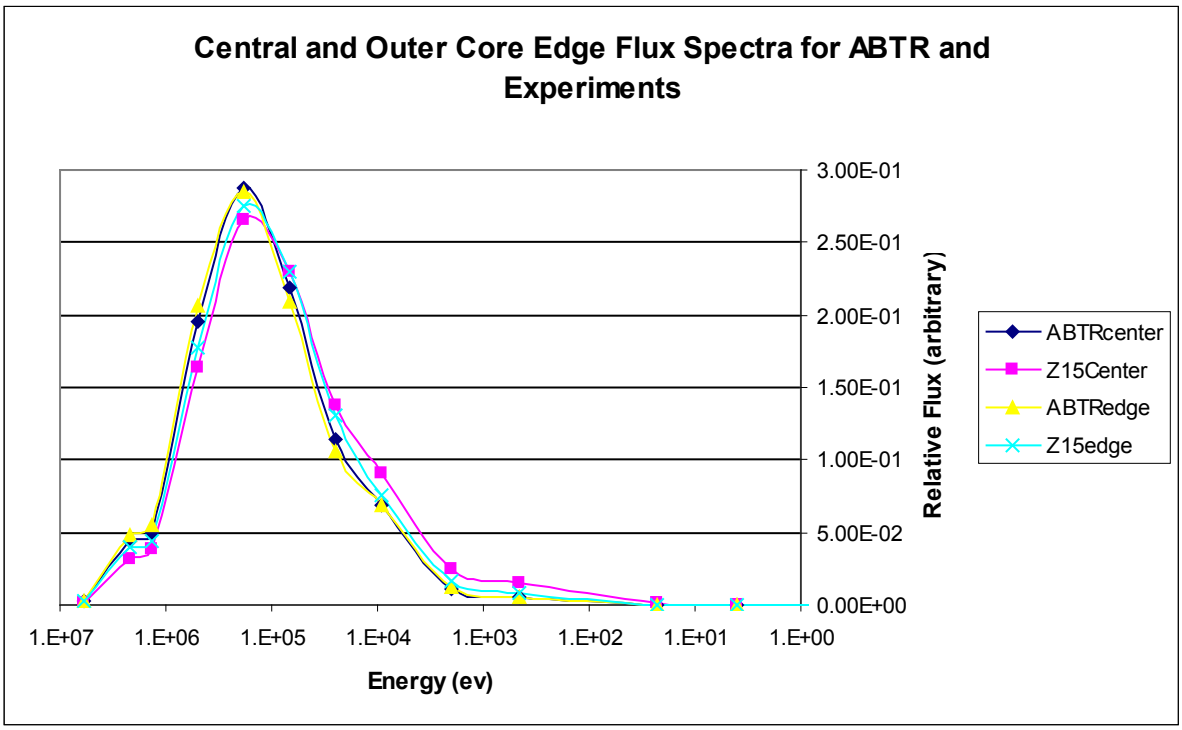

Figure 2.3 : ZPPR-15B flux spectrum compared to ABTR.

2.1.3. ZPPR as a Neutron Source

Countless irradiation experiments over the course of the ZPPR program indicate that it was used extensively as a fast neutron source. What make this particular experiment so attractive for this work is that its normalized neutron spectrum closely matches the one calculated for ABTR. While the absolute values of neutron passing a given area per second varies about 11 orders of magnitude between the ABTR and the ZPPR, the shape of the energy spectra are nearly identical. Further, the designers of ABTR put great effort into assuring that the normalized start-up core spectrum was nearly the same as the normalized equilibrium core spectrum, which means ZPPR-15B supports nuclear data assimilation applicable to both the ABTR start-up and equilibrium cores. Since fission and capture

reaction rates are directly scaleable from the flux spectrum, then for any given composition the same reactions should be taking place in ZPPR-15B as in ABTR, just on a lower order of absolute magnitude. This provides an environment to analyze the less understood reactions such as fission and capture of the higher minor actinides.

2.1.4. ZPPR as a Reactor Mock-Up

A survey of the ZPPR program history shows that reactors were used various times to mock-up future full scale facilities. These included the Fast Test Reactor, FTR, the Fast Flux Test reactor, FFT, and the Clinch River Breeder Reactor, CRBR. ZPPR provided an environment to mock up fuel assemblies for these reactors, determine void worth, perform power distribution calculations, and examine relative reaction rates. What the ZPPR could not do was to determined full scale, temperature dependent properties such as Doppler reactivity coefficient and axial or radial expansion coefficient since the ZPPR was a room temperature facility where the core was not allowed to exceed certain temperatures. It was also difficult to gather any information on radiation damage to materials over long times since neutron fluence is proportional to the time integrated flux, but both ZPPR flux level and experiment duration, at most a few days, are orders of magnitude too low versus what is needed. In summary, ZPPR could be used as a reactor mock-up facility for some integral parameters and reaction rate calculations, but temperature and fluence are much less representative of the real environment the fuel would experience in an actual power reactor facility.

2.2. Selection of Key Observables, Attributes, and Responses

In reviewing the various references looking for observables and attributes typically measured and also those that would limit a reactor like ABTR, one finds a considerable list of limiting factors for reactor operation. The ABTR report lists numerous neutronics, thermal hydraulics, mechanical and materials factors that limit the reactor [2]. Wade and Fujita build an entire safety analysis around four reactivity coefficients [13]. Aliberti, et. al. list both operating metrics such as k-effective and discharge metrics such as heat load as areas needing improvement for total fuel cycle performance [14]. As will be seen, many observables and attributes were examined for the initial generation of experiment perturbations. For the optimization problem, however, a more focused group of values was chosen and assigned monetary significance. Eventually, the selected outputs for this work met essentially two criteria: 1) what could be calculated with the modeling codes or their outputs and 2) what attributes are most important to the various aspects of a new reactor design.

The code REBUS, which will be discussed more in Chapter 3, is a neutronics and fuel cycle simulation code, so immediately all mechanical, thermal hydraulic, and materials limits are beyond our scope of analysis. This leaves neutronics based metrics such as peaking factors, reaction rates, reactivity coefficients, and fuel composition changes. For ABTR safety it was decided to look at void worth, Doppler reactivity coefficient, radial expansion reactivity coefficient, and axial expansion coefficient, from which the safety analysis developed by Wade and Fujita can be built. For waste disposal concerns, end of cycle nuclide masses and decay heat were examined for the start-up core, and for the equilibrium

core also discharge decay heat and masses. The time integral of decay heat, i.e. power generation, of the discharged fuel was also examined. For materials concerns, peak neutron flux and peak neutron fluence were examined. For reactor operations, BOC and EOC k-effectives, peaking factor, and peak power density were examined. For general fuel cycle information, this work examined conversion ratio, total and elastic scatter reaction rates for iron and Na-23, and fission and capture reaction rates for U-235, U-238, Np-237, Pu-238, Pu-239, Pu-240, Pu-241, Pu-242, Am-241, Am-242m, Am-243, Cm-242, Cm-244, and Cm-245. Reaction rates were taken at numerous spatial nodes in the active fuel and then averaged. Note in ZPPR only reaction rates, void worth, and Doppler coefficient were assumed to be directly measurable and used in data assimilation.

The optimization problem had a much more focused group of parameters. Reaction rates and k-effective from ZPPR experiments were used in the data assimilation to produce posteriori ABTR uncertainties. The ZPPR experiment is optimized over the specification of number and location of instruments, and choice and placement of SNF and TRU fuel drawers. The ABTR design is optimized over the specifications of cycle length, inner core and outer core Pu-239 content, middle core TRU enrichment, boron content which is equated to changing the number or size of control rods, and sodium content which is equated to changing the fuel rod size. The overall decision variable for the optimization is net cost savings, but the decision variables for the ABTR optimization are burnup, cycle length, and the three unitless safety parameters discussed in the next subsection. These are based on of k-effective, fluence, void worth, Doppler coefficient, and axial and radial expansion

coefficients. The ABTR decision variables must meet prescribed limits or a penalty is applied to the objective function.

2.3. Unitless Safety Parameters

A 1989 paper by Wade and Fujita [13] suggests that the ability of a fast reactor to mitigate primary accidents of loss of heat sink, transient over power, loss of coolant flow, chilled coolant inlet, and coolant pump overspeed, all without trip, can be evaluated by the values of three unitless parameters that are combinations of the reactivity coefficients of sodium density, Doppler, axial and radial expansion. To make evaluations of these unitless parameters possible each of these reactivity parameters, their uncertainties and covariances with each other must be determined. Let these four reactivity coefficients be denoted as α_{Na}, $\alpha_{Doppler}$, α_{axial}, and α_{radial}.

Once these reactivity coefficients are determined, the three parameters, A, B, and C defined by Wade

$$\begin{aligned} A &= \left(\alpha_{Doppler} + \alpha_{axial}\right)\Delta T_f \\ B &= \left(\alpha_{Doppler} + \alpha_{axial} + \alpha_{Na} + 2\alpha_{radial}\right)\frac{\Delta T_c}{2} \\ C &= \left(\alpha_{Doppler} + \alpha_{axial} + \alpha_{Na} + \alpha_{radial}\right) \end{aligned} \tag{2.1}$$

can be calculated. The reactor in question can mitigate the various accident scenarios if these unitless safety parameters are within the following ranges:

$$\frac{A}{B} \le 1, \quad 1 \le C\frac{\Delta T_c}{B} \le 2, \quad \text{and} \quad \frac{\Delta \rho_{TOP}}{|B|} \le 1 \tag{2.2}$$

where:

$$\begin{aligned}
&\Delta T_f = \text{average coolant to fuel temperature rise at full power} = 148.3K \\
&\Delta T_c = \text{average coolant temperature rise at full power} = 148.3K \\
&\Delta\rho_{TOP} = \frac{\text{BOEC hot excess reactivity}}{\text{number of contorl rods}}(\text{first control rod interaction factor}) = 0.451\$ \\
&\quad \text{where BOEC = beginning of equilibrium cycle}
\end{aligned} \tag{2.3}$$

The values of ΔT_f and ΔT_c are indicated as the same value of 148.3 K based on the information in the ABTR report and the original cross section file provided from ANL. The value $\Delta\rho_{TOP}$ is the worst stuck rod out shutdown margin divided by the number of control rods, which from the ABTR report is a nominal value of 0.451\$. Establishing the nominal values of these parameter is the first goal of the analysis, however, as this is a work on uncertainty analysis with adaption their uncertainties will also be evaluted. The 4 x 4 a priori covariance matrix for the four reactivity coefficients is determined directly from ESM uncertainty analysis. The posteriori covariance matrix can be calculated using the adapted values just like any of the other non-measurable, derived parameters. The reactivity coefficient covariance information and sensitivities are used to generate a 3 x 3 covariance matrix for the parameters A, B and C. Referring to $\frac{A}{B} \le 1$, $1 \le C\frac{\Delta T_c}{B} \le 2$, and $\frac{\Delta\rho_{TOP}}{|B|} \le 1$ as parameters 1, 2, and 3 respectively, the relative covariance information from A, B, and C was propagated to these parameters by:

$$\begin{aligned}
&\text{VAR(1)} = \text{VAR(A)} + \text{VAR(B)} - 2\text{COV(A,B)} \\
&\text{VAR(2)} = \text{VAR(C)} + \text{VAR(B)} - 2\text{COV(C,B)} \\
&\text{VAR(3)} = \text{VAR(B)}
\end{aligned} \tag{2.4}$$

It should be noted that there is indeed uncertainty on $\Delta\rho_{TOP}$, and arguably the temperatures as well. However, due to a lack of uncertainty information for these values only nominal

values were assumed. If uncertainty information was available for $\Delta\rho_{TOP}$ or the temperature changes it would add to the uncertainty on parameters A, B, 1, 2 and 3.

3. MATHEMATICAL AND COMPUTATIONAL METHODOLOGIES

3.1. Modeling Software Verification

First, a verification step was completed to confirm that REBUS with its current data is accurately predicting the ZPPR-15B experimental results and further to verify REBUS against another code, in this case MCNP. To verify the REBUS model, fission and capture reaction rate ratios for uranium-238 and uranium-235, normalized to plutonium-239 fission along with k-effective were compared with the original reported results in terms of Calculation / Experimental (C/E) values. In the original experiment, reaction rate ratios were computed for rates measured in each drawer radially along the reactor midplane and axially along the core centerline [18]. For verification purposes, the reaction rate ratios at 17 points extending radially from the center of the core to the outer core / blanket interface were used. Reaction rates were calculated in the REBUS model for these same points so that comparison could be made. Comparing the k-effective and reaction rate ratios computed by REBUS to the experimental results and the original C/E values validates REBUS is properly representing the experiment. To further verify the REBUS results, MCNP was used to model ZPPR 15B using the same geometry and compositions as the REBUS model. Reaction rate ratios and k-effective were obtained from MCNP and compared both to REBUS and to the original experimental results. Good agreement between REBUS and MCNP verifies the REBUS model and good agreement with the experimental results validates MCNP. The verification step is very important and is currently the focus of much work in the nuclear industry, especially since the migration of much of nuclear research from physical

experiments to computer simulation. Finally, where available, experimental uncertainties due to counting statistics, sample impurities, and positioning were compared to computational uncertainties due to cross section data. So as not to detract from the main body of this work, the quantitative results associated with models' verification and validation are presented in Appendix A.

3.2. ESM Methodology

As already discussed, the Efficient Subspace Method is used to propagate uncertainty through the model. Since the sensitivity and uncertainty analysis used are first-order with respect to the measured observables and key attributes and responses dependence on nuclear data, the first objective is to confirm that the model in question behaves linearly over the range of perturbations to be introduced. If the model is approximately linear over the range of possible perturbations, then higher order terms are negligible and ESM can be reliably used.

Let some model $\mathbf{\Omega}$, in this case the REBUS core simulator code, be defined by:

$$\bar{y}_0 = \mathbf{\Omega}\left(\bar{\sigma}_0\right) \tag{3.1}$$

where $\bar{\sigma}_0$ are the input cross-sections, $\bar{y}_0$ are the calculated observables, and the subscript "0" denotes the unperturbed values. Given arbitrary cross-sections perturbations, $\delta\bar{\sigma}_i, i = 1 \to n$, calculate the output responses:

$$\delta\bar{y}_i = \mathbf{\Omega}\left(\bar{\sigma}_0 + \delta\bar{\sigma}_i\right) - \mathbf{\Omega}\left(\bar{\sigma}_0\right), i = 1 \to n \tag{3.2}$$

Then, for arbitrary but bounded a_i and prescribed numerical error tolerance limit, ε, the model $\mathbf{\Omega}$ is judged to behave linearly for the range of perturbations considered if the following condition is satisfied:

$$\left| \mathbf{\Omega}\left(\bar{\sigma}_0 + \sum_{i=1}^{n} a_i \delta\bar{\sigma}_i \right) - \mathbf{\Omega}\left(\bar{\sigma}_0\right) - \sum_{i=1}^{n} a_i \delta\bar{y}_i \right| < \varepsilon \tag{3.3}$$

It has been shown in other work that the REBUS model behaves linearly for the range of cross section perturbations introduced [34]. A demonstration of this linearity is also provided in Appendix B so as not to detract from the main body of this work.

After confirming the model is linear, now consider *n* input data and *m* output data calculated by using the model $\mathbf{\Omega}$. For *n* inputs, at most *n* runs are required to fully characterize the distributions of the output. Define $\bar{y}$ as the vector of *m* outputs calculated by:

$$\bar{y} = \bar{\bar{\Omega}}\bar{\sigma} = \bar{y}_0 + \bar{\bar{\Omega}}\left(\bar{\sigma} - \bar{\sigma}_0\right) + O\left(\left(\bar{\sigma} - \bar{\sigma}_0\right)^2\right) \tag{3.4}$$

where $\bar{\sigma}$ are the *n* cross-section inputs. The second-order term can be ignored because of the linearity over the range of cross-section perturbations, and the matrix $\bar{\bar{\Omega}}$ is the absolute sensitivity matrix for the REBUS simulator. The second moments of the input and output data are characterized by the symmetric, positive definite covariance matrices, $\bar{\bar{C}}_\sigma$ and $\bar{\bar{C}}_y$, which can be decomposed as:

$$\bar{\bar{C}}_\sigma = \bar{\bar{U}}_\sigma \, \bar{\bar{\Sigma}}_\sigma \, \bar{\bar{U}}_\sigma^{\,T} \text{ and } \bar{\bar{C}}_y = \bar{\bar{\Omega}} \, \bar{\bar{C}}_\sigma \bar{\bar{\Omega}}^T \tag{3.5}$$

Combing these yields:

$$\overline{\overline{C}}_y = \overline{\overline{\Omega}}\,\overline{\overline{U}}_\sigma\,\overline{\overline{\Sigma}}_\sigma\,\overline{\overline{U}}_\sigma^{\,T}\,\overline{\overline{\Omega}}^T = \overline{\overline{\Omega}}\,\overline{\overline{U}}_\sigma\,\overline{\overline{\Sigma}}_\sigma^{\,1/2}\left(\overline{\overline{\Omega}}\,\overline{\overline{U}}_\sigma\,\overline{\overline{\Sigma}}_\sigma^{\,1/2}\right)^T \tag{3.6}$$

The matrix $\overline{\overline{\Omega}}$ is not available a priori, and in practice is rarely calculated. A stochastic sampling method would build, by sampling, only the diagonal values of $\overline{\overline{C}}_y$; whereas, ESM directly calculates $\overline{\overline{C}}_y$ by the following:

$$\overline{\overline{C}}_y = \overline{\overline{Y}}_\Sigma \overline{\overline{Y}}_\Sigma^{\,T} \text{ where } \overline{\overline{Y}}_\Sigma = \left[\delta\bar{y}_1\ \delta\bar{y}_2\ \ldots\ \delta\bar{y}_r\right] \tag{3.7}$$

where $\delta\bar{y}_i$ is given by:

$$\delta\bar{y}_i = \mathbf{\Omega}\left(\bar{\sigma}_0 + s_i\bar{u}_i\right) - \mathbf{\Omega}\left(\bar{\sigma}_0\right),\ \mathrm{i} = 1,\ldots,r \tag{3.8}$$

with r the effective rank of the input data covariance matrix, $s_i\bar{u}_i$ the input perturbations, and s_i the square root of the ith diagonal element of $\overline{\overline{\Sigma}}_\sigma$. The ith perturbation is along the ith singular vector of the input covariance matrix and proportional to the ith singular value. When repeated r times, this procedure propagates the second moments of the input data through the model. The effective rank, r, denotes the number of singular values of $\overline{\overline{C}}_\sigma$ whose magnitudes are considered sufficiently large to not ignore.

The value of r, which is typically much less than n, is determined by numerical evaluation of the percent change in attributes' uncertainties as the number of neglected singular values is increased. To determine r, the evaluator must first set some lower limit, ζ, of perturbations in the output responses that signify no further significant change due to perturbations in some input cross section, i:

$$\left|\mathbf{\Omega}\left(\overline{\sigma}_0 + \delta\overline{\sigma}_i\right) - \mathbf{\Omega}\left(\overline{\sigma}_0\right)\right| < \zeta \tag{3.9}$$

where $\delta\overline{\sigma}_i = s_i\overline{u}_i$. The smallest singular value/vector perturbation that does not make Equation 3.9 true for any cross section is assumed to be the last perturbation that will significantly contribute to the propagated uncertainty. This assumption would be violated if a singular vector with a smaller singular value was associated with an exceptionally large uncertainty. The index of this singular value then becomes *r*, the effective numerical rank of the cross section covariance matrix. For the cross section covariance matrix used in this work *n* = 5091 and *r* = 915, thus using ESM significantly reduces the number of executions of REBUS required to propagate the uncertainty.

In general, the preceding method is implemented in the program or subroutine used to generate the few-group cross sections input. This typically involves the process of introducing the prescribed perturbations into the cross-section library directly, before it is used by the model for calculations. In the REBUS model, this involves rewriting the cross section libraries produced by MC^2, the lattice physics code, to include perturbations before each sample is run. Previous work has shown that ESM produces equivalent results to traditional methods such as stochastic sampling [35].

This analysis uses a method to calculate $\delta\overline{y_i}$ which ensures that the model is constrained to its linear region. This is done by exploiting the linear behavior of the ESM process by rewriting $\delta\overline{y_i}$ as:

$$\delta\overline{y_i} = \left(\mathbf{\Omega}\left(\overline{\sigma_o} + \varepsilon_i\overline{u_i}\right) - \mathbf{\Omega}\left(\overline{\sigma_o}\right)\right)\frac{s_i}{\varepsilon_i} \tag{3.10}$$

where ε_i is a scaling factor that is calculated such that the perturbation is constrained to a user-defined magnitude, because two-norm of $\overline{u_i}$ is unity. Linearity allows this scaling factor to be divided out and the square root of the singular value multiplied in during post processing.

3.3. Representativity Methodology

The representativity of an experiment, e.g. ZPPR, to a design, e.g. ABTR, is quantified by a factor, the representativity factor, which is bounded between 0 and 1, with 1 indicating an experiment which perfectly represents the sensitivities of the design [3]. Let $\overline{S}_R$ and $\overline{S}_E$ be the sensitivity vectors of a parameter, b_x, to n input parameters for a reactor design and an experiment, respectively.

$$\overline{S}_R = \begin{vmatrix} S_{R1} \\ S_{R2} \\ \vdots \\ S_{Rn} \end{vmatrix} \text{ and } \overline{S}_E = \begin{vmatrix} S_{E1} \\ S_{E2} \\ \vdots \\ S_{En} \end{vmatrix}, \text{ where } S_{x,i} = \frac{\partial b_x}{\partial \sigma_i} \cdot \frac{\sigma_i}{b_x} \tag{3.11}$$

Note for the reactor design, the parameters of interest are those that influence the design; whereas, for the experiment the parameters of interest are those that can be measured, i.e. observables. The representativity factor is then defined as:

$$r_{RE} = \frac{\left(\overline{S}_R \overline{\overline{C}}_\sigma \overline{S}_E{}^T\right)}{\sqrt{\left(\overline{S}_R \overline{\overline{C}}_\sigma \overline{S}_R{}^T\right)\left(\overline{S}_E \overline{\overline{C}}_\sigma \overline{S}_E{}^T\right)}} \tag{3.12}$$

The optimal experiment for a reactor design is one in which r_{RE} is as close to 1 as possible, which means $\overline{S}_R$ and $\overline{S}_E$ are as similar as possible.

When more than one parameter is of interest, we can extend the representativity factor to a matrix $\overline{\overline{R}}_{RE}$, whose diagonals are the r_{RE} for each parameter:

$$\overline{\overline{R}}_{RE} = \left[\left(\overline{\overline{S}}_R \overline{\overline{C}}_\sigma \overline{\overline{S}}_R{}^T \right)^{-1} \left(\overline{\overline{S}}_R \overline{\overline{C}}_\sigma \overline{\overline{S}}_E{}^T \right) \left(\overline{\overline{S}}_E \overline{\overline{C}}_\sigma \overline{\overline{S}}_E{}^T \right)^{-1} \left(\overline{\overline{S}}_E \overline{\overline{C}}_\sigma \overline{\overline{S}}_R{}^T \right) \right]^{1/2} \tag{3.13}$$

Then, for the ideal experiment for a design concept, $\overline{\overline{R}}_{RE}$ would be as close as possible to the identity matrix. Once the representativity is available, calculation of the posterior covariance matrix $\overline{\overline{C}}_R^{(P)}$ can be made using the formula:

$$\overline{\overline{C}}_R^{(P)} = \overline{\overline{C}}_R^{(o)} \left(\overline{\overline{I}} - \left(\overline{\overline{S}}_R{}^T \right)^{-1} \overline{\overline{S}}_E{}^T \left(\overline{\overline{S}}_E \overline{\overline{C}}_\sigma \overline{\overline{S}}_E{}^T + \overline{\overline{C}}_e \right)^{-1} \overline{\overline{S}}_E \overline{\overline{C}}_\sigma \overline{\overline{S}}_R{}^T \right) \tag{3.14}$$

where $\overline{\overline{C}}_R^{(o)}$ represents the prior covariance for the reactor design and is defined as $\overline{\overline{C}}_R^{(o)} = \overline{\overline{S}}_R \overline{\overline{C}}_\sigma \overline{\overline{S}}_R{}^T$. $\overline{\overline{C}}_e$ represents the experimental uncertainties covariance matrix (geometry uncertainties, counting statistics, etc.). With some algebraic manipulation, the posteriori covariance matrix can be written in terms of the representativity matrix:

$$\overline{\overline{C}}_R^{(P)} = \overline{\overline{C}}_R^{(o)} \left(\overline{\overline{I}} - \overline{\overline{R}}_{RE}{}^2 \left[\overline{\overline{I}} - \left(\overline{\overline{S}}_E \overline{\overline{C}}_\sigma \overline{\overline{S}}_R{}^T \right)^{-1} \overline{\overline{C}}_e \left(\overline{\overline{S}}_E{}^{-1} \overline{\overline{S}}_R{}^T \right) \right]^{-1} \right) \tag{3.15}$$

and denoting the second matrix product in the bracket as $\overline{\overline{E}}$:

$$\overline{\overline{C}}_R^{(P)} = \overline{\overline{C}}_R^{(o)} \left(\overline{\overline{I}} - \overline{\overline{R}}_{RE}{}^2 \left[\overline{\overline{I}} - \overline{\overline{E}} \right]^{-1} \right) \tag{3.16}$$

The posterior covariance matrix $\overline{\overline{C}}_R^{(P)}$ denotes the design concept parameters' uncertainties if the experiment were to be conducted and the results assimilated to adapt the

input data. It is clear from this formulation that the uncertainty reduction depends on how representative the experiment is of the design and is limited by the experimental errors term, $\overline{\overline{E}}$, except in the case of a "perfect" experiment where $\overline{\overline{C}}_e \equiv 0$. Preliminary work examined cases both with and without experimental error to demonstrate the affect of experiment inaccuracy when trying to reduce data uncertainties. Subsequent work assumed a more realistic experimental error distribution that will be discussed later.

3.4. Adaptive Simulation Methodology

Before proceeding with the adaptive simulation/data assimilation section, it should be noted that the sensitivity matrices, $\overline{\overline{S}}_R$ and $\overline{\overline{S}}_E$, are not explicitly calculated in this work. Instead the uncertainty propagation technique computes only the product

$$\overline{\overline{Y}}_{\Sigma,x} = \overline{\overline{S}}_x \overline{\overline{U}}_\sigma \overline{\overline{\Sigma}}_\sigma^{1/2}, \; x = R, E \tag{3.17}$$

From this product all necessary components of the posteriori covariance matrix formula can be computed.

If this problem had matrices where all matrices are well-conditioned, then a direct calculation of Equation 3.14 could be made. However since the sensitivity matrices and the cross section covariance matrix may be ill-conditioned, some mathematical procedure must be introduced enabling Equation 3.14 to be computationally evaluated. Recognizing that

$$\overline{\overline{C}}_R^{(P)} = \overline{\overline{S}}_R \overline{\overline{C}}_\sigma^{(P)} \overline{\overline{S}}_R^{\,T} \tag{3.18}$$

where $\overline{\overline{C}}_{\sigma}^{(P)}$ is the posteriori cross section covariance matrix, there needs to be an expression for $\overline{\overline{C}}_{\sigma}^{(P)}$ such that it can be computed without numerical failures. Such an expression is derived, at length, in the work of Jessee [11].

Jessee derives an expression for $\overline{\overline{C}}_{\sigma}^{(P)}$ in terms of the solution procedure used to solve the minimization problem of adjusting the original input cross sections $\bar{\sigma}_o$ to some new values $\bar{\sigma}$, which will reduce the discrepancy between observed experimental parameters $\bar{y}_{Em}$ and calculated experimental parameters $\bar{y}_E$. Following Jessee's work henceforth:

$$\bar{\sigma}' = \underset{\bar{\sigma}}{\mathbf{min}} \left\{ \left[\bar{y}_{Em} - \bar{y}_E - \overline{\overline{S}}_E \left(\bar{\sigma} - \bar{\sigma}_o \right) \right]^T \overline{\overline{C}}_e^{-1} \left[\bar{y}_{Em} - \bar{y}_E - \overline{\overline{S}}_E \left(\bar{\sigma} - \bar{\sigma}_o \right) \right] + \left(\bar{\sigma} - \bar{\sigma}_o \right)^T \overline{\overline{C}}_{\sigma}^{-1} \left(\bar{\sigma} - \bar{\sigma}_o \right) \right\} \tag{3.19}$$

this equation originating from Bayes Theorem and imposing maximum likelihood. The matrix inverse $\overline{\overline{C}}_e^{-1}$ and $\overline{\overline{C}}_{\sigma}^{-1}$ in general can be replaced by pseudo-inverses. If one of these matrices is non-singular, which would be expected of $\overline{\overline{C}}_e$, nothing is lost in doing this. Also adjustments $\left(\bar{\sigma} - \bar{\sigma}_o \right)$ must be constrained to the space spanned by the uncertainty $\overline{\overline{C}}_{\sigma}$ which is the range of the singular vectors, $R\left(\overline{\overline{U}}_{\sigma} \right)$:

$$\bar{\sigma} = \bar{\sigma}_o + \overline{\overline{U}}_{\sigma} \overline{\overline{\Sigma}}_{\sigma}^{1/2} \bar{z}_{\sigma} \tag{3.20}$$

where $\bar{z}_{\sigma}$ is some vector. The problem can also include a regularization term, α, to restrain adjustments to be within a range of the a priori uncertainty. The preferred value for α is determined by computation experiments, i.e. adjust to find the "knee" of the "L-curve" [73]

when plotting the mismatch term as a function of the regularization term as α is varied. Note that when $\alpha = 1$ an unbiased adjustment results. Equation 3.19 then becomes:

$$\bar{\sigma}' = \underset{\bar{\sigma}}{\mathbf{min}} \left\{ \left\| \bar{y}_{Em} - \bar{y}_E - \bar{\bar{S}}_E \left(\bar{\sigma} - \bar{\sigma}_0 \right) \right\|^2_{\bar{\bar{C}}_e^{-1}} + \alpha \left\| \left(\bar{\sigma} - \bar{\sigma}_0 \right) \right\|^2_{\bar{\bar{C}}_\sigma^{-1}} \right\} \tag{3.21}$$

By this definition α = 0 implies no regularization. Using the decomposition $\bar{\bar{C}}_e = \bar{\bar{U}}_e \bar{\bar{\Sigma}}_e^{1/2} \bar{\bar{\Sigma}}_e^{1/2} \bar{\bar{U}}_e^T$, Equation 3.21 is rewritten as:

$$\bar{\sigma}' = \underset{\bar{\sigma}}{\mathbf{min}} \left\{ \left\| \begin{bmatrix} \bar{\bar{\Sigma}}_e^{-1/2} \bar{\bar{U}}_e^T \left(\bar{y}_{Em} - \bar{y}_E \right) \\ 0 \end{bmatrix} - \begin{bmatrix} \bar{\bar{\Sigma}}_e^{-1/2} \bar{\bar{U}}_e^T \bar{\bar{S}}_E \\ \alpha^2 \bar{\bar{\Sigma}}_\sigma^{-1/2} \bar{\bar{U}}_\sigma^T \end{bmatrix} \left(\bar{\sigma} - \bar{\sigma}_0 \right) \right\|_2^2 \right\} \tag{3.22}$$

Equation 3.20 is substituted into Equation 3.22 to yield:

$$\bar{z}'_\sigma = \underset{\bar{z}_\sigma}{\mathbf{min}} \left\{ \left\| \begin{bmatrix} \bar{\bar{\Sigma}}_e^{-1/2} \bar{\bar{U}}_e^T \left(\bar{y}_{Em} - \bar{y}_E \right) \\ 0 \end{bmatrix} - \begin{bmatrix} \bar{\bar{\Sigma}}_e^{-1/2} \bar{\bar{U}}_e^T \bar{\bar{S}}_E \bar{\bar{U}}_\sigma \bar{\bar{\Sigma}}_\sigma^{1/2} \\ \alpha^2 \bar{\bar{I}} \end{bmatrix} \bar{z}_\sigma \right\|_2^2 \right\} \tag{3.23}$$

The quantity $\bar{\bar{\Sigma}}_e^{-1/2} \bar{\bar{U}}_e^T \bar{\bar{S}}_E \bar{\bar{U}}_\sigma \bar{\bar{\Sigma}}_\sigma^{1/2}$ is decomposed via SVD such that:

$$\bar{\bar{\Sigma}}_e^{-1/2} \bar{\bar{U}}_e^T \bar{\bar{S}}_E \bar{\bar{U}}_\sigma \bar{\bar{\Sigma}}_\sigma^{1/2} = \bar{\bar{\Sigma}}_e^{-1/2} \bar{\bar{U}}_e^T \bar{\bar{Y}}_{\Sigma,E} = \bar{\bar{U}} \; \bar{\bar{\Sigma}}^{1/2} \; \bar{\bar{\Sigma}}^{1/2} \; \bar{\bar{V}}^T \tag{3.24}$$

The solution of the minimization problem is:

$$\bar{z}'_\sigma = \bar{\bar{V}} \left(\bar{\bar{\Sigma}}^2 + \alpha^2 \bar{\bar{I}} \right)^{-1} \bar{\bar{\Sigma}} \; \bar{\bar{U}}^T \bar{\bar{\Sigma}}_E^{-1/2} \bar{\bar{U}}_E^T \left(\bar{y}_{Em} - \bar{y}_E \right) \tag{3.25}$$

It then follows that:

$$\bar{\bar{C}}_\sigma^{(P)} = \bar{\bar{U}}_\sigma \bar{\bar{\Sigma}}_\sigma^{1/2} \bar{\bar{C}}_{\bar{z}} \bar{\bar{\Sigma}}_\sigma^{1/2} \bar{\bar{U}}_\sigma^T \tag{3.26}$$

where

$$\overline{\overline{C}}_z = \overline{\overline{V}}\,\overline{\overline{\Sigma}}_z\,\overline{\overline{V}}^T = \overline{\overline{V}}\left(\overline{\overline{\Sigma}}^2 + \alpha^2\overline{\overline{I}}\right)^{-2}\left(\overline{\overline{\Sigma}}^2 + \alpha^4\overline{\overline{I}}\right)\overline{\overline{V}}^T \tag{3.27}$$

Substituting Equation 3.26 in Equation 3.18 produces

$$\overline{\overline{C}}_R^{(P)} = \overline{\overline{S}}_R\,\overline{\overline{U}}_\sigma\,\overline{\overline{\Sigma}}_\sigma^{1/2}\,\overline{\overline{C}}_z\,\overline{\overline{\Sigma}}_\sigma^{1/2}\,\overline{\overline{U}}_\sigma^{\,T}\,\overline{\overline{S}}_R^{\,T} \tag{3.28}$$

for the posteriori covariance matrix for the reactor parameters. As expected, $\overline{\overline{C}}_R^{(P)}$ is seen to be independent of both $\bar{y}_{Em}$ and $\bar{y}_E$. Equation 3.28 is well-conditioned and can therefore be numerically evaluated. Using Equation 3.17 in Equation 3.28, the equation used in the calculations is obtained:

$$\overline{\overline{C}}_R^{(P)} = \overline{\overline{Y}}_{\Sigma,R}\,\overline{\overline{C}}_z\,\overline{\overline{Y}}_{\Sigma,R}^{\,T} \tag{3.29}$$

The preceding derivation indicates that Equation 3.29 is the expression for $\overline{\overline{C}}_R^{(P)}$ with regularization that can be computed with acceptable numerical errors. Obtaining $\overline{\overline{Y}}_{\Sigma,R}$ and $\overline{\overline{Y}}_{\Sigma,E}$ which appear in Equation 3.29 and Equation 3.17, respectively, along with SVD to obtain $\overline{\overline{V}}$ appearing in Equation 3.27 for $\overline{\overline{C}}_z$ defines the computations required to evaluate Equation 3.29 to obtain $\overline{\overline{C}}_R^{(P)}$.

To realistically assimilate data from an experiment, uncertainties must be included in the analysis, i.e. $\overline{\overline{C}}_e \neq 0$. Experimental uncertainty will be discussed first. The most evident source of uncertainty is the intrinsic counting statistics uncertainty of one divided by the square root of the number of counts [30]. Beyond this there are uncertainties due to sample impurities, sample or detector positioning, and reactor table positioning. As seen from the original ZPPR reports, these sources of uncertainties and the counting statistics uncertainty

were typically lumped into a single reported uncertainty on reaction rate counting that was about 1% relative standard deviation over all the reaction rates counted [18][29]. The effect of these experimental uncertainties on posteriori uncertainties is evaluated for 0%, 1% and 7.5% experimental uncertainties, with 1% assumed to be the most realistic according to the original experiment reports.

The other noticeable source of uncertainty is fission product yield and decay constant uncertainty, which are two parameters affecting the measured reaction rates. As indicated in the paper by de Saint Jean [36], parameters with a priori uncertainty, such as fission product yield and decay constant, can be addressed by the same method as used to treat experimental uncertainties. So in determining $\overline{\overline{C}}_e$ the experimental uncertainties noted in the previous paragraph were combined with the just noted uncertainties to obtain the overall experimental uncertainties.

Specifically, fission product decay constant uncertainty and yield data uncertainty were considered for the fission rates, and capture product decay constant uncertainty was considered for the capture rates. It was assumed that all the fission rates were counted by the decay of the Mo-99 fission product into Tc-99, with a nominal half life of 65.94 hours. Table 3.1 presents fission yield data for the actinides tracked in this work. The uncertainties are in percent of fissions. For example, since the fission product yield for U-235 has an uncertainty of 0.1336% then the predicted U-235 fission reaction rate should also have an uncertainty of 0.1336% from the fission product yield data uncertainty.

The decay constant of Mo-99 is nominally 65.94 hours with an uncertainty of 36 seconds, or 0.0152% [43]. Since activity has the time dependent form of

$$A(t) = \lambda N_o \exp(-\lambda t) \tag{3.30}$$

where λ is the decay constant, the uncertainty on the observed change in rate with respect to time, dA/dt must be integrated over some counting time to get the uncertainty in counts. The activity at any time relative to the initial activity is then

$$\frac{A(t)}{\lambda N_o} = \exp(-\lambda t) \tag{3.31}$$

Therefore, to obtain the relative counts observed in some time interval t_1 to t_2, the expression is integrated

$$\int_{t_1}^{t_2} \frac{A(t)}{\lambda N_o} dt = \int_{t_1}^{t_2} \exp(-\lambda t)\, dt = \frac{1}{\lambda}\left(\exp(-\lambda t_1) - \exp(-\lambda t_2)\right) \tag{3.32}$$

yielding a value bounded by 0 and $1/\lambda$. One standard deviation of the value of the decay constant, σ_λ, is applied and the equation integrated with both $+\sigma_\lambda$ and $-\sigma_\lambda$ to yield perturbed values:

$$\int_{t_1}^{t_2} \frac{A(t)}{(\lambda \pm \sigma_\lambda) N_o} dt = \int_{t_1}^{t_2} \exp\left(-(\lambda \pm \sigma_\lambda)t\right) dt = \frac{1}{\lambda}\left(\exp\left(-(\lambda \pm \sigma_\lambda)t_1\right) - \exp\left(-(\lambda \pm \sigma_\lambda)t_1\right)\right) \tag{3.33}$$

The change in observed relative counts is evaluated for both cases and the average taken as the uncertainty in the counts contributed by the decay constant. For counting of Mo-99, the counting time was integrated from 2 hours to 3 half-lives, and the relative uncertainty in the counts applied to the predicted reaction rate value. Two hours was chosen as the approximate time to get the sample from the experiment to a counting chamber.

Decay constant uncertainty on the capture daughters for the capture reaction rates were treated in the same manner as for the fission product Mo-99. Counting times were

assumed to be 2 hours to 200 hours, or about the same time as the fission product counts. The capture products and decay constant relative uncertainties are shown in Table 3.2. Once evaluated, these uncertainties, which were assumed to be uncorrelated to each other, were added to the diagonal values of $\overline{\overline{C}}_e$ as additional variances.

It should be noted that in the original ZPPR experiments, an uncertainly on k-effective of 0.1 cents [28] was also reported. However, this translates into 3.36E-4 % for k-effective and 6.72E-4 % for the Doppler coefficients and void worth measurements. While this value is insignificant it is included in the error term for these data for completeness.

Table 3.1 : Fission product yield uncertainty for Mo-99.

	Fission Product Yield for Fast Fission	
	% of Fissions	Uncertainty, %
U-235	5.80470	0.1336
U-238	6.18130	0.0990
Np-237	7.62180	1.2424
Pu-238	6.00290	1.9810
Pu-239	5.82270	0.1281
Pu-240	6.05930	0.4787
Pu-241	4.11740	2.3181
Pu-242	3.78950	2.5769
Am-241	5.32860	0.2771
Am-242m	4.73840	1.6111
Am-243	4.45820	1.4890
Cm-242	5.42580	0.8681
Cm-244	4.56790	1.4937
Cm-245	3.99120	1.2852

Table 3.2 : Decay constant uncertainties.

Capture Parent	Daughter	% Uncertainty
U-235	U-236	0.1281
U-238	U-239	0.0853
Np-237	Np-238	0.0945
Pu-238	Pu-239	0.1244
Pu-239	Pu-240	0.1067
Pu-240	Pu-241	0.0420
Pu-241	Pu-242	0.5333
Pu-242	Pu-243	0.0605
Am-241	Am-242	0.1248
Am-242m	Am-243	0.5427
Am-243	Am-244	0.9901
Cm-242	Cm-243	0.3436
Cm-244	Cm-245	1.1765
Cm-245	Cm-246	0.8404

3.5. Optimization Problem Development

The objective of this problem is to maximize ABTR Reactor Cost Savings by reducing the margins required, accounting for the offsetting cost of performing experiments. Therefore the objective to be maximized can be stated as follows:

(ABTR Reactor Cost using a priori ABTR Optimum Design Specs) - (ABTR Reactor Cost using posteriori ABTR Optimum Design Specs) - (ZPPR Experiment Cost) = Net Savings

The problem can also be viewed as a minimization problem by simply saying that it is desired to minimize the cost of a given reactor design introduced by the need for margin. Therefore the objective is to minimize the following problem:

(ABTR Reactor Cost using posteriori ABTR Optimum Design Specs) - (ABTR Reactor Cost using a priori ABTR Optimum Design Specs) + (ZPPR Experiment Cost) = Net Cost

By this definition if the net cost is not substantially less than zero then the experiment is not economically beneficial. To achieve this objective, an experiment setup of optimized ZPPR design specifications (plate compositions and locations, detector locations and number) which are constrained to the feasibility space of the ZPPR reactor facility is selected.

To solve this problem cost data as a function of the ABTR design specifications is needed. The following information is also required:

- A priori uncertainties on ABTR design attributes, propagated from parameters (cross sections)
- Posteriori uncertainties on ABTR design attributes, propagated from parameters (which depends on the ZPPR design specifications)

This would in turn be used to determine the uncertainties of ABTR design responses which must be constrained to a space such that there is a stated probability of not exceeding a certain set of ABTR design limits which may be financial or safety related.

The ABTR core attributes are calculated based on the input parameters as well as the reactor specifications. The optimum ABTR design specifications are drawn from some allowable design specification range as constrained by the ABTR design limits and are the specifications that minimize the cost of the reactor. The objective problem then is to select a set of ZPPR design specifications, the decision variables, to produce an optimal experiment in which the net savings are maximized.

Starting with the following definitions:

$\Gamma^{(p)} = \left(\text{ABTR Reactor Cost using ABTR Optimum Design Specs based upon posteriori ABTR Design Specs Range}\right)$
$\Gamma^{(o)} = \left(\text{ABTR Reactor Cost using ABTR Optimum Design Specs based upon a priori ABTR Design Specs Range}\right)$
$\Gamma_E = \left(\text{ZPPR Experiment Cost}\right)$
Then the objective is to solve:

$$\min\left\{\Gamma^{(p)} - \Gamma^{(o)} + \Gamma_E\right\} \text{ with respect to ZPPR Design Specifications} \tag{3.34}$$

3.5.1. Definition of Experiment Cost

The cost of the experiment is determined by the number and types of plates, number and location of detectors, base cost of the facility, and the labor costs to do the experiments. Facility costs, e.g. refurbishing ZPPR, are a fixed cost which can be assumed invariant to the number of experiments being performed. So the definition of experimental cost is:

$$\Gamma_E = \left(\overline{C}_{Ex}{}^T \overline{D}_{Ex}\right) + C_{Fixed} \tag{3.35}$$

where $\overline{D}_{Ex}$ is the vector of the selected values of the decision variables, $\overline{C}_{Ex}$ is a vector of per unit costs for each of the decision variables, and C_{Fixed} is the facility cost. Clearly, an assumption has been made that unit costs are independent of number of units, e.g. no economy of scale. For example if $\overline{D}_{Ex} = 5$ TRU drawers and $\overline{C}_{Ex} =$ \$2000/TRU drawer than $\Gamma_E = \$10,000$ if all other costs were zero. Since this set of decision variables is what we will chose to minimize the objective function of Net Cost, the problem is now defined as the minimized cost over the possible selections of $\overline{D}_{Ex}$:

$$\min_{\overline{D}_{Ex}}\left\{\Gamma^{(p)} - \Gamma^{(o)} + \Gamma_E\right\} \tag{3.36}$$

However $\overline{D}_{Ex}$ cannot be anything. ZPPR has a finite size, finite number of drawers, and must be operated within certain limits due to the nature of the facility (radiation limits, heat load, run times, etc.). Therefore $\overline{D}_{Ex}$ must be constrained to some set of values that the ZPPR facility can physically accommodate, i.e. the feasibility space of the experiment:

$$\overline{D}_{Ex} \in s_{F_{Ex}} \tag{3.37}$$

where $s_{F_{Ex}}$ is the allowable range of the ZPPR design specifications, the decision variables. There are only 896 fuel drawer locations in the ZPPR-15B experiment, or 224 per symmetric quarter core. Note that although ZPPR is a split core reactor, each drawer is modeled as spanning the entire axial length of the reactor. Given that we assume there are four feasible types of fuel drawers, the total number of single column Pu, double column Pu, TRU, and SNF drawers must be no greater than and no less than 224 (quarter core symmetry maintained). So this is the problem now:

$$\min_{\overline{D}_{Ex} \in s_{F_{Ex}}} \left\{ \Gamma^{(p)} - \Gamma^{(o)} + \Gamma_E \right\} \tag{3.38}$$

Note that the ZPPR uncertainties are addressed in the data assimilation that permits the posteriori optimized design of the ABTR, i.e. they are included implicitly in $\Gamma^{(p)}$.

3.5.2. Definition of ABTR Design Limits and Responses

For every reactor design there are some set of design limits which are required to be met at all times, within a stated probability of not being exceeded, for the design to operate safely and economically. These limits bound the ABTR design responses, i.e. every response

must be within some limits. Some examples of ABTR design responses which have associated limits could be:

- Wade-Fujita Safety Parameters – a combination of reactivity coefficients that if within a certain range of values ensure the reactor can safely mitigate most severe accident scenarios (e.g. Overpower, Loss of Heat Sink and Loss of Flow events without trip)
- Cycle Length – to destroy a desired quantity of minor actinides while producing an economically sustainable amount of electricity
- Burnup – to protect fuel from failures and to ensure economic cycles

Let these, and/or any other, ABTR design responses be defined as $\gamma_j, j = 1 \ldots n$ for a set of n responses.

3.5.3. Definition of ABTR Core Attributes

All the ABTR design responses are defined by some set of ABTR core attributes, which are a set of values calculated and then used to determine the responses. For example, say that the set of ABTR design responses in the previous section may be related to the following set of ABTR core attributes:

- k-effective at EOC
- Fluence
- Void worth
- Doppler reactivity coefficient
- Axial Expansion coefficient

- Radial Expansion coefficient

The ABTR core attributes noted above are obtainable from REBUS outputs.

Define $\bar{\eta}_{\gamma j}, j = 1 \ldots n$ as the vector of core attributes that produces the j-th design response γ_j, i.e. $\gamma_j = f\left(\bar{\eta}_{\gamma j}\right)$.

3.5.4. Definition of ABTR Design Specifications

The ABTR core attributes $\bar{\eta}_{\gamma j}$ are calculated in REBUS utilizing two sources of input. The first source is the parameters, i.e. cross sections, which are known and have associated a priori and posteriori uncertainties which propagate through to determine the ABTR core attributes' uncertainties. The other source of data used to calculate the attributes is the ABTR design specifications which are input into REBUS. These can include but are not limited to:

- Cycle length
- Composition of control elements
- Composition (Pu, U and TRU) of each fuel zone
- Core size
- Core thermal power density
- Number of control elements
- Fuel pin size
- Core coolant flow rate

Note that ABTR design specifications can also be ABTR core attributes, e.g. cycle length, since the core physics does not change such core attribute values. Also note that changes in

one ABTR design specification could necessitate changes in other ABTR design specifications, e.g. core flow rate impacts pump and heat exchanger sizes.

Given a set of ABTR design specifications, $\overline{\beta}$, this will produce a set of ABTR core attributes and their associated uncertainties due to the uncertainties in the parameters, i.e. cross-sections. In turn the ABTR core attributes and their uncertainties will produce the ABTR design responses and their uncertainties, which can be used to determine whether the ABTR design limits are satisfied. The larger the cross-sections uncertainties the less freedom there is to select $\overline{\beta}$. By reducing the cross-sections uncertainties by data assimilations using ZPPR experiments, more freedom in selecting values of $\overline{\beta}$ that satisfy the ABTR design limits is gained.

3.5.5. Design Limits and Final Problem Statement

Let the ABTR design response γ_j be subject to the design limits of $\gamma_{j,\max}$ and $\gamma_{j,\min}$ Then for a given set of ABTR design specs, $\overline{\beta}$, the design response γ_j must satisfy the limits to within XX% probability:

$$O_{\gamma j}\left(\overline{\beta}\right) = \int_{\gamma j,\min}^{\gamma j,\max} p_{\gamma j}\left(\gamma_j, \overline{\beta}\right) d\gamma_j \geq 0.\text{XX} \tag{3.39}$$

This implies given some design limits on γ_j, there is a range of ABTR design specifications, denoted $s_{\beta\gamma_j}$ such that when $\overline{\beta} \in s_{\beta\gamma_j}$ will assure a XX% probability of not exceeding the ABTR design limits. Note this formula implicitly includes the cross section induced uncertainties which propagate from the relevant ABTR design attributes, $\overline{\eta}_{\gamma j}$, into γ_j.

Within the framework of using a risk informed approach, one cannot directly use design responses. Instead one is interested in consequences, which could imply retaining the integrity of some system, structure or component (SCC). Now the failure probability of a SSC would be dependent upon a number of the design responses, so to obtain the failure probability of an SSC would involve the convolution of the joint probability distribution of the design responses with the probability distribution of SSC failure given values for the design responses. This is too complex for the current work, so it will be assumed that if each design response is retained within its limits, the SSC probability of failure will satisfy the risk informed limits imposed.

To obtain the j-th design response probability distribution, $p_{\gamma j}\left(\gamma_j, \overline{\beta}\right)$, in general would involve the solution of a complex set of partial differential equations to obtain the relationship $\gamma_j = f\left(\overline{\eta}_{\gamma j}\right)$. This in turn would provide the basis for determining $p_{\gamma j}\left(\gamma_j, \overline{\beta}\right)$ by accounting for the uncertainties in the ABTR core responses, $\overline{\eta}_{\gamma j}$, which in turn were previously determined using the uncertainties in the parameters. To simplify the problem, in this work it will be assumed that there is no need to solve a set of PDEs to obtain the relationship between the ABTR core attributes and ABTR design responses since it is given by an algebraic expression.

Since there are n design responses and associated design limits, then there will be n design specifications ranges, $s_{\beta\gamma_j}$. To obtain the range of the ABTR design specifications that satisfies all design limits simultaneously, one determines the range defined by the common intersects of all n design specifications ranges as now indicated.

$$s_\beta = s_{\beta\gamma 1} \bigcap s_{\beta\gamma 2} \bigcap \ldots \bigcap s_{\beta\gamma n} \tag{3.40}$$

Clearly s_β is dependent upon the uncertainties in the parameters, i.e. cross-sections. So if the cross-sections uncertainties are reduced using data assimilation based upon ZPPR experiments, then the range of s_β will be increased. In turn this increased range can be utilized to decrease the ABTR reactor cost.

For the remainder of this discussion assume that when we refer to $\overline{\beta}$ that it both assures the ABTR design limits are satisfied, i.e. $\overline{\beta} \in s_\beta$, and that it has been selected to minimize the ABTR reactor cost. That $\overline{\beta}$ is referred to as the ABTR optimum design specifications, i.e. those such that the a priori cost is

$$\Gamma^{(o)} = \min_{\overline{\beta} \in s_\beta^{(o)}} \left(\overline{C}_\beta{}^T \overline{\beta} \right) \tag{3.41}$$

where $\overline{C}_\beta$ is the cost associated with each of the design specifications in $\overline{\beta}$ being applied to the ABTR reactor design and $s_\beta^{(o)}$ is the design spec range permitted by the a priori uncertainties on the parameters. For example one of the elements of $\overline{\beta}$ would be the composition of fuel in a particular region and the corresponding value in $\overline{C}_\beta$ would be the dollar cost for that composition. In this manner the inner product is simply the transpose of the cost vector times the design specifications vector. Again, this assumes a simple cost relationship.

Likewise we also define the posteriori ABTR reactor cost as that associated with a $\overline{\beta}$ constrained to the design specification range of $s_\beta^{(p)}$ which is the range permitted by the posteriori uncertainties of the parameters.

$$\Gamma^{(p)} = \min_{\overline{\beta} \in s_\beta^{(p)}} \left(\overline{C}_\beta{}^T \overline{\beta} \right) \tag{3.42}$$

So the minimization problem now reads as follows.

$$\min_{\overline{D}_{Ex} \in s_{F_{Ex}}} \left\{ \min_{\overline{\beta} \in s_\beta^{(p)}} \left(\overline{C}_\beta{}^T \overline{\beta} \right) - \min_{\overline{\beta} \in s_\beta^{(o)}} \left(\overline{C}_\beta{}^T \overline{\beta} \right) + \left(\overline{C}_{Ex}{}^T \overline{D}_{Ex} \right) + C_{Fixed} \right\} \tag{3.43}$$

This is a complicated problem with two inner minimization problems within an outer minimization problem. As discussed there are closed form expressions to determine the a priori and posteriori covariance matrices of the ABTR design attributes, $\overline{\overline{C}}_R^{(o)}$ and $\overline{\overline{C}}_R^{(p)}$, respectively. Values are set for C_{Fixed}, $\overline{C}_\beta$ and $\overline{C}_{Ex}$. Values are selected for the ABTR design specifications and checked to see if the resulting attributes generate responses that are still within the limits. Now all that is needed is a method to solve the minimization problems and simulated annealing will be applied for this.

3.5.6. Solution of the Optimization Problem

The a priori ABTR reactor cost will be a constant, i.e. $\Gamma^{(o)}$ is not dependent upon the choice of experimental setup, so this value need only be computed once. The a priori ABTR optimum design specifications will be determined via a simulated annealing (SA) algorithm with the objective of minimizing the cost while still meeting the design limits. Given the ABTR core attributes a priori covariance matrix , $\overline{\overline{C}}_R^{(o)}$, and given specified values of the

design limits it can be determined if the chosen set of ABTR design specifications produced core attributes with some uncertainty that produced responses with some uncertainty that meet the design limits to within an XX% probability. If not, the magnitude of violation is used to determine the penalty function which is added to the objective function to form the augmented objective function. These specifications are used to compute the cost of the ABTR, the objective function. The augmented objective function is then used to determine whether this set of specifications is accepted outright or accepted with a certain probability. The SA algorithm then proceeds until the near-optimum ABTR design specifications have been determined. The solution of this SA problem is the minimum ABTR cost using the optimum a priori design specs: $\min_{\overline{\beta} \in s_{\beta}^{(o)}} \left(\overline{C}_{\beta}^{\,T} \overline{\beta} \right)$.

The minimization problem now has two fixed values and two variable values that depend upon the choice of ZPPR design specs, $\overline{D}_{Ex}$.

$$\min_{\overline{D}_{Ex} \in s_{F_{Ex}}} \left\{ \min_{\overline{\beta} \in s_{\beta}^{(p)}} \left(\overline{C}_{\beta}^{\,T} \overline{\beta} \right) + \left(\overline{C}_{Ex}^{\,T} \overline{D}_{Ex} \right) + C_{Fixed} - \Gamma^{(o)} \right\} \tag{3.44}$$

The solution of this is a two tiered, or inner and outer, SA solution. First, a set of allowed ZPPR design specifications are chosen: $\overline{D}_{Ex} \in s_{F_{Ex}}$. The non-fixed ZPPR experiment cost, $\left(\overline{C}_{Ex}^{\,T} \overline{D}_{Ex} \right)$, is then computed. The ZPPR experiment is then modeled and the resulting ZPPR observables used in the adaption methodology already developed to compute parameters posteriori uncertainties and subsequently core ABTR attributes posteriori uncertainties, $\overline{\overline{C}}_{R}^{\,(p)}$. Now the ABTR design response uncertainties can be evaluated. The

optimum posteriori design specifications which minimize the cost of ABTR, $\min_{\beta \in s_\beta^{(p)}} \left(\overline{C}_\beta{}^T \overline{\beta} \right)$, is then determined using the same SA algorithm as the a priori optimum design specifications, only with the ABTR design responses uncertainties based upon the ABTR core attributes posteriori uncertainty instead of the a priori uncertainty. This is the inner SA optimization which must be computed for each choice of ZPPR design specifications.

The outer SA optimization is the one in which the optimum ZPPR design specifications are selected by minimizing the cost function. Once the inner SA optimization is complete for the current selection of ZPPR design specifications the objective function $\left\{ \min_{D_{Ex} \in s_{F_{Ex}}} \left(\overline{C}_\beta{}^T \overline{\beta} \right) + \left(\overline{C}_{Ex}{}^T \overline{D}_{Ex} \right) + C_{Fixed} - \Gamma^{(o)} \right\}$ is evaluated.

Depending on this value, the SA algorithm will either accept outright or accept with some probability the ZPPR design specifications that produced this result. Another set of ZPPR design specifications will then be selected, the inner SA optimization repeated, and the resulting objective function value fed back into the outer SA optimization when the inner optimization is completed. The outer SA algorithm proceeds to determine the near-optimum ZPPR design specifications. At the conclusion of the optimization, not only the family of near-optimum ZPPR design specifications but also the family of near-optimum ABTR design specifications will have been determined.

3.5.7. Simulated Annealing Procedure

This discussion is kept general as the same SA procedure will be used for determining the inner and the outer SA optimizations. Let F_i be the current generation augmented

objective function value, i.e. an evaluated cost plus penalty function if constraints are violated, and F_{i+1} be the perturbed augmented objective function. Perturbations are introduced by randomly perturbing design specifications within their specified ranges. With several different design specifications, all are perturbed each ith sample. If $F_{i+1} < F_i$ then the decision variables, $\overline{D}_{i+1}$, producing F_{i+1} are always accepted. If $F_{i+1} > F_i$ then the decision variables, $\overline{D}_{i+1}$, producing F_{i+1} are accepted with the following probability [51]:

$$p = \exp\left(-\frac{F'_{i+1} - F_i}{T_k}\right) \tag{3.45}$$

where k denotes the k-th generation of trials, i.e. Markov chain.

T_k is the temperature for the k-th generation of trials and a cooling schedule must be determined for the SA algorithm. The initial temperature is estimated by surveying the space of possible augmented objective function values [55][56]. The standard deviation of these values, $\sigma_{obj,0}$, is computed. The initial temperature is then:

$$T_0 = A\sigma_{obj,0} \tag{3.46}$$

where the magnitude of the proportionality constant, A, is determined by whether a local or global search is desired [53].

After a user selected number of acceptances occurs to form a pseudo-equilibrium the temperature is updated, i.e. cooled. The next generation temperature is determined by

$$T_{k+1} = \alpha_k T_k \tag{3.47}$$

where α_k can be a user selected value between 0.5 and 0.99 [53][51][52] or a more elaborate schedule [56][51]:

$$\alpha_k = \exp\left(-\frac{cT_k}{\sigma_{obj,k}}\right) \tag{3.48}$$

A typical value for c is 0.7 [56] and $\sigma_{obj,k}$ is the standard deviation of the accepted objective function values for the k-th generation. The method employed for this work will use the minimum of either Equation 3.48 or 0.5 [54]. The SA proceeds through a number of generations to arrive at an optimized solution within a user defined tolerance in terms of the change in the augment objective function value.

In addition to the criteria on the monetary value of the objective function, trials can be rejected because they violate a hard limit. The only hard limit imposed in this work is exceeding one of the three Wade-Fujita safety parameters. Finally, as mentioned above, penalties are added to the objective function values if constraint violations occur to create the augmented objective function value F_{i+1}:

$$F_{i+1} = \text{cost}_{i+1} + \zeta_{i+1}\sum_n \lambda_n \Theta_{n,i+1} \tag{3.49}$$

Since this optimization problem is based on monetary cost, the penalties take the simple form of cost associated with violating some soft constraint. Here the penalty function $\Theta_{n,i+1}$ is dependent upon the magnitude of the violation of the n-th penalty type and λ_n is the per unit cost of that violation which is independent of generation. The ζ_{i+1} values are increased as the optimization proceeds such that small values are used early on to accept trials with violation and large values are used later to assure trials with constraint violations are not accepted. This assures the infeasible decision variable space is transversed allowing the vicinity of the global optimum to be located. To avoid adding elaborate schemes to the

demonstration problem, ζ_{i+1} was defined to be 0.2 for the 0th generation, 0.4 for the 1st generation, 0.6 for the 2nd generation, 0.8 for the 3rd generation, and 1 for all generations 4 and beyond. The reader will note that penalty functions like this one were only developed for the inner ABTR optimization and that the method was satisfactorily demonstrated with this simplified formula for ζ_{i+1}.

The algorithm used to solve this optimization problem is as follows:

Determine the a priori optimized ABTR design specifications w.r.t. cost:
Survey the ABTR a priori cost objective function space:
- Select ABTR design specs
- Run ABTR model in REBUS
- Use ABTR core attributes to compute ABTR design responses and uncertainties
- Use the ABTR design responses a priori uncertainty to determine any violations
- Compute the objective function cost, augmented as necessary
- Reject only rouge trials
- Repeat for a number of trials and determine the standard deviation of those trials

Use the standard deviation of the trials to set the initial temperature.
Run the k-th generation of the simulated annealing algorithm:
- Select ABTR design specs
- Run ABTR model in REBUS
- Use ABTR core attributes to compute ABTR design responses and uncertainties
- Use the ABTR design responses a priori uncertainty to determine any violations
- Compute the objective function cost, augmented as necessary
- Determine acceptance
- Repeat for a number of trials and determine the standard deviation of those trials

Determine the k+1 temperature from the standard deviation of the k-th set of accepted trials
Repeat the SA until the desired convergence on an optimized solution is reached.

The ABTR reactor cost based on the a priori optimized ABTR design specifications is a constant in the following problem.

Determine the optimized ZPPR design specs
Survey the outer objective function (OOF) space:
- Select a set of ZPPR design specifications and evaluate their cost
- Run the ZPPR experiment and uncertainty analysis in REBUS
- Use the ZPPR observables with data assimilation to determine ABTR core attributes posteriori uncertainty
- *Survey the inner objective function space, the ABTR posteriori cost objective function space:*
  - *Select ABTR design specs*
  - *Run ABTR model in REBUS*

Use ABTR core attributes to compute ABTR design responses and uncertainties
Use the ABTR design responses posteriori uncertainty to determine any violations
Compute the objective function cost, augmented as necessary
Reject only rouge cases
Repeat for a number of trials and determine the standard deviation of those trials
Use the standard deviation of the trials to set the initial temperature.
Run the k-th generation of the simulated annealing algorithm:
Select ABTR design specs
Run ABTR model in REBUS
Use ABTR core attributes to compute ABTR design responses and uncertainties
Use the ABTR design responses posteriori uncertainty to determine any violations
Compute the objective function cost, augmented as necessary
Determine acceptance, with penalty if necessary
Repeat for a number of trials and determine the standard deviation of those trials
Determine the k+1 temperature from the standard deviation of the k-th set of accepted trials
Repeat the SA until the desired convergence on an optimized solution is reached.
Compute the value of the OOF, augmented as necessary
Reject only rouge cases
Repeat for a number of trials and determined the standard deviation of those trials
Use the standard deviation of the trials to set the initial temperature for the OOF.
Run the k-th generation of the simulated annealing algorithm for the OOF:
Select a set of ZPPR design specifications and evaluate their cost
Run the ZPPR experiment and uncertainty analysis in REBUS
Use the ZPPR observables with data assimilation to determine ABTR core attributes posteriori uncertainty
Survey the inner objective function space, the ABTR posteriori cost objective function space:
Select ABTR design specs
Run ABTR model in REBUS
Use ABTR core attributes to compute ABTR design responses and uncertainties
Use the ABTR design responses posteriori uncertainty to determine any violations
Compute the objective function cost, augmented as necessary
Reject only rouge cases
Repeat for a number of trials and determine the standard deviation of those trials
Use the standard deviation of the trials to set the initial temperature.
Run the k-th generation of the simulated annealing algorithm:
Select ABTR design specs
Run ABTR model in REBUS
Use ABTR core attributes to compute ABTR design responses and uncertainties
Use the ABTR design responses posteriori uncertainty to determine any violations
Compute the objective function cost, augmented as necessary
Determine acceptance
Repeat for a number of trials and determine the standard deviation of those trials
Determine the k+1 temperature from the standard deviation of the k-th set of accepted trials
Repeat the SA until the desired convergence on an optimized solution is reached.
Compute the value of the OOF, augmented as necessary
Determine acceptance
Repeat for a number of trials and determine the standard deviation of those trials
Determine the k+1 temperature from the standard deviation of the k-th set of accepted trials
Repeat the OOF SA until the desired convergence on an optimized solution is reached.

3.6. Optimization Experiment

The following is an attempt to derive a set of values to use in the optimization of the ZPPR experiment to reduce costs of the ABTR. These values are to be used for a representative experiment only and not as an exhaustive economic analysis.

3.6.1. ABTR Costs

The ABTR is expected to have a total assumed cost of $1,500,000,000. Since no official cost breakdown was published, a distribution among the capital, fuel and operations and maintenance costs is developed based on references where available and engineering judgment elsewhere. Unless otherwise stated the data used to support the assumptions is the nominal ABTR values from the ABTR Preconceptual Design Report [2]. Since most of the cost data available is several years old, the dollar values given will be updated to a 2009 dollar worth using the Consumer Price Index. The costs will be divided into three categories – capital, fuel, and operations and maintenance. These will be further subdivided into pertinent components for this work.

Capital Cost

This cost includes construction of the power plant and associated facilities. In addition to the physical buildings, this will include the reactor vessel, control system, internals/instrumentation, coolant, piping, steam supply system, generators, and any other costs not associated with the fuel or operations.

The capital is expected to be the largest component of the reactor cost. Reference [67] gives a LMR capital conservative cost of $2280/kWe in 1978 or $7500/kWe in 2009

dollars. Reference [68] states a fast reactor must be no more than \$400/kWe different from LWRs to be economic, but may be as high as \$900/kWe (\$1050 in 2009 dollars) different. Drawing upon a 2009 news report [69], the average cost of new LWRs in the U.S. is expected to be between \$2500 and \$4500 per kWe with a maximum estimate of \$8071/kWe. Using the most conservative estimate of \$8071/kWe plus \$1050/kWe and adding an additional conservatism of 10% due to the experimental, first of a kind nature of ABTR, the capital cost is estimated at \$10033/kWe or \$953,144,500 which is 63.5% of the total projected ABTR cost.

The ABTR Design Report provides little information about the cost distribution of the various components of capital cost. It does address the cost of one of the most expensive single non-nuclear components, the heat exchanger which was found to be optimized at very approximately \$6,000,000. Since a detailed study of the breakdown of these costs is beyond the scope of this work, we will examine in detail only the two components of capital cost which we intend to be perturbed in the optimization routine proof. These are coolant requirements (analogous to changing the volume of fuel) and control element requirements.

The coolant is metallic sodium. Reference [70] gives the prices of reactor grade sodium at \$3,520/m^3 (\$3,400 in 2007). The primary side requires 320 m^3 of sodium and the secondary side requires 9.70 m^3. This gives a total cost of \$1,160,544 for the coolant alone. Unlike LWRs with numerous control rods that insert into or between assemblies, the ABTR is controlled by 10 full size assemblies of control elements. These assemblies are the same dimension as fuel assemblies and composed of 217 control rods. A 21-finger control rod is currently priced at about \$50,000 [71] so the ABTR control assemblies' rods would cost

about $516,667/control assembly. Allowing for different machining costs and fabrication, a price of $525,000/control assembly is assumed. Assuming a fixed number of control assemblies for simplicity the amount of control material is perturbed which will be equivalent in concept to replacing expensive control rods with inexpensive inert steel rods.

Fuel Cost

This cost includes material, reprocessing, fabrication, transportation, security, and storage costs of the fuel. The largest component of fuel cost is expected to be the reprocessing, especially since an industrial reprocessing plant does not exist in the U.S. Reference [68] gives an estimated reprocessing cost of $2,000 (in 2003) per kgHM for the fast reactor fuel cycle to be competitive. However, the most conservative value in that report is $6,700/kgHM, which is based on the riskiest scenario where the reprocessing facility is financed by non-guaranteed private sector loans. This cost's present worth is $7,810/kgHM for reprocessing cost which is closer to the estimate in Reference [67], $7,500/kgHM (or $2,280 in 1978 dollars).

For the fabrication and storage the present worth values in References [67] and [68] are very close, with Reference [68] being slightly more conservative. Reference [67] gave a transportation cost of $178/kgHM ($54/kgHM in 1978). Conservatism for security personnel/equipment is added at the rate of 25% of the transportation and storage cost.

Using the nominal mass flow rates, the first cycle fuel cost is $44,903,280. The total lifetime cost, without adjusting for inflation/deflation over the reactor lifetime, would be $357,791,235 or 23.8% of the ABTR total cost. The inner, middle and outer core fractions are given and 6 inner, 6 outer, and 1.5 middle core assemblies are replaced annually. The

cost breakdown of the fuel and the mass distribution of ABTR's core can be seen in the following tables.

Table 3.3 : Reprocessed Fuel Cost Breakdown.

COMPONENT	REFERENCE COST	REFERENCE YEAR	PRESENT COST
Reprocessing	$6,700/kgHM	2003	$7,810/kgHM
Fabrication	$2,300/kgHM	2003	$2,680/kgHM
Transportation	$54/kgHM	1978	$178/kgHM
Storage	$300/kgHM	2003	$350/kgHM
Security	---	---	$132/kgHM
TOTAL*	---	---	**$11,150/kgHM**

Table 3.4 : ABTR Fuel by Mass Distribution.

CORE LOCATION	TOTAL MASS IN CORE (CYCLE 1)	ANNUAL FLOW	LIFETIME REQUIREMENTS	PERCENT OF TOTAL CORE
Total Core	4027.2 kg	945.9 kg	32088.9 kg	100%
Inner Core	1610.8 kg	420.7 kg	14211.3 kg	44.3%
Middle Core	402.7 kg	100.7 kg	3088.1 kg	9.6%
Outer Core	2013.7 kg	425.6 kg	14789.5 kg	46.1%

Therefore the correlated cost of the inner, middle and outer core compositions are $1,585,015/(% change in HM loading), $343,480/(% change in HM loading), and $1,649,417/(% change in HM loading) respectively.

Operations and Maintenance Cost

This is the cost associated with an operating ABTR and maintaining the facility through the reactor lifetime. In the absence of a detailed study of fast reactor O&M costs it is assumed to be the difference between the total assumed cost and the capital plus fuel costs noted above, which is $189,064,265 or 12.6% of the ABTR cost without adjusting for inflation/deflation over the reactor lifetime. This will be a fixed ABTR cost which cannot be modified within the scope of this work.

3.6.2. ABTR Penalties

The values described in this section are the per unit cost factors, λ_n. For this demonstration three types of penalties are assumed. The penalties associated with ABTR will be monetary costs for not making cycle length, not making average burnup, and coming within 2% of safety factor limits. Exceeding maximum burnup or the safety factor limits will be counted as a rouge case that cannot be accepted. It is recognized these are very generalized limits and are meant only as a demonstration of the procedure for solving the optimization problem.

A value of \$9,500/pcm will be assumed for not making cycle length. This is based on an estimate that a 1000 MWe LWR plant will sell \$1,000,000 of electricity in one EFPD, or about \$1000 per MWe assuming full power operation. ABTR should provide \$95,0000 per day income with a nominal 120 day cycle over which there is a nominal reactivity change of 1.2% Δk per cycle or 10 pcm per day.

A value of \$431,891/MWD/kgHM will be assumed for not making average burnup. This is based on a nominal average discharge burnup of 97.7 MWD/kgHM over 12 cycles (~8.14 MWD/kgHM per cycle) and a nominal flow of 315.3 kg/cycle which costs \$3,515,595. Then by division the per cycle fuel to burnup worth is \$431,891/MWD/kgHM which will be the penalty for not meeting the average burnup. This is the highest value penalty because it equates to wasting fuel.

A value of \$50,000/violation value is assumed for being less than 1% to the bounds for the three Wade-Fujita safety parameters. This is analogous to a fine a regulator would impose on a utility for operating too close to a limit. The utility, in practice, would alter

operation to return to safer conditions rather than be continuously fined. Furthermore, a violation of the limit is a hard constraint and such a design is rejected. Thus this value need not be increased as violation size increases.

3.6.3. ZPPR Costs

The ZPPR fixed costs are first established. A value of $60,000,000 for program restart [15] has been discussed but this is prohibitively high for a single value fixed cost. Further it is unrealistic that an entire facility would be set up for one experiment. Therefore it is assumed that the experiment in question is one of many the facility does and a fixed cost usage for $300,000 for a single experiment is assumed. This choice is somewhat arbitrary for demonstrations purposes as the ZPPR fixed cost serves to bias the value of the objective function.

A value of $3,500 fixed cost per experiment for having three ZPPR technicians running the reactor for one week (assumed cost $29/hr). A value of $2,700 fixed cost per experiment for having one professional scientist conducting his experiment for 1.5 weeks (assumed cost $45/hr) is assumed. A value of $1,184/TRU drawer, which contains only a small amount of Am and Cm, is based on 106.2 grams of reprocessed TRU per drawer. A value of $51,780/SNF drawer based on 4.644 kg of reprocessed SNF per drawer is assumed. The SNF drawers are a full fuel drawer composed of reprocessed spent nuclear fuel. These compositions are discussed in Chapter 4. A value of $2,700/detector based on a professional scientist's salary of $45/hour and 60 hr/detector (i.e. one and a half days to process the results) is assumed. This is based on a typical time between a ZPPR experiment and the

corresponding technical report containing the results, which was about 6 weeks. A typical study might report results for up to 10 counted irradiations, sometimes less, sometimes more. One cannot simply divide 240 hours of work by 10 counting sets since most samples were counted immediately after irradiation and then the results took some time to process. It is assumed that in 6 weeks, one week of the time will be spent counting (assuming a reasonable number of different types of reactions are observed) and then a processing time of 5 weeks / 10 detector, or 0.5 weeks work time per set of detector results. This gives a total of 60 hours work time per set of detectors. Note since counting facilities are common infrastructure in any nuclear laboratory no cost is assumed for usage of these machines. In practice, a "detector" refers to the results of counting an irradiated foil of a given isotope or element, from which a particular reaction rate of that isotope or element in the core can be determined. Computationally this is a numerical calculation of a particular reaction rate for a given isotope or element at a specified node in the core. The $2,700 cost is meant to include counting of all reaction rates that are computed for a single detector node in the model.

3.6.4. Optimization Demonstration Parameters

The following are the definitions of what ZPPR design specifications, ZPPR observables, ZPPR experiment costs, ABTR design specifications, ABTR core attributes, ABTR design responses, and ABTR design limits which will be used in the example problem. The reader will note that for the ABTR decision variables (design specifications) since these are in terms of relative changes there is a continuous distribution of possible values. Simulated annealing works for discrete values. So that simulated annealing can still

be used in this case, the possible ATBR design specification relative perturbations are kept to five significant figures so that they are effectively discretized. Even with this discretization it is recognized that the sampling space is still large, requiring up to $4x10^4$ samples which is beyond the computational capabilities of this work. The average ATBR optimization examined 400 samples, or about 1% of this space. This limitation is recognized but accepted as this is a demonstration problem only.

ZPPR

1. ZPPR Design Specifications: items that define the experimental setup and are the decision variables
    - Number of SNF drawers
    - Number of TRU drawers
    - Location of SNF drawers
    - Location of TRU drawers
    - Number of detectors
    - Location of detectors
2. ZPPR Observables: the instrument readings that are used for adaption
    - k-effective
    - Reaction rates for Na, Fe, Pu, U, Np, Am, and Cm. Na and Fe are elemental compositions and individual pure isotopic samples for Pu, U, Np, Am, and Cm. Isotopic samples of Pu, U and Np-237 are common. Section 1.3.3 discusses some of the history of Am and Cm pure isotopic samples.

3. ZPPR Experiment Cost: function of the ZPPR Design Specs and associated with multiple experiments
    - $306,200 fixed cost
    - $1,184 per TRU drawer
    - $51,780 per SNF drawer
    - $2,700 per detector

ABTR

1. ABTR Design Specifications: items that define the design of the reactor
    - Cycle length
    - Inner core TRU enrichment
    - Outer core TRU enrichment
    - Middle core TRU enrichment
    - Control elements – analogous to boron concentration since homogenized assemblies
    - Fuel outer diameter – analogous to sodium content since homogenized assemblies
2. ABTR Core Attributes: Items that the design responses are dependent upon and for which uncertainties can be determined from the uncertainties in the parameters
    - EOC k-effective
    - Fluence or Burnup
    - Void worth
    - Doppler coefficient

- Axial expansion coefficient
- Radial expansion coefficient

3. ABTR Design Responses: responses that have limits whose uncertainty distributions can be determined from the ABTR Core Attributes uncertainty distributions and the ABTR Design Specs
    - Three Wade-Fujita safety parameters, based on reactivity coefficients
    - Burnup
    - Cycle length
4. ABTR Design Limits: values that the ABTR Design Responses should not exceed for a stated probability
    - Three wade-Fujita safety parameters, based on reactivity coefficients
        - WF1 –must be less than or equal to 1
        - WF2 –must be contained in [1,2]
        - WF3 –must be less than or equal to 1
        - Penalty for inadequate margin to the limits
    - Burnup - penalty on a burnup too low and a hard upper limit
    - Cycle length - penalty on not making 120 day nominal length
5. ABTR Design Specification Costs: dollar value assigned to the relative change in each of the design specifications mentioned in item 1.
    - $95,000/(full power day of operation)
    - $1,585,015/(% change in HM loading) for inner core composition.
    - $343,479.6/(% change in HM loading) for middle core composition

- $1,649,417/(% change in HM loading) for outer core composition
- $52,500/(% change in boron) per an estimated cost of $525,000 for each of the 10 ABTR control elements already mentioned
- $123/(% change in sodium content), based on the $3,520/$m^3$ sodium cost mentioned earlier and a 10.896 m^3 active core of which 32.1% by volume is coolant [2].

6. ABTR Limit Violation Costs:
    - $50,000 for having less than 2% margin to the limit for any of the three Wade-Fujita safety parameters
    - $431,891/MWD/kgHM for not meeting target burnup
    - $9,500/pcm for missing target cycle length of 120 days

Even with this simplified problem, further assumptions needed to be made in considerations of the time commitment needed to run each iteration of optimization routine. The uncertainty propagation and data assimilation for each ZPPR variation took several hours of computational time and the ABTR optimization with posteriori information took several more hours. The additional ZPPR simplifications include maintaining quarter core symmetry, allowing only inner core fuel drawers to be replaced with SNF or TRU drawers, limiting TRU drawers to 50 per quarter core, limiting SNF drawers to 15 per quarter core, limiting detector locations to one quarter of the core, and limiting detector number to between 4 and 10. The placement of the SNF and TRU drawers was also not allowed to be truly randomized but restricted to rings, clusters, and checkerboard patterns as seen in

Appendix C. These restrictions reduced the problem to a manageable amount of computational time to prove the methodology developed in this work.

3.7. Software Used in Analysis

A survey of the ZPR Technical Memos shows that the bulk of the original computational analyses were done with the same few codes. Most of these are predecessors to the codes referenced and discussed in the following sections. Cross sections were typically processed using the Argonne National Lab code MC^2 (also written MC**2) and ultimately reduced from the ENDF-B data to 28 to 30 energy groups. The criticality and reaction rate calculations were done in usually 2-D rz and xy geometries in DIFF2D with one model essentially compensating for the other's lack of detail in one direction or the other. Numerous transport codes as well experimental data and professional experience were used to make necessary corrections to the values produced from DIFF2D. As computational power evolved, the models moved almost exclusively to xyz 3-D models in DIF3D. Finally, when Monte Carlo techniques began to improve and expand, Argonne developed its own Monte Carlo transport code called VIM and this code was also used to model the ZPPR experiments.

3.7.1. REBUS and DIF3D

The primary model used in this study is the REBUS 3 Variant 8.0 code system from Argonne National Laboratory [37]. REBUS is a fast reactor fuel cycle analysis code that is built around the deterministic 3-D nodal diffusion code DIF3D and the deterministic 3-D transport code VARIANT. Diffusion was chosen over transport due to computational

resources available, the complex nature of the ZPPR 15B reactor, the good agreement between experimental results and the diffusion results, and the intrinsic memory limitations in REBUS. REBUS has the ability to simulate reactor operations at any power over any cycle length, perform recycle, and many other closed fuel cycle aspects. The ABTR model utilized some of the aspects by simulating one cycle of operation at full power. The ZPPR 15B model however was set to operate at zero power and a zero day cycle length, as per the actual operation of the experiment.

The model is given an input geometry, region compositions in the form of isotopic number densities, reactor operating parameters, cycle length, and the cross section library file ISOTXS. REBUS processes the neutronics parameters followed by fuel cycle parameters. Finally the DIF3D nodal diffusion calculation is initiated. Since all of the working models analyzed in this study were non-equilibrium, single cycle models, DIF3D is only executed once and the final output saved. Equilibrium problems process the information at the end of the cycle, create a new fuel loading as per the fuel cycle specifications and run DIF3D, repeating this processes as many times as specified. The equilibrium core model was only run once to give the equilibrium fuel compositions and discharge mass flows. The ABTR core used a triangular meshing of the hexagonal fuel assemblies, 6 triangles per assembly, with 20 axial nodes, symmetric about the midplane, with 8 nodes evenly spaced in the active fuel. The ZPPR core used rectangular meshing with each drawer as a xy-planar node and 24 axial nodes, symmetric about the midplane, with 12 nodes evenly spaced in the active fuel.

3.7.2. MC^2-2

Cross section data for the REBUS system was prepared by the Argonne National Lab code MC^2 – 2 [38]. MC^2 uses the basic nuclear data available in the ENDF-B Version V to solve the neutron slowing down equation in 0-, 1- and 2-D geometries, generate fundamental mode spectra and use those spectra to collapse the many-group ENDF-B data down to few-group cross sections, in this case the 15-energy group structure shown in Table 2.1. The 15-group structure was chosen primarily due to the fact that cross section covariance data is available for many of the common fuel and structural materials in this particular group structure [39]. Explicitly, "MC^2 solves the extended transport P^1, B^1, consistent P^1, and consistent B^1 fundamental mode ultra-fine-group equations continuous slowing down theory and multigroup methods. Fast and accurate resonance integral methods are used in the narrow resonance resolved and unresolved resonance treatment. A fundamental mode homogenous unit cell calculation is performed using either multigroup or a continuous slowing-down treatment." [38]

For this study, MC^2 was provided as inputs the 15-group energy structure, the homogenized composition of a given region, operating temperature, isotope labels, and required input parameters on the BCD input card. For the ABTR and the ZPPR 15B models, regional fuel compositions were modeled separately in 0-D geometry with only the homogenized isotopic compositions provided. Each region was individually labeled and combined into a final cross section file which would be provided to REBUS. The code was instructed to search for a critical buckling in 0-D geometry. MC^2 then computed the flux spectrum which satisfied these criteria. Next the ultra fine group structure was collapsed to

the 15-group structure with corrections to the flux spectrum for the proper resonance treatment and spatial weighting, with iterations made as necessary to capture these effects.

It is noted that for this study the MC^2 option to discard the thermal broad group cross-section data was chosen. This is due to the fact that when the option to replace thermal groups by last epithermal value was selected the power peaking factor and k-effective values became unreasonably high. It was also decided to use finite difference in the ABTR model as opposed to the nodal method, to further improve the power peaking factor and k-effective agreement with reported values.

3.7.3. MCNP 5.0

The Monte Carlo n-particle transport code MCNP 5.0 available from Los Alamos National Lab was also used in this study. MCNP is a Monte Carlo type code that solves various transport problems concerning electrons, neutrons, and/or photons [40]. While all of its capabilities are too diverse and numerous to discuss for this paper, it is sufficient to note that MCNP was used in neutron transport mode with continuous energy cross sections from the ENDF-B Version VI libraries. The purpose of employing this model was only to verify the results obtained in REBUS for the ZPPR 15B model.

3.7.4. In-House Generated Software

Several in-house codes were generated for this work and can be divided into five distinct groups. The first group consists of a series of programs that takes a nominal cross section library and a set of provided cross section covariance information, reads in that data,

generates a set of perturbation vector according to the ESM method described earlier, and uses them to create perturbed cross section libraries which are subsequently supplied to REBUS. The second group is a set of scripts and codes to generate scripts which will execute sequential or parallel sampling on UNIX or LINUX based computing systems at North Carolina State University. These submit and process the output of REBUS runs using the perturbed cross section libraries generated with the first set of codes. The third group post processes the outputted REBUS results to obtain a priori uncertainties on different models, perform adaptive simulation, and sort the final results into presentable data. The fourth group is a collection of various auxiliary codes developed during the course of this study which perform such tasks as writing the ZPPR geometry in REBUS input format, calculating power maps from REBUS output data, expanding geometry and adjusting number densities for expansion coefficient models, and reading ENDF formatted fission yield files. The fifth group of codes implements the simulated annealing process necessary for this work, and acts as a wrapper to encompass the uncertainty propagation and the data assimilation sequences and apply them toward the solution of the optimization problem.

4. REACTOR MODELING AND VARIATIONS

4.1. ABTR Models

4.1.1. Start-Up Core

The initial model of the Advanced Burner Test Reactor, ABTR, was provided to North Carolina State University in 2006 by Argonne National Laboratory and was the start-up core as specified in the pre-conceptual design report [1]. The model specified weapons grade plutonium fuel for the inner and outer cores and contained a middle core region of spent nuclear fuel assemblies. The model was provided in REBUS input format, triangular geometry, single cycle, and third core symmetry. Figure 4.1 shows the ABTR with the third of the core that is modeled shown in the triangular grid. Inner, middle, and outer fuel regions are shown in pink, purple, and red, respectively. Dark blue and teal represent primary and secondary control assemblies, respectively. Gray and light blue are the reflector and shield, respectively. Detector nodes were placed at one inner core, one outer core, and two middle core assembly locations, repeated on five symmetric axial planes: one in the active fuel mid-plane, two in the active fuel halfway between the mid-plane and the reflector, and two at the active fuel reflector interface.

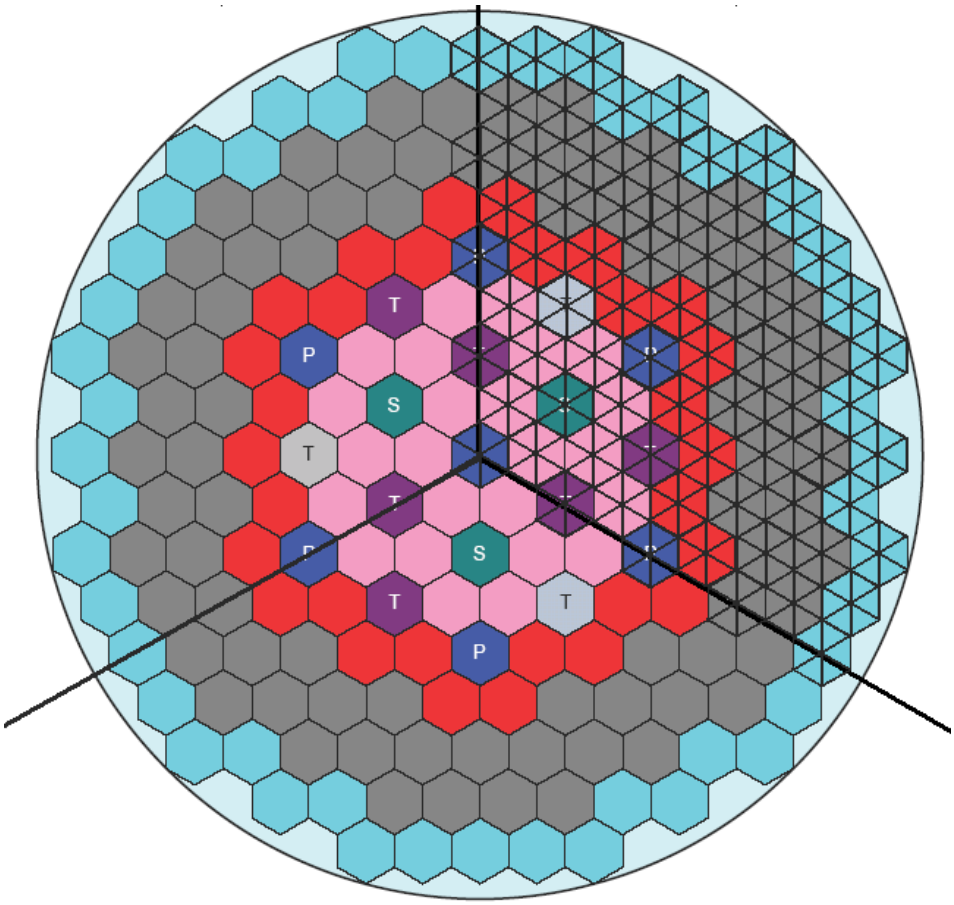

Figure 4.1 : ABTR core showing triangular discretization.

4.1.2. Equilibrium Core

The first modification made was to create a second model which reflected the compositions of an equilibrium recycle core, i.e. one that is made entirely of recycled SNF coming from both the ABTR itself and from LWR SNF. REBUS has the ability to search for and determine an equilibrium fuel composition and the associated mass flow rates by going through several cycles with a given energy output requirement and specified available fuel sources. The model received from Argonne was modified and this feature was used to determine discharge mass flow rates and an equilibrium fuel composition. This composition

was then provided to a single cycle model, like the initial model only now reflecting the fuel composition loaded for an equilibrium cycle. Geometry, energy requirements, and detector locations were not modified.

4.1.3. Sodium Voided Core

To obtain the sodium void worth for the start-up and equilibrium cores, coolant sodium was voided from the active fuel regions and above in each model. The sodium content acting as a bonding agent inside the fuel pins themselves was not voided, but it was assumed that it was pushed up into the gas plenum of the fuel rod by the thermal expansion of the fuel. Geometry, power requirements, and detector locations were not modified. The total void worth is given by the formula

$$\alpha_{Void} = \frac{\Delta k}{\beta} \tag{4.1}$$

where Δk is the change in the k-effective value, and β the effective delayed neutron fraction. Uncertainty on β is not treated in this work and the nominal value of 0.0033 is used. Conservatively assuming that the voiding which occurs is that which creates the total void worth in Equation 4.1, the sodium density coefficient can be calculated by

$$\alpha_{Na} = \frac{\Delta k}{\beta}\left[\frac{1}{\rho}\frac{d\rho}{dT}\right] \tag{4.2}$$

where the volumetric coefficient of expansion, $\left[\frac{1}{\rho}\frac{d\rho}{dT}\right]$, is 0.28 x 10^{-3}/K, where ρ is density, such that α_{Na} is in the expected units of \$/K.

4.1.4. Cross Section Adjustment for Doppler Coefficient

To obtain the Doppler reactivity coefficient for the start-up and equilibrium cores, the models themselves were not adjusted, but the cross sections provided were. The code MC**2 requires the user to enter the average temperature of each nuclide in each composition provided to the code. For the ABTR the fuel operates at an average temperature of 854 K with coolant being approximately 705 K. To obtain the Doppler coefficient input temperatures were adjusted by +250 K and -250 K and the average of the two calculated reactivity coefficients taken. Geometry, power requirements, and simulated detector locations were not modified. Each Doppler reactivity coefficient is given by

$$a_{Dopp} = \frac{\Delta k}{\Delta T}\frac{1}{\beta} \tag{4.3}$$

4.1.5. Axial and Radial Expansion Coefficient Models

To obtain the axial and radial expansion coefficients for the start-up and equilibrium cores, the geometry was expanded and the compositions' atom densities reduced to reflect geometry changes as a result of a +100 K temperature increase. The linear expansion coefficients for the fuel and clad are $\alpha_f = 17.6e-6 \ m/(m\cdot K)$ and $\alpha_c = 19.5e-6 \ m/(m\cdot K)$, respectively.

For the axial expansion, the original height of the core is $H_o = 3.4568\ m$. Using $\Delta T = 100\ K$, the expanded structure height is $H_c = 3.4635\ m$ and the expanded fuel height is $H_f = 3.4629\ m$. Assuming a constant effective cross-sectional area for the core, the new

volume will simply be the initial volume times the ratio of the new height to the initial height:

$$V = (Area)H$$
$$V_c = V_o \frac{H_c}{H_o} = V_o(1.00195) \tag{4.4}$$
$$V_f = V_o \frac{H_f}{H_o} = V_o(1.00176)$$

The actinide and zirconium atom densities are divided by 1.00176, all other number densities are divided by 1.00195, and the z-coordinates are multiplied by 1.00195. The final formula for the axial expansion reactivity coefficient, assuming linearity of the reactivity over a small range, is:

$$\alpha_{axial} = \frac{\Delta k}{\Delta H}\frac{1}{\beta} H \alpha_c \tag{4.5}$$

For the radial expansion, the effective radius, R_o, of a single assembly is 14.6850 *cm*. Using $\Delta T = 100\ K$, the expanded structure radius is $R_c = 14.7136\ cm$ such that $R_c / R_o = 1.00195$. The total cross sectional area of a hexagonal fuel assembly is given by:

$$A = 6R^2 \tan\left(\frac{180^o}{6}\right) \tag{4.6}$$

Therefore the new expanded area is given by

$$A = A_o R^2 / R_o^2 \tag{4.7}$$

Assuming a constant height for the core, the new volume will simply be the initial volume times the ratio of the new area to the initial area:

$$V = (Area)H$$
$$V_c = V_o \frac{R_c^{\,2}}{R_o^{\,2}} = V_o(1.00390) \tag{4.8}$$
$$V_f = V_o \frac{R_f^{\,2}}{R_o^{\,2}} = V_o(1.00345)$$

where the fuel radii were based on the radii of a single slug, i.e. $R_o = 0.00348\ m$ and $R_f = 0.003486\ m$. The actinide and zirconium atom densities are divided by 1.00345, all other number densities are divided by 1.00390, and the assembly pitch is increased to 14.7136 *cm*. The final formula for the radial reactivity expansion coefficient, assuming linearity of the reactivity over a small range, is:

$$\alpha_{radial} = \frac{\Delta k}{\Delta R}\frac{1}{\beta} R\alpha_c \tag{4.9}$$

Energy requirements and detector locations were not modified. Note that these two coefficients are not measurable in the ZPPR reactor because the temperature differences allowed there are too small to see this effect on a reactor wide scale. Individual small samples may have been heated to expansion in ZPPR, but the whole reactor core itself was not capable of this type of experiment.

4.2. ZPPR Models

4.2.1. Base Models

The Zero Power Physics Reactor Assembly 15-B was modeled as is [28] in both MCNP and REBUS. The MCNP model, along with the original experimental results, were used for verification and validation for the deterministic REBUS model (see Appendix A). All other models were developed solely in REBUS. Given good agreement with the

experiment in the REBUS model, infinitely thin "foils" of minor actinides were added to the model to provide preliminary data on minor actinide reaction rates and so that the codes tracked the appropriate number of nuclides. These infinitely thin foils had no affect on the reactor operation, i.e. integral parameters remained the same within numerical precision of the codes. Detector nodes were placed at two inner core and two outer core locations, repeated on five symmetric axial planes: one in the active fuel mid-plane, two in the active fuel halfway between the mid-plane and the reflector, and two at the active fuel blanket interface. The model assumes 100 W power and a cycle length of 1 hour, which is an assumed experimental time. Each drawer was homogenized and modeled as a single node, axially discretized by region and quarter core symmetry maintained throughout this work. While searching for an optimal experiment, numerous iterations of this model were created and are briefly discussed in the following subsections. Figure 4.2 shows the ZPPR-15B model, as built. Orange, blue and red denote reflector, blanket and narrow control assembly, respectively. The pink is the inner core fuel and the yellow-green checkered area is the outer core, a mixture of lower and higher enrichment fuel drawers with a higher effective enrichment than the inner core.

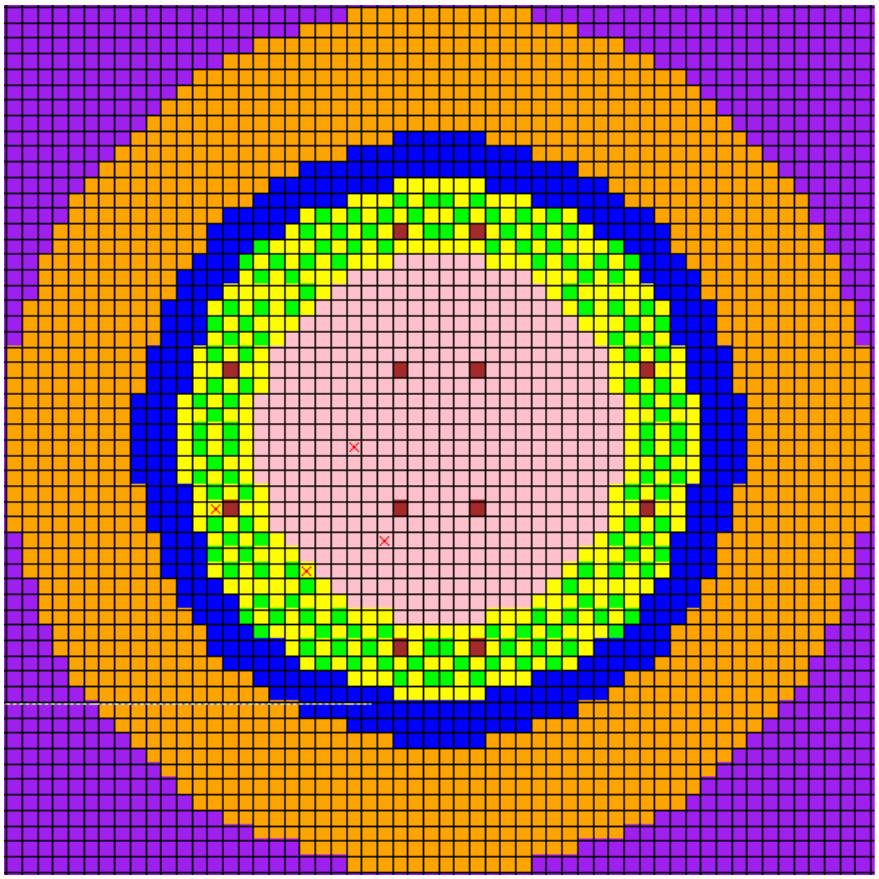

Figure 4.2 : ZPPR-15B as built.

4.2.2. Sodium Voided Inner Core

In accordance with ZPPR experimental procedures, sodium void worth was determined for each model variation by removing the sodium content of the inner core assemblies only. The worth was determined as indicated previously with geometry, power specifications, and simulated detector locations unchanged.

4.2.3. Cross Section Adjustment for Doppler Coefficient

The ZPPR could not perform very large temperature swings because it was an air cooled reactor. Core wide Doppler experiments in the ZPPR involved simply turning off the cooling fans and letting the reactor heat up slightly. To determine Doppler reactivity coefficient for the ZPPR, cross sections were allowed to change temperature from 300 K to 320 K. The coefficient was determined as indicated previously with geometry, power specifications, and detector locations unchanged.

4.2.4. Preliminary ZPPR Variations

The preliminary ZPPR variations, hereinafter referred to as the 0^{th} generation, were "hand optimizations" of the experiment. These variations were based on engineering judgment and modeling experience and were intended to provide data representative of ABTR by placing in the ZPPR-15B reactor configuration sample fuel drawers of materials analogous in composition to what is in the ABTR core. Note that a subset of these preliminary trails was used as the scoping or survey generation to set the initial "temperature" for the simulated annealing optimization of the experimental setup.

The first trial in optimizing the ZPPR for applicability to ABTR was to add sample drawers of transuranics, TRU, to the inner core of the reactor so as to expose them to a neutron flux spectrum similar to what would be experienced in ABTR. Two models were created, one with 16 drawers of transuranics (Figure 4.3) and one with 32 drawers (Figure 4.4). Different analyses placed the detectors in two distinct sets of location: 1) one inner core, one outer core, two in sample drawers, and 2) all four detectors in central sample

drawers. Axial detector locations were unchanged. Table 4.1 gives the nomenclature for these models that will be used throughout the rest of this paper. The sample drawers were created by replacing, by volume, the plutonium content of the fuel with minor actinides alloyed with zirconium, emulating the work of Hilton [3], the composition of which is listed in Table 4.2. If implemented in practice, this would mean replacing only the plutonium plates in a drawer with plates having the composition specified in Table 4.2.

Table 4.1 : ZPPR-15B TRU model variation nomenclature.

Model Variation	Number of TRU Trays	Detector Location
TRU v.1	16	1 outer core, 1 inner core, 2 in test assemblies
TRU v. 1-B	32	1 outer core, 1 inner core, 2 in test assemblies
TRU v. 1-C	32	1 outer core, 2 inner core, 1 in test assemblies
TRU v. 2	16	4 in test assemblies
TRU v. 2-B	32	4 in test assemblies

Table 4.2 : TRU plate composition by weight percent.

Isotope	Weight Percent
Am-241	33.041
Am-242m	0.065
Am-243	5.724
Cm-244	1.106
Cm-245	0.065
Zr	60.000

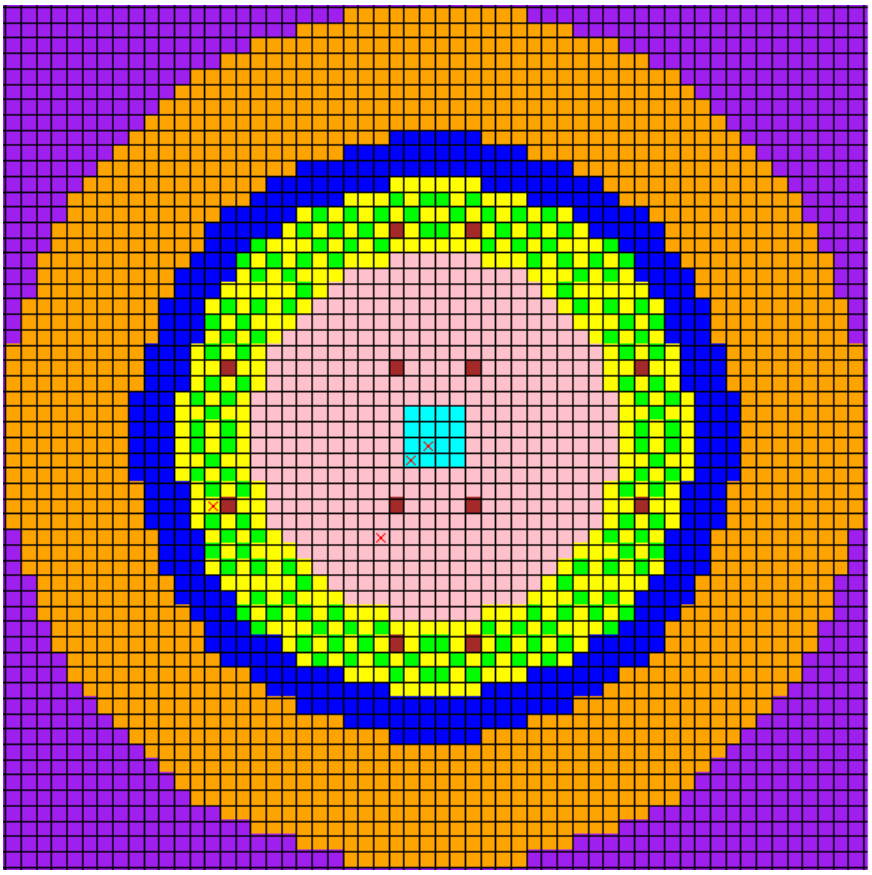

Figure 4.3 : ZPPR-15B with 16 TRU drawers in the center.

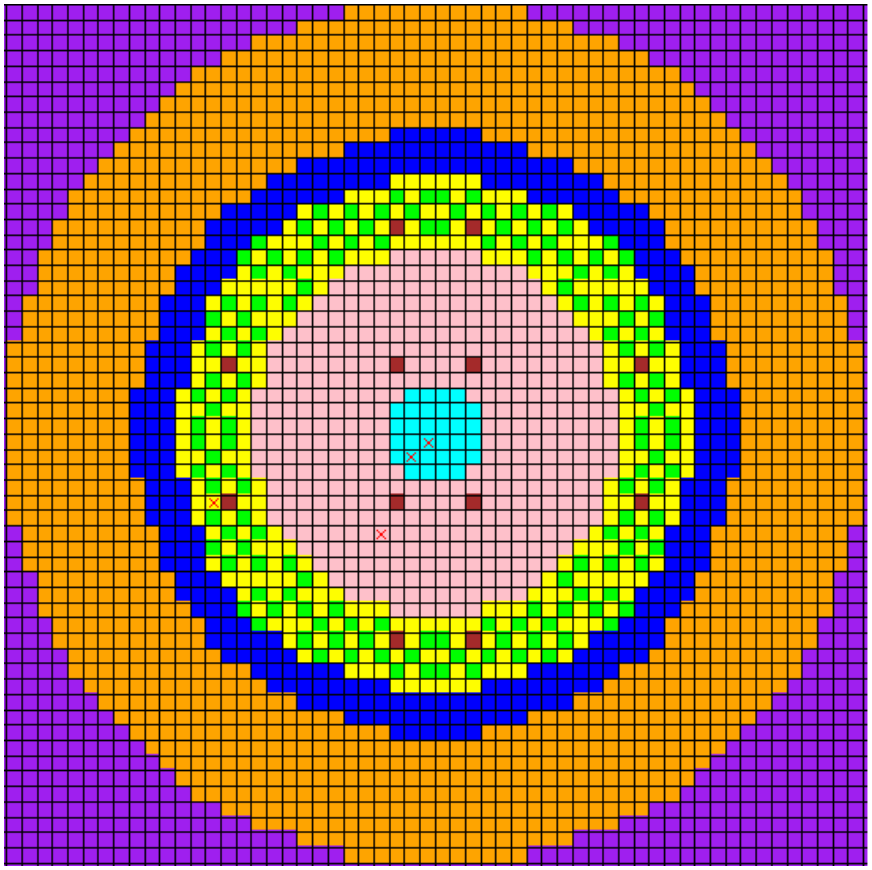

Figure 4.4 : ZPPR-15B with 32 TRU drawers in the center.

The next variation involved moving the 32 sample drawers to be symmetrically placed around the inner core and inner/outer core interface, similarly to the locations of the SNF test assemblies in ABTR (Figure 4.5). Detector positions were one inner core, one outer core, one inner sample drawer, and one interface sample drawer. This variation is hereinafter referred to as TRU v. 3.

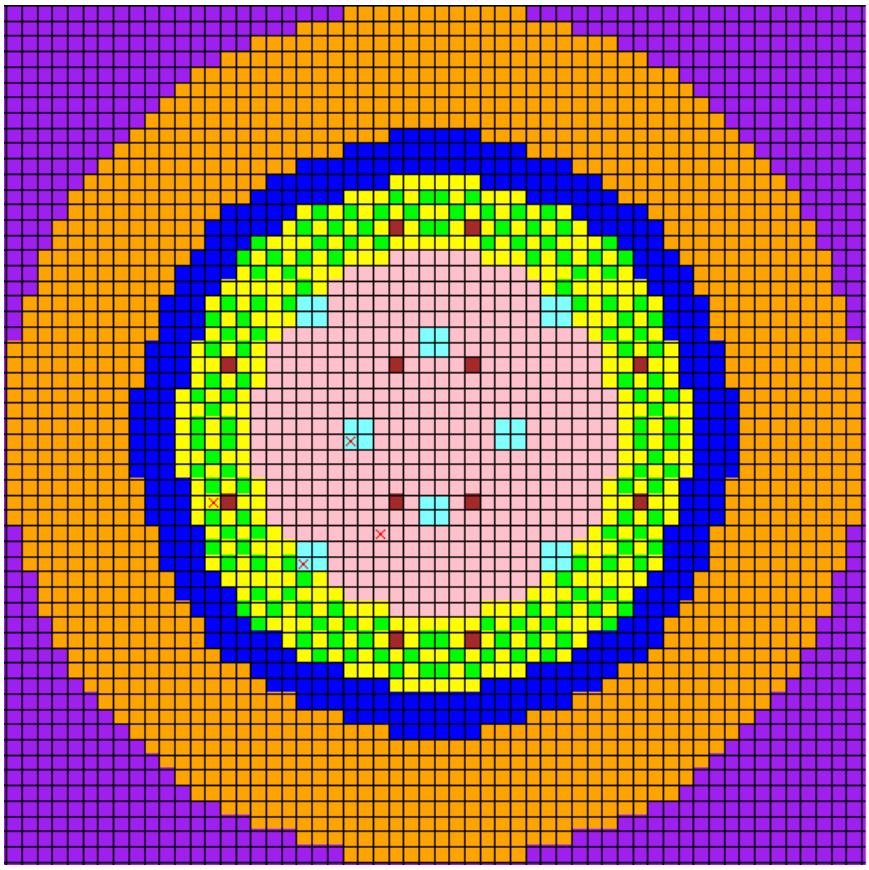

Figure 4.5 : ZPPR-15B with distributed TRU drawers.

The next variation attempted to emulate the ABTR start-up core. Eight 3 x 3 blocks of drawers were filled with the homogenized composition of the SNF test assemblies loaded into the ABTR start-up core (Figure 4.6), shown in dark purple. This mock-up preserves the approximate loading of SNF assemblies that would be in ABTR. The relative loadings of plutonium and minor actinides are taken from 3.3 w/o enriched UOX fuel that was burned for 33 GWD/MT in an LWR. Detector positions were one inner core, one outer core, one inner SNF drawer, and one interface SNF drawer. This variation is hereinafter referred to as ZPPR-SNF.

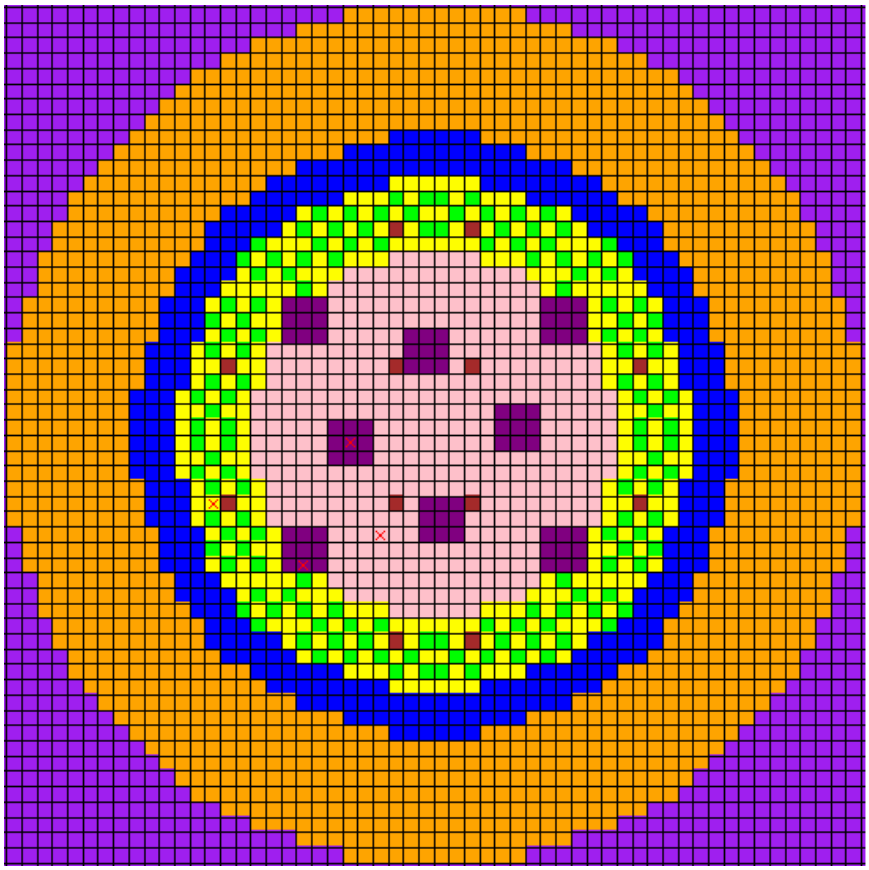

Figure 4.6 : ZPPR-15B with mock SNF assemblies.

The last preliminary ZPPR-15B variation considered is a mock-up of the ABTR with the equilibrium fuel compositions taken directly from the ABTR equilibrium model (Figure 4.7). This is a theoretical exercise only as the actual fuel compositions do not exist as of now and would be far too great of a radiological hazard to physically construct in the ZPPR facility. The blanket was removed and replaced with reflector. Control materials were placed symmetrically in enough quantity so as to maintain the relative loading of ABTR. The outer core was homogenized into one fuel composition. Detector positions were one inner core, one outer core, and two middle core drawers. This variation is hereinafter known as ZPPR-ABTR.

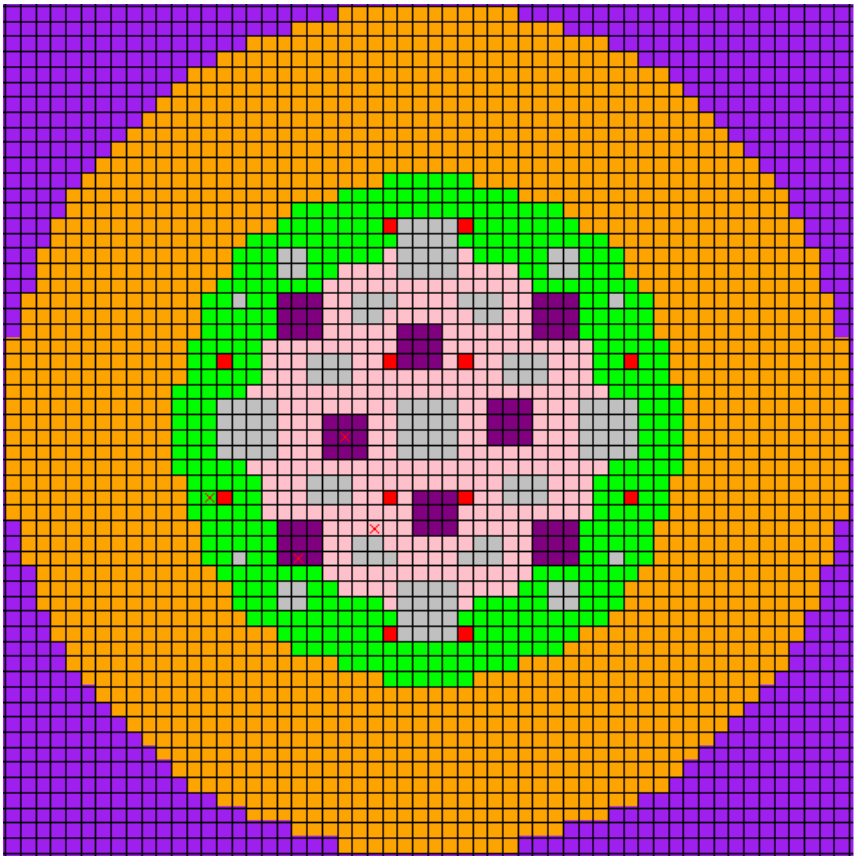

Figure 4.7 : ZPPR-15B ABTR mock-up.

4.2.5. Optimization Variations

For the subsequent generations of the optimization demonstration problem 30 additional ZPPR variations were examined as computational time allowed. These variations used differing combinations of SNF and TRU drawers and varying detector locations and numbers. These variations were subject to the constraints already discussed in Section 3.5.4. All of the variations are displayed in Appendix C using quarter core format and having the same coloring scheme as in previous sections. So as not to add to the main body of this work, only the final optimized ZPPR variation is displayed in this section (Figure 4.8). The

ZPPR optimization variations are referred to as a numerical identifier of ZPPR_(generation)_(variant). Of the thirty-five histories (including the survey generation) and six generations spanned by the overall optimization, variant ZPPR_5_3 emerged as the optimal choice. Section 5.5 discusses this experiment, the results of the search for it, and the resulting optimized ABTR design associated with the posteriori data obtained for this experiment.

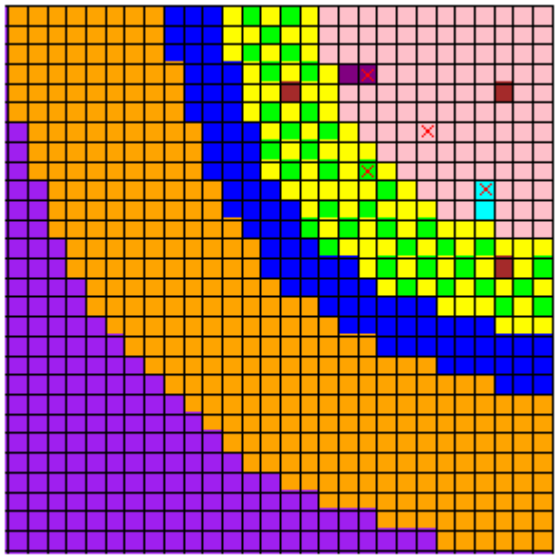

Figure 4.8 : Optimized ZPPR Experiment, ZPPR_5_3.

5. RESULTS AND INTERPRETATIONS

5.1. ZPPR Models' Uncertainties

Uncertainties in the cross sections for the reactions listed in Table 5.1 were propagated through REBUS for each of the ZPPR models using the ESM method described herein. The a priori uncertainties for the ABTR models were propagated in the same manner but are presented in a later section for comparison with the posteriori results. A review of the reactor model nomenclature used throughout the remainder of this paper is presented in Table 5.2. Results were propagated through to the parameters already discussed. Integral parameters' nominal values and relative uncertainties (% standard deviation) are given in Table 5.3 and Table 5.4 for the preliminary or 0^{th} generation ZPPR perturbations, and reaction rate relative uncertainties are given in Table 5.5 and Table 5.6 for the preliminary or 0^{th} generation ZPPR perturbations. Observe that some modeled k-effectives are sub- or super- critical but note that there is typically an 0.85% (or 850 pcm) standard deviation on that value and also that the fine tuning control rods of the ZPPR were included. Note that numerous reaction rates at different spatial nodes were considered, but only the spatial averages are presented here due to space limitations in this document. By default, these data were also computed for each of the ZPPR perturbations used in the optimization problem, but are not presented due to space limitations in this document.

The final optimized experiment nominal values and relative uncertainties are deferred to Section 5.5. To demonstrate that the uncertainties in the ZPPR perturbations for subsequent generations are similar to those examined in the 0^{th} generation, a subset of the

perturbations is selected to be presented. This subset includes ZPPR_1_3, ZPPR_2_3, ZPPR_3_5, ZPPR_4_1, ZPPR_6_2, and ZPPR_3_1. The first five represent the best values in each generation and ZPPR_3_1 is presented as its design bounds the radiological hazards of all other experiments except ZPPR-ABTR (see Section 6.0). These integral parameter data are given in Table 5.7 and the averaged reaction rate uncertainties are given in Table 5.8. For a description of each experiment's design specifications see Appendix C. Note Doppler coefficient and void worth were not presented for the ZPPR perturbations as only k-effective and reaction rates were used in the optimization.

All uncertainties presented are in percent standard deviation relative to the nominal value of the attribute or response. The reader will first note that the k-effective uncertainty is very low due to its strong dependence on the very well known cross section of Pu-239 fission, which also has a low reaction rate uncertainty. Since the Pu-239 fission cross section is known so well, these uncertainties depend mainly on the other cross sections affecting the flux spectrum. Conversion ratio consistently has an uncertainty of about 2%. Void worth and Doppler reactivity coefficient have larger uncertainties and vary between different reactors. The power related parameters' uncertainties are about 1% throughout, limited mainly by the certainty of the Pu-239 fission reaction which is the primary power producing reaction. As expected, the ZPPR-15B integral parameters are unchanged, to numerical precision, by the presence of infinitely thin foils in ZPPR-15B w/ TRU. Less well known minor actinide reaction rates have the largest uncertainties, with a maximum of approximately 40% for Cm-244 fission. The neutron spectrum is affected by iron and sodium cross sections, and as can be seen the reaction rates for these materials have average

uncertainties in the (3-8)% range depending upon which model is examined. Having uncertainty information for each of the ZPPR models allows for the computation of representativity factors for each of these listed parameters in regards to the two ABTR cores. Uncertainties were similar for the 0^{th} generation as well as all subsequent perturbations examined during the demonstration of the optimization method.

Table 5.1 : Cross section uncertainties available.

Isotope	Reactions	Isotope	Reactions
H-1	(n,el), (n,gamma)	Pb-208	(n,el), (n,n'), (n,2n), (n,gamma)
F-19	(n,el), (n,n'), (n,2n), (n,gamma)	Bi-209	(n,el), (n,n'), (n,2n), (n,gamma)
Na-23	(n,el), (n,n'), (n,2n), (n,gamma)	Th-232	(n,el), (n,n'), (n,2n), (n,gamma), (n,f)
Cr-52	(n,el), (n,n'), (n,2n), (n,gamma)	U-233	(n,el), (n,n'), (n,2n), (n,gamma), (n,f) nu-bar
Fe-56	(n,el), (n,n'), (n,2n), (n,gamma)	U-234	(n,el), (n,n'), (n,2n), (n,gamma), (n,f)
Fe-57	(n,el), (n,n'), (n,2n), (n,gamma)	U-235	nu-bar
Ni-58	(n,el), (n,n'), (n,2n), (n,gamma)	U-236	(n,el), (n,n'), (n,2n), (n,gamma), (n,f)
Zr-90	(n,el), (n,n'), (n,2n), (n,gamma)	U-238	(n,el), (n,n'), (n,2n), (n,gamma), (n,f), nu-bar
Zr-91	(n,el), (n,n'), (n,2n), (n,gamma)	Np-237	(n,el), (n,n'), (n,2n), (n,gamma), (n,f), nu-bar
Zr-92	(n,el), (n,n'), (n,2n), (n,gamma)	Pu-238	(n,el), (n,n'), (n,2n), (n,gamma), (n,f)
Zr-94	(n,el), (n,n'), (n,2n), (n,gamma)	Pu-239	(n,el), (n,n'), (n,2n), (n,gamma), (n,f), nu-bar
Gd-155	(n,el), (n,n'), (n,2n), (n,gamma)	Pu-240	(n,el), (n,n'), (n,2n), (n,gamma), (n,f), nu-bar
Gd-156	(n,el), (n,n'), (n,2n), (n,gamma)	Pu-241	(n,el), (n,n'), (n,2n), (n,gamma), (n,f), nu-bar
Gd-157	(n,el), (n,n'), (n,2n), (n,gamma)	Pu-242	(n,el), (n,n'), (n,2n), (n,gamma), (n,f)
Gd-158	(n,el), (n,n'), (n,2n), (n,gamma)	Am-241	(n,el), (n,n'), (n,2n), (n,gamma), (n,f), nu-bar
Gd-160	(n,el), (n,n'), (n,2n), (n,gamma)	Am-242m	(n,el), (n,n'), (n,2n), (n,gamma), (n,f), nu-bar
Er-166	(n,el), (n,n'), (n,2n), (n,gamma)	Am-243	(n,el), (n,n'), (n,2n), (n,gamma), (n,f), nu-bar
Er-167	(n,el), (n,n'), (n,2n), (n,gamma)	Cm-242	(n,el), (n,n'), (n,2n), (n,gamma), (n,f)
Er-168	(n,el), (n,n'), (n,2n), (n,gamma)	Cm-243	(n,el), (n,n'), (n,2n), (n,gamma), (n,f)
Er-170	(n,el), (n,n'), (n,2n), (n,gamma)	Cm-244	(n,el), (n,n'), (n,2n), (n,gamma), (n,f)
Pb-206	(n,el), (n,n'), (n,2n), (n,gamma)	Cm-245	(n,el), (n,n'), (n,2n), (n,gamma), (n,f)
Pb-207	(n,el), (n,n'), (n,2n), (n,gamma)		

Table 5.2 : Reactor model nomenclature.

Model Nomenclature	TRU Included	Description
ABTR-SU	6 SNF test assemblies	ABTR start-up core, single cycle, 1/3 core as designed.
ABTR-EQ	SNF whole core	ABTR equilibrium core, single cycle, 1/3 core as designed.
ZPPR-15B	None, original experiment	ZPPR-15B exactly as built, full core model.
ZPPR-15B w/TRU	Infinitely thin foils	ZPPR-15B including infinitely thin foils of minor actinides for reaction rate tracking.
TRU v.1	16 trays	ZPPR with inner core TRU sample trays and detectors in varying locations.
TRU v. 1-B	32 trays	ZPPR with inner core TRU sample trays and detectors in varying locations.
TRU v. 1-C	32 trays	ZPPR with inner core TRU sample trays and detectors in varying locations.
TRU v. 2	16 trays	ZPPR with inner core TRU sample trays and detectors in varying locations.
TRU v. 2-B	32 trays	ZPPR with inner core TRU sample trays and detectors in varying locations.
TRU v. 3	32 trays	ZPPR with distributed TRU samples trays in 2 x 2 blocks and detectors in varying locations.
ZPPR-SNF	8 mock-up SNF assemblies	ZPPR with eight 3 x 3 blocks of trays containing SNF fuel composition identical to that in the ABTR-SU SNF test assemblies.
ZPPR-ABTR	SNF whole core	ZPPR core designed to emulate the ABTR equilibrium core.
ZPPR_*x*_*y*	Varies	ZPPR optimization perturbations where x indicates the generation and y indicates the perturbation. The number and location of TRU and SNF trays and the number and location of detectors varies with each perturbation.

Table 5.3 : ZPPR integral parameter values for original ZPPR-15B and all TRU v.1 models.

Parameter	Nominal Values	Uncertainty
ZPPR-15B		
k-eff,	1.000403233	0.8612
Void ($)	6.522602779	10.1670
Doppler ($/K)	-0.005723132	5.2780
Peak Fluence (n/cm^2)	16743800	1.0245
Peaking Factor	1.99667	0.3923
Peak Flux (n/cm^2-s)	7254.12	0.8402
Peak Power Density (W/cm^3)	7.41414E-10	0.6380
Conversion Ratio	0.71927	2.0328
ZPPR-15B w/ TRU		
k-eff	1.000403233	0.8612
Void ($)	6.522602779	10.1670
Doppler ($/K)	-0.005723132	5.2780
Peak Fluence (n/cm^2)	16743800	1.0245
Peaking Factor	1.99667	0.3923
Peak Flux (n/cm^2-s)	7254.12	0.8402
Peak Power Density (W/cm^3)	7.41414E-10	0.6380
Conversion Ratio	0.71927	2.0328
TRU v. 1		
k-eff	0.990397931	0.8582
Void ($)	6.340525949	5.3849
Doppler ($/K)	-0.005697623	3.1377
Peak Fluence (n/cm^2)	16804800	1.0952
Peaking Factor	2.02698	0.3667
Peak Flux (n/cm^2-s)	6960.25	0.9694
Peak Power Density (W/cm^3)	7.62684E-10	0.6372
Conversion Ratio	0.709699	2.0251
TRU v. 1-B		
k-eff	0.982372734	0.8540
Void ($)	6.060045854	5.2810
Doppler ($/K)	-0.005652062	3.8960
Peak Fluence (n/cm^2)	17216700	1.1062
Peaking Factor	2.0419	0.3813
Peak Flux (n/cm^2-s)	7001.58	1.0529
Peak Power Density (W/cm^3)	7.79712E-10	0.6494
Conversion Ratio	0.701269	2.0207
TRU v. 1-C		
k-eff	0.982372734	0.8540
Void ($)	6.060045854	5.2810
Doppler ($/K)	-0.005652062	3.8960
Peak Fluence (n/cm^2)	17216700	1.1062
Peaking Factor	2.0419	0.3813
Peak Flux (n/cm^2-s)	7001.58	1.0529
Peak Power Density (W/cm^3)	7.79712E-10	0.6494
Conversion Ratio	0.701269	2.0207

Table 5.4 : ZPPR integral parameter uncertainties on all other 0th generation models.

Parameter	Nominal Values	Uncertainty
TRU v. 2		
k-eff	0.990397931	0.8582
Void ($)	6.340525949	5.3849
Doppler ($/K)	-0.005697623	3.1377
Peak Fluence (n/cm^2)	16804800	1.0952
Peaking Factor	2.02698	0.3667
Peak Flux (n/cm^2-s)	6960.25	0.9694
Peak Power Density (W/cm^3)	7.62684E-10	0.6372
Conversion Ratio	0.709699	2.0251
TRU v. 2-B		
k-eff	0.982372734	0.8540
Void ($)	6.060045854	5.2810
Doppler ($/K)	-0.005652062	3.8960
Peak Fluence (n/cm^2)	17216700	1.1062
Peaking Factor	2.0419	0.3813
Peak Flux (n/cm^2-s)	7001.58	1.0529
Peak Power Density (W/cm^3)	7.79712E-10	0.6494
Conversion Ratio	0.701269	2.0207
TRU v. 3		
k-eff, EOC	0.982462887	0.8748
Void ($)	5.217968734	7.0326
Doppler ($/K)	-0.078369377	4.3967
Peak Fluence (n/cm^2)	17011900	1.0873
Peaking Factor	2.01146	0.3420
Peak Flux (n/cm^2-s)	7097.27	0.8989
Peak Power Density (W/cm^3)	7.66404E-10	0.6225
Conversion Ratio	0.703918	2.0434
ZPPR-SNF		
k-eff	0.983615122	0.8718
Void ($)	6.815347138	5.4260
Doppler ($/K)	-0.0050513	3.3738
Peak Fluence (n/cm^2)	16688500	1.2166
Peaking Factor	2.01304	0.3590
Peak Flux (n/cm^2-s)	7230.4	0.8415
Peak Power Density (W/cm^3)	7.62024E-10	0.6540
Conversion Ratio	0.707461	2.0248
ZPPR-ABTR		
k-eff	1.005562817	1.0813
Void ($)	5.7330666	2.8179
Doppler ($/K)	-0.001936754	34.7057
Peak Fluence (n/cm^2)	16716100	1.3179
Peaking Factor	1.64183	0.8306
Peak Flux (n/cm^2-s)	6333.55	1.4226
Peak Power Density (W/cm^3)	7.7319E-10	0.8282
Conversion Ratio	0.77782	2.4168

Table 5.5 : Average reaction rates uncertainties for original ZPPR-15B and all TRU v.1 models.

Reaction	ZPPR-15B	ZPPR-15B w/ TRU	TRU v. 1	TRU v. 1-B	TRU v.1-C
Fe Total	4.0572	4.0572	4.1228	4.1772	4.1291
Na-23 Total	1.7583	1.7583	1.7345	1.7407	1.7698
U-235 Capture	1.6188	1.6188	1.5781	1.5904	1.6319
U-238 Capture	1.9308	1.9308	1.6962	1.6413	1.8282
Np-237 Capture	--N/A--	3.4501	3.5355	3.5694	3.4971
Pu-238 Capture	12.1149	12.1149	12.0562	12.0237	12.0626
Pu-239 Capture	4.2935	4.2935	4.1349	4.1068	4.2459
Pu-240 Capture	10.0402	10.0402	9.4449	9.2556	9.7469
Pu-241 Capture	9.1788	9.1788	8.4634	8.2894	8.8857
Pu-242 Capture	22.0082	22.0082	22.0799	22.0727	21.9832
Am-241 Capture	--N/A--	4.8547	4.7876	4.7668	4.8200
Am-242m Capture	--N/A--	14.5033	14.6210	14.6841	14.5902
Am-243 Capture	--N/A--	4.9059	4.9722	5.0035	4.9503
Cm-242 Capture	--N/A--	13.4731	12.6420	12.4039	13.0842
Cm-244 Capture	--N/A--	13.2202	12.6935	12.5281	12.9630
Cm-245 Capture	--N/A--	11.0508	10.8313	10.7966	10.9842
Fe (n,el)	3.4128	3.4128	4.8108	5.5839	4.6711
Na-23 (n,el)	3.6205	3.6205	5.0712	5.8705	4.9262
U-235 Fission	1.1903	1.1903	1.1982	1.2375	1.2491
U-238 Fission	2.6243	2.6243	4.0098	4.7703	3.8222
Np-237 Fission	--N/A--	6.2601	6.3804	6.4789	6.3948
Pu-238 Fission	12.4260	12.4260	11.6317	11.3407	11.9844
Pu-239 Fission	0.8042	0.8042	1.0205	1.1195	1.0014
Pu-240 Fission	4.0908	4.0908	4.3745	4.5212	4.3294
Pu-241 Fission	10.9271	10.9271	10.3889	10.2011	10.6508
Pu-242 Fission	16.2655	16.2655	16.3129	16.3132	16.3021
Am-241 Fission	--N/A--	8.1900	8.3117	8.3988	8.3242
Am-242m Fission	--N/A--	11.9528	11.4171	11.2537	11.6992
Am-243 Fission	--N/A--	6.2801	6.6407	6.8786	6.6283
Cm-242 Fission	--N/A--	29.5786	28.7338	28.4579	29.0351
Cm-244 Fission	--N/A--	40.0308	40.1234	40.0458	40.0507
Cm-245 Fission	--N/A--	30.8572	29.2644	28.6416	29.9686

Table 5.6 : Average reaction rates uncertainties for all other 0th generation ZPPR models.

Reaction	TRU v. 2	TRU v. 2-B	TRU v. 3	ZPPR-SNF	ZPPR-ABTR
Fe Total	4.1797	4.2936	4.0841	4.0733	4.2114
Na-23 Total	1.7159	1.7466	1.7758	1.7522	1.7110
U-235 Capture	1.5373	1.5734	1.6267	1.6186	1.7598
U-238 Capture	1.4641	1.3692	1.8805	1.9081	2.2994
Np-237 Capture	3.6358	3.7123	3.4873	3.4613	3.1293
Pu-238 Capture	11.9756	11.9184	12.0667	12.0910	12.1725
Pu-239 Capture	3.9445	3.8933	4.2348	4.2491	4.8960
Pu-240 Capture	8.7822	8.4010	9.7928	9.8911	11.2611
Pu-241 Capture	7.6694	7.3080	8.8804	8.9802	10.8669
Pu-242 Capture	22.1318	22.1271	21.9748	22.0267	21.6485
Am-241 Capture	4.7159	4.6806	4.8264	4.8372	4.9883
Am-242m Capture	14.7514	14.8790	14.5298	14.4978	14.2608
Am-243 Capture	5.0510	5.1196	4.9364	4.9169	4.6918
Cm-242 Capture	11.6812	11.2053	13.0804	13.2087	15.7926
Cm-244 Capture	12.1046	11.7707	13.0053	13.0819	14.3673
Cm-245 Capture	10.5824	10.5107	10.9580	10.9859	11.7877
Fe (n,el)	6.1193	7.7778	4.2283	3.6826	3.0007
Na-23 (n,el)	6.4287	8.1471	4.4870	3.9046	3.1134
U-235 Fission	1.1943	1.2862	1.2008	1.1961	1.4497
U-238 Fission	5.3213	6.9306	3.2255	2.8675	2.8235
Np-237 Fission	6.4882	6.6898	6.2834	6.2748	6.2821
Pu-238 Fission	10.7845	10.1828	12.1230	12.2565	13.1866
Pu-239 Fission	1.2260	1.4213	0.8569	0.8415	1.2834
Pu-240 Fission	4.6552	4.9653	4.2098	4.1457	3.7260
Pu-241 Fission	9.7998	9.4218	10.7341	10.7872	11.1916
Pu-242 Fission	16.3647	16.3734	16.3172	16.2835	15.9633
Am-241 Fission	8.4149	8.5983	8.2241	8.2044	8.2199
Am-242m Fission	10.8229	10.4927	11.7438	11.8158	13.0114
Am-243 Fission	6.9802	7.4778	6.4051	6.3208	6.2550
Cm-242 Fission	27.8154	27.2114	29.1018	29.4342	30.6194
Cm-244 Fission	40.2401	40.1077	40.2019	40.0556	39.7630
Cm-245 Fission	27.5491	26.2874	30.3126	30.5062	33.2520

Table 5.7 : Selected ZPPR perturbation integral parameter uncertainties.

Parameter	Nominal Values	Uncertainty	Nominal Values	Uncertainty
	ZPPR_1_3		ZPPR_2_3	
k-eff	0.963438879	0.8804	0.98143473	0.8557
Peak Fluence (n/cm^2)	1.91412E+07	0.9835	1.72132E+07	1.1122
Peaking Factor	1.91329	0.2868	2.04393	0.3702
Peak Flux (n/cm^2-s)	8215.64	0.8909	6993.29	1.0710
Peak Power Density (W/cm^3)	7.51180E-10	0.5663	7.79596E-10	0.6555
Conversion Ratio	0.713087	2.0305	0.701768	2.0181
	ZPPR_3_5		ZPPR_4_1	
k-eff	0.995495583	0.8608	0.98143473	0.8557
Peak Fluence (n/cm^2)	1.65386E+07	1.0979	1.72132E+07	1.1122
Peaking Factor	2.01124	0.8822	2.04393	0.3702
Peak Flux (n/cm^2-s)	6991.94	0.3781	6993.29	1.0710
Peak Power Density (W/cm^3)	7.51635E-10	0.6315	7.79596E-10	0.6555
Conversion Ratio	0.712517	2.0283	0.701768	2.0181
	ZPPR_6_2		ZPPR_3_1	
k-eff, EOC	0.963438879	0.8804	0.927879362	0.8912
Peak Fluence (n/cm^2)	1.91412E+07	0.9835	2.12587E+07	0.9836
Peaking Factor	1.91329	0.2868	1.84254	0.3214
Peak Flux (n/cm^2-s)	8215.64	0.2868	9043.5	0.9453
Peak Power Density (W/cm^3)	7.51180E-10	0.5663	7.66561E-10	0.6519
Conversion Ratio	0.713087	2.0305	0.700249	2.0182

Table 5.8 : Average reaction rates uncertainties for selected ZPPR perturbations.

Reaction	ZPPR_1_3	ZPPR_2_3	ZPPR_3_5	ZPPR_4_1	ZPPR_6_2	ZPPR_3_1
Fe Total	4.0907	4.0292	4.0317	4.0292	4.0700	4.1103
Na-23 Total	1.7361	1.7150	1.7139	1.7150	1.6832	1.7437
U-235 Capture	1.5767	1.5756	1.5687	1.5756	1.5714	1.5779
U-238 Capture	1.7564	1.8755	1.8712	1.8755	1.7537	1.7009
Np-237 Capture	3.5146	3.4126	3.4212	3.4126	3.4470	3.5495
Pu-238 Capture	12.1505	12.2260	12.2452	12.2260	12.3971	12.1211
Pu-239 Capture	4.1986	4.3682	4.3571	4.3682	4.4183	4.1590
Pu-240 Capture	9.6318	10.2341	10.2077	10.2341	10.2139	9.4299
Pu-241 Capture	8.5520	9.2918	9.2334	9.2918	9.0832	8.3175
Pu-242 Capture	22.1800	22.1439	22.1934	22.1439	22.4534	22.1711
Am-241 Capture	4.8021	4.8512	4.8492	4.8512	4.8706	4.7708
Am-242m Capture	14.5120	14.4541	14.4591	14.4541	14.3885	14.5561
Am-243 Capture	4.9375	4.8617	4.8641	4.8617	4.8456	4.9655
Cm-242 Capture	12.8740	13.8042	13.7726	13.8042	13.8547	12.5724
Cm-244 Capture	12.8604	13.3694	13.3412	13.3694	13.3450	12.6770
Cm-245 Capture	10.8346	11.0726	11.0510	11.0726	11.0080	10.7634
Fe (n,el)	4.3549	3.1644	3.1725	3.1644	3.1924	4.7291
Na-23 (n,el)	4.6226	3.3655	3.3785	3.3655	3.3639	5.0192
U-235 Fission	1.1435	1.1498	1.1494	1.1498	1.2079	1.1506
U-238 Fission	3.2367	2.3350	2.3632	2.3350	2.5096	3.5826
Np-237 Fission	6.2600	6.2388	6.2428	6.2388	6.2721	6.2764
Pu-238 Fission	11.8577	12.5764	12.5205	12.5764	12.3781	11.5986
Pu-239 Fission	0.7312	0.7063	0.6957	0.7063	0.7471	0.7854
Pu-240 Fission	4.2250	4.0373	4.0446	4.0373	4.0921	4.2909
Pu-241 Fission	8.5520	9.2918	9.2334	9.2918	9.0832	8.3175
Pu-242 Fission	16.3026	16.2475	16.2385	16.2475	16.1993	16.3082
Am-241 Fission	8.1923	8.1671	8.1726	8.1671	8.1791	8.2061
Am-242m Fission	11.5666	12.0898	12.0589	12.0898	12.0267	11.3851
Am-243 Fission	6.3895	6.2306	6.2389	6.2306	6.2698	6.4718
Cm-242 Fission	28.9428	29.7291	29.7060	29.7291	29.8230	28.6717
Cm-244 Fission	40.2100	40.0150	40.0104	40.0150	39.8984	40.2518
Cm-245 Fission	29.8551	31.2209	31.1246	31.2209	30.9580	29.3331

5.2. Representativity of Experiments to ABTR

Representativity was calculated for each 0^{th} generation ZPPR model to the ABTR start-up and ABTR equilibrium cores integral parameters and reaction rates. The representativity results for the ABTR start-up core, with respect to the 0^{th} generation ZPPR

perturbations, are presented in Table 5.9 and Table 5.10 and for the equilibrium core in Table 5.11 and Table 5.12. Since the ABTR start-up core was the one used in the demonstration optimization problem, the representativity for a selection of ZPPR experiment perturbations to their respective optimized ABTR start-up cores is shown in Table 5.13.

For the ABTR start-up core, the reader will first notice that k-effective representativity is very high, >0.9, which indicates any of these models will be overall representative of ABTR criticality. Void worth and Doppler reactivity coefficient seem difficult to capture in ZPPR and vary greatly depending on model from 0.1 up to 0.7, but ZPPR-SNF seems to be the most representative, which is expected since that model tends to emulate the ABTR start-up core. Peaking factor, power density, and Pu-239 fission rates all have low representativities due to the fact that Pu-239 is so well known that the uncertainties are more sensitive to cross sections affecting the flux spectrum, such as iron or sodium scatter. The sensitivities to these cross sections vary from reactor to reactor so representativity is lower for these parameters. Peak flux, fluence, and conversion ratio are all also well represented except in the ZPPR-ABTR model, which is expected since that models the ABTR equilibrium core. The other result the reader should note is that all of the minor actinide reactions have very high representativities. This is because these reaction rates' uncertainties are sensitive primarily to the reaction cross section itself which is very uncertain. This makes these uncertainties much less reactor dependent because the uncertainty source is in the reaction microscopic cross section itself.

For the ABTR equilibrium core, the reader will notice that k-effective is less representative, ~0.75, except for the ZPPR-ABTR core which mocks up the ABTR-EQ core.

The remaining integral parameters tend to follow the same trends as when compared with the ABTR start-up core for the same reasons. The exception to that trend is the Doppler reactivity coefficient which has a very low representativity in the ZPPR-ABTR model. The minor actinide reaction rates also follow the same tendency as before.

The selected ZPPR perturbations shown demonstrate that the experiments examined for the optimization demonstration also follow these same representativity trends as the 0^{th} generation. The representativity of the optimized ZPPR experiment will be deferred until Section 5.5.

Using the representativity values, one can qualitatively gauge how well a particular experiment variation will perform in reducing uncertainties on an ABTR. For parameters with very low representativities, it is expected that little uncertainty reduction will be seen and what is seen will come from correlations with parameters of higher representativity. This affect can be seen by using only the diagonal elements of the covariance information which removes these helpful cross-correlations. For parameters with very high representativity it is expected there will be substantial uncertainty reduction. However, whether or not that amount of reduction could be physically achievable with current instrumentation is a source of contention. Comparing the a priori uncertainties on the parameters and the corresponding representativities, it is clear that accuracy is not an indicator of representativity. A very accurate parameter may have low representativity because it is affected by reactor dependent physics causing dissimilarity between the sensitivity profiles. Conversely, a very uncertain parameter can have a high representativity

because it is more sensitive to its own microscopic cross section than to reactor dependent physics.

Table 5.9 : Representativity to ABTR-SU of original ZPPR-15B, TRU v. 1 and 1-B.

Parameter	ZPPR-15B	ZPPR-15B w/ TRU	TRU v. 1	TRU v. 1-B
k-eff, EOC	0.9142	0.9142	0.9179	0.9211
Void	0.3929	0.3929	0.6992	0.7029
Doppler	0.5493	0.5493	0.8771	0.7357
Peak Fluence	0.8059	0.8059	0.8270	0.8156
Peaking Factor	0.3833	0.3833	0.3846	0.4018
Peak Flux	0.7034	0.7034	0.8690	0.8635
Peak Power Density	0.2907	0.2907	0.2990	0.2971
Conversion Ratio	0.9930	0.9930	0.9930	0.9932
Fe Total	0.9659	0.9659	0.9196	0.8974
Na-23 Total	0.9165	0.9165	0.8278	0.7904
U-235 Capture	0.9209	0.9209	0.8257	0.7803
U-238 Capture	0.9696	0.9696	0.9297	0.8986
Np-237 Capture	--N/A--	0.9539	0.9250	0.9121
Pu-238 Capture	0.9932	0.9932	0.9884	0.9860
Pu-239 Capture	0.9745	0.9745	0.9440	0.9288
Pu-240 Capture	0.9966	0.9966	0.9930	0.9909
Pu-241 Capture	0.9780	0.9780	0.9498	0.9322
Pu-242 Capture	0.9821	0.9821	0.9757	0.9729
Am-241 Capture	--N/A--	0.9757	0.9491	0.9357
Am-242m Capture	--N/A--	0.9712	0.9499	0.9414
Am-243 Capture	--N/A--	0.8298	0.7928	0.7790
Cm-242 Capture	--N/A--	0.9775	0.9629	0.9556
Cm-244 Capture	--N/A--	0.9895	0.9791	0.9731
Cm-245 Capture	--N/A--	0.9319	0.9112	0.9005
Fe (n,el)	0.9533	0.9533	0.9369	0.9280
Na-23 (n,el)	0.9564	0.9564	0.9395	0.9298
U-235 Fission	0.8804	0.8804	0.7381	0.6841
U-238 Fission	0.9250	0.9250	0.8826	0.8748
Np-237 Fission	--N/A--	0.9892	0.9743	0.9625
Pu-238 Fission	0.9937	0.9937	0.9803	0.9693
Pu-239 Fission	0.6148	0.6148	0.3942	0.3810
Pu-240 Fission	0.9803	0.9803	0.9530	0.9365
Pu-241 Fission	0.9905	0.9905	0.9805	0.9739
Pu-242 Fission	0.9974	0.9974	0.9932	0.9893
Am-241 Fission	--N/A--	0.9940	0.9788	0.9663
Am-242m Fission	--N/A--	0.9864	0.9699	0.9595
Am-243 Fission	--N/A--	0.9258	0.8969	0.8767
Cm-242 Fission	--N/A--	0.9960	0.9876	0.9788
Cm-244 Fission	--N/A--	0.9993	0.9974	0.9959
Cm-245 Fission	--N/A--	0.9927	0.9901	0.9883

Table 5.10 : Representativity to ABTR-SU of all other ZPPR models.

Parameter	TRU v. 1-C	TRU v. 2	TRU v. 2-B	TRU v. 3	ZPPR-SNF	ZPPR-ABTR
k-eff, EOC	0.92107	0.91790	0.92107	0.91708	0.91780	0.76566
Void	0.70291	0.69917	0.70291	0.73125	0.68808	0.68330
Doppler	0.73573	0.87713	0.73573	0.12904	0.92545	0.09693
Peak Fluence	0.81560	0.82704	0.81560	0.83890	0.76770	0.58139
Peaking Factor	0.40183	0.38464	0.40183	0.39147	0.36898	0.59128
Peak Flux	0.86345	0.86901	0.86345	0.80592	0.67738	0.64327
Peak Power Density	0.29707	0.29900	0.29707	0.28577	0.28796	0.58224
Conversion Ratio	0.99318	0.99300	0.99318	0.99309	0.99263	0.87205
Fe Total	0.93477	0.88091	0.83818	0.95164	0.95964	0.96385
Na-23 Total	0.85596	0.75673	0.67969	0.89496	0.90979	0.74869
U-235 Capture	0.85189	0.74484	0.65552	0.89942	0.91234	0.77290
U-238 Capture	0.93308	0.90018	0.83827	0.96218	0.96666	0.87097
Np-237 Capture	0.93565	0.90108	0.87645	0.94643	0.95082	0.90970
Pu-238 Capture	0.99026	0.98394	0.97929	0.99188	0.99260	0.99365
Pu-239 Capture	0.95315	0.91784	0.88806	0.96491	0.96892	0.96283
Pu-240 Capture	0.99374	0.99007	0.98586	0.99557	0.99627	0.99395
Pu-241 Capture	0.95640	0.92679	0.89317	0.97039	0.97449	0.98885
Pu-242 Capture	0.97880	0.97118	0.96600	0.98031	0.98098	0.98675
Am-241 Capture	0.95931	0.92886	0.90381	0.96838	0.97200	0.97215
Am-242m Capture	0.96162	0.93489	0.91960	0.96385	0.96747	0.98425
Am-243 Capture	0.81047	0.76709	0.74260	0.81735	0.82238	0.84742
Cm-242 Capture	0.96818	0.95081	0.93694	0.97240	0.97482	0.98238
Cm-244 Capture	0.98251	0.97097	0.95984	0.98685	0.98809	0.99270
Cm-245 Capture	0.91874	0.89500	0.87516	0.92628	0.92880	0.94192
Fe (n,el)	0.93503	0.91132	0.88887	0.94882	0.95825	0.91837
Na-23 (n,el)	0.93862	0.91251	0.88840	0.95041	0.96008	0.92052
U-235 Fission	0.78995	0.62188	0.51305	0.85235	0.87004	0.70777
U-238 Fission	0.88416	0.82875	0.80820	0.90776	0.92558	0.88961
Np-237 Fission	0.97270	0.96111	0.93632	0.98667	0.98863	0.98141
Pu-238 Fission	0.98024	0.96746	0.94555	0.99046	0.99245	0.99540
Pu-239 Fission	0.62369	0.25146	0.21271	0.55423	0.58898	0.64683
Pu-240 Fission	0.95520	0.92804	0.89346	0.97467	0.97887	0.95944
Pu-241 Fission	0.98235	0.97220	0.95939	0.98804	0.98928	0.99193
Pu-242 Fission	0.99235	0.98922	0.98114	0.99657	0.99723	0.99653
Am-241 Fission	0.97629	0.96432	0.93797	0.99079	0.99357	0.98969
Am-242m Fission	0.97376	0.95611	0.93621	0.98192	0.98418	0.99106
Am-243 Fission	0.89591	0.87023	0.82874	0.91852	0.92464	0.92240
Cm-242 Fission	0.98487	0.98023	0.96209	0.99383	0.99561	0.99639
Cm-244 Fission	0.99727	0.99563	0.99256	0.99872	0.99914	0.99933
Cm-245 Fission	0.99048	0.98789	0.98440	0.99201	0.99235	0.99328

Table 5.11 : Representativity to ABTR-EQ of original ZPPR-15B, TRU v. 1 and 1-B.

Parameter	ZPPR-15B	ZPPR-15B w/ TRU	TRU v. 1	TRU v. 1-B
k-eff, EOC	0.73121	0.73121	0.73501	0.73826
Void	0.38371	0.38371	0.68571	0.68726
Doppler	0.59496	0.59496	0.69444	0.71896
Peak Fluence	0.57304	0.57304	0.68565	0.68292
Peaking Factor	0.50373	0.50373	0.47765	0.50260
Peak Flux	0.62460	0.62460	0.72888	0.72461
Peak Power Density	0.46084	0.46084	0.46377	0.46097
Conversion Ratio	0.86845	0.86845	0.86971	0.87076
Fe TOT	0.93140	0.93140	0.88061	0.85713
Na-23 TOT	0.76491	0.76491	0.69534	0.66623
U-235 CAP	0.79909	0.79909	0.72798	0.69128
U-238 CAP	0.88876	0.88876	0.85680	0.82896
Np-237 CAP	--N/A--	0.91877	0.89212	0.88014
Pu-238 CAP	0.98964	0.98964	0.98442	0.98190
Pu-239 CAP	0.95180	0.95180	0.92168	0.90684
Pu-240 CAP	0.99377	0.99377	0.99044	0.98839
Pu-241 CAP	0.96981	0.96981	0.93873	0.92013
Pu-242 CAP	0.98819	0.98819	0.98045	0.97717
Am-241 CAP	--N/A--	0.95067	0.92185	0.90777
Am-242m CAP	--N/A--	0.95279	0.92648	0.91673
Am-243 CAP	--N/A--	0.88428	0.84586	0.83170
Cm-242 CAP	--N/A--	0.97105	0.95479	0.94707
Cm-244 CAP	--N/A--	0.98597	0.97405	0.96755
Cm-245 CAP	--N/A--	0.95499	0.93100	0.91913
Fe (n,el)	0.91006	0.91006	0.88882	0.87937
Na-23 (n,el)	0.91575	0.91575	0.89364	0.88284
U-235 FIS	0.70696	0.70696	0.59947	0.55552
U-238 FIS	0.87103	0.87103	0.80893	0.80031
Np-237 FIS	--N/A--	0.98504	0.96415	0.94997
Pu-238 FIS	0.99299	0.99299	0.97836	0.96686
Pu-239 FIS	0.55030	0.55030	0.37823	0.33899
Pu-240 FIS	0.96272	0.96272	0.92585	0.90638
Pu-241 FIS	0.98962	0.98962	0.97842	0.97125
Pu-242 FIS	0.99740	0.99740	0.99210	0.98769
Am-241 FIS	--N/A--	0.98961	0.96947	0.95506
Am-242m FIS	--N/A--	0.98410	0.96582	0.95482
Am-243 FIS	--N/A--	0.97684	0.93958	0.91649
Cm-242 FIS	--N/A--	0.99531	0.98581	0.97637
Cm-244 FIS	--N/A--	0.99932	0.99724	0.99567
Cm-245 FIS	--N/A--	0.99761	0.99476	0.99282

Table 5.12 : Representativity to ABTR-EQ of all other ZPPR models.

Parameter	TRU v. 1-C	TRU v. 2	TRU v. 2-B	TRU v. 3	ZPPR-SNF	ZPPR-ABTR
k-eff, EOC	0.73826	0.73501	0.73826	0.73309	0.76346	0.98066
Void	0.68726	0.68571	0.68726	0.71321	0.68899	0.72862
Doppler	0.71896	0.69444	0.71896	0.03866	0.78043	0.25879
Peak Fluence	0.68292	0.68565	0.68292	0.68897	0.63000	0.96492
Peaking Factor	0.50260	0.47765	0.50260	0.48683	0.45787	0.77896
Peak Flux	0.72461	0.72888	0.72461	0.70330	0.55700	0.95210
Peak Power Density	0.46097	0.46377	0.46097	0.45128	0.44153	0.78459
Conversion Ratio	0.87076	0.86971	0.87076	0.86942	0.86672	0.99037
Fe TOT	0.90021	0.83789	0.79261	0.91532	0.92517	0.98687
Na-23 TOT	0.72538	0.64573	0.58490	0.74937	0.77055	0.92719
U-235 CAP	0.75225	0.67018	0.59793	0.78473	0.80367	0.93548
U-238 CAP	0.86208	0.83584	0.78095	0.88459	0.89279	0.96061
Np-237 CAP	0.90478	0.87243	0.84952	0.91240	0.91950	0.97095
Pu-238 CAP	0.98651	0.98032	0.97560	0.98814	0.98901	0.99723
Pu-239 CAP	0.93251	0.89690	0.86797	0.94184	0.94746	0.98597
Pu-240 CAP	0.99121	0.98753	0.98343	0.99281	0.99375	0.99812
Pu-241 CAP	0.94711	0.91288	0.87710	0.96114	0.96587	0.99259
Pu-242 CAP	0.98442	0.97470	0.96874	0.98594	0.98681	0.99772
Am-241 CAP	0.93442	0.89898	0.87242	0.94257	0.94748	0.98921
Am-242m CAP	0.94185	0.90684	0.88916	0.94338	0.94807	0.99096
Am-243 CAP	0.86591	0.81199	0.78456	0.87104	0.87839	0.95944
Cm-242 CAP	0.96111	0.94068	0.92583	0.96518	0.96814	0.98768
Cm-244 CAP	0.97852	0.96496	0.95289	0.98287	0.98443	0.99694
Cm-245 CAP	0.94084	0.91191	0.88967	0.94815	0.95130	0.97900
Fe (n,el)	0.89541	0.87599	0.85482	0.89932	0.89508	0.96202
Na-23 (n,el)	0.89947	0.87500	0.85129	0.90319	0.90126	0.96397
U-235 FIS	0.64894	0.52172	0.43405	0.68683	0.70286	0.92298
U-238 FIS	0.84138	0.79441	0.77146	0.83835	0.83927	0.94689
Np-237 FIS	0.96621	0.95056	0.92246	0.97999	0.98090	0.99341
Pu-238 FIS	0.97898	0.96644	0.94395	0.98929	0.99123	0.99839
Pu-239 FIS	0.51672	0.28238	0.21067	0.50999	0.52517	0.89225
Pu-240 FIS	0.93607	0.90323	0.86527	0.95267	0.95416	0.98240
Pu-241 FIS	0.98117	0.96946	0.95576	0.98683	0.98820	0.99569
Pu-242 FIS	0.99184	0.98829	0.97966	0.99605	0.99662	0.99888
Am-241 FIS	0.96974	0.95525	0.92639	0.98392	0.98631	0.99540
Am-242m FIS	0.97086	0.95058	0.92949	0.97897	0.98154	0.99730
Am-243 FIS	0.94361	0.91266	0.86594	0.96498	0.97054	0.98923
Cm-242 FIS	0.98348	0.97839	0.95952	0.99258	0.99448	0.99695
Cm-244 FIS	0.99723	0.99559	0.99246	0.99866	0.99909	0.99978
Cm-245 FIS	0.99531	0.99242	0.98872	0.99685	0.99723	0.99926

Table 5.13 : Representativity of the selected ZPPR perturbations to their respective optimized ABTR-SU core.

Parameter	ZPPR_1_3	ZPPR_2_3	ZPPR_3_5	ZPPR_4_1	ZPPR_6_2	ZPPR_3_1
k-eff, EOC	0.91069	0.92056	0.91691	0.92056	0.91069	0.90971
Void	0.69917	0.69917	0.69917	0.69917	0.69917	0.69917
Doppler	0.87713	0.87713	0.87713	0.87713	0.87713	0.87713
Peak Fluence	0.83521	0.81341	0.83157	0.81341	0.83521	0.80952
Peaking Factor	0.34946	0.3836	0.40396	0.38360	0.34946	0.38389
Peak Flux	0.77021	0.87448	0.82479	0.87448	0.77021	0.77175
Peak Power Density	0.23758	0.29821	0.30274	0.29821	0.23758	0.24335
Conversion Ratio	0.99273	0.99306	0.99296	0.99306	0.99273	0.99248
Fe TOT	0.96284	0.98450	0.98398	0.81815	0.93296	0.95186
Na-23 TOT	0.90227	0.93393	0.93352	0.71111	0.86614	0.88112
U-235 CAP	0.96020	0.72548	0.84256	0.94500	0.95794	0.94312
U-238 CAP	0.98044	0.98132	0.97991	0.96232	0.98099	0.97791
Np-237 CAP	0.97624	0.90819	0.93623	0.93002	0.98343	0.96802
Pu-238 CAP	0.98809	0.98799	0.98066	0.99724	0.99640	0.98796
Pu-239 CAP	0.97467	0.97332	0.97537	0.99104	0.98826	0.97239
Pu-240 CAP	0.99225	0.99129	0.99185	0.99844	0.99838	0.99187
Pu-241 CAP	0.96969	0.96759	0.96921	0.99075	0.98927	0.96814
Pu-242 CAP	0.93155	0.93079	0.93134	0.93554	0.93384	0.93116
Am-241 CAP	0.97995	0.95997	0.96164	0.94148	0.96348	0.97962
Am-242m CAP	0.95062	0.90795	0.92161	0.94863	0.98099	0.93953
Am-243 CAP	0.88077	0.80910	0.83116	0.75429	0.81189	0.86438
Cm-242 CAP	0.95849	0.92748	0.92748	0.92277	0.91815	0.95473
Cm-244 CAP	0.98940	0.96877	0.97627	0.98369	0.99383	0.98608
Cm-245 CAP	0.93756	0.89405	0.91007	0.92711	0.96616	0.92936
Fe (n,el)	0.95701	0.94667	0.94704	0.94512	0.93283	0.95213
Na-23 (n,el)	0.93422	0.90334	0.90521	0.87636	0.89241	0.93012
U-235 FIS	0.92484	0.94924	0.95176	0.90376	0.89799	0.91578
U-238 FIS	0.86490	0.84416	0.86103	0.92220	0.93916	0.87054
Np-237 FIS	0.99177	0.96559	0.97349	0.96868	0.99592	0.98810
Pu-238 FIS	0.99676	0.97659	0.97155	0.99768	0.99637	0.99458
Pu-239 FIS	0.63422	0.52981	0.58302	0.67168	0.63164	0.61565
Pu-240 FIS	0.98369	0.97535	0.98170	0.98011	0.97814	0.98307
Pu-241 FIS	0.98028	0.97958	0.98013	0.99698	0.99651	0.97963
Pu-242 FIS	0.98663	0.98650	0.97178	0.99750	0.99739	0.98627
Am-241 FIS	0.99082	0.98844	0.99015	0.98775	0.99585	0.98946
Am-242m FIS	0.98254	0.95042	0.96321	0.97107	0.99089	0.97655
Am-243 FIS	0.97794	0.94085	0.94910	0.89366	0.93596	0.97097
Cm-242 FIS	0.99394	0.99398	0.98349	0.96494	0.95497	0.99409
Cm-244 FIS	0.99842	0.99620	0.99655	0.99433	0.99783	0.99771
Cm-245 FIS	0.99576	0.99077	0.99264	0.99007	0.99330	0.99489

5.3. Adaptive Simulation Posteriori Results

The following pages present the posteriori results for each 0^{th} generation ZPPR model adapted to the ABTR start-up core and the ABTR equilibrium core. The adaption results from the optimized experiment will be deferred to Section 5.5, but selected results from the optimization search are shown here. Each table in this section includes a selection of integral parameters, spatially averaged reaction rates, and safety analysis responses discussed earlier. For the ABTR equilibrium models, the tables also include a selection of spent fuel discharge parameters. Each 0^{th} generation table includes the nominal values of the attribute or response for the ABTR being adapted, the a priori uncertainty on that attribute or response, and posteriori results for four cases: 0% experimental error, 1% experimental errors, 1% experimental errors plus fission product yield (FPY), decay constant, and eigenvalue uncertainty, and 7.5% experimental error. The later generation optimization search table does not include the nominal values because nominal values change with each optimization of ATBR but remain similar to those of the original ABTR model. Table 5.14 - Table 5.23 are the ABTR start-up core adaption results and Table 5.24 - Table 5.33 are the ABTR equilibrium core adaption results. Table 5.34 shows a selection of ABTR posteriori uncertainties for several of the ZPPR perturbations seen during the optimization search. Additional results including capture and elastic scatter reaction rates and end of cycle/discharge isotopics are included in Appendix D. All uncertainties presented are in percent standard deviation relative to the nominal value of the attribute or response.

Throughout the results the a priori uncertainties are significantly larger than the calculated posteriori uncertainties. This is true even when assimilating data from the original

ZPPR-15B experiment, even though data for that experiment was possibly included in much earlier ENDF cross section evaluations. The reason for this is quite simple; by the nature of the data assimilation method, the posteriori uncertainty must always be less than or equal to the a priori uncertainty.

As indicated by the mathematics, experimental errors limit the amount of uncertainty reduction achievable. The 0% error case is, as expected, always the best, and the 7.5% error is the worst of the ones examined. It is also seen that there is little difference between the 1% error results and the 1% error results that also include fission product yield, decay constant, and eigenvalue uncertainty. This implies that these errors are quite small, and in some cases even negligible. However it is proper to include these sources of error since they do occur in reality. Based upon the errors reported in the ZPPR experimental results and these additional uncertainties, it is assumed in this work that the 1% error with fission product yield uncertainty is the most realistic of the possible adaption results. As such subsequent results will focus exclusively on those results for determining optimal experiments for ABTR adaption.

Table 5.14 : ABTR-SU adapted with ZPPR-15B.

Parameter	Nominal Values	A Priori	0%	1%	1% + FPY	7.50%
k-eff, EOC	1.00538786	**0.7920**	0.0654	0.2781	0.2838	0.5893
Void ($)	1.759085	**16.9421**	3.2838	8.4255	8.4728	12.7435
Doppler Coeff. ($/K)	-8.8693E-04	**3.3897**	0.8267	1.6729	1.6845	2.5545
Peak Fluence (n/cm^2)	2.47144E+22	**0.8677**	*0.1266*	*0.4633*	*0.4687*	*0.7530*
Peaking Factor	1.575	**0.4760**	*0.1570*	*0.3570*	*0.3585*	*0.4199*
Peak Flux (n/cm^2-s)	4.09059E+15	**0.9883**	*0.1637*	*0.3769*	*0.3789*	*0.6043*
Peak Power Density (W/cm^3)	406.022	**0.4784**	*0.1569*	*0.3632*	*0.3647*	*0.4270*
Conversion Ratio	0.551	**2.0303**	*0.0634*	*0.2726*	*0.2853*	*1.2069*
Axial Expansion Coeff. ($/C)	-5.70792E-04	**5.0190**	*1.6502*	*2.4349*	*2.4463*	*4.3157*
Radial Expansion Coeff. ($/C)	-7.09128E-03	**4.4571**	*1.1748*	*1.8151*	*1.8285*	*3.7738*
EOC Decay Heat (W, 1/3 core)	7110.470	**1.8201**	*0.1237*	*0.2525*	*0.2538*	*0.6859*
k-eff, BOC	1.019409486	**0.8042**	*0.0640*	*0.2768*	*0.2826*	*0.5977*
Average Reaction Rates						
Fe Total	3.06713E+11	**4.0119**	0.1508	0.5774	0.5782	1.7295
Na-23 Total	1.42611E+10	**1.5533**	0.1466	0.3929	0.3941	0.8535
U-238 Capture	4.70672E+12	**2.1331**	0.1137	0.3703	0.3824	1.3003
U-235 Fission	5.64742E+10	**1.0189**	0.0895	0.2444	0.2459	0.5596
U-238 Fission	1.21327E+12	**2.7973**	0.1847	0.4948	0.4982	1.5138
Np-237 Fission	5.04398E+10	**6.2319**	6.1123	6.1254	6.1256	6.1662
Pu-238 Fission	7.08204E+10	**13.1966**	0.3002	0.7247	1.0217	2.1017
Pu-239 Fission	6.34917E+12	**0.5575**	0.0881	0.2064	0.2080	0.3372
Pu-240 Fission	4.31025E+11	**3.9874**	0.1212	0.4075	0.4242	1.5628
Pu-241 Fission	3.92393E+11	**11.1955**	0.1379	0.5559	0.9418	1.9305
Pu-242 Fission	4.79160E+10	**16.1724**	0.1317	0.4512	0.7599	1.7447
Am-241 Fission	4.90637E+10	**8.2289**	0.1365	0.4518	0.4587	1.7241
Am-242m Fission	1.24016E+10	**12.0382**	11.8962	11.9057	11.9057	11.9267
Am-243 Fission	8.16183E+09	**6.6916**	6.0287	6.0523	6.0525	6.1278
Cm-242 Fission	1.04283E+09	**30.1371**	29.8479	29.9467	29.9474	30.0264
Cm-244 Fission	3.86831E+09	**39.6675**	39.5152	39.6003	39.6009	39.6510
Cm-245 Fission	1.54605E+09	**31.8290**	31.6713	31.7514	31.7520	31.8032
Safety Analysis Parameters						
A ($)	-0.2162	**5.8887**	*1.7747*	*2.5660*	*2.5764*	*4.6237*
B ($)	-1.1232	**16.5360**	*4.2074*	*9.0386*	*9.0843*	*13.2412*
C ($/K)	-8.0565E-03	**16.0790**	*3.9530*	*8.7733*	*8.8155*	*12.6269*
Parameter 1	0.1925	**22.3973**	*4.2978*	*9.9460*	*10.0071*	*16.8035*
Parameter 2	1.0637	**29.8584**	*5.5065*	*13.3079*	*13.3914*	*22.3064*
Parameter 3	0.4016	**16.5360**	*4.2074*	*9.0386*	*9.0843*	*13.2412*

Table 5.15 : ABTR-SU adapted with ZPPR-15B w/ TRU.

Parameter	Nominal Values	A Priori	0%	1%	1% + FPY	7.50%
k-eff, EOC	1.00538786	**0.7920**	0.0616	0.2691	0.2763	0.5822
Void ($)	1.759085	**16.9421**	2.9279	8.2668	8.3491	12.4238
Doppler Coeff. ($/K)	-8.8693E-04	**3.3897**	0.7777	1.6140	1.6350	2.4894
Peak Fluence (n/cm^2)	2.47144E+22	**0.8677**	*0.1180*	*0.4482*	*0.4565*	*0.7445*
Peaking Factor	1.575	**0.4760**	*0.1465*	*0.3523*	*0.3549*	*0.4138*
Peak Flux (n/cm^2-s)	4.09059E+15	**0.9883**	*0.1506*	*0.3735*	*0.3765*	*0.5878*
Peak Power Density (W/cm^3)	406.022	**0.4784**	*0.1461*	*0.3583*	*0.3611*	*0.4206*
Conversion Ratio	0.551	**2.0303**	*0.0609*	*0.2710*	*0.2838*	*1.1833*
Axial Expansion Coeff. ($/C)	-5.70792E-04	**5.0190**	*1.3903*	*2.2777*	*2.3038*	*4.1424*
Radial Expansion Coeff. ($/C)	-7.09128E-03	**4.4571**	*1.0326*	*1.7104*	*1.7389*	*3.6416*
EOC Decay Heat (W, 1/3 core)	7110.470	**1.8201**	*0.0289*	*0.2213*	*0.2229*	*0.6748*
k-eff, BOC	1.019409486	**0.8042**	*0.0603*	*0.2678*	*0.2752*	*0.5909*
Average Reaction Rates						
Fe Total	3.06713E+11	**4.0119**	0.1440	0.5746	0.5759	1.7283
Na-23 Total	1.42611E+10	**1.5533**	0.1344	0.3866	0.3886	0.8191
U-238 Capture	4.70672E+12	**2.1331**	0.1064	0.3657	0.3787	1.2707
U-235 Fission	5.64742E+10	**1.0189**	0.0819	0.2410	0.2431	0.5372
U-238 Fission	1.21327E+12	**2.7973**	0.1712	0.4835	0.4908	1.4975
Np-237 Fission	5.04398E+10	**6.2319**	0.2863	0.4946	0.5722	1.6934
Pu-238 Fission	7.08204E+10	**13.1966**	0.2102	0.6922	0.9992	2.0911
Pu-239 Fission	6.34917E+12	**0.5575**	0.0806	0.2025	0.2049	0.3300
Pu-240 Fission	4.31025E+11	**3.9874**	0.1123	0.4040	0.4218	1.5620
Pu-241 Fission	3.92393E+11	**11.1955**	0.1305	0.5535	0.9409	1.9294
Pu-242 Fission	4.79160E+10	**16.1724**	0.1221	0.4470	0.7583	1.7440
Am-241 Fission	4.90637E+10	**8.2289**	0.1266	0.4464	0.4549	1.7232
Am-242m Fission	1.24016E+10	**12.0382**	0.1428	0.6117	0.9139	2.1390
Am-243 Fission	8.16183E+09	**6.6916**	0.2496	0.6171	0.7254	1.7923
Cm-242 Fission	1.04283E+09	**30.1371**	0.1661	0.6516	0.7334	2.1515
Cm-244 Fission	3.86831E+09	**39.6675**	0.1472	0.5439	0.7402	1.8961
Cm-245 Fission	1.54605E+09	**31.8290**	0.1193	0.5928	0.8046	2.1825
Safety Analysis Parameters						
A ($)	-0.2162	**5.8887**	*1.5206*	*2.4250*	*2.4464*	*4.4834*
B ($)	-1.1232	**16.5360**	*3.6897*	*8.8052*	*8.8844*	*13.0227*
C ($/K)	-8.0565E-03	**16.0790**	*3.4653*	*8.5706*	*8.6435*	*12.4142*
Parameter 1	0.1925	**22.3973**	*3.8155*	*9.6871*	*9.8038*	*16.1569*
Parameter 2	1.0637	**29.8584**	*4.9132*	*12.9922*	*13.1473*	*21.5002*
Parameter 3	0.4016	**16.5360**	*3.6897*	*8.8052*	*8.8844*	*13.0227*

Table 5.16 : ABTR-SU adapted with TRU v. 1.

Parameters	Nominal Values	A Priori	0%	1%	1% + FPY	7.50%
k-eff, EOC	1.00538786	**0.7920**	0.0559	0.2548	0.2614	0.5743
Void ($)	1.759085	**16.9421**	2.9772	7.6758	7.7724	12.3557
Doppler Coeff. ($/K)	-8.8693E-04	**3.3897**	0.5959	1.3150	1.3265	2.4572
Peak Fluence (n/cm^2)	2.47144E+22	**0.8677**	*0.1091*	*0.4079*	*0.4159*	*0.7353*
Peaking Factor	1.575	**0.4760**	*0.1432*	*0.3145*	*0.3195*	*0.4029*
Peak Flux (n/cm^2-s)	4.09059E+15	**0.9883**	*0.1468*	*0.3623*	*0.3683*	*0.5946*
Peak Power Density (W/cm^3)	406.022	**0.4784**	*0.1427*	*0.3201*	*0.3251*	*0.4088*
Conversion Ratio	0.551	**2.0303**	*0.0581*	*0.3007*	*0.3140*	*1.1915*
Axial Expansion Coeff. ($/C)	-5.70792E-04	**5.0190**	*1.4366*	*2.5290*	*2.6034*	*4.2968*
Radial Expansion Coeff. ($/C)	-7.09128E-03	**4.4571**	*1.1491*	*2.0434*	*2.1173*	*3.7749*
EOC Decay Heat (W, 1/3 core)	7110.470	**1.8201**	*0.0251*	*0.2220*	*0.2240*	*0.7383*
k-eff, BOC	1.019409486	**0.8042**	*0.0546*	*0.2536*	*0.2604*	*0.5832*
Average Reaction Rates						
Fe Total	3.06713E+11	**4.0119**	0.1294	0.5858	0.5869	1.8878
Na-23 Total	1.42611E+10	**1.5533**	0.1288	0.3853	0.3888	0.8400
U-238 Capture	4.70672E+12	**2.1331**	0.0992	0.3900	0.4045	1.2878
U-235 Fission	5.64742E+10	**1.0189**	0.0785	0.2318	0.2351	0.5507
U-238 Fission	1.21327E+12	**2.7973**	0.1563	0.4805	0.4925	1.3916
Np-237 Fission	5.04398E+10	**6.2319**	0.2844	0.5202	0.6138	1.7443
Pu-238 Fission	7.08204E+10	**13.1966**	0.2461	0.6930	1.0918	2.5014
Pu-239 Fission	6.34917E+12	**0.5575**	0.0777	0.1875	0.1913	0.3124
Pu-240 Fission	4.31025E+11	**3.9874**	0.1099	0.4376	0.4655	1.5958
Pu-241 Fission	3.92393E+11	**11.1955**	0.1155	0.5591	1.0833	2.2281
Pu-242 Fission	4.79160E+10	**16.1724**	0.1205	0.4611	0.9143	1.9181
Am-241 Fission	4.90637E+10	**8.2289**	0.1250	0.4637	0.4777	1.8600
Am-242m Fission	1.24016E+10	**12.0382**	0.1279	0.5932	0.9473	2.5265
Am-243 Fission	8.16183E+09	**6.6916**	0.2448	0.5909	0.7774	1.9527
Cm-242 Fission	1.04283E+09	**30.1371**	0.1601	0.5807	0.6677	2.6219
Cm-244 Fission	3.86831E+09	**39.6675**	0.1447	0.5127	0.7623	2.2981
Cm-245 Fission	1.54605E+09	**31.8290**	0.1141	0.5861	0.8329	2.6167
Safety Analysis Parameters						
A ($)	-0.2162	**5.8887**	*1.6297*	*2.9700*	*3.0558*	*4.8237*
B ($)	-1.1232	**16.5360**	*4.2942*	*8.8394*	*8.9470*	*12.9567*
C ($/K)	-8.0565E-03	**16.0790**	*3.9738*	*8.4412*	*8.5301*	*12.3181*
Parameter 1	0.1925	**22.3973**	*2.9886*	*8.6411*	*8.8266*	*16.2912*
Parameter 2	1.0637	**29.8584**	*4.0205*	*11.7653*	*12.0112*	*21.6971*
Parameter 3	0.4016	**16.5360**	*4.2942*	*8.8394*	*8.9470*	*12.9567*

Table 5.17 : ABTR-SU adapted with TRU v. 1-B.

Parameter	Nominal Values	A Priori	0%	1%	1% + FPY	7.50%
k-eff, EOC	1.00538786	**0.7920**	0.0549	0.2533	0.2594	0.5692
Void ($)	1.759085	**16.9421**	2.9198	7.5111	7.6230	12.3285
Doppler Coeff. ($/K)	-8.8693E-04	**3.3897**	0.5074	1.3882	1.4098	2.4680
Peak Fluence (n/cm^2)	2.47144E+22	**0.8677**	*0.1056*	*0.4075*	*0.4156*	*0.7294*
Peaking Factor	1.575	**0.4760**	*0.1377*	*0.3167*	*0.3224*	*0.3998*
Peak Flux (n/cm^2-s)	4.09059E+15	**0.9883**	*0.1394*	*0.3545*	*0.3607*	*0.5973*
Peak Power Density (W/cm^3)	406.022	**0.4784**	*0.1369*	*0.3215*	*0.3272*	*0.4052*
Conversion Ratio	0.551	**2.0303**	*0.0583*	*0.3073*	*0.3209*	*1.1830*
Axial Expansion Coeff. ($/C)	-5.70792E-04	**5.0190**	*1.5511*	*2.6056*	*2.6646*	*4.3060*
Radial Expansion Coeff. ($/C)	-7.09128E-03	**4.4571**	*1.2217*	*2.0784*	*2.1356*	*3.7743*
EOC Decay Heat (W, 1/3 core)	7110.470	**1.8201**	*0.0245*	*0.2084*	*0.2103*	*0.7575*
k-eff, BOC	1.019409486	**0.8042**	*0.0537*	*0.2521*	*0.2584*	*0.5782*
Average Reaction Rates						
Fe Total	3.06713E+11	**4.0119**	0.1283	0.5613	0.5624	1.9361
Na-23 Total	1.42611E+10	**1.5533**	0.1250	0.3838	0.3874	0.8464
U-238 Capture	4.70672E+12	**2.1331**	0.0971	0.3950	0.4099	1.2794
U-235 Fission	5.64742E+10	**1.0189**	0.0755	0.2312	0.2347	0.5549
U-238 Fission	1.21327E+12	**2.7973**	0.1600	0.4889	0.4984	1.3617
Np-237 Fission	5.04398E+10	**6.2319**	0.2919	0.5262	0.6316	1.7687
Pu-238 Fission	7.08204E+10	**13.1966**	0.2289	0.6654	1.0513	2.5861
Pu-239 Fission	6.34917E+12	**0.5575**	0.0745	0.1878	0.1918	0.3103
Pu-240 Fission	4.31025E+11	**3.9874**	0.1082	0.4329	0.4632	1.6234
Pu-241 Fission	3.92393E+11	**11.1955**	0.1207	0.5292	1.0621	2.3129
Pu-242 Fission	4.79160E+10	**16.1724**	0.1190	0.4474	0.9382	2.0098
Am-241 Fission	4.90637E+10	**8.2289**	0.1256	0.4566	0.4705	1.9295
Am-242m Fission	1.24016E+10	**12.0382**	0.1273	0.5565	0.8936	2.5921
Am-243 Fission	8.16183E+09	**6.6916**	0.2450	0.5765	0.7702	2.0234
Cm-242 Fission	1.04283E+09	**30.1371**	0.1592	0.5575	0.6410	2.6778
Cm-244 Fission	3.86831E+09	**39.6675**	0.1423	0.4927	0.7373	2.3829
Cm-245 Fission	1.54605E+09	**31.8290**	0.1103	0.5486	0.7828	2.6921
Safety Analysis Parameters						
A ($)	-0.2162	**5.8887**	*1.6628*	*2.7066*	*2.7342*	*4.7279*
B ($)	-1.1232	**16.5360**	*4.3159*	*8.5682*	*8.6719*	*12.9942*
C ($/K)	-8.0565E-03	**16.0790**	*3.9689*	*8.1879*	*8.2838*	*12.3526*
Parameter 1	0.1925	**22.3973**	*3.0848*	*8.9517*	*9.1703*	*16.2561*
Parameter 2	1.0637	**29.8584**	*4.0700*	*11.9118*	*12.1776*	*21.5987*
Parameter 3	0.4016	**16.5360**	*4.3159*	*8.5682*	*8.6719*	*12.9942*

Table 5.18 : ABTR-SU adapted to TRU v. 1-C.

Parameter	Nominal Values	A Priori	0%	1%	1% + FPY	7.50%
k-eff, EOC	1.00538786	**0.7920**	0.0536	0.2573	0.2637	0.5640
Void ($)	1.759085	**16.9421**	2.4875	7.5553	7.6769	12.1200
Doppler Coeff. ($/K)	-8.8693E-04	**3.3897**	0.5073	1.3313	1.3502	2.4596
Peak Fluence (n/cm^2)	2.47144E+22	**0.8677**	*0.1028*	*0.4157*	*0.4242*	*0.7317*
Peaking Factor	1.575	**0.4760**	*0.1279*	*0.3122*	*0.3182*	*0.3976*
Peak Flux (n/cm^2-s)	4.09059E+15	**0.9883**	*0.1277*	*0.3508*	*0.3566*	*0.5830*
Peak Power Density (W/cm^3)	406.022	**0.4784**	*0.1269*	*0.3173*	*0.3234*	*0.4036*
Conversion Ratio	0.551	**2.0303**	*0.0559*	*0.2724*	*0.2856*	*1.1539*
Axial Expansion Coeff. ($/C)	-5.70792E-04	**5.0190**	*1.5520*	*2.4581*	*2.5094*	*4.0906*
Radial Expansion Coeff. ($/C)	-7.09128E-03	**4.4571**	*1.2163*	*1.9265*	*1.9760*	*3.5662*
EOC Decay Heat (W, 1/3 core)	7110.470	**1.8201**	*0.0247*	*0.1765*	*0.1782*	*0.6994*
k-eff, BOC	1.019409486	**0.8042**	*0.0525*	*0.2559*	*0.2623*	*0.5727*
Average Reaction Rates						
Fe Total	3.06713E+11	**4.0119**	0.1092	0.4891	0.4906	1.7926
Na-23 Total	1.42611E+10	**1.5533**	0.1185	0.3691	0.3725	0.8240
U-238 Capture	4.70672E+12	**2.1331**	0.0926	0.3578	0.3722	1.2432
U-235 Fission	5.64742E+10	**1.0189**	0.0711	0.2252	0.2286	0.5389
U-238 Fission	1.21327E+12	**2.7973**	0.1502	0.4602	0.4694	1.3599
Np-237 Fission	5.04398E+10	**6.2319**	0.2828	0.4897	0.5826	1.7113
Pu-238 Fission	7.08204E+10	**13.1966**	0.2149	0.5961	0.8863	2.1969
Pu-239 Fission	6.34917E+12	**0.5575**	0.0698	0.1837	0.1876	0.3076
Pu-240 Fission	4.31025E+11	**3.9874**	0.1008	0.3774	0.4022	1.5724
Pu-241 Fission	3.92393E+11	**11.1955**	0.1166	0.4538	0.8771	2.0265
Pu-242 Fission	4.79160E+10	**16.1724**	0.1114	0.3918	0.7962	1.8330
Am-241 Fission	4.90637E+10	**8.2289**	0.1174	0.4042	0.4157	1.7908
Am-242m Fission	1.24016E+10	**12.0382**	0.1225	0.4840	0.7461	2.2149
Am-243 Fission	8.16183E+09	**6.6916**	0.2357	0.5340	0.6848	1.8649
Cm-242 Fission	1.04283E+09	**30.1371**	0.1494	0.4985	0.5626	2.2850
Cm-244 Fission	3.86831E+09	**39.6675**	0.1334	0.4364	0.6251	2.0425
Cm-245 Fission	1.54605E+09	**31.8290**	0.1054	0.4729	0.6518	2.2723
Safety Analysis Parameters						
A ($)	-0.2162	**5.8887**	*1.6719*	*2.6643*	*2.6889*	*4.5933*
B ($)	-1.1232	**16.5360**	*3.8819*	*8.5182*	*8.6233*	*12.9650*
C ($/K)	-8.0565E-03	**16.0790**	*3.5252*	*8.1814*	*8.2816*	*12.3257*
Parameter 1	0.1925	**22.3973**	*2.9607*	*8.7626*	*8.9794*	*15.4822*
Parameter 2	1.0637	**29.8584**	*3.8036*	*11.7701*	*12.0396*	*20.6905*
Parameter 3	0.4016	**16.5360**	*3.8819*	*8.5182*	*8.6233*	*12.9650*

Table 5.19 : ABTR-SU adapted with TRU v. 2.

Parameter	Nominal Values	A Priori	0%	1%	1% + FPY	7.50%
k-eff, EOC	1.00538786	**0.7920**	0.0733	0.2741	0.2813	0.6109
Void ($)	1.759085	**16.9421**	4.2246	7.8781	7.9395	13.6350
Doppler Coeff. ($/K)	-8.8693E-04	**3.3897**	0.6698	1.3960	1.4041	2.4884
Peak Fluence (n/cm^2)	2.47144E+22	**0.8677**	*0.1522*	*0.4349*	*0.4405*	*0.7542*
Peaking Factor	1.575	**0.4760**	*0.1807*	*0.3345*	*0.3358*	*0.4163*
Peak Flux (n/cm^2-s)	4.09059E+15	**0.9883**	*0.1878*	*0.4037*	*0.4066*	*0.6571*
Peak Power Density (W/cm^3)	406.022	**0.4784**	*0.1815*	*0.3394*	*0.3407*	*0.4216*
Conversion Ratio	0.551	**2.0303**	*0.0761*	*0.4085*	*0.4178*	*1.2712*
Axial Expansion Coeff. ($/C)	-5.70792E-04	**5.0190**	*1.4904*	*2.7301*	*2.8245*	*4.4816*
Radial Expansion Coeff. ($/C)	-7.09128E-03	**4.4571**	*1.2020*	*2.2537*	*2.3452*	*3.9599*
EOC Decay Heat (W, 1/3 core)	7110.470	**1.8201**	*0.0409*	*0.5572*	*0.5587*	*0.8490*
k-eff, BOC	1.019409486	**0.8042**	*0.0719*	*0.2735*	*0.2809*	*0.6207*
Average Reaction Rates						
Fe Total	3.06713E+11	**4.0119**	0.2068	1.5213	1.5223	2.1872
Na-23 Total	1.42611E+10	**1.5533**	0.1661	0.4558	0.4579	0.8991
U-238 Capture	4.70672E+12	**2.1331**	0.1295	0.4952	0.5055	1.3774
U-235 Fission	5.64742E+10	**1.0189**	0.1035	0.2734	0.2760	0.6086
U-238 Fission	1.21327E+12	**2.7973**	0.2099	0.6897	0.7054	1.4691
Np-237 Fission	5.04398E+10	**6.2319**	0.3056	0.7315	0.7968	1.9283
Pu-238 Fission	7.08204E+10	**13.1966**	0.2746	1.7955	2.5890	3.6315
Pu-239 Fission	6.34917E+12	**0.5575**	0.0988	0.2159	0.2183	0.3286
Pu-240 Fission	4.31025E+11	**3.9874**	0.1366	0.8059	0.8249	1.7376
Pu-241 Fission	3.92393E+11	**11.1955**	0.1961	1.6504	2.1127	2.8882
Pu-242 Fission	4.79160E+10	**16.1724**	0.1523	1.1338	1.5414	2.3749
Am-241 Fission	4.90637E+10	**8.2289**	0.1591	1.0390	1.0562	2.2410
Am-242m Fission	1.24016E+10	**12.0382**	0.2035	2.1821	2.7625	3.6389
Am-243 Fission	8.16183E+09	**6.6916**	0.2797	1.2705	1.5149	2.4138
Cm-242 Fission	1.04283E+09	**30.1371**	0.2013	1.6282	1.9726	4.8361
Cm-244 Fission	3.86831E+09	**39.6675**	0.1781	1.5981	2.2856	3.6107
Cm-245 Fission	1.54605E+09	**31.8290**	0.1489	2.0622	2.6135	3.8886
Safety Analysis Parameters						
A ($)	-0.2162	**5.8887**	*1.7629*	*3.2109*	*3.3151*	*4.9743*
B ($)	-1.1232	**16.5360**	*5.1060*	*9.0327*	*9.1332*	*13.8073*
C ($/K)	-8.0565E-03	**16.0790**	*4.8522*	*8.5844*	*8.6578*	*13.2429*
Parameter 1	0.1925	**22.3973**	*4.5615*	*9.1933*	*9.3566*	*18.0305*
Parameter 2	1.0637	**29.8584**	*6.2414*	*12.4668*	*12.6747*	*24.0345*
Parameter 3	0.4016	**16.5360**	*5.1060*	*9.0327*	*9.1332*	*13.8073*

Table 5.20 : ABTR-SU adapted with TRU v. 2-B.

Parameter	Nominal Values	A Priori	0%	1%	1% + FPY	7.50%
k-eff, EOC	1.00538786	**0.7920**	0.0723	0.2800	0.2857	0.6129
Void ($)	1.759085	**16.9421**	4.1092	7.7545	7.8094	13.3557
Doppler Coeff. ($/K)	-8.8693E-04	**3.3897**	0.5948	1.4971	1.5158	2.5213
Peak Fluence (n/cm^2)	2.47144E+22	**0.8677**	*0.1603*	*0.4385*	*0.4438*	*0.7456*
Peaking Factor	1.575	**0.4760**	*0.1819*	*0.3418*	*0.3440*	*0.4133*
Peak Flux (n/cm^2-s)	4.09059E+15	**0.9883**	*0.1874*	*0.4051*	*0.4079*	*0.6649*
Peak Power Density (W/cm^3)	406.022	**0.4784**	*0.1825*	*0.3457*	*0.3480*	*0.4180*
Conversion Ratio	0.551	**2.0303**	*0.0923*	*0.4584*	*0.4670*	*1.2802*
Axial Expansion Coeff. ($/C)	-5.70792E-04	**5.0190**	*1.6603*	*2.7299*	*2.7895*	*4.4378*
Radial Expansion Coeff. ($/C)	-7.09128E-03	**4.4571**	*1.3058*	*2.2102*	*2.2684*	*3.9054*
EOC Decay Heat (W, 1/3 core)	7110.470	**1.8201**	*0.0442*	*0.6460*	*0.6476*	*0.9106*
k-eff, BOC	1.019409486	**0.8042**	*0.0709*	*0.2797*	*0.2856*	*0.6230*
Average Reaction Rates						
Fe Total	3.06713E+11	**4.0119**	0.2073	1.8198	1.8207	2.3509
Na-23 Total	1.42611E+10	**1.5533**	0.1571	0.4798	0.4821	0.9241
U-238 Capture	4.70672E+12	**2.1331**	0.1386	0.5443	0.5540	1.3929
U-235 Fission	5.64742E+10	**1.0189**	0.1056	0.2866	0.2893	0.6226
U-238 Fission	1.21327E+12	**2.7973**	0.2247	0.7697	0.7805	1.4636
Np-237 Fission	5.04398E+10	**6.2319**	0.3118	0.8703	0.9321	2.0186
Pu-238 Fission	7.08204E+10	**13.1966**	0.2808	2.3975	3.3930	4.4484
Pu-239 Fission	6.34917E+12	**0.5575**	0.0993	0.2277	0.2304	0.3319
Pu-240 Fission	4.31025E+11	**3.9874**	0.1488	1.0074	1.0292	1.8300
Pu-241 Fission	3.92393E+11	**11.1955**	0.2144	2.1258	2.6129	3.3329
Pu-242 Fission	4.79160E+10	**16.1724**	0.1685	1.5132	2.0346	2.7876
Am-241 Fission	4.90637E+10	**8.2289**	0.1712	1.3951	1.4144	2.5247
Am-242m Fission	1.24016E+10	**12.0382**	0.2174	2.8423	3.4615	4.2646
Am-243 Fission	8.16183E+09	**6.6916**	0.2914	1.6719	1.9694	2.7467
Cm-242 Fission	1.04283E+09	**30.1371**	0.2137	2.1889	2.7082	6.6779
Cm-244 Fission	3.86831E+09	**39.6675**	0.1913	2.2836	3.1897	4.5668
Cm-245 Fission	1.54605E+09	**31.8290**	0.1606	2.7432	3.3988	4.6871
Safety Analysis Parameters						
A ($)	-0.2162	**5.8887**	*1.8103*	*2.7908*	*2.8166*	*4.8069*
B ($)	-1.1232	**16.5360**	*5.2603*	*8.7470*	*8.8315*	*13.7197*
C ($/K)	-8.0565E-03	**16.0790**	*4.9417*	*8.3516*	*8.4211*	*13.1438*
Parameter 1	0.1925	**22.3973**	*4.3584*	*9.5146*	*9.6475*	*17.6122*
Parameter 2	1.0637	**29.8584**	*5.9190*	*12.5937*	*12.7420*	*23.4048*
Parameter 3	0.4016	**16.5360**	*5.2603*	*8.7470*	*8.8315*	*13.7197*

Table 5.21 : ABTR-SU adapted with TRU v. 3.

Parameter	Nominal Values	A Priori	0%	1%	1% + FPY	7.50%
k-eff, EOC	1.00538786	**0.7920**	0.0559	0.2640	0.2701	0.5800
Void ($)	1.759085	**16.9421**	3.1964	7.5504	7.6129	11.9007
Doppler Coeff. ($/K)	-8.8693E-04	**3.3897**	0.6094	1.4899	1.5059	2.4716
Peak Fluence (n/cm^2)	2.47144E+22	**0.8677**	*0.1139*	*0.4180*	*0.4244*	*0.7292*
Peaking Factor	1.575	**0.4760**	*0.1530*	*0.3263*	*0.3309*	*0.4041*
Peak Flux (n/cm^2-s)	4.09059E+15	**0.9883**	*0.1557*	*0.3664*	*0.3713*	*0.5817*
Peak Power Density (W/cm^3)	406.022	**0.4784**	*0.1532*	*0.3317*	*0.3363*	*0.4106*
Conversion Ratio	0.551	**2.0303**	*0.0505*	*0.2796*	*0.2929*	*1.1794*
Axial Expansion Coeff. ($/C)	-5.70792E-04	**5.0190**	*1.5942*	*2.5464*	*2.6178*	*4.3018*
Radial Expansion Coeff. ($/C)	-7.09128E-03	**4.4571**	*1.2871*	*2.0475*	*2.1181*	*3.7882*
EOC Decay Heat (W, 1/3 core)	7110.470	**1.8201**	*0.0247*	*0.2315*	*0.2332*	*0.6979*
k-eff, BOC	1.019409486	**0.8042**	*0.0547*	*0.2627*	*0.2689*	*0.5886*
Average Reaction Rates						
Fe Total	3.06713E+11	**4.0119**	0.1294	0.6074	0.6088	1.7909
Na-23 Total	1.42611E+10	**1.5533**	0.1248	0.3825	0.3859	0.8144
U-238 Capture	4.70672E+12	**2.1331**	0.0976	0.3625	0.3768	1.2756
U-235 Fission	5.64742E+10	**1.0189**	0.0804	0.2316	0.2347	0.5341
U-238 Fission	1.21327E+12	**2.7973**	0.1613	0.4836	0.4968	1.4066
Np-237 Fission	5.04398E+10	**6.2319**	0.2906	0.5082	0.5897	1.7063
Pu-238 Fission	7.08204E+10	**13.1966**	0.2345	0.7095	1.0856	2.2593
Pu-239 Fission	6.34917E+12	**0.5575**	0.0804	0.1884	0.1921	0.3128
Pu-240 Fission	4.31025E+11	**3.9874**	0.1139	0.4302	0.4517	1.5573
Pu-241 Fission	3.92393E+11	**11.1955**	0.1149	0.5765	1.0234	2.0345
Pu-242 Fission	4.79160E+10	**16.1724**	0.1249	0.4737	0.8383	1.7979
Am-241 Fission	4.90637E+10	**8.2289**	0.1297	0.4745	0.4865	1.7724
Am-242m Fission	1.24016E+10	**12.0382**	0.1323	0.6322	0.9804	2.3051
Am-243 Fission	8.16183E+09	**6.6916**	0.2371	0.6175	0.7745	1.8508
Cm-242 Fission	1.04283E+09	**30.1371**	0.1651	0.6254	0.7193	2.4373
Cm-244 Fission	3.86831E+09	**39.6675**	0.1454	0.5463	0.7936	2.1032
Cm-245 Fission	1.54605E+09	**31.8290**	0.1171	0.6167	0.8635	2.3624
Safety Analysis Parameters						
A ($)	-0.2162	**5.8887**	*1.6730*	*2.9601*	*3.0330*	*4.8585*
B ($)	-1.1232	**16.5360**	*4.4382*	*8.6055*	*8.6744*	*12.5358*
C ($/K)	-8.0565E-03	**16.0790**	*4.0982*	*8.2063*	*8.2581*	*11.8510*
Parameter 1	0.1925	**22.3973**	*3.7043*	*8.8177*	*8.9872*	*15.9268*
Parameter 2	1.0637	**29.8584**	*4.8448*	*11.8984*	*12.1103*	*21.1844*
Parameter 3	0.4016	**16.5360**	*4.4382*	*8.6055*	*8.6744*	*12.5358*

Table 5.22 : ABTR-SU adapted with ZPPR-SNF.

Parameter	Nominal Values	A Priori	0%	1%	1% + FPY	7.50%
k-eff, EOC	1.00538786	**0.7920**	0.0566	0.2658	0.2729	0.5838
Void ($)	1.759085	**16.9421**	3.5746	8.0020	8.0539	12.3518
Doppler Coeff. ($/K)	-8.8693E-04	**3.3897**	0.5337	1.2340	1.2422	2.4337
Peak Fluence (n/cm^2)	2.47144E+22	**0.8677**	*0.1172*	*0.4229*	*0.4304*	*0.7429*
Peaking Factor	1.575	**0.4760**	*0.1565*	*0.3294*	*0.3333*	*0.4072*
Peak Flux (n/cm^2-s)	4.09059E+15	**0.9883**	*0.1589*	*0.3673*	*0.3718*	*0.5875*
Peak Power Density (W/cm^3)	406.022	**0.4784**	*0.1570*	*0.3351*	*0.3389*	*0.4140*
Conversion Ratio	0.551	**2.0303**	*0.0575*	*0.2748*	*0.2877*	*1.1824*
Axial Expansion Coeff. ($/C)	-5.70792E-04	**5.0190**	*1.6929*	*2.5383*	*2.6023*	*4.2481*
Radial Expansion Coeff. ($/C)	-7.09128E-03	**4.4571**	*1.3627*	*2.0288*	*2.0919*	*3.7393*
EOC Decay Heat (W, 1/3 core)	7110.470	**1.8201**	*0.0253*	*0.2382*	*0.2399*	*0.6901*
k-eff, BOC	1.019409486	**0.8042**	*0.0557*	*0.2645*	*0.2717*	*0.5923*
Average Reaction Rates						
Fe Total	3.06713E+11	**4.0119**	0.1508	0.6145	0.6158	1.7611
Na-23 Total	1.42611E+10	**1.5533**	0.1341	0.3872	0.3897	0.8165
U-238 Capture	4.70672E+12	**2.1331**	0.1040	0.3666	0.3800	1.2741
U-235 Fission	5.64742E+10	**1.0189**	0.0829	0.2326	0.2355	0.5385
U-238 Fission	1.21327E+12	**2.7973**	0.1626	0.4725	0.4828	1.4595
Np-237 Fission	5.04398E+10	**6.2319**	0.2881	0.4969	0.5758	1.6976
Pu-238 Fission	7.08204E+10	**13.1966**	0.2333	0.7193	1.0726	2.1872
Pu-239 Fission	6.34917E+12	**0.5575**	0.0809	0.1915	0.1945	0.3219
Pu-240 Fission	4.31025E+11	**3.9874**	0.1115	0.4171	0.4359	1.5576
Pu-241 Fission	3.92393E+11	**11.1955**	0.1111	0.5809	0.9796	1.9916
Pu-242 Fission	4.79160E+10	**16.1724**	0.1235	0.4661	0.7881	1.7626
Am-241 Fission	4.90637E+10	**8.2289**	0.1278	0.4600	0.4696	1.7375
Am-242m Fission	1.24016E+10	**12.0382**	0.1352	0.6529	0.9934	2.2508
Am-243 Fission	8.16183E+09	**6.6916**	0.2377	0.6232	0.7426	1.8084
Cm-242 Fission	1.04283E+09	**30.1371**	0.1650	0.6633	0.7571	2.2420
Cm-244 Fission	3.86831E+09	**39.6675**	0.1449	0.5664	0.7932	1.9686
Cm-245 Fission	1.54605E+09	**31.8290**	0.1206	0.6357	0.8771	2.3010
Safety Analysis Parameters						
A ($)	-0.2162	**5.8887**	*1.7729*	*2.8129*	*2.8755*	*4.7515*
B ($)	-1.1232	**16.5360**	*4.8358*	*9.1481*	*9.2379*	*13.0303*
C ($/K)	-8.0565E-03	**16.0790**	*4.4818*	*8.7556*	*8.8259*	*12.3759*
Parameter 1	0.1925	**22.3973**	*4.0218*	*8.8863*	*8.9863*	*16.1025*
Parameter 2	1.0637	**29.8584**	*5.3386*	*12.1044*	*12.2315*	*21.4896*
Parameter 3	0.4016	**16.5360**	*4.8358*	*9.1481*	*9.2379*	*13.0303*

Table 5.23 : ABTR-SU adapted with ZPPR-ABTR.

Parameter	Nominal Values	A Priori	0%	1%	1% + FPY	7.50%
k-eff, EOC	1.00538786	**0.7920**	0.0735	0.3052	0.3099	0.5366
Void ($)	1.759085	**16.9421**	2.2597	8.3466	8.4207	13.2776
Doppler Coeff. ($/K)	-8.8693E-04	**3.3897**	0.6479	2.3383	2.3617	2.8064
Peak Fluence (n/cm^2)	2.47144E+22	**0.8677**	*0.0939*	*0.5084*	*0.5179*	*0.7512*
Peaking Factor	1.575	**0.4760**	*0.0647*	*0.2172*	*0.2215*	*0.3635*
Peak Flux (n/cm^2-s)	4.09059E+15	**0.9883**	*0.0652*	*0.2907*	*0.2980*	*0.6140*
Peak Power Density (W/cm^3)	406.022	**0.4784**	*0.0656*	*0.2267*	*0.2310*	*0.3717*
Conversion Ratio	0.551	**2.0303**	*0.0744*	*0.3037*	*0.3180*	*1.2365*
Axial Expansion Coeff. ($/C)	-5.70792E-04	**5.0190**	*1.0614*	*2.3031*	*2.3279*	*2.8873*
Radial Expansion Coeff. ($/C)	-7.09128E-03	**4.4571**	*0.8469*	*1.9322*	*1.9555*	*2.5747*
EOC Decay Heat (W, 1/3 core)	7110.470	**1.8201**	*0.0207*	*0.1240*	*0.1268*	*0.6110*
k-eff, BOC	1.019409486	**0.8042**	*0.0745*	*0.3039*	*0.3087*	*0.5445*
Average Reaction Rates						
Fe Total	3.06713E+11	**4.0119**	0.1124	0.4325	0.4372	1.5857
Na-23 Total	1.42611E+10	**1.5533**	0.0991	0.4162	0.4247	0.9439
U-238 Capture	4.70672E+12	**2.1331**	0.0869	0.3843	0.3994	1.3176
U-235 Fission	5.64742E+10	**1.0189**	0.0465	0.2044	0.2101	0.5937
U-238 Fission	1.21327E+12	**2.7973**	0.1040	0.4886	0.5003	1.4260
Np-237 Fission	5.04398E+10	**6.2319**	0.2584	0.4908	0.5718	1.7174
Pu-238 Fission	7.08204E+10	**13.1966**	0.2343	0.5120	0.6989	1.7804
Pu-239 Fission	6.34917E+12	**0.5575**	0.0415	0.1595	0.1629	0.3160
Pu-240 Fission	4.31025E+11	**3.9874**	0.0665	0.3528	0.3752	1.6760
Pu-241 Fission	3.92393E+11	**11.1955**	0.0748	0.3380	0.6336	1.7314
Pu-242 Fission	4.79160E+10	**16.1724**	0.0771	0.3902	0.7051	1.7611
Am-241 Fission	4.90637E+10	**8.2289**	0.0806	0.4150	0.4274	1.7279
Am-242m Fission	1.24016E+10	**12.0382**	0.0875	0.3751	0.5312	1.7008
Am-243 Fission	8.16183E+09	**6.6916**	0.1862	0.5331	0.6422	1.7830
Cm-242 Fission	1.04283E+09	**30.1371**	0.1028	0.5140	0.5731	1.9440
Cm-244 Fission	3.86831E+09	**39.6675**	0.0962	0.4097	0.5487	1.7806
Cm-245 Fission	1.54605E+09	**31.8290**	0.0736	0.3516	0.4669	1.7455
Safety Analysis Parameters						
A ($)	-0.2162	**5.8887**	*1.1916*	*2.8086*	*2.8283*	*3.4732*
B ($)	-1.1232	**16.5360**	*2.8867*	*8.7985*	*8.8725*	*13.1973*
C ($/K)	-8.0565E-03	**16.0790**	*2.6656*	*8.4572*	*8.5280*	*12.9222*
Parameter 1	0.1925	**22.3973**	*2.9142*	*10.3797*	*10.4899*	*16.0193*
Parameter 2	1.0637	**29.8584**	*3.8018*	*13.8167*	*13.9562*	*21.6228*
Parameter 3	0.4016	**16.5360**	*2.8867*	*8.7985*	*8.8725*	*13.1973*

Table 5.24 : ABTR-EQ adapted to ZPPR-15B.

Parameter	Nominal Values	A Priori	0%	1%	1% + FPY	7.50%
k-eff, EOC	1.009293719	**1.0275**	0.2552	0.4129	0.4177	0.6514
Void ($)	2.901985	**8.7046**	2.0582	4.1050	4.2584	6.1949
Doppler Coeff. ($/K)	-5.8325E-04	**4.5878**	1.2647	2.1611	2.2084	3.2993
Peak Fluence (n/cm^2)	2.49590E+22	**1.2424**	*0.2415*	*0.4776*	*0.4857*	*0.7636*
Peaking Factor	1.804	**0.5442**	*0.1628*	*0.3448*	*0.3502*	*0.4490*
Peak Flux (n/cm^2-s)	4.09383E+15	**1.3921**	*0.2736*	*0.4378*	*0.4421*	*0.6885*
Peak Power Density (W/cm^3)	466.215	**0.5538**	*0.1630*	*0.3516*	*0.3572*	*0.4602*
Conversion Ratio	0.764	**2.2458**	*0.0771*	*0.2700*	*0.2845*	*1.1158*
Axial Expansion Coeff. ($/C)	-4.83061E-04	**7.8448**	*3.5046*	*4.5594*	*4.5806*	*6.9356*
Radial Expansion Coeff. ($/C)	-5.96788E-03	**3.7178**	*1.4726*	*1.9947*	*2.0136*	*3.2086*
EOC Decay Heat (W, 1/3 core)	63345.700	**1.5558**	*0.1482*	*0.2200*	*0.2214*	*0.5670*
DIS Decay Heat (W, 1/3 core)	10324.9	**35.4703**	5.4732	9.8924	11.9937	15.3563
k-eff, BOC	1.009311528	**1.0275**	*0.2553*	*0.4130*	*0.4179*	*0.6513*
Average Reaction Rates						
Fe Total	2.40915E+11	**4.1955**	0.2786	0.7376	0.7407	1.8767
Na-23 Total	1.23629E+10	**1.7626**	0.2735	0.4687	0.4714	0.8571
U-238 Capture	5.28064E+12	**2.3021**	0.2596	0.4615	0.4736	1.3153
U-235 Fission	6.39618E+10	**1.3625**	0.2236	0.3361	0.3407	0.6369
U-238 Fission	1.44365E+12	**2.6937**	0.2811	0.6282	0.6325	1.4964
Np-237 Fission	5.87333E+10	**6.1865**	6.0729	6.0833	6.0836	6.1136
Pu-238 Fission	2.35308E+11	**13.0457**	0.2233	0.5879	0.9430	2.0370
Pu-239 Fission	5.93414E+12	**1.2048**	0.2227	0.3227	0.3287	0.5313
Pu-240 Fission	9.55335E+11	**3.6882**	0.2220	0.4500	0.4663	1.4567
Pu-241 Fission	5.61278E+11	**10.8653**	0.2532	0.6454	1.0504	1.9695
Pu-242 Fission	1.40619E+11	**15.8698**	0.2281	0.5017	0.7876	1.7367
Am-241 Fission	9.13075E+10	**8.1269**	0.2265	0.5398	0.5481	1.7464
Am-242m Fission	5.20438E+10	**12.2534**	12.1487	12.1578	12.1579	12.1733
Am-243 Fission	3.73546E+10	**6.2131**	5.9983	6.0107	6.0110	6.0601
Cm-242 Fission	1.77931E+09	**30.3575**	30.0739	30.1731	30.1738	30.2477
Cm-244 Fission	3.20464E+10	**39.4914**	39.3414	39.4248	39.4254	39.4731
Cm-245 Fission	3.05065E+10	**32.1604**	32.0073	32.0840	32.0846	32.1310
Safety Analysis Parameters						
A ($)	-0.1581	**9.7661**	*3.7924*	*4.9806*	*5.0203*	*7.9419*
B ($)	-0.9039	**14.0924**	*5.5865*	*8.0089*	*8.0533*	*12.0207*
C ($/K)	-6.2216E-03	**12.8171**	*4.9976*	*7.2709*	*7.3156*	*10.8103*
Parameter 1	0.1750	**14.2237**	*4.3533*	*6.9215*	*7.1622*	*10.5659*
Parameter 2	1.0208	**17.6832**	*4.6007*	*7.8428*	*8.2073*	*12.4576*
Parameter 3	0.4991	**14.0924**	*5.5865*	*8.0089*	*8.0533*	*12.0207*
Decay Heat Integral (W-s)						
100 years	5.05582E+12	**59.0669**	7.321	12.4577	15.03365	18.7967
500 years	1.16064E+13	**46.1908**	5.922	9.93916	11.73318	14.6341
1000 years	1.56835E+13	**44.2799**	5.515	9.3655	11.09587	13.9066
1500 years	1.84655E+13	**43.4953**	5.3231	9.11073	10.84228	13.6249
2500 years	2.25724E+13	**42.6915**	5.1173	8.84561	10.60814	13.3692
5000 years	3.03256E+13	**41.6755**	4.8611	8.51852	10.34105	13.0779
10000 years	4.16153E+13	**40.5924**	4.6186	8.199	10.06219	12.7629

Table 5.25 : ABTR-EQ adapted with ZPRR-15B w/ TRU.

Parameter	Nominal Values	A Priori	0%	1%	1% + FPY	7.50%
k-eff, EOC	1.009293719	**1.0275**	0.1790	0.3703	0.3764	0.6276
Void ($)	2.901985	**8.7046**	1.6846	3.9590	4.1268	5.9696
Doppler Coeff. ($/K)	-5.8325E-04	**4.5878**	1.1404	2.0824	2.1389	3.2143
Peak Fluence (n/cm^2)	2.49590E+22	**1.2424**	*0.1171*	*0.4200*	*0.4318*	*0.7338*
Peaking Factor	1.804	**0.5442**	*0.1490*	*0.3358*	*0.3436*	*0.4350*
Peak Flux (n/cm^2-s)	4.09383E+15	**1.3921**	*0.1569*	*0.3761*	*0.3828*	*0.6421*
Peak Power Density (W/cm^3)	466.215	**0.5538**	*0.1493*	*0.3428*	*0.3507*	*0.4457*
Conversion Ratio	0.764	**2.2458**	*0.0723*	*0.2685*	*0.2831*	*1.0959*
Axial Expansion Coeff. ($/C)	-4.83061E-04	**7.8448**	*3.1933*	*4.3753*	*4.4345*	*6.7523*
Radial Expansion Coeff. ($/C)	-5.96788E-03	**3.7178**	*1.2877*	*1.8788*	*1.9140*	*3.0823*
EOC Decay Heat (W, 1/3 core)	63345.700	**1.5558**	*0.0418*	*0.1669*	*0.1689*	*0.5487*
DIS Decay Heat (W, 1/3 core)	10324.9	**35.4703**	4.3718	9.4556	11.6432	15.1273
k-eff, BOC	1.009311528	**1.0275**	*0.1790*	*0.3704*	*0.3765*	*0.6275*
Average Reaction Rates						
Fe Total	2.40915E+11	**4.1955**	0.1780	0.7029	0.7066	1.8639
Na-23 Total	1.23629E+10	**1.7626**	0.1600	0.4123	0.4162	0.8102
U-238 Capture	5.28064E+12	**2.3021**	0.1435	0.4066	0.4212	1.2740
U-235 Fission	6.39618E+10	**1.3625**	0.1007	0.2696	0.2762	0.5921
U-238 Fission	1.44365E+12	**2.6937**	0.2129	0.5976	0.6053	1.4787
Np-237 Fission	5.87333E+10	**6.1865**	0.1328	0.4016	0.4930	1.6586
Pu-238 Fission	2.35308E+11	**13.0457**	0.1021	0.5502	0.9209	2.0264
Pu-239 Fission	5.93414E+12	**1.2048**	0.0934	0.2476	0.2569	0.4824
Pu-240 Fission	9.55335E+11	**3.6882**	0.1199	0.4066	0.4257	1.4431
Pu-241 Fission	5.61278E+11	**10.8653**	0.1413	0.6085	1.0289	1.9565
Pu-242 Fission	1.40619E+11	**15.8698**	0.1326	0.4633	0.7643	1.7250
Am-241 Fission	9.13075E+10	**8.1269**	0.1414	0.5066	0.5169	1.7359
Am-242m Fission	5.20438E+10	**12.2534**	0.1414	0.6873	1.0744	2.3384
Am-243 Fission	3.73546E+10	**6.2131**	0.1416	0.5335	0.6611	1.7220
Cm-242 Fission	1.77931E+09	**30.3575**	0.1614	0.7274	0.8233	2.2536
Cm-244 Fission	3.20464E+10	**39.4914**	0.1248	0.5007	0.7091	1.8668
Cm-245 Fission	3.05065E+10	**32.1604**	0.1070	0.6374	0.8988	2.2925
Safety Analysis Parameters						
A ($)	-0.1581	**9.7661**	*3.4244*	*4.7526*	*4.8303*	*7.7356*
B ($)	-0.9039	**14.0924**	*4.9985*	*7.6807*	*7.7882*	*11.7866*
C ($/K)	-6.2216E-03	**12.8171**	*4.4815*	*6.9904*	*7.0895*	*10.6170*
Parameter 1	0.1750	**14.2237**	*3.8860*	*6.6789*	*6.9441*	*10.0402*
Parameter 2	1.0208	**17.6832**	*3.9669*	*7.5323*	*7.9170*	*11.7559*
Parameter 3	0.4991	**14.0924**	*4.9985*	*7.6807*	*7.7882*	*11.7866*
Decay Heat Integral (W-s)						
100 years	5.05582E+12	**59.0669**	9.8874	14.1166	16.53309	19.8133
500 years	1.16064E+13	**46.1908**	7.3926	11.8321	14.25425	17.5274
1000 years	1.56835E+13	**44.2799**	6.412	10.6991	12.97344	16.0826
1500 years	1.84655E+13	**43.4953**	5.9365	10.0828	12.25191	15.2322
2500 years	2.25724E+13	**42.6915**	5.4083	9.32616	11.34008	14.1229
5000 years	3.03256E+13	**41.6755**	4.7762	8.35529	10.14071	12.6333
10000 years	4.16153E+13	**40.5924**	4.3114	7.62173	9.204506	11.4553

Table 5.26 : ABTR-EQ adapted with TRU v. 1.

Parameter	Nominal Values	A Priori	0%	1%	1% + FPY	7.50%
k-eff, EOC	1.009293719	**1.0275**	0.1758	0.3603	0.3662	0.6298
Void ($)	2.901985	**8.7046**	1.6255	3.7369	3.8386	5.8415
Doppler Coeff. ($/K)	-5.8325E-04	**4.5878**	1.1224	1.9088	1.9559	3.2543
Peak Fluence (n/cm^2)	2.49590E+22	**1.2424**	*0.1003*	*0.3889*	*0.4011*	*0.7220*
Peaking Factor	1.804	**0.5442**	*0.1383*	*0.3088*	*0.3174*	*0.4191*
Peak Flux (n/cm^2-s)	4.09383E+15	**1.3921**	*0.1402*	*0.3719*	*0.3824*	*0.6335*
Peak Power Density (W/cm^3)	466.215	**0.5538**	*0.1386*	*0.3150*	*0.3239*	*0.4289*
Conversion Ratio	0.764	**2.2458**	*0.0553*	*0.2998*	*0.3160*	*1.1118*
Axial Expansion Coeff. ($/C)	-4.83061E-04	**7.8448**	*2.9341*	*4.4357*	*4.5535*	*6.9478*
Radial Expansion Coeff. ($/C)	-5.96788E-03	**3.7178**	*1.2013*	*1.8807*	*1.9302*	*3.0879*
EOC Decay Heat (W, 1/3 core)	63345.700	**1.5558**	*0.0335*	*0.1723*	*0.1747*	*0.5939*
DIS Decay Heat (W, 1/3 core)	10324.9	**35.4703**	3.7421	9.2413	11.5928	16.4245
k-eff, BOC	1.009311528	**1.0275**	*0.1758*	*0.3603*	*0.3663*	*0.6297*
Average Reaction Rates						
Fe Total	2.40915E+11	**4.1955**	0.1457	0.6751	0.6792	2.0394
Na-23 Total	1.23629E+10	**1.7626**	0.1357	0.4119	0.4183	0.8108
U-238 Capture	5.28064E+12	**2.3021**	0.1105	0.4324	0.4494	1.2837
U-235 Fission	6.39618E+10	**1.3625**	0.0845	0.2593	0.2692	0.5945
U-238 Fission	1.44365E+12	**2.6937**	0.1516	0.5654	0.5779	1.3714
Np-237 Fission	5.87333E+10	**6.1865**	0.1197	0.4290	0.5389	1.7141
Pu-238 Fission	2.35308E+11	**13.0457**	0.0865	0.5537	1.0124	2.4423
Pu-239 Fission	5.93414E+12	**1.2048**	0.0800	0.2338	0.2482	0.4557
Pu-240 Fission	9.55335E+11	**3.6882**	0.1088	0.4293	0.4581	1.4775
Pu-241 Fission	5.61278E+11	**10.8653**	0.1171	0.5916	1.1484	2.2605
Pu-242 Fission	1.40619E+11	**15.8698**	0.1222	0.4698	0.9123	1.8941
Am-241 Fission	9.13075E+10	**8.1269**	0.1252	0.5026	0.5185	1.8788
Am-242m Fission	5.20438E+10	**12.2534**	0.1080	0.6387	1.0615	2.7449
Am-243 Fission	3.73546E+10	**6.2131**	0.1269	0.5061	0.7220	1.8944
Cm-242 Fission	1.77931E+09	**30.3575**	0.1398	0.6209	0.7137	2.7246
Cm-244 Fission	3.20464E+10	**39.4914**	0.1132	0.4745	0.7309	2.2709
Cm-245 Fission	3.05065E+10	**32.1604**	0.0896	0.6156	0.8991	2.7365
Safety Analysis Parameters						
A ($)	-0.1581	**9.7661**	*3.2678*	*5.0717*	*5.2373*	*8.2142*
B ($)	-0.9039	**14.0924**	*4.9666*	*7.8960*	*8.1151*	*12.1508*
C ($/K)	-6.2216E-03	**12.8171**	*4.4756*	*7.1847*	*7.3814*	*10.9578*
Parameter 1	0.1750	**14.2237**	*2.9668*	*5.7364*	*5.8347*	*9.5213*
Parameter 2	1.0208	**17.6832**	*2.7604*	*6.4815*	*6.6265*	*11.1969*
Parameter 3	0.4991	**14.0924**	*4.9666*	*7.8960*	*8.1151*	*12.1508*
Decay Heat Integral (W-s)						
100 years	5.05582E+12	**59.0669**	4.5868	11.1952	14.08531	19.6965
500 years	1.16064E+13	**46.1908**	3.6689	9.01505	11.05053	15.3133
1000 years	1.56835E+13	**44.2799**	3.4648	8.5244	10.48349	14.5921
1500 years	1.84655E+13	**43.4953**	3.373	8.29883	10.25326	14.318
2500 years	2.25724E+13	**42.6915**	3.2743	8.05072	10.02999	14.0709
5000 years	3.03256E+13	**41.6755**	3.1493	7.73235	9.763821	13.7884
10000 years	4.16153E+13	**40.5924**	3.028	7.42487	9.488689	13.4762

Table 5.27 : ABTR-EQ adapted with TRU v. 1-B.

Parameter	Nominal Values	A Priori	0%	1%	1% + FPY	7.50%
k-eff, EOC	1.009293719	**1.0275**	0.1750	0.3597	0.3651	0.6262
Void ($)	2.901985	**8.7046**	1.6463	3.6801	3.7694	5.8220
Doppler Coeff. ($/K)	-5.8325E-04	**4.5878**	1.1028	1.8897	1.9213	3.2226
Peak Fluence (n/cm^2)	2.49590E+22	**1.2424**	*0.0969*	*0.3909*	*0.4030*	*0.7199*
Peaking Factor	1.804	**0.5442**	*0.1333*	*0.3158*	*0.3245*	*0.4171*
Peak Flux (n/cm^2-s)	4.09383E+15	**1.3921**	*0.1345*	*0.3667*	*0.3777*	*0.6379*
Peak Power Density (W/cm^3)	466.215	**0.5538**	*0.1334*	*0.3220*	*0.3308*	*0.4266*
Conversion Ratio	0.764	**2.2458**	*0.0570*	*0.3050*	*0.3217*	*1.1082*
Axial Expansion Coeff. ($/C)	-4.83061E-04	**7.8448**	*2.9746*	*4.5050*	*4.5934*	*6.9428*
Radial Expansion Coeff. ($/C)	-5.96788E-03	**3.7178**	*1.2384*	*1.8831*	*1.9209*	*3.0726*
EOC Decay Heat (W, 1/3 core)	63345.700	**1.5558**	*0.0339*	*0.1660*	*0.1684*	*0.6095*
DIS Decay Heat (W, 1/3 core)	10324.9	**35.4703**	4.2163	9.1169	11.2013	16.6114
k-eff, BOC	1.009311528	**1.0275**	*0.1750*	*0.3598*	*0.3652*	*0.6261*
Average Reaction Rates						
Fe Total	2.40915E+11	**4.1955**	0.1484	0.6376	0.6420	2.0899
Na-23 Total	1.23629E+10	**1.7626**	0.1346	0.4108	0.4180	0.8159
U-238 Capture	5.28064E+12	**2.3021**	0.1116	0.4362	0.4542	1.2789
U-235 Fission	6.39618E+10	**1.3625**	0.0831	0.2594	0.2695	0.5985
U-238 Fission	1.44365E+12	**2.6937**	0.1552	0.5671	0.5787	1.3467
Np-237 Fission	5.87333E+10	**6.1865**	0.1170	0.4344	0.5574	1.7402
Pu-238 Fission	2.35308E+11	**13.0457**	0.0849	0.5177	0.9632	2.5298
Pu-239 Fission	5.93414E+12	**1.2048**	0.0781	0.2350	0.2498	0.4561
Pu-240 Fission	9.55335E+11	**3.6882**	0.1032	0.4224	0.4532	1.5045
Pu-241 Fission	5.61278E+11	**10.8653**	0.1242	0.5531	1.1116	2.3410
Pu-242 Fission	1.40619E+11	**15.8698**	0.1144	0.4563	0.9339	1.9839
Am-241 Fission	9.13075E+10	**8.1269**	0.1206	0.4894	0.5052	1.9500
Am-242m Fission	5.20438E+10	**12.2534**	0.1134	0.5877	0.9828	2.7969
Am-243 Fission	3.73546E+10	**6.2131**	0.1226	0.4899	0.7119	1.9703
Cm-242 Fission	1.77931E+09	**30.3575**	0.1371	0.5915	0.6797	2.7685
Cm-244 Fission	3.20464E+10	**39.4914**	0.1072	0.4569	0.7067	2.3555
Cm-245 Fission	3.05065E+10	**32.1604**	0.0882	0.5663	0.8318	2.8004
Safety Analysis Parameters						
A ($)	-0.1581	**9.7661**	*3.3128*	*4.8744*	*4.9469*	*8.0732*
B ($)	-0.9039	**14.0924**	*5.0645*	*7.6773*	*7.7926*	*12.0690*
C ($/K)	-6.2216E-03	**12.8171**	*4.5524*	*6.9706*	*7.0711*	*10.8790*
Parameter 1	0.1750	**14.2237**	*2.8996*	*6.3576*	*6.5629*	*9.6610*
Parameter 2	1.0208	**17.6832**	*2.6732*	*7.0546*	*7.3034*	*11.2620*
Parameter 3	0.4991	**14.0924**	*5.0645*	*7.6773*	*7.7926*	*12.0690*
Decay Heat Integral (W-s)						
100 years	5.05582E+12	**59.0669**	5.0699	11.0002	13.54969	19.8485
500 years	1.16064E+13	**46.1908**	4.0518	8.87688	10.67977	15.4383
1000 years	1.56835E+13	**44.2799**	3.8359	8.39372	10.12858	14.7148
1500 years	1.84655E+13	**43.4953**	3.7388	8.16926	9.898513	14.4387
2500 years	2.25724E+13	**42.6915**	3.6339	7.91979	9.667976	14.1878
5000 years	3.03256E+13	**41.6755**	3.5002	7.59782	9.387283	13.899
10000 years	4.16153E+13	**40.5924**	3.3692	7.28797	9.102047	13.5805

Table 5.28 : ABTR-EQ adapted with TRU v. 1-C.

Parameter	Nominal Values	A Priori	0%	1%	1% + FPY	7.50%
k-eff, EOC	1.009293719	**1.0275**	0.1740	0.3615	0.3664	0.6162
Void ($)	2.901985	**8.7046**	1.5379	3.6866	3.7865	5.7610
Doppler Coeff. ($/K)	-5.8325E-04	**4.5878**	1.0683	1.8727	1.9024	3.2176
Peak Fluence (n/cm^2)	2.49590E+22	**1.2424**	*0.0943*	*0.3964*	*0.4075*	*0.7167*
Peaking Factor	1.804	**0.5442**	*0.1284*	*0.3084*	*0.3180*	*0.4113*
Peak Flux (n/cm^2-s)	4.09383E+15	**1.3921**	*0.1282*	*0.3616*	*0.3710*	*0.6256*
Peak Power Density (W/cm^3)	466.215	**0.5538**	*0.1283*	*0.3143*	*0.3240*	*0.4202*
Conversion Ratio	0.764	**2.2458**	*0.0547*	*0.2699*	*0.2852*	*1.0783*
Axial Expansion Coeff. ($/C)	-4.83061E-04	**7.8448**	*2.9950*	*4.2845*	*4.3638*	*6.6159*
Radial Expansion Coeff. ($/C)	-5.96788E-03	**3.7178**	*1.2622*	*1.8138*	*1.8461*	*2.9266*
EOC Decay Heat (W, 1/3 core)	63345.700	**1.5558**	*0.0318*	*0.1428*	*0.1449*	*0.5675*
DIS Decay Heat (W, 1/3 core)	10324.9	**35.4703**	3.6838	8.8732	10.5602	15.2574
k-eff, BOC	1.009311528	**1.0275**	*0.1740*	*0.3616*	*0.3665*	*0.6161*
Average Reaction Rates						
Fe Total	2.40915E+11	**4.1955**	0.1429	0.5682	0.5722	1.9308
Na-23 Total	1.23629E+10	**1.7626**	0.1278	0.3992	0.4053	0.7999
U-238 Capture	5.28064E+12	**2.3021**	0.1075	0.4001	0.4166	1.2465
U-235 Fission	6.39618E+10	**1.3625**	0.0796	0.2531	0.2612	0.5829
U-238 Fission	1.44365E+12	**2.6937**	0.1490	0.5550	0.5665	1.3562
Np-237 Fission	5.87333E+10	**6.1865**	0.1102	0.3902	0.5011	1.6836
Pu-238 Fission	2.35308E+11	**13.0457**	0.0815	0.4392	0.7865	2.1413
Pu-239 Fission	5.93414E+12	**1.2048**	0.0747	0.2291	0.2407	0.4457
Pu-240 Fission	9.55335E+11	**3.6882**	0.0982	0.3720	0.3973	1.4575
Pu-241 Fission	5.61278E+11	**10.8653**	0.1227	0.4788	0.9264	2.0485
Pu-242 Fission	1.40619E+11	**15.8698**	0.1099	0.4046	0.7959	1.8149
Am-241 Fission	9.13075E+10	**8.1269**	0.1150	0.4404	0.4540	1.8126
Am-242m Fission	5.20438E+10	**12.2534**	0.1109	0.5110	0.8264	2.3890
Am-243 Fission	3.73546E+10	**6.2131**	0.1177	0.4416	0.6177	1.8124
Cm-242 Fission	1.77931E+09	**30.3575**	0.1316	0.5331	0.6013	2.3649
Cm-244 Fission	3.20464E+10	**39.4914**	0.1017	0.3987	0.5928	2.0136
Cm-245 Fission	3.05065E+10	**32.1604**	0.0853	0.4866	0.6938	2.3627
Safety Analysis Parameters						
A ($)	-0.1581	**9.7661**	*3.3116*	*4.7380*	*4.8070*	*7.7623*
B ($)	-0.9039	**14.0924**	*4.9928*	*7.4154*	*7.5229*	*11.7415*
C ($/K)	-6.2216E-03	**12.8171**	*4.4659*	*6.7484*	*6.8442*	*10.6168*
Parameter 1	0.1750	**14.2237**	*2.9786*	*6.1681*	*6.3694*	*9.2656*
Parameter 2	1.0208	**17.6832**	*2.7948*	*6.9797*	*7.2336*	*10.8120*
Parameter 3	0.4991	**14.0924**	*4.9928*	*7.4154*	*7.5229*	*11.7415*
Decay Heat Integral (W-s)						
100 years	5.05582E+12	**59.0669**	4.4975	10.7347	12.85181	18.3841
500 years	1.16064E+13	**46.1908**	3.6244	8.68266	10.16341	14.3443
1000 years	1.56835E+13	**44.2799**	3.4207	8.20649	9.62938	13.6571
1500 years	1.84655E+13	**43.4953**	3.326	7.98373	9.403345	13.3901
2500 years	2.25724E+13	**42.6915**	3.2209	7.73487	9.174046	13.1429
5000 years	3.03256E+13	**41.6755**	3.0858	7.41291	8.893088	12.8553
10000 years	4.16153E+13	**40.5924**	2.9567	7.10413	8.610574	12.5442

Table 5.29 : ABTR-EQ adapted with TRU v. 2.

Parameter	Nominal Values	A Priori	0%	1%	1% + FPY	7.50%
k-eff, EOC	1.009293719	**1.0275**	0.1959	0.3782	0.3882	0.6696
Void ($)	2.901985	**8.7046**	2.2597	3.9364	4.0169	6.6482
Doppler Coeff. ($/K)	-5.8325E-04	**4.5878**	1.2160	2.0576	2.0962	3.3527
Peak Fluence (n/cm^2)	2.49590E+22	**1.2424**	*0.1426*	*0.4168*	*0.4356*	*0.7454*
Peaking Factor	1.804	**0.5442**	*0.1744*	*0.3408*	*0.3444*	*0.4548*
Peak Flux (n/cm^2-s)	4.09383E+15	**1.3921**	*0.1907*	*0.4177*	*0.4297*	*0.6741*
Peak Power Density (W/cm^3)	466.215	**0.5538**	*0.1763*	*0.3471*	*0.3510*	*0.4657*
Conversion Ratio	0.764	**2.2458**	*0.0759*	*0.4240*	*0.4380*	*1.1818*
Axial Expansion Coeff. ($/C)	-4.83061E-04	**7.8448**	*3.0278*	*4.7676*	*4.9032*	*7.2306*
Radial Expansion Coeff. ($/C)	-5.96788E-03	**3.7178**	*1.2813*	*2.0381*	*2.0953*	*3.2737*
EOC Decay Heat (W, 1/3 core)	63345.700	**1.5558**	*0.0482*	*0.4165*	*0.4190*	*0.6724*
DIS Decay Heat (W, 1/3 core)	10324.9	**35.4703**	4.8778	14.236	16.9972	19.6916
k-eff, BOC	1.009311528	**1.0275**	*0.1960*	*0.3782*	*0.3882*	*0.6694*
Average Reaction Rates						
Fe Total	2.40915E+11	**4.1955**	0.2443	1.7392	1.7428	2.3556
Na-23 Total	1.23629E+10	**1.7626**	0.1782	0.4747	0.4821	0.8483
U-238 Capture	5.28064E+12	**2.3021**	0.1534	0.5434	0.5571	1.3502
U-235 Fission	6.39618E+10	**1.3625**	0.1198	0.3089	0.3231	0.6383
U-238 Fission	1.44365E+12	**2.6937**	0.2441	0.7067	0.7251	1.4138
Np-237 Fission	5.87333E+10	**6.1865**	0.1443	0.6532	0.7267	1.8686
Pu-238 Fission	2.35308E+11	**13.0457**	0.1301	1.7363	2.5689	3.5702
Pu-239 Fission	5.93414E+12	**1.2048**	0.1120	0.2960	0.3145	0.5111
Pu-240 Fission	9.55335E+11	**3.6882**	0.1339	0.7695	0.7916	1.5926
Pu-241 Fission	5.61278E+11	**10.8653**	0.2018	1.7424	2.2211	2.9205
Pu-242 Fission	1.40619E+11	**15.8698**	0.1571	1.1184	1.5185	2.3076
Am-241 Fission	9.13075E+10	**8.1269**	0.1680	1.0762	1.0956	2.2347
Am-242m Fission	5.20438E+10	**12.2534**	0.1977	2.4350	3.0963	3.9440
Am-243 Fission	3.73546E+10	**6.2131**	0.1665	1.2053	1.4726	2.3223
Cm-242 Fission	1.77931E+09	**30.3575**	0.1939	1.7115	2.0723	4.9824
Cm-244 Fission	3.20464E+10	**39.4914**	0.1571	1.5618	2.2645	3.5701
Cm-245 Fission	3.05065E+10	**32.1604**	0.1281	2.1834	2.8045	4.0544
Safety Analysis Parameters						
A ($)	-0.1581	**9.7661**	*3.4511*	*5.5634*	*5.7398*	*8.5752*
B ($)	-0.9039	**14.0924**	*5.3046*	*8.4657*	*8.7111*	*12.5410*
C ($/K)	-6.2216E-03	**12.8171**	*4.8029*	*7.6779*	*7.8982*	*11.3141*
Parameter 1	0.1750	**14.2237**	*3.5295*	*5.9760*	*6.0431*	*10.8370*
Parameter 2	1.0208	**17.6832**	*3.8466*	*6.8565*	*6.9378*	*13.1452*
Parameter 3	0.4991	**14.0924**	*5.3046*	*8.4657*	*8.7111*	*12.5410*
Decay Heat Integral (W-s)						
100 years	5.05582E+12	**59.0669**	5.8636	17.1999	20.33037	23.3423
500 years	1.16064E+13	**46.1908**	4.6485	13.324	15.63854	18.0392
1000 years	1.56835E+13	**44.2799**	4.4032	12.6739	14.91175	17.2217
1500 years	1.84655E+13	**43.4953**	4.2948	12.4298	14.65351	16.9234
2500 years	2.25724E+13	**42.6915**	4.179	12.2146	14.44217	16.6674
5000 years	3.03256E+13	**41.6755**	4.0328	11.9739	14.21829	16.3844
10000 years	4.16153E+13	**40.5924**	3.8896	11.7072	13.9521	16.0571

Table 5.30 : ABTR-EQ adapted with TRU v. 2-B.

Parameter	Nominal Values	A Priori	0%	1%	1% + FPY	7.50%
k-eff, EOC	1.009293719	**1.0275**	0.1982	0.3891	0.4003	0.6809
Void ($)	2.901985	**8.7046**	2.2394	3.9218	3.9979	6.5219
Doppler Coeff. ($/K)	-5.8325E-04	**4.5878**	1.1726	2.0282	2.0586	3.3234
Peak Fluence (n/cm^2)	2.49590E+22	**1.2424**	*0.1509*	*0.4305*	*0.4523*	*0.7567*
Peaking Factor	1.804	**0.5442**	*0.1799*	*0.3537*	*0.3576*	*0.4495*
Peak Flux (n/cm^2-s)	4.09383E+15	**1.3921**	*0.1944*	*0.4359*	*0.4500*	*0.6969*
Peak Power Density (W/cm^3)	466.215	**0.5538**	*0.1817*	*0.3596*	*0.3640*	*0.4599*
Conversion Ratio	0.764	**2.2458**	*0.0876*	*0.4794*	*0.4940*	*1.1989*
Axial Expansion Coeff. ($/C)	-4.83061E-04	**7.8448**	*2.9941*	*4.7283*	*4.8164*	*7.1568*
Radial Expansion Coeff. ($/C)	-5.96788E-03	**3.7178**	*1.2634*	*2.0076*	*2.0518*	*3.2365*
EOC Decay Heat (W, 1/3 core)	63345.700	**1.5558**	*0.0510*	*0.4922*	*0.4951*	*0.7225*
DIS Decay Heat (W, 1/3 core)	10324.9	**35.4703**	5.4155	16.1948	19.0253	21.5991
k-eff, BOC	1.009311528	**1.0275**	*0.1982*	*0.3892*	*0.4004*	*0.6808*
Average Reaction Rates						
Fe Total	2.40915E+11	**4.1955**	0.2412	2.0474	2.0513	2.5290
Na-23 Total	1.23629E+10	**1.7626**	0.1771	0.5090	0.5188	0.8753
U-238 Capture	5.28064E+12	**2.3021**	0.1605	0.5998	0.6148	1.3725
U-235 Fission	6.39618E+10	**1.3625**	0.1238	0.3383	0.3552	0.6626
U-238 Fission	1.44365E+12	**2.6937**	0.2514	0.7809	0.7986	1.4134
Np-237 Fission	5.87333E+10	**6.1865**	0.1502	0.8027	0.8704	1.9596
Pu-238 Fission	2.35308E+11	**13.0457**	0.1406	2.3551	3.3800	4.3971
Pu-239 Fission	5.93414E+12	**1.2048**	0.1146	0.3320	0.3541	0.5372
Pu-240 Fission	9.55335E+11	**3.6882**	0.1399	0.9566	0.9818	1.6800
Pu-241 Fission	5.61278E+11	**10.8653**	0.2152	2.2119	2.7117	3.3609
Pu-242 Fission	1.40619E+11	**15.8698**	0.1721	1.4892	1.9995	2.7102
Am-241 Fission	9.13075E+10	**8.1269**	0.1781	1.4301	1.4518	2.5209
Am-242m Fission	5.20438E+10	**12.2534**	0.2144	3.1274	3.8185	4.5911
Am-243 Fission	3.73546E+10	**6.2131**	0.1745	1.6230	1.9388	2.6597
Cm-242 Fission	1.77931E+09	**30.3575**	0.2044	2.2809	2.8162	6.8506
Cm-244 Fission	3.20464E+10	**39.4914**	0.1713	2.2553	3.1727	4.5295
Cm-245 Fission	3.05065E+10	**32.1604**	0.1410	2.8749	3.6020	4.8681
Safety Analysis Parameters						
A ($)	-0.1581	**9.7661**	*3.3404*	*5.1204*	*5.1930*	*8.3196*
B ($)	-0.9039	**14.0924**	*5.1957*	*7.9841*	*8.1054*	*12.3510*
C ($/K)	-6.2216E-03	**12.8171**	*4.7066*	*7.2290*	*7.3338*	*11.1378*
Parameter 1	0.1750	**14.2237**	*3.6227*	*6.9199*	*7.1049*	*10.8731*
Parameter 2	1.0208	**17.6832**	*3.9182*	*7.7889*	*8.0030*	*13.0157*
Parameter 3	0.4991	**14.0924**	*5.1957*	*7.9841*	*8.1054*	*12.3510*
Decay Heat Integral (W-s)						
100 years	5.05582E+12	**59.0669**	6.4411	19.3449	22.52415	25.4121
500 years	1.16064E+13	**46.1908**	5.0602	14.9342	17.30892	19.6139
1000 years	1.56835E+13	**44.2799**	4.8057	14.2312	16.52687	18.7431
1500 years	1.84655E+13	**43.4953**	4.6982	13.9734	16.25126	18.4278
2500 years	2.25724E+13	**42.6915**	4.588	13.7521	16.02689	18.1589
5000 years	3.03256E+13	**41.6755**	4.4515	13.5083	15.78897	17.8618
10000 years	4.16153E+13	**40.5924**	4.3136	13.2298	15.50162	17.514

Table 5.31 : ABTR-EQ adapted with TRU v. 3.

Parameter	Nominal Values	A Priori	0%	1%	1% + FPY	7.50%
k-eff, EOC	1.009293719	**1.0275**	0.1763	0.3647	0.3703	0.6311
Void ($)	2.901985	**8.7046**	1.8051	3.7098	3.8477	5.7115
Doppler Coeff. ($/K)	-5.8325E-04	**4.5878**	1.1000	2.0891	2.1432	3.2852
Peak Fluence (n/cm^2)	2.49590E+22	**1.2424**	*0.1022*	*0.3976*	*0.4074*	*0.7165*
Peaking Factor	1.804	**0.5442**	*0.1469*	*0.3245*	*0.3337*	*0.4277*
Peak Flux (n/cm^2-s)	4.09383E+15	**1.3921**	*0.1510*	*0.3753*	*0.3842*	*0.6310*
Peak Power Density (W/cm^3)	466.215	**0.5538**	*0.1478*	*0.3313*	*0.3407*	*0.4384*
Conversion Ratio	0.764	**2.2458**	*0.0486*	*0.2763*	*0.2919*	*1.0995*
Axial Expansion Coeff. ($/C)	-4.83061E-04	**7.8448**	*3.0474*	*4.4598*	*4.5714*	*6.9480*
Radial Expansion Coeff. ($/C)	-5.96788E-03	**3.7178**	*1.2568*	*1.8806*	*1.9298*	*3.1112*
EOC Decay Heat (W, 1/3 core)	63345.700	**1.5558**	*0.0322*	*0.1750*	*0.1774*	*0.5652*
DIS Decay Heat (W, 1/3 core)	10324.9	**35.4703**	3.8061	9.455	11.8767	15.6748
k-eff, BOC	1.009311528	**1.0275**	*0.1764*	*0.3648*	*0.3704*	*0.6309*
Average Reaction Rates						
Fe Total	2.40915E+11	**4.1955**	0.1430	0.7256	0.7299	1.9368
Na-23 Total	1.23629E+10	**1.7626**	0.1293	0.4082	0.4145	0.8020
U-238 Capture	5.28064E+12	**2.3021**	0.1062	0.3992	0.4160	1.2808
U-235 Fission	6.39618E+10	**1.3625**	0.0856	0.2606	0.2696	0.5876
U-238 Fission	1.44365E+12	**2.6937**	0.1628	0.5771	0.5901	1.3954
Np-237 Fission	5.87333E+10	**6.1865**	0.1182	0.4180	0.5138	1.6775
Pu-238 Fission	2.35308E+11	**13.0457**	0.0908	0.5758	1.0145	2.2014
Pu-239 Fission	5.93414E+12	**1.2048**	0.0826	0.2372	0.2502	0.4564
Pu-240 Fission	9.55335E+11	**3.6882**	0.1081	0.4278	0.4507	1.4434
Pu-241 Fission	5.61278E+11	**10.8653**	0.1096	0.6273	1.1104	2.0686
Pu-242 Fission	1.40619E+11	**15.8698**	0.1202	0.4863	0.8428	1.7819
Am-241 Fission	9.13075E+10	**8.1269**	0.1252	0.5243	0.5382	1.7929
Am-242m Fission	5.20438E+10	**12.2534**	0.1106	0.7059	1.1381	2.5248
Am-243 Fission	3.73546E+10	**6.2131**	0.1273	0.5384	0.7237	1.7947
Cm-242 Fission	1.77931E+09	**30.3575**	0.1480	0.6815	0.7845	2.5579
Cm-244 Fission	3.20464E+10	**39.4914**	0.1126	0.5058	0.7634	2.0799
Cm-245 Fission	3.05065E+10	**32.1604**	0.0899	0.6599	0.9551	2.4865
Safety Analysis Parameters						
A ($)	-0.1581	**9.7661**	*3.3241*	*5.1391*	*5.2938*	*8.2322*
B ($)	-0.9039	**14.0924**	*5.0429*	*7.9173*	*8.1021*	*12.1262*
C ($/K)	-6.2216E-03	**12.8171**	*4.5323*	*7.2054*	*7.3722*	*10.9186*
Parameter 1	0.1750	**14.2237**	*3.4235*	*5.9275*	*6.1368*	*9.4401*
Parameter 2	1.0208	**17.6832**	*3.4503*	*6.6503*	*6.9564*	*11.0575*
Parameter 3	0.4991	**14.0924**	*5.0429*	*7.9173*	*8.1021*	*12.1262*
Decay Heat Integral (W-s)						
100 years	5.05582E+12	**59.0669**	4.6548	11.5423	14.53829	18.9375
500 years	1.16064E+13	**46.1908**	3.7202	9.23949	11.34043	14.7358
1000 years	1.56835E+13	**44.2799**	3.5149	8.74084	10.76241	14.031
1500 years	1.84655E+13	**43.4953**	3.4237	8.51821	10.53656	13.762
2500 years	2.25724E+13	**42.6915**	3.3267	8.28004	10.32797	13.519
5000 years	3.03256E+13	**41.6755**	3.2045	7.97917	10.08766	13.2416
10000 years	4.16153E+13	**40.5924**	3.0844	7.68493	9.832179	12.9374

Table 5.32 : ABTR-EQ adapted with ZPPR-SNF.

Parameter	Nominal Values	A Priori	0%	1%	1% + FPY	7.50%
k-eff, EOC	1.009293719	**1.0275**	0.0814	0.3620	0.3684	0.6308
Void ($)	2.901985	**8.7046**	1.7745	3.9148	4.0428	5.9205
Doppler Coeff. ($/K)	-5.8325E-04	**4.5878**	1.0213	1.8104	1.8518	3.2269
Peak Fluence (n/cm^2)	2.49590E+22	**1.2424**	*0.1032*	*0.3987*	*0.4088*	*0.7270*
Peaking Factor	1.804	**0.5442**	*0.1493*	*0.3234*	*0.3315*	*0.4278*
Peak Flux (n/cm^2-s)	4.09383E+15	**1.3921**	*0.1507*	*0.3742*	*0.3830*	*0.6347*
Peak Power Density (W/cm^3)	466.215	**0.5538**	*0.1506*	*0.3300*	*0.3383*	*0.4383*
Conversion Ratio	0.764	**2.2458**	*0.0538*	*0.2721*	*0.2877*	*1.0985*
Axial Expansion Coeff. ($/C)	-4.83061E-04	**7.8448**	*2.9573*	*4.3924*	*4.4971*	*6.8508*
Radial Expansion Coeff. ($/C)	-5.96788E-03	**3.7178**	*1.2148*	*1.8711*	*1.9165*	*3.0865*
EOC Decay Heat (W, 1/3 core)	63345.700	**1.5558**	*0.0332*	*0.1777*	*0.1801*	*0.5591*
DIS Decay Heat (W, 1/3 core)	10324.9	**35.4703**	3.3476	9.5836	11.8948	15.5259
k-eff, BOC	1.009311528	**1.0275**	*0.0814*	*0.3622*	*0.3685*	*0.6307*
Average Reaction Rates						
Fe Total	2.40915E+11	**4.1955**	0.1661	0.7409	0.7449	1.9011
Na-23 Total	1.23629E+10	**1.7626**	0.1342	0.4116	0.4168	0.8029
U-238 Capture	5.28064E+12	**2.3021**	0.1104	0.4072	0.4229	1.2777
U-235 Fission	6.39618E+10	**1.3625**	0.0869	0.2616	0.2705	0.5892
U-238 Fission	1.44365E+12	**2.6937**	0.1734	0.5770	0.5865	1.4416
Np-237 Fission	5.87333E+10	**6.1865**	0.1184	0.4054	0.4977	1.6663
Pu-238 Fission	2.35308E+11	**13.0457**	0.0963	0.5904	1.0054	2.1261
Pu-239 Fission	5.93414E+12	**1.2048**	0.0841	0.2386	0.2498	0.4655
Pu-240 Fission	9.55335E+11	**3.6882**	0.1084	0.4185	0.4383	1.4423
Pu-241 Fission	5.61278E+11	**10.8653**	0.1050	0.6366	1.0657	2.0265
Pu-242 Fission	1.40619E+11	**15.8698**	0.1220	0.4818	0.7936	1.7453
Am-241 Fission	9.13075E+10	**8.1269**	0.1261	0.5187	0.5296	1.7540
Am-242m Fission	5.20438E+10	**12.2534**	0.1109	0.7358	1.1642	2.4663
Am-243 Fission	3.73546E+10	**6.2131**	0.1276	0.5447	0.6846	1.7427
Cm-242 Fission	1.77931E+09	**30.3575**	0.1516	0.7401	0.8471	2.3568
Cm-244 Fission	3.20464E+10	**39.4914**	0.1159	0.5253	0.7639	1.9425
Cm-245 Fission	3.05065E+10	**32.1604**	0.0920	0.6851	0.9780	2.4225
Safety Analysis Parameters						
A ($)	-0.1581	**9.7661**	*3.2688*	*4.9078*	*5.0419*	*8.0555*
B ($)	-0.9039	**14.0924**	*4.9656*	*7.8706*	*8.0666*	*12.0607*
C ($/K)	-6.2216E-03	**12.8171**	*4.4711*	*7.1717*	*7.3502*	*10.8767*
Parameter 1	0.1750	**14.2237**	*3.1030*	*5.9060*	*6.0627*	*9.5905*
Parameter 2	1.0208	**17.6832**	*3.0939*	*6.7222*	*6.9416*	*11.3015*
Parameter 3	0.4991	**14.0924**	*4.9656*	*7.8706*	*8.0666*	*12.0607*
Decay Heat Integral (W-s)						
100 years	5.05582E+12	**59.0669**	4.122	11.7399	14.56233	18.7785
500 years	1.16064E+13	**46.1908**	3.2959	9.37651	11.37009	14.6224
1000 years	1.56835E+13	**44.2799**	3.109	8.87047	10.79067	13.9217
1500 years	1.84655E+13	**43.4953**	3.0253	8.64731	10.56376	13.6534
2500 years	2.25724E+13	**42.6915**	2.9356	8.4117	10.35364	13.4103
5000 years	3.03256E+13	**41.6755**	2.8227	8.11648	10.11107	13.1321
10000 years	4.16153E+13	**40.5924**	2.7129	7.82633	9.853288	12.8278

Table 5.33 : ABTR-EQ adapted with ZPPR-ABTR.

Parameter	Nominal Values	A Priori	0%	1%	1% + FPY	7.50%
k-eff, EOC	1.009293719	**1.0275**	0.0286	0.3297	0.3343	0.5463
Void ($)	2.901985	**8.7046**	0.9327	3.7620	3.8320	6.4879
Doppler Coeff. ($/K)	-5.8325E-04	**4.5878**	0.9884	2.8269	2.8698	3.4665
Peak Fluence (n/cm^2)	2.49590E+22	**1.2424**	*0.0647*	*0.4368*	*0.4473*	*0.6917*
Peaking Factor	1.804	**0.5442**	*0.0491*	*0.1850*	*0.1938*	*0.3710*
Peak Flux (n/cm^2-s)	4.09383E+15	**1.3921**	*0.0508*	*0.2689*	*0.2752*	*0.6061*
Peak Power Density (W/cm^3)	466.215	**0.5538**	*0.0496*	*0.1921*	*0.2010*	*0.3796*
Conversion Ratio	0.764	**2.2458**	*0.0480*	*0.2416*	*0.2535*	*1.1135*
Axial Expansion Coeff. ($/C)	-4.83061E-04	**7.8448**	*1.9794*	*4.3842*	*4.4248*	*5.1238*
Radial Expansion Coeff. ($/C)	-5.96788E-03	**3.7178**	*0.8159*	*1.8961*	*1.9207*	*2.4517*
EOC Decay Heat (W, 1/3 core)	63345.700	**1.5558**	*0.0190*	*0.0998*	*0.1010*	*0.5050*
DIS Decay Heat (W, 1/3 core)	10324.9	**35.4703**	3.4926	8.7919	9.7839	12.9231
k-eff, BOC	1.009311528	**1.0275**	*0.0286*	*0.3297*	*0.3343*	*0.5464*
Average Reaction Rates						
Fe Total	2.40915E+11	**4.1955**	0.1019	0.3838	0.3854	1.5891
Na-23 Total	1.23629E+10	**1.7626**	0.0662	0.3183	0.3217	0.8388
U-238 Capture	5.28064E+12	**2.3021**	0.0612	0.3288	0.3415	1.2591
U-235 Fission	6.39618E+10	**1.3625**	0.0378	0.1896	0.1930	0.5791
U-238 Fission	1.44365E+12	**2.6937**	0.0799	0.3701	0.3794	1.3219
Np-237 Fission	5.87333E+10	**6.1865**	0.0584	0.3081	0.4163	1.6370
Pu-238 Fission	2.35308E+11	**13.0457**	0.0358	0.3093	0.5545	1.6780
Pu-239 Fission	5.93414E+12	**1.2048**	0.0347	0.1607	0.1708	0.4531
Pu-240 Fission	9.55335E+11	**3.6882**	0.0464	0.2945	0.3165	1.5085
Pu-241 Fission	5.61278E+11	**10.8653**	0.0483	0.3033	0.6050	1.6498
Pu-242 Fission	1.40619E+11	**15.8698**	0.0517	0.3209	0.6585	1.6962
Am-241 Fission	9.13075E+10	**8.1269**	0.0569	0.3273	0.3389	1.6714
Am-242m Fission	5.20438E+10	**12.2534**	0.0468	0.2980	0.4799	1.6373
Am-243 Fission	3.73546E+10	**6.2131**	0.0570	0.3354	0.4764	1.6566
Cm-242 Fission	1.77931E+09	**30.3575**	0.0673	0.4047	0.4625	1.8757
Cm-244 Fission	3.20464E+10	**39.4914**	0.0479	0.3411	0.4933	1.7144
Cm-245 Fission	3.05065E+10	**32.1604**	0.0390	0.3005	0.4354	1.6882
Safety Analysis Parameters						
A ($)	-0.1581	**9.7661**	*2.2482*	*5.0192*	*5.0745*	*6.0208*
B ($)	-0.9039	**14.0924**	*3.2265*	*7.5786*	*7.6470*	*9.4646*
C ($/K)	-6.2216E-03	**12.8171**	*2.8865*	*6.8573*	*6.9190*	*8.6869*
Parameter 1	0.1750	**14.2237**	*2.3860*	*7.4347*	*7.5714*	*10.9211*
Parameter 2	1.0208	**17.6832**	*2.3423*	*8.3030*	*8.4823*	*13.2765*
Parameter 3	0.4991	**14.0924**	*3.2265*	*7.5786*	*7.6470*	*9.4646*
Decay Heat Integral (W-s)						
100 years	5.05582E+12	**59.0669**	4.3668	10.7998	12.13398	18.7785
500 years	1.16064E+13	**46.1908**	3.479	8.68865	9.615228	14.6224
1000 years	1.56835E+13	**44.2799**	3.2793	8.21381	9.099039	13.9217
1500 years	1.84655E+13	**43.4953**	3.1919	7.99895	8.881219	13.6534
2500 years	2.25724E+13	**42.6915**	3.101	7.76669	8.662334	13.4103
5000 years	3.03256E+13	**41.6755**	2.9885	7.47206	8.396602	13.1321
10000 years	4.16153E+13	**40.5924**	2.8785	7.18676	8.130023	12.8278

Table 5.34 : Selected ABTR posteriori results from selected ZPPR perturbations.

Parameter	A Priori	ZPPR_1_3	ZPPR_2_3	ZPPR_3_5	ZPPR_4_1	ZPPR_6_2	ZPPR_3_1
k-eff, EOC	**0.7920**	0.1428	0.1434	0.1422	0.1352	0.1353	0.1414
Void	**16.9421**	8.0020	8.0539	7.6230	7.7545	7.8094	7.6769
Doppler Coeff.	**3.3897**	1.2340	1.2422	1.4098	1.4971	1.5158	1.3502
Peak Fluence	**0.8677**	0.4543	0.4533	0.4511	0.4276	0.4331	0.4513
Peaking Factor	**0.4760**	0.3523	0.3463	0.3454	0.3364	0.3435	0.3523
Peak Flux	**0.9883**	0.3879	0.3942	0.3926	0.3784	0.3764	0.3891
Peak Power Density	**0.4784**	0.3581	0.3513	0.3505	0.3413	0.3495	0.3580
Conversion Ratio	**2.0303**	0.2775	0.3119	0.3036	0.2827	0.2436	0.2856
Axial Expansion Coeff.	**5.0190**	2.7268	2.6057	2.7133	2.5519	2.5932	2.9606
Radial Expansion Coeff.	**4.4571**	2.2070	2.0842	2.1849	2.0317	2.0756	2.4411
EOC Decay Heat	**1.8201**	0.2823	0.2766	0.2887	0.2297	0.2538	0.2838
k-eff, BOC	**0.8042**	0.1410	0.1411	0.1399	0.1330	0.1334	0.1394
Average Reaction Rates							
Fe Total	**4.0119**	0.7749	0.7465	0.7888	0.6091	0.8581	0.7733
Na-23 Total	**1.5533**	0.3856	0.3980	0.3912	0.3776	0.3896	0.3898
U-238 Capture	**2.1331**	0.3993	0.4318	0.4236	0.4026	0.4156	0.4084
U-235 Fission	**1.0189**	0.2764	0.2861	0.2823	0.2692	0.2639	0.2780
U-238 Fission	**2.7973**	0.5032	0.4922	0.4890	0.4697	0.4793	0.5208
Np-237 Fission	**6.2319**	0.6401	0.7257	0.6960	0.6786	0.5677	0.6739
Pu-238 Fission	**13.1966**	1.3515	1.3539	1.3606	1.1115	1.2253	1.3553
Pu-239 Fission	**0.5575**	0.2648	0.2606	0.2594	0.2527	0.2582	0.2634
Pu-240 Fission	**3.9874**	0.4626	0.4770	0.4685	0.4042	0.4075	0.4595
Pu-241 Fission	**11.1955**	1.2447	1.2641	1.2608	1.0626	1.0853	1.2430
Pu-242 Fission	**16.1724**	0.9667	0.9795	0.9010	0.7492	0.8167	0.9656
Am-241 Fission	**8.2289**	0.4648	0.4962	0.4899	0.4461	0.4257	0.4663
Am-242m Fission	**12.0382**	1.6675	2.5740	2.4311	2.4657	1.5935	1.9450
Am-243 Fission	**6.6916**	0.9717	1.2253	1.0758	1.2119	0.9196	1.1177
Cm-242 Fission	**30.1371**	0.6813	0.8065	0.7184	0.8024	0.7529	0.7438
Cm-244 Fission	**39.6675**	1.5643	2.0719	1.6519	1.9093	1.5234	1.8664
Cm-245 Fission	**31.8290**	1.7788	2.6768	2.5782	2.4783	1.6750	2.0627
Safety Analysis Parameters							
Parameter 1	**22.3973**	10.3139	10.5636	10.2195	10.1885	9.9328	10.5916
Parameter 2	**29.8584**	13.9111	14.3010	13.7765	13.7835	13.3968	14.1755
Parameter 3	**16.5360**	9.3174	9.5235	9.2450	9.2505	8.9485	9.3146

5.4. Key Parameters Response Analysis

When presented with the dozens of ABTR attributes and responses analyzed in this study, one must decide upon an intelligent and intuitive way to interpret those results since it is often impractical to consider all aspects at once. The tabulated form in the preceding section is often too much information to be of use other than for reference. The results in this section show that the choice of experiment can depend upon which design attributes and responses are being examined and which design is being considered. The large number of results can be subdivided into groups of data that are of interest to various aspects of the reactor design, e.g. safety, power, waste considerations, etc.

5.4.1. Reactor Safety

For the engineers concerned with reactor safety and stability, the reactivity coefficients are of importance. Void worth, and the Doppler, axial expansion, and radial expansion reactivity coefficients are key to the reactor's safety. Further it has been suggested that the ability of the reactor to mitigate certain accidents can be determined by parameters listed by Wade and Fujita [13]. These parameters are listed for the ABTR start-up core in Table 5.35 and for the ABTR equilibrium core in Table 5.36.

In both the ABTR start-up and ABTR equilibrium cores, the values of parameter 1 and parameter 3 never exceed the allowable values, to within the numerical precision of the calculation. In the ABTR start-up core, the a priori probability of parameter 2 not exceeding the limits is 57.8%. After adapting to TRU v. 1-C, TRU v. 1-B and TRU v. 3 the probabilities are 69.1%, 68.9%, and 68.95%, respectively, far from the desired 95%

probability but a definite improvement. In the ABTR equilibrium core, the a priori probability of parameter 2 not exceeding the limits is 54.6%. After adapting to ABTR-SU, TRU v. 1-C and TRU v. 1 the probabilities are 80.6%, 61.1% and 62.1%, respectively. It is clear here that the best understanding of ABTR equilibrium safety could only come from an actual ABTR. The other two experiments show potential as well but much less than ABTR start-up. To meet the objective of 95% probability on parameter 2, uncertainty on parameter 2 would have to be no more than 3.65% in the start-up core and no more than 1.25% in the equilibrium core. Parameter 2 sensitivity is dominated by sodium density and axial expansion coefficients of reactivity. To achieve the targeted accuracy, reactivity coefficients would have to have uncertainties of less than 1.58% in the start-up core. To achieve the targeted accuracy in the equilibrium core would require all reactivity parameters to have uncertainties of less than 0.6%. Note the probabilities are based on a Gaussian distribution of the data.

Table 5.35 : Posteriori uncertainty for reactor safety parameters in ABTR-SU.

Parameter	A priori	ZPPR-15B	ZPPR w/ TRU	TRU v. 1	TRU v. 2	TRU v. 3
Void	**16.9421**	8.4728	8.3491	7.7724	7.9395	7.6129
Doppler	**3.3897**	1.6845	1.6350	1.3265	1.4041	1.5059
Axial Expansion Coeff.	**5.0190**	2.4463	2.3038	2.6034	2.8245	2.6178
Radial Expansion Coeff.	**4.4571**	1.8285	1.7389	2.1173	2.3452	2.1181
A	**5.8887**	2.5764	2.4464	3.0558	3.3151	3.0330
B	**16.5360**	9.0843	8.8844	8.9470	9.1332	8.6744
C	**16.0790**	8.8155	8.6435	8.5301	8.6578	8.2581
Parameter 1	**22.3973**	10.0071	9.8038	8.8266	9.3566	8.9872
Parameter 2	**29.8584**	13.3914	13.1473	12.0112	12.6747	12.1103
Parameter 3	**16.5360**	9.0843	8.8844	8.9470	9.1332	8.6744
Parameter	**ZPPR-SNF**	**TRU v. 1-B**	**TRU v. 2-B**	**TRU v. 1-C**	**ZPPR-ABTR**	
Void	8.0539	7.6230	7.8094	7.6769	8.4207	
Doppler	1.2422	1.4098	1.5158	1.3502	2.3617	
Axial Expansion Coeff.	2.6023	2.6646	2.7895	2.5094	2.3279	
Radial Expansion Coeff.	2.0919	2.1356	2.2684	1.9760	1.9555	
A	2.8755	2.7342	2.8166	2.6889	2.8283	
B	9.2379	8.6719	8.8315	8.6233	8.8725	
C	8.8259	8.2838	8.4211	8.2816	8.5280	
Parameter 1	8.9863	9.1703	9.6475	8.9794	10.4899	
Parameter 2	12.2315	12.1776	12.7420	12.0396	13.9562	
Parameter 3	9.2379	8.6719	8.8315	8.6233	8.8725	

Table 5.36 : Posteriori uncertainty for reactor safety parameters in ABTR-EQ.

Parameter	A priori	ZPPR-15B	ZPPR w/ TRU	TRU v. 1	TRU v. 2	TRU v. 3
Void	**8.7046**	4.2584	4.1268	3.8386	4.0169	3.8477
Doppler	**4.5878**	2.2084	2.1389	1.9559	2.0962	2.1432
Axial Expansion Coeff.	**7.8448**	4.5806	4.4345	4.5535	4.9032	4.5714
Radial Expansion Coeff.	**3.7178**	2.0136	1.9140	1.9302	2.0953	1.9298
A	**9.7661**	5.0203	4.8303	5.2373	5.7398	5.2938
B	**14.0924**	8.0533	7.7882	8.1151	8.7111	8.1021
C	**12.8171**	7.3156	7.0895	7.3814	7.8982	7.3722
Parameter 1	**14.2237**	7.1622	6.9441	5.8347	6.0431	6.1368
Parameter 2	**17.6832**	8.2073	7.9170	6.6265	6.9378	6.9564
Parameter 3	**14.0924**	8.0533	7.7882	8.1151	8.7111	8.1021
Parameter	**ZPPR-SNF**	**TRU v. 1-B**	**TRU v. 2-B**	**TRU v. 1-C**	**ZPPR-ABTR**	
Void	4.0428	3.7694	3.9979	3.7865	3.8320	
Doppler	1.8518	1.9213	2.0586	1.9024	2.8698	
Axial Expansion Coeff.	4.4971	4.5934	4.8164	4.3638	4.4248	
Radial Expansion Coeff.	1.9165	1.9209	2.0518	1.8461	1.9207	
A	5.0419	4.9469	5.1930	4.8070	5.0745	
B	8.0666	7.7926	8.1054	7.5229	7.6470	
C	7.3502	7.0711	7.3338	6.8442	6.9190	
Parameter 1	6.0627	6.5629	7.1049	6.3694	7.5714	
Parameter 2	6.9416	7.3034	8.0030	7.2336	8.4823	
Parameter 3	8.0666	7.7926	8.1054	7.5229	7.6470	

5.4.2. Power

For the engineers designing the reactor's operating cycle, the k-effectives at BOC and EOC are important. The power and thermal hydraulic analysts will also be interested in peak power and peak power density. Since these aspects are based on the power generated by fission, the reaction rates of U-235 fission, Pu-239 fission, and U-238 capture will also be of importance. These parameters are given for the ABTR start-up core in Table 5.37 and for the equilibrium core in Table 5.38.

Table 5.37 : Posteriori uncertainties for power parameters in ABTR-SU.

Parameter	A priori	ZPPR-15B	ZPPR w/ TRU	TRU v. 1	TRU v. 2	TRU v. 3
k-eff, EOC	**0.7920**	0.2838	0.2763	0.2614	0.2813	0.2701
k-eff, BOC	**0.8042**	*0.2826*	*0.2752*	*0.2604*	0.2809	*0.2689*
Peaking Factor	**0.4760**	*0.3585*	*0.3549*	*0.3195*	*0.3358*	*0.3309*
Peak Power Density	**0.4784**	*0.3647*	*0.3611*	*0.3251*	*0.3407*	*0.3363*
U-235 Fission	**1.0189**	0.2459	0.2431	0.2351	0.2760	0.2347
Pu-239 Fission	**0.5575**	0.2080	0.2049	0.1913	0.2183	0.1921
U-238 Capture	**2.1331**	0.3824	0.3787	0.4045	0.5055	0.3768
Parameter	**ZPPR-SNF**	**TRU v. 1-B**	**TRU v. 2-B**	**TRU v. 1-C**	**ZPPR-ABTR**	
k-eff, EOC	0.2729	0.2594	0.2857	0.2637	0.3099	
k-eff, BOC	*0.2717*	*0.2584*	*0.2856*	*0.2623*	*0.3087*	
Peaking Factor	*0.3333*	*0.3224*	*0.3440*	*0.3182*	*0.2215*	
Peak Power Density	*0.3389*	*0.3272*	*0.3480*	*0.3234*	*0.2310*	
U-235 Fission	0.2355	0.2347	0.2893	0.2286	0.2101	
Pu-239 Fission	0.1945	0.1918	0.2304	0.1876	0.1629	
U-238 Capture	0.3800	0.4099	0.5540	0.3722	0.3994	

Table 5.38 : Posteriori uncertainty for power parameters in ABTR-EQ.

Parameter	A priori	ZPPR-15B	ZPPR w/ TRU	TRU v. 1	TRU v. 2	TRU v. 3
k-eff, EOC	**1.0275**	0.4177	0.3764	0.3662	0.3882	0.3703
k-eff, BOC	**1.0275**	*0.4179*	*0.3765*	*0.3663*	0.3882	*0.3704*
Peaking Factor	**0.5442**	*0.3502*	*0.3436*	*0.3174*	*0.3444*	*0.3337*
Peak Power Density	**0.5538**	*0.3572*	*0.3507*	*0.3239*	*0.3510*	*0.3407*
U-235 Fission	**1.3625**	0.3407	0.2762	0.2692	0.3231	0.2696
Pu-239 Fission	**1.2048**	0.3287	0.2569	0.2482	0.3145	0.2502
U-238 Capture	**2.3021**	0.4736	0.4212	0.4494	0.5571	0.4160
Parameter	**ZPPR-SNF**	**TRU v. 1-B**	**TRU v. 2-B**	**TRU v. 1-C**	**ZPPR-ABTR**	
k-eff, EOC	0.3684	0.3651	0.4003	0.3664	0.3343	
k-eff, BOC	*0.3685*	*0.3652*	*0.4004*	*0.3665*	*0.3343*	
Peaking Factor	*0.3315*	*0.3245*	*0.3576*	*0.3180*	*0.1938*	
Peak Power Density	*0.3383*	*0.3308*	*0.3640*	*0.3240*	*0.2010*	
U-235 Fission	0.2705	0.2695	0.3552	0.2612	0.1930	
Pu-239 Fission	0.2498	0.2498	0.3541	0.2407	0.1708	
U-238 Capture	0.4229	0.4542	0.6148	0.4166	0.3415	

5.4.3. Fuels and Materials

When designing fuel forms and selecting structural materials, engineers will look at how well a composition endures in the high radiation environment of a fast reactor. The integral parameters of interest are the peak flux and its integrated counterpart peak fluence. Since iron is the primary non-actinide structural material in ABTR, total and scatter reaction rates of this element is of importance for analysis of cladding and structural damage. Table 5.39 presents these parameters for the ABTR start-up core and Table 5.40 for the equilibrium core.

Table 5.39 : Posteriori uncertainties for material parameters in ABTR-SU.

Parameter	A priori	ZPPR-15B	ZPPR w/ TRU	TRU v. 1	TRU v. 2	TRU v. 3
Peak Fluence	**0.8677**	*0.4687*	*0.4565*	*0.4159*	*0.4405*	*0.4244*
Peak Flux	**0.9883**	*0.3789*	*0.3765*	*0.3683*	*0.4066*	*0.3713*
Fe Total	**4.0119**	0.5782	0.5759	0.5869	1.5223	0.6088
Fe (n,el)	**3.1362**	0.5806	0.5764	0.5534	0.8190	0.5577
Parameter	**ZPPR-SNF**	**TRU v. 1-B**	**TRU v. 2-B**	**TRU v. 1-C**	**ZPPR-ABTR**	
Peak Fluence	*0.4304*	*0.4156*	*0.4438*	*0.4242*	*0.5179*	
Peak Flux	*0.3718*	*0.3607*	*0.4079*	*0.3566*	*0.2980*	
Fe Total	0.6158	0.5624	1.8207	0.4906	0.4372	
Fe (n,el)	0.5774	0.5498	0.9751	0.5421	0.5795	

Table 5.40 : Posteriori uncertainties for material parameters in ABTR-EQ.

Parameter	A priori	ZPPR-15B	ZPPR w/ TRU	TRU v. 1	TRU v. 2	TRU v. 3
Peak Fluence	**1.2424**	*0.4857*	*0.4318*	*0.4011*	*0.4356*	*0.4074*
Peak Flux	**1.3921**	*0.4421*	*0.3828*	*0.3824*	*0.4297*	*0.3842*
Fe Total	**4.1955**	0.7407	0.7066	0.6792	1.7428	0.7299
Fe (n,el)	**2.7838**	0.7690	0.7514	0.7372	0.8938	0.7293
Parameter	**ZPPR-SNF**	**TRU v. 1-B**	**TRU v. 2-B**	**TRU v. 1-C**	**ZPPR-ABTR**	
Peak Fluence	*0.4088*	*0.4030*	*0.4523*	*0.4075*	*0.4473*	
Peak Flux	*0.3830*	*0.3777*	*0.4500*	*0.3710*	*0.2752*	
Fe Total	0.7449	0.6420	2.0513	0.5722	0.3854	
Fe (n,el)	0.7497	0.7334	1.0051	0.7305	0.4007	

5.4.4. Discharged Waste

In planning for recycle or disposal, the waste handling engineer will need to know some key parameters of the fuel being discharged. As this topic tends more toward equilibrium discharged fuel, the results here will be restricted to the ABTR equilibrium model. The engineer will need to know the EOC decay heat associated with the fuel as it is coming out of the core for recycle and the decay heat of the fuel being discharged for disposal. In performing either recycling or repository analysis, isotopics are also of great importance so the discharge isotopic uncertainties are also given. Finally for the engineers designing the waste repository, decay heat integrals up to 10,000 years are given. All values given represent one third of the total core's content of material, which is the fraction of the core discharged each cycle. These parameters for ABTR equilibrium are given in Table 5.41 and Table 5.42.

Table 5.41 : Posteriori uncertainties on waste parameters for ABTR-EQ, 1 of 2.

Parameter	A priori	ZPPR-15B	ZPPR w/ TRU	TRU v. 1	TRU v. 2	TRU v. 3
EOC Decay Heat, Start-Up Core	**1.8201**	*0.2538*	*0.2229*	*0.2240*	*0.5587*	*0.2332*
EOC Decay Heat	**1.5558**	*0.2214*	*0.1689*	*0.1747*	*0.4190*	*0.1774*
DIS Decay Heat	**35.4703**	*11.9937*	*11.6432*	*11.5928*	*16.9972*	*11.8767*
DIS U-235 Mass	**7.3322**	*1.6387*	*1.6271*	*1.5917*	*2.4404*	*1.6582*
DIS U-238 Mass	**10.0496**	*2.5283*	*2.4564*	*2.4290*	*3.4398*	*2.4873*
DIS NP237 Mass	**73.4646**	*21.5153*	*20.8677*	*19.7432*	*29.6490*	*20.9429*
DIS PU238 Mass	**21.4872**	*8.0331*	*7.4756*	*7.4324*	*8.2935*	*7.4042*
DIS PU239 Mass	**16.8644**	*4.1480*	*4.1336*	*3.9326*	*6.1478*	*4.1642*
DIS PU240 Mass	**31.8332**	*7.9313*	*7.7881*	*7.5809*	*11.2411*	*7.8951*
DIS PU241 Mass	**35.1597**	*7.3207*	*7.1907*	*7.3005*	*10.3487*	*7.3476*
DIS PU242 Mass	**80.3409**	*18.2240*	*18.0660*	*17.7664*	*26.7642*	*18.4156*
DIS AM241 Mass	**44.2526**	*11.0456*	*10.6863*	*10.6234*	*14.5373*	*10.8017*
DIS AM242 Mass	**48.9414**	*14.4000*	*11.7559*	*11.5538*	*16.2167*	*11.8566*
DIS AM243 Mass	**99.3120**	*23.2499*	*22.7251*	*22.2212*	*33.9221*	*23.1592*
DIS CM242 Mass	**38.2103**	*8.7162*	*8.4991*	*8.5575*	*11.9726*	*8.6520*
DIS CM244 Mass	**118.1987**	*28.1601*	*27.0416*	*26.3283*	*40.7080*	*27.5602*
DIS CM245 Mass	**140.3874**	*37.7136*	*32.1599*	*31.1981*	*48.4420*	*32.7567*
Heat Integral, 100 y	**59.0669**	15.0337	16.5331	14.0853	20.3304	14.5383
Heat Integral, 500 y	**46.1908**	11.7332	14.2543	11.0505	15.6385	11.3404
Heat Integral, 1000 y	**44.2799**	11.0959	12.9734	10.4835	14.9118	10.7624
Heat Integral, 1500 y	**43.4953**	10.8423	12.2519	10.2533	14.6535	10.5366
Heat Integral, 2500 y	**42.6915**	10.6081	11.3401	10.0300	14.4422	10.3280
Heat Integral, 3500 y	**42.2015**	10.4775	10.7413	9.9002	14.3338	10.2108
Heat Integral, 5000 y	**41.6755**	10.3410	10.1407	9.7638	14.2183	10.0877
Heat Integral, 10000 y	**40.5924**	10.0622	9.2045	9.4887	13.9521	9.8322

Table 5.42 : Posteriori uncertainties for waste parameters for ABTR-EQ, 2 of 2.

Parameter	ZPPR-SNF	TRU v. 1-B	TRU v. 2-B	TRU v. 1-C	ZPPR-ABTR
EOC Decay Heat, Start-Up Core	*0.2399*	*0.2103*	*0.6476*	*0.1782*	*0.1268*
EOC Decay Heat	*0.1801*	*0.1684*	*0.4951*	*0.1449*	*0.1010*
DIS Decay Heat	*11.8948*	*11.2013*	*19.0253*	*10.5602*	*9.7839*
DIS U-235 Mass	*1.6638*	*1.5182*	*2.7316*	*1.4215*	*1.3545*
DIS U-238 Mass	*2.4979*	*2.3517*	*3.8139*	*2.2391*	*2.1127*
DIS NP237 Mass	*20.9321*	*18.5942*	*32.5455*	*17.7161*	*17.4563*
DIS PU238 Mass	*7.4655*	*7.3588*	*8.7031*	*7.2844*	*7.2009*
DIS PU239 Mass	*4.1603*	*3.7038*	*6.8349*	*3.4742*	*3.3276*
DIS PU240 Mass	*7.9256*	*7.2500*	*12.4761*	*6.8610*	*6.5082*
DIS PU241 Mass	*7.3614*	*7.1399*	*11.6534*	*6.7463*	*6.2526*
DIS PU242 Mass	*18.4196*	*17.0233*	*29.9116*	*15.9980*	*14.8469*
DIS AM241 Mass	*10.8527*	*10.3602*	*16.0651*	*9.9242*	*9.3773*
DIS AM242 Mass	*11.9307*	*11.2002*	*17.8911*	*10.7051*	*10.2766*
DIS AM243 Mass	*23.1519*	*21.2021*	*37.9141*	*19.8831*	*18.4942*
DIS CM242 Mass	*8.6751*	*8.3508*	*13.3748*	*7.9344*	*7.3956*
DIS CM244 Mass	*27.5419*	*25.0293*	*45.5140*	*23.4171*	*21.8197*
DIS CM245 Mass	*32.7413*	*29.5971*	*54.1122*	*27.6858*	*25.8998*
Heat Integral, 100 y	14.5623	13.5497	22.5241	12.8518	12.1340
Heat Integral, 500 y	11.3701	10.6798	17.3089	10.1634	9.6152
Heat Integral, 1000 y	10.7907	10.1286	16.5269	9.6294	9.0990
Heat Integral, 1500 y	10.5638	9.8985	16.2513	9.4033	8.8812
Heat Integral, 2500 y	10.3536	9.6680	16.0269	9.1740	8.6623
Heat Integral, 3500 y	10.2354	9.5311	15.9121	9.0369	8.5325
Heat Integral, 5000 y	10.1111	9.3873	15.7890	8.8931	8.3966
Heat Integral, 10000 y	9.8533	9.1020	15.5016	8.6106	8.1300

5.4.5. Minor Actinide Conversion

Finally, one of the main purposes of having a burner reactor is to transmute minor actinides into short lived capture daughters or short lived fission products. To examine this property the engineer will first look at conversion ratio and then also at the individual fission and capture reaction rates of the minor actinides. The adaption results for ABTR start-up are given in Table 5.43 and Table 5.44, and the results for ABTR equlibrium are in Table 5.45 and Table 5.46.

Table 5.43 : Posteriori uncertainties for conversion parameters in ABTR-SU, 1 of 2.

Parameter	A priori	ZPPR-15B	ZPPR w/ TRU	TRU v. 1	TRU v. 2	TRU v. 3
Conversion Ratio	**2.0303**	*0.2853*	*0.2838*	*0.3140*	*0.4178*	*0.2929*
Np-237 Capture	**3.0851**	2.4887	0.5459	0.5555	0.6802	0.5381
Pu-238 Capture	**11.8061**	0.8000	0.7734	0.7852	1.4999	0.7925
Pu-239 Capture	**4.6378**	0.5693	0.5650	0.5976	1.2132	0.5917
Pu-240 Capture	**10.9878**	0.5046	0.4994	0.5243	0.7612	0.5051
Pu-241 Capture	**10.8240**	0.6563	0.6530	0.6426	2.4842	0.6830
Pu-242 Capture	**19.7742**	1.3819	1.3710	1.2887	2.7110	1.3424
Am-241 Capture	**4.7001**	0.5650	0.5621	0.5676	1.3187	0.5796
Am-242m Capture	**14.2233**	13.9603	0.8920	0.8514	3.4397	0.9001
Am-243 Capture	**5.1920**	4.2171	1.4001	1.3524	2.1409	1.4158
Cm-242 Capture	**15.6376**	15.2430	0.9852	0.9241	3.4184	0.9961
Cm-244 Capture	**14.0488**	13.9150	0.7161	0.7173	2.1349	0.7425
Cm-245 Capture	**12.3336**	12.1623	0.7128	0.7000	2.4366	0.7388
Np-237 Fission	**6.2319**	6.1256	0.5722	0.6138	0.7968	0.5897
Pu-238 Fission	**13.1966**	1.0217	0.9992	1.0918	2.5890	1.0856
Pu-239 Fission	**0.5575**	0.2080	0.2049	0.1913	0.2183	0.1921
Pu-240 Fission	**3.9874**	0.4242	0.4218	0.4655	0.8249	0.4517
Pu-241 Fission	**11.1955**	0.9418	0.9409	1.0833	2.1127	1.0234
Pu-242 Fission	**16.1724**	0.7599	0.7583	0.9143	1.5414	0.8383
Am-241 Fission	**8.2289**	0.4587	0.4549	0.4777	1.0562	0.4865
Am-242m Fission	**12.0382**	11.9057	0.9139	0.9473	2.7625	0.9804
Am-243 Fission	**6.6916**	6.0525	0.7254	0.7774	1.5149	0.7745
Cm-242 Fission	**30.1371**	29.9474	0.7334	0.6677	1.9726	0.7193
Cm-244 Fission	**39.6675**	39.6009	0.7402	0.7623	2.2856	0.7936
Cm-245 Fission	**31.8290**	31.7520	0.8046	0.8329	2.6135	0.8635

Table 5.44 : Posteriori uncertainties for conversion parameters in ABTR-SU, 2 of 2.

Parameter	ZPPR-SNF	TRU v. 1-B	TRU v. 2-B	TRU v. 1-C	ZPPR-ABTR
Conversion Ratio	*0.2877*	*0.3209*	*0.4670*	*0.2856*	*0.3180*
Np-237 Capture	0.5443	0.5548	0.7329	0.5207	0.5553
Pu-238 Capture	0.8060	0.7534	1.7410	0.6748	0.5786
Pu-239 Capture	0.6016	0.5802	1.4368	0.5037	0.5022
Pu-240 Capture	0.5066	0.5238	0.8710	0.4711	0.4731
Pu-241 Capture	0.7035	0.6033	3.2903	0.5168	0.4236
Pu-242 Capture	1.3970	1.2332	3.1778	1.1689	1.1337
Am-241 Capture	0.5940	0.5425	1.5423	0.4714	0.4065
Am-242m Capture	0.9317	0.8103	4.2554	0.7346	0.7652
Am-243 Capture	1.4446	1.2869	2.2951	1.1851	0.8665
Cm-242 Capture	1.0332	0.8776	4.0972	0.8077	0.7448
Cm-244 Capture	0.7618	0.6764	2.6973	0.5891	0.5105
Cm-245 Capture	0.7659	0.6545	3.0980	0.5626	0.5230
Np-237 Fission	0.5758	0.6316	0.9321	0.5826	0.5718
Pu-238 Fission	1.0726	1.0513	3.3930	0.8863	0.6989
Pu-239 Fission	0.1945	0.1918	0.2304	0.1876	0.1629
Pu-240 Fission	0.4359	0.4632	1.0292	0.4022	0.3752
Pu-241 Fission	0.9796	1.0621	2.6129	0.8771	0.6336
Pu-242 Fission	0.7881	0.9382	2.0346	0.7962	0.7051
Am-241 Fission	0.4696	0.4705	1.4144	0.4157	0.4274
Am-242m Fission	0.9934	0.8936	3.4615	0.7461	0.5312
Am-243 Fission	0.7426	0.7702	1.9694	0.6848	0.6422
Cm-242 Fission	0.7571	0.6410	2.7082	0.5626	0.5731
Cm-244 Fission	0.7932	0.7373	3.1897	0.6251	0.5487
Cm-245 Fission	0.8771	0.7828	3.3988	0.6518	0.4669

Table 5.45 : Posteriori uncertainties for conversion parameters in ABTR-EQ, 1 of 2.

Parameter	A priori	ZPPR-15B	ZPPR w/ TRU	TRU v. 1	TRU v. 2	TRU v. 3
Conversion Ratio	**2.2458**	*0.2845*	*0.2831*	*0.3160*	*0.4380*	*0.2919*
Np-237 Capture	**3.0616**	2.3741	0.5060	0.5216	0.6604	0.5017
Pu-238 Capture	**11.9504**	0.7607	0.7275	0.7292	1.5970	0.7560
Pu-239 Capture	**4.9738**	0.7286	0.6921	0.7103	1.4203	0.7114
Pu-240 Capture	**11.4211**	0.5622	0.5163	0.5546	0.8098	0.5295
Pu-241 Capture	**11.3481**	0.8220	0.7897	0.7449	2.8499	0.8145
Pu-242 Capture	**21.0632**	0.9014	0.8698	0.8258	2.6728	0.8931
Am-241 Capture	**4.8517**	0.7191	0.6856	0.6622	1.5558	0.6999
Am-242m Capture	**14.3345**	14.1304	1.0940	0.9919	4.2856	1.0895
Am-243 Capture	**4.6468**	4.2215	1.4146	1.3626	2.2422	1.4446
Cm-242 Capture	**16.6336**	16.2588	1.2454	1.1207	4.2093	1.2415
Cm-244 Capture	**14.4697**	14.3445	0.7920	0.7690	2.4496	0.8194
Cm-245 Capture	**12.1820**	12.0267	0.8234	0.7761	2.7597	0.8483
Np-237 Fission	**6.1865**	6.0836	0.4930	0.5389	0.7267	0.5138
Pu-238 Fission	**13.0457**	0.9430	0.9209	1.0124	2.5689	1.0145
Pu-239 Fission	**1.2048**	0.3287	0.2569	0.2482	0.3145	0.2502
Pu-240 Fission	**3.6882**	0.4663	0.4257	0.4581	0.7916	0.4507
Pu-241 Fission	**10.8653**	1.0504	1.0289	1.1484	2.2211	1.1104
Pu-242 Fission	**15.8698**	0.7876	0.7643	0.9123	1.5185	0.8428
Am-241 Fission	**8.1269**	0.5481	0.5169	0.5185	1.0956	0.5382
Am-242m Fission	**12.2534**	12.1579	1.0744	1.0615	3.0963	1.1381
Am-243 Fission	**6.2131**	6.0110	0.6611	0.7220	1.4726	0.7237
Cm-242 Fission	**30.3575**	30.1738	0.8233	0.7137	2.0723	0.7845
Cm-244 Fission	**39.4914**	39.4254	0.7091	0.7309	2.2645	0.7634
Cm-245 Fission	**32.1604**	32.0846	0.8988	0.8991	2.8045	0.9551

Table 5.46 : Posteriori uncertainties for conversion parameters in ABTR-EQ, 2 of 2.

Parameter	ZPPR-SNF	TRU v. 1-B	TRU v. 2-B	TRU v. 1-C	ZPPR-ABTR
Conversion Ratio	*0.2877*	*0.3217*	*0.4940*	*0.2852*	*0.2535*
Np-237 Capture	0.5075	0.5202	0.7237	0.4826	0.3713
Pu-238 Capture	0.7719	0.6828	1.8730	0.5921	0.3459
Pu-239 Capture	0.7284	0.6839	1.6644	0.6035	0.4048
Pu-240 Capture	0.5262	0.5554	0.9398	0.4965	0.3460
Pu-241 Capture	0.8467	0.6898	3.7103	0.5987	0.3593
Pu-242 Capture	0.9273	0.7583	3.2722	0.6634	0.4087
Am-241 Capture	0.7235	0.6226	1.7909	0.5463	0.3329
Am-242m Capture	1.1426	0.9280	5.1955	0.8536	0.5220
Am-243 Capture	1.4704	1.2828	2.4080	1.1676	0.6850
Cm-242 Capture	1.2994	1.0518	4.9561	0.9866	0.5312
Cm-244 Capture	0.8472	0.7108	3.0575	0.6159	0.3819
Cm-245 Capture	0.8854	0.7119	3.4507	0.6150	0.3849
Np-237 Fission	0.4977	0.5574	0.8704	0.5011	0.4163
Pu-238 Fission	1.0054	0.9632	3.3800	0.7865	0.5545
Pu-239 Fission	0.2498	0.2498	0.3541	0.2407	0.1708
Pu-240 Fission	0.4383	0.4532	0.9818	0.3973	0.3165
Pu-241 Fission	1.0657	1.1116	2.7117	0.9264	0.6050
Pu-242 Fission	0.7936	0.9339	1.9995	0.7959	0.6585
Am-241 Fission	0.5296	0.5052	1.4518	0.4540	0.3389
Am-242m Fission	1.1642	0.9828	3.8185	0.8264	0.4799
Am-243 Fission	0.6846	0.7119	1.9388	0.6177	0.4764
Cm-242 Fission	0.8471	0.6797	2.8162	0.6013	0.4625
Cm-244 Fission	0.7639	0.7067	3.1727	0.5928	0.4933
Cm-245 Fission	0.9780	0.8318	3.6020	0.6938	0.4354

5.4.6. Experiment Choice for Design Concept

The exercise seen in this section served to demonstrate that the choice of design concept, here the ABTR start-up or ABTR equilibrium core, and the set of attributes and responses of interest tend to affect what type of experiment is best suited for reducing uncertainties on those attributes and responses. Therefore it is in the interest of designers to have a way to optimize both the experiment and the design to best satisfy the desired limits on the responses. The final section of this chapter presents the results of the optimization

method developed in this work. The demonstration of this method selected the ABTR start-up core for optimization and chose a set of responses, based on a set of attributes, which reflect reactor safety and economics. The ABTR was then optimized around a chosen set of design specifications (decision variables) for specified values of uncertainty in the attributes. A ZPPR experiment is then optimized around a chosen set of ZPPR design specifications (decision variables) to best reduce the uncertainty on the ABTR attributes so as to allow for the optimal design specifications for the ATBR.

5.5. Optimized ZPPR Experiment and ABTR Start-up Core

The previous sections have served to establish the results of the preliminary, or 0th generation, of using ZPPR experiments to reduce the uncertainty on ABTR designs. The data gained from each of those preliminary ZPPR perturbations was shown to reduce the posteriori uncertainty on key attributes and responses of the ABTR start-up and equilibrium cores. The reader can see from these sections that indeed using the ZPPR platform for integral experiments and assimilating those results will reduce the posteriori uncertainty on the ABTR.

This section presents the capstone of this study. The optimization method developed in this work evaluated numerous ZPPR experiment perturbations, collecting the criticality and reaction rate data from each, and then assimilating that data to reduce the a priori uncertainty on the cross sections input to the ABTR to some significantly improved posteriori value. These posteriori values were then used to compute posteriori uncertainties for ABTR on the attributes of EOC k-effective, neutron fluence, void worth, Doppler coefficient, axial expansion coefficient and radial expansion coefficient. From these values the posteriori uncertainties on the design responses of the three Wade-Fujita safety parameters, cycle length (determined by linear change with burnup in k-effective), and the discharge burnup, which was assumed to have the same uncertainty as fluence since power was invariant and uncertainty on the primary fissioning isotope (Pu-239) is very low, were also determined and used to check the design limits and apply necessary penalties. Having values of the posteriori uncertainties allowed the ABTR design specifications to be altered to reach an optimized design. The values of expected cycle length, inner core TRU enrichment,

outer core TRU enrichment, middle core TRU enrichment, boron concentration in control assemblies, and sodium content relative to fuel content for the ABTR model were randomly perturbed by relative amounts until the simulated annealing algorithm reached an optimized ABTR start-up core. As this is a demonstration, rigorously relating these relative perturbations to physical quantities in the ABTR design space is beyond the scope of this work. It is noted that changing the relative boron concentration is analogous to changing the amount of control rods necessary for the core or enriching the boron in B^{10}. Likewise, changing the relative sodium loading is analogous to changing the size of the fuel rods. Perturbations were introduced in the REBUS models by manipulating the homogenized compositions' number densities to reflect the desired change.

The result of applying this optimization method is an optimized ZPPR experiment which produces an optimized ABTR start-up core. As indicated, with each ZPPR perturbation a posteriori ABTR optimization was also required. The ABTR optimization can be referred to as the inner optimization problem. Figure 5.1 shows the bounding ABTR results and a selection of samples, where each optimization began with an initial guess of 8E+6 for the objective function standard deviation, which thus set the 0^{th} generation temperature as well. The dataset "A priori" shows the cost savings (negative dollars relative to the original ARN ABTR design) objective function of the ABTR as optimized with the a priori uncertainty information and optimizing over the design specifications listed above. The dataset "0 Uncer" is meant as a bounding set which shows the optimized value if no uncertainty is applied to the responses and therefore there are no penalties. The optimized objective function values are meant to be bounding and all of the posteriori optimizations are

to fall between these two values. Three trial ABTR posteriori optimizations are shown for example (ZPPR_1_2, ZPPR_3_3, and ZPPR_6_2). Note these are not the same subset of ZPPR trials that other results have been shown for. These were chosen because they were not necessarily the best results and thus show the distribution of posteriori ABTR designs possible due to different experiments. Each objective function data point marks a SA generation (i.e. Markov chain at a constant annealing temperature) and each generation consists of forty ABTR perturbations or five ABTR acceptances, whichever occurred first. This resulted in six executions of REBUS for each ABTR sample (one nominal and five perturbed cases to calculate the various reactivity coefficients). It is typical for the simulated annealing algorithm to have a large distribution of objective function values in early generations and progressively more narrow ranges as a solution is approached. The data presented here is averaged for clarity.

Figure 5.2 shows the progression of the ZPPR optimization cooling algorithm with penalty multipliers included, which is the overall optimization problem. Plotted is the overall objective function, which is the net cost penalty of the optimized ABTR design including the cost penalty of performing the experiment. Now the net cost is measured with respect to the a priori optimized ABTR design specifications and the ZPPR experiments performed. Negative values indicate savings. The axis has been scaled to match Figure 5.1 for comparison. Also plotted is the cost difference for each successive generation of ABTR designs. The span between each of the two points is the cost space occupied by penalties and experiment cost. The survey, or 0^{th}, generation was used to initialize the annealing temperature and six additional generations of ZPPR perturbations were analyzed following

that. Each generation is limited to five ZPPR experiment perturbations, mainly due to the computational time required to analyze each, including each associated inner optimization. Table 5.47 and Figure 5.4 describe the optimized ZPPR experimental setup including cost. Red X's indicate the location of detectors. Table 5.48 shows the ZPPR uncertainties for the optimized experiment, as well as the nominal values for selected integral parameters.

The corresponding optimized ABTR start-up core is described in terms of the relative changes to the six design specifications used as decision variables in the ABTR optimization (Table 5.49). This table also shows the penalty cost and final reactor cost. The changes are relative to the original values in the model provided from Argonne National Laboratory. Table 5.49 also presents the a priori optimized ABTR design specifications for comparison. Its values are more representative since the a priori and posteriori ABTR design specifications are being determined using the same objective function and constraints, which is not the case for the ANL design specifications. The rightmost column shows the percent change of the posteriori optimized ABTR relative to the a priori optimized ABTR. Table 5.50 shows the representativity of the optimized ZPPR experiment to its associated optimized ABTR design. Table 5.51 shows the nominal values, and a priori and posteriori uncertainties on many of the attributes and observables of the optimized ABTR, including those attributes used in the optimization. Finally, Table 5.52 shows the nominal and a priori and posteriori values of the design responses. All design limits were met with nominal values and all were met within 95% probability except for the second Wade-Fujita safety parameter. Appendix C describes each of the ZPPR perturbations examined and Appendix D shows further, select adaption results.

Two aspects of these results will immediately catch the reader's attention and are addressed now. First, the Markov chains associated with optimizing the ZPPR for each ZPPR generation are indeed short, so the question of whether each chain reached thermal equilibrium may be posed. Figure 5.3 shows the progressive standard deviation of the acceptances for each chain. All five perturbations were accepted during the first and second generations, and these can be seen trending toward equilibrium. In the third generation there were only four acceptances so the chain is one value shorter but still shows a trend toward equilibrium. The fourth generation had only two acceptances so there is only a single value for the standard deviation, and then only a measure of the average distance between the two accepted values. The fifth generation had only one acceptance, so by definition the standard deviation was 0. The sixth and final generation have 0 acceptances and the algorithm was stopped. Note that the number of acceptances is, as expected, less than the number of perturbations and that the acceptance ratio, also as expected, decreased to 0 as the algorithm progressed. Second, one will notice a relatively smooth behavior of the overall objective function's annealing results. As discussed in Section 3.6.4, due to computational limitations further simplifications and restrictions had to be imposed on the possible feasibility space of ZPPR experiments. As can be seen in Appendix C, this resulted in a series of 30 ZPPR perturbations that were chosen to span the range of possible ZPPR configurations within these simplified bounds of Section 3.6.4. By not being truly randomly selected, climbing out of local minima is forcibly avoided which accounts for the smooth appearance of Figure 5.2.

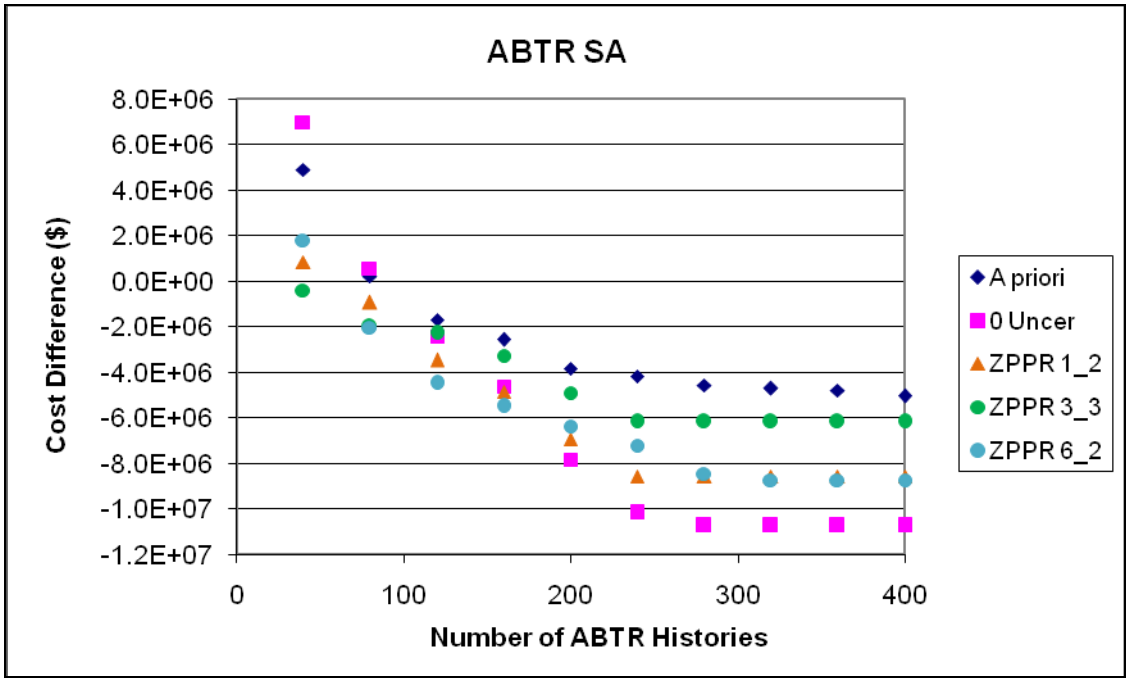

Figure 5.1 : Bounding and example inner ABTR optimizations.

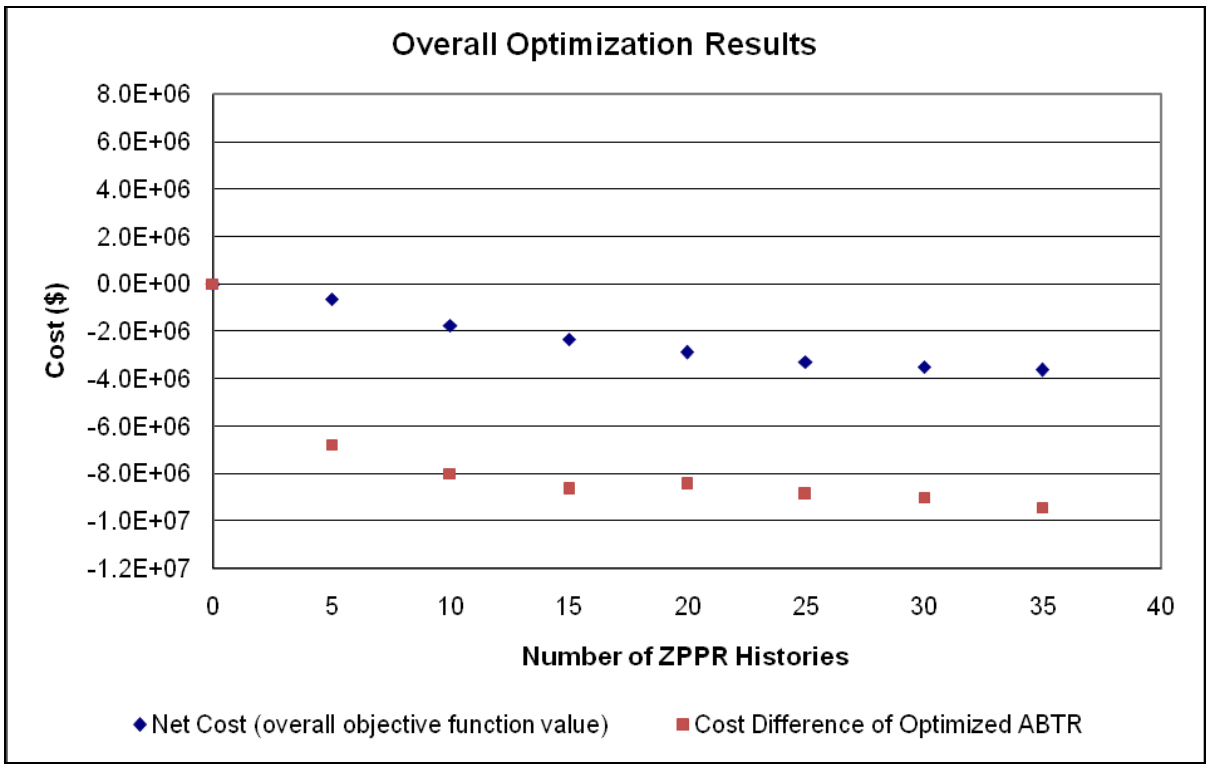

Figure 5.2 : Overall optimization of ZPPR experiment and ABTR design.

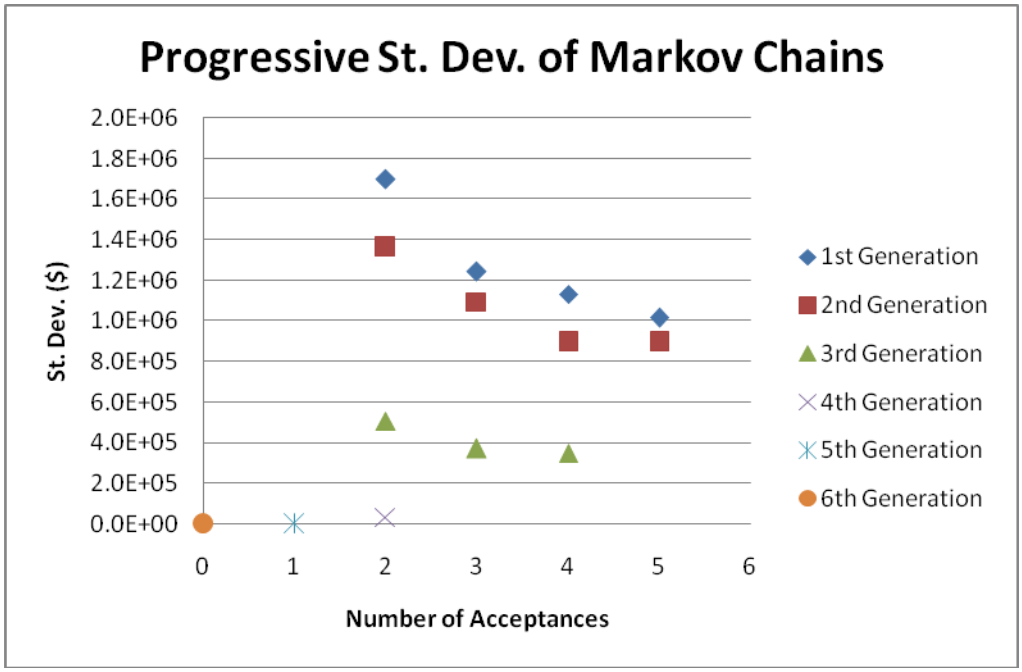

Figure 5.3 : Progressive standard deviation of the ZPPR Markov chains, by generation.

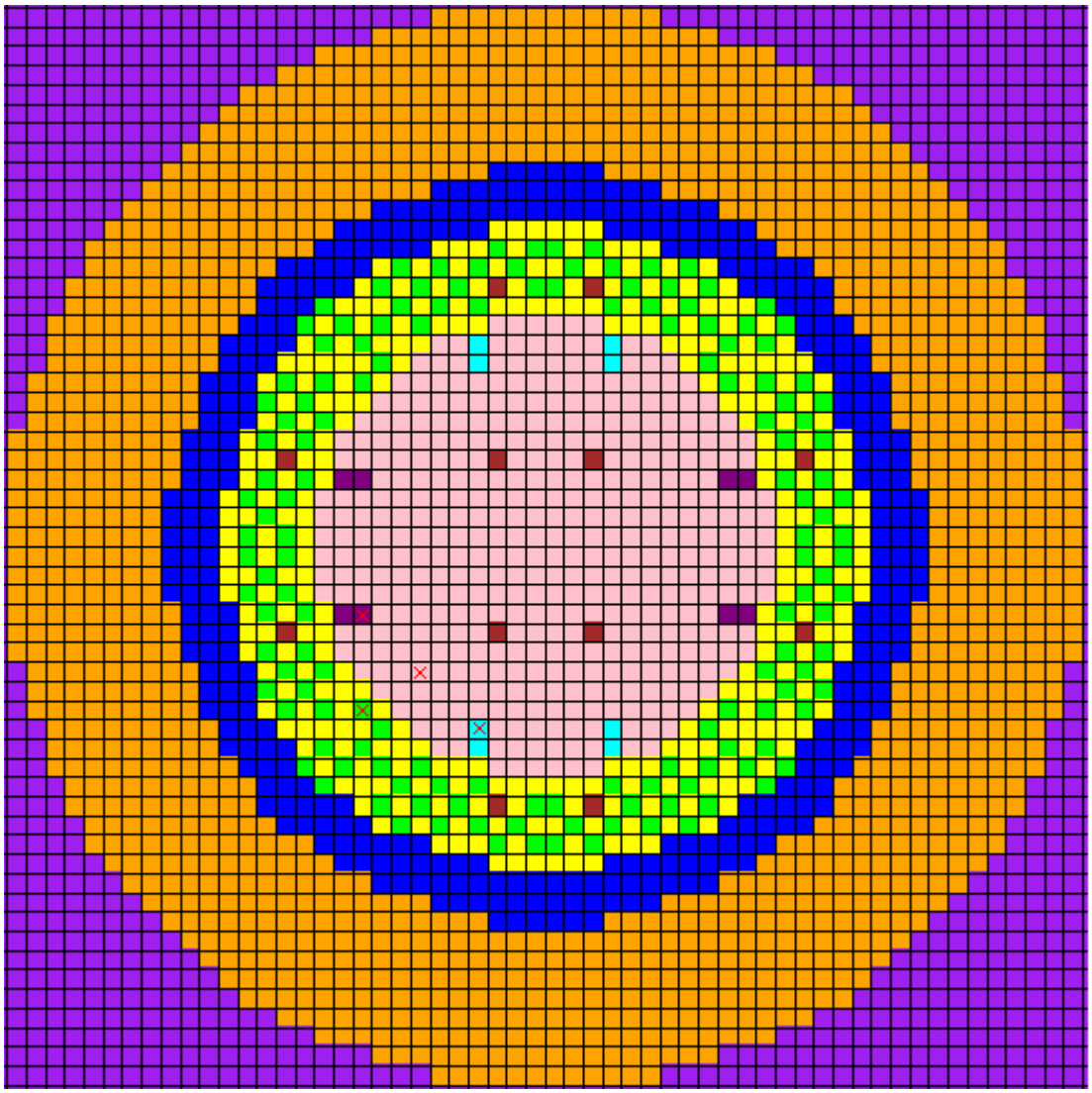

Figure 5.4 : Optimized ZPPR experiment (ZPPR_5_3) in full core.

Table 5.47 : Design specifications of ZPPR_5_3.

Design Specification	Value
Number of SNF Drawers	8
Location of SNF Drawers*	(19,25), (18,25)
Number of TRU Drawers	8
Location of TRU Drawers*	(25,19), (25,18)
Number of Detectors	4
Location of Detectors	(22,22), (19,20), (19,25), (25,19)
Experiment Cost	$740,712

*There are four quarter core symmetric locations.

Table 5.48 : Optimized ZPPR perturbations uncertainties.

Parameter	Nominal Value	Uncertainty
k-eff, EOC	0.994264692	0.8645
Peak Fluence (n/cm^2)	1.70048E+07	1.0194
Peaking Factor	2.00209	0.3786
Peak Flux (n/cm^2-s)	7356.83	0.8445
Peak Power Density (W/cm^3)	7.49977E-10	0.6427
Conversion Ratio	0.716465	2.0308

Reaction	Uncertainty	Reaction	Uncertainty
Fe Total	4.1053	Fe (n,el)	4.8865
Na-23 Total	1.7351	Na-23 (n,el)	5.1797
U-235 Capture	1.5578	U-235 Fission	1.1398
U-238 Capture	1.6592	U-238 Fission	3.8995
Np-237 Capture	3.5561	Np-237 Fission	6.3003
Pu-238 Capture	12.1390	Pu-238 Fission	11.5501
Pu-239 Capture	4.1375	Pu-239 Fission	0.8130
Pu-240 Capture	9.4223	Pu-240 Fission	4.3329
Pu-241 Capture	8.2798	Pu-241 Fission	8.2798
Pu-242 Capture	22.2577	Pu-242 Fission	16.3306
Am-241 Capture	4.8020	Am-241 Fission	8.2381
Am-242m Capture	14.5471	Am-242m Fission	11.3688
Am-243 Capture	4.9685	Am-243 Fission	6.5421
Cm-242 Capture	12.5820	Cm-242 Fission	28.5474
Cm-244 Capture	12.6736	Cm-244 Fission	40.3037
Cm-245 Capture	10.7500	Cm-245 Fission	29.2795

Table 5.49 : Optimized ABTR design specifications and cost.

Design Specification	Relative Scaling of Posteriori Optimized Design	Relative Scaling of A Priori Optimized Design	% Difference
Expected Cycle Length	0.99258	1.00906	-1.63
Inner Core Pu-239 Loading	0.96336	0.98276	-1.97
Outer Core Pu-239 Loading	1.03739	1.00214	3.52
Middle Core TRU Loading	0.96764	0.97895	-1.16
Boron Concentration	1.00621	0.99071	1.56
Sodium Concentration	1.00471	0.97566	2.98
Penalty ($)	392,950	1,133,000	---
Cost ($)	1,490,563,600	1,494,951,800	---

Table 5.50 : Optimized ZPPR representativity to optimized ABTR.

k-eff, EOC	0.91501	Cm-242 Capture	0.94796
Peak Fluence (n/cm^2)	0.80719	Cm-244 Capture	0.99028
Peaking Factor	0.38786	Cm-245 Capture	0.93958
Peak Flux (n/cm^2-s)	0.70784	Fe (n,el)	0.95337
Peak Power Density (W/cm^3)	0.30422	Na-23 (n,el)	0.93556
Conversion Ratio	0.99286	U-235 Fission	0.90533
Fe Total	0.95061	U-238 Fission	0.91657
Na-23 Total	0.87419	Np-237 Fission	0.99475
U-235 Capture	0.96650	Pu-238 Fission	0.99295
U-238 Capture	0.98108	Pu-239 Fission	0.79223
Np-237 Capture	0.97934	Pu-240 Fission	0.98796
Pu-238 Capture	0.98755	Pu-241 Fission	0.98494
Pu-239 Capture	0.98834	Pu-242 Fission	0.98597
Pu-240 Capture	0.99385	Am-241 Fission	0.99690
Pu-241 Capture	0.98508	Am-242m Fission	0.98450
Pu-242 Capture	0.98208	Am-243 Fission	0.98412
Am-241 Capture	0.97843	Cm-242 Fission	0.99437
Am-242m Capture	0.95494	Cm-244 Fission	0.99910
Am-243 Capture	0.88539	Cm-245 Fission	0.99608

Table 5.51 : Optimized ABTR attributes uncertainty using data from ZPPR_5_3.

Attributes	Nominal	A Priori	Posteriori
k-eff, EOC	1.017999352	**0.792**	0.1448
Void ($)	1.8513	**16.9421**	7.6129
Doppler ($/K)	-8.592988E-04	**3.3897**	1.5059
Peak Fluence (n/cm^2)	2.950950E+22	**0.8677**	0.4758
Peaking Factor	1.5463	**0.476**	0.3606
Peak Flux (n/cm^2-s)	4.052050E+15	**0.9883**	0.4000
Peak Power Density (W/cm^3)	398.667	**0.4784**	0.3651
Conversion Ratio	0.550304	**2.0303**	0.2943
Axial Expansion Coeff. ($/C)	-5.836070E-04	**5.019**	2.9714
Radial Expansion Coeff. ($/C)	-7.100615E-03	**4.4571**	2.4312
EOC Decay Heat (W, 1/3 core)	7110.47	**1.8201**	0.3072
k-eff, BOC	1.003999201	**0.8042**	0.1426
Fe Total	3.067131E+11	**4.0119**	0.8581
Na-23 Total	1.426114E+10	**1.5533**	0.3896
U-238 Capture	4.706723E+12	**2.1331**	0.4156
U-235 Fission	5.647421E+10	**1.0189**	0.2846
U-238 Fission	1.213269E+12	**2.7973**	0.5515
Np-237 Fission	5.043978E+10	**6.2319**	0.6535
Pu-238 Fission	7.082039E+10	**13.1966**	1.2343
Pu-239 Fission	6.349173E+12	**0.5575**	0.2706
Pu-240 Fission	4.310251E+11	**3.9874**	0.4468
Pu-241 Fission	3.923926E+11	**11.1955**	1.1854
Pu-242 Fission	4.791604E+10	**16.1724**	0.8069
Am-241 Fission	4.906375E+10	**8.2289**	0.5453
Am-242m Fission	1.240164E+10	**12.0382**	1.7473
Am-243 Fission	8.161827E+09	**6.6916**	0.9559
Cm-242 Fission	1.042832E+09	**30.1371**	0.7193
Cm-244 Fission	3.868309E+09	**39.6675**	1.4575
Cm-245 Fission	1.546049E+09	**31.829**	1.8620

Table 5.52 : Optimized ABTR responses uncertainty using data from ZPPR_5_3.

Parameter	Nominal	A Priori	Posteriori
Wade-Fujita Parameter 1	0.1909	**22.3973**	11.1381
Wade-Fujita Parameter 2	1.0612	**29.8584**	14.9872
Wade-Fujita Parameter 3	-0.4021	**16.536**	9.8885
Burnup (MWD/MTHM)	7232.95	**0.8677**	0.4758
Cycle Length (Days)	119.1	**1.1201**	0.2048

6. Feasibility Analysis

The main body of this report concludes with a discussion on the feasibility of the concepts contained herein. When talking about an engineered system, feasibility can have many meanings. For this purpose it will be restricted to three topics: 1) cost of experiments, 2) quantifying benefits of improved data, and 3) ability to perform the experiment. Due to a large lack of nominal information, the first two topics, and partially the third, will be largely qualitative, with the quantitative portion being developed from the values in this work.

The cost of the experiments is difficult to estimate, therefore experimental cost values were developed for this work as discussed in section 3.6.3 and 3.6.4. The restart cost is estimated at $60 million to restart the program, which is currently in standby. A fixed cost of $300,000 cost for each experiment was assumed. This work also assumed, based on expert judgment, a fixed cost of $6,200 for operating fees for any one experiment. A fixed cost of $2,700 for each detector was assumed which allowed handling and data processing costs. There is also the cost of reprocessing to obtain the TRU material from spent LWR fuel to be considered; each SNF and TRU fuel drawer was assigned a cost of $1,184 and $51,780, respectively, based on the mass of reprocessed fuel in each drawer type. These assumptions were then assigned to each experiment. The ZPPR perturbations, excluding ZPPR-ABTR, had costs that range from $335,944 to $4,045,160 (Appendix C). The ZPPR-ABTR variation required reprocessed ABTR equilibrium fuel, which could only come from several years of ABTR operation and therefore the cost of that experiment would greatly exceed the reactor cost and it is judged infeasible.

The value of the experiments must exceed the cost of performing them for funding to become available either from the government or from a potential ABTR operator. For an experiment to be economically feasible, some agency would have to fund it because that agency sees it as worth the investment. Therefore the agency looking to fund the experiment must have a means of quantifying exactly how much benefit will be gained by the new data, i.e. how much will cost be reduced. Here cost is used very loosely. Cost could be monetary capital, operating costs, delays in construction, meeting regulatory compliance, safety requirements, or personnel requirements. Cost in this work has been gauged by change in margin allowing for a change in the design specifications. Each time an ABTR optimization was run with posteriori data assimilated from a ZPPR experiment, modifications were made to six design specifications. The reactor cost was determined by a monetary value assigned to each design specification and each penalty. The more negative the cost, the most savings were realized for the ABTR design. With a final optimized ABTR design that reduced the nominal cost by more than $9 million, the benefit of the experiment can exceed the cost of the experiment.

Even if the facilities were available, and even if funding were available for the experiment, the experiment of choice may not be possible due to limitations on materials and safety. As discussed in the introduction, plutonium fuel is available for ZPPR and small samples of minor actinides could be produced if necessary. Spent nuclear fuel from LWRs on the other hand is assumed to still be in its raw form, i.e. sitting in either dry or wet storage somewhere, with a very limited inventory of reprocessed material from past reprocessing. To create a SNF sample of fuel would require reprocessing of the LWR waste, which is

currently achievable in only limited capacities. Idaho National Lab does some reprocessing, primarily of fuel from Experimental Breeder Reactor II and the Savannah River Site does industrial scale defense waste processing, but not back into fuel forms. However both of these facilities are currently designed for the reprocessing of metal fuel (from EBR-II and naval vessels) and not for the ceramic fuel used in LWR power plants. SNF fuel forms for an experiment would have to be created on a laboratory scale. For the composition of the ABTR equilibrium core used in the ZPPR-ABTR variation, it does not even physically exist.

There is also the issue of radiological hazard of the fuel. Plutonium fuel can be handled safely in glove boxes but reprocessed LWR fuel would require more shielding. This aspect of the feasibility is easily calculated by knowing the fuel and/or core composition and associated specific activities. Following evaluation of the various versions of ZPPR analyzed, it was decided to examine the feasibility of physically assembling each experiment. Radioactivity, gamma radiation heating, total decay heat and radiotoxicity were examined for each individual fuel drawer type and for each whole ZPPR experiment of 1,784 trays. Note radiotoxicity in air is based on the unshielded values for the actinides in each composition. Table 6.1 gives the drawer type values and Table 6.2 gives the whole core values where the minimum and maximum values are highlighted and the ZPPR-ABTR is shown in red text.

Although activities seem high in all cases, a simple comparison with the gamma heating or an examination of the table of nuclides reveals that most of the radiation is alpha radiation which will effectively not make it out of the cladding material. Americium and plutonium isotopes are strong alpha emitters. It is seen that the SNF and TRU trays have gamma radiation about 1 and 0.5 orders of magnitude larger than the original trays,

respectively. In terms of the whole core, most ZPPR variations have decay heat 20% to 30% higher, respectively, and gamma radiation 40% to 50% higher, respectively. The unshielded radiotoxicity is about the same however. Therefore it is concluded that most ZPPR variations are feasible, but the trays will need to be assembled and transported in closed glove boxes, which were available in the ZPPR facility.

The ABTR mock-up seems physically impossible without a completely remote facility, however. The gamma radiation is two orders of magnitude higher than the original experiment and would therefore require sealed hot cells with very thick shielding. It appears possible for the fuel processing line at Idaho National Laboratory to handle the compositions for the ABTR mock-up, but this would require very specialized skills of the workforce and some infrastructure overhauling to switch from rod fuel to small plate fuel reprocessing. Needless to say, the radiotoxity is 20 times higher as well. The total decay heat is also two orders of magnitude higher which would require more than just air cooling of the facility. Compare 50-60 light bulbs in a large room to 5000+ light bulbs in the same space. While the ABTR mock-up would provide very useful data to assimilate, it is judged to not be safe from a worker's viewpoint to build this experiment in a facility such as ZPPR.

Alpha radiation will be stopped mostly by the cladding around the fuel plates and therefore the basic plutonium fuel drawers may be handled with limited exposure via face/hand/arm coverings such as gloves or the sliding window workstations at the ZPPR vault facility. The primary concern therefore is gamma radiation. Plutonium isotopes are the most energetic of the gammas that would be associated with ZPPR ranging from about 43 keV up to 340-380 keV. However these occur in very small amounts. The greater concern is

therefore the much more intense gamma sources of Am-241, Cm-242, and Cm-244. Am-241 gammas have energies from 14 keV up to 59.5 keV. Cm-244 have energies between 42 keV and 153 keV, and Cm-242 is the most limiting with energies between 44 keV and 160 keV. Decay data were taken from the Table of Nuclides and ENFD available from Brookhaven National Laboratory [42][43].

In conclusion, an experiment may be performed if the facilities are available, the cost is worth the benefit derived from new information, and the experiment is physically able to be constructed. Results show that indeed the benefit of the experiment can exceed the cost and that nearly all of the ZPPR perturbations examined in this work are feasible. The reader should recognize that the economic conclusions are based upon assumed costs used in this study, which may be unrealistic.

Table 6.1 : Radiation hazard from the worst single tray in a ZPPR experiment.

Reactor	Worst Single Tray			
	Ci	Gamma W	W	m^3 Air to Dilute
ZPPR-15B	1407.88	0.00524	4.07820	1.0468E+16
TRU 1-C	543.82	0.05480	18.46437	2.5725E+16
SNF	4914.93	0.01983	12.02702	2.6794E+16
ZPPR-ABTR	15931.54	0.15591	319.10644	1.7604E+17

Table 6.2 : Radiation hazard from the whole ZPPR core in an experiment.

Experiment	(Ci)	Gamma (W)	(W)	m^3 Air to Dilute
ZPPR-15B	1.67257E+06	6.22487	4844.92030	1.24358E+19
TRU 1, 2	1.66744E+06	7.89467	5370.52846	1.30916E+19
TRU 1 B, 1 C, 2 B	1.66232E+06	9.56447	5896.13662	1.37473E+19
TRU 3	1.65669E+06	9.54352	5879.82396	1.37054E+19
SNF	2.26769E+06	8.66138	6250.55245	1.54568E+19
ZPPR-ABTR	2.13027E+07	202.95124	430378.16488	2.23163E+20
ZPPR_1_1	1.87469E+06	7.05101	5324.33945	1.34707E+19
ZPPR_1_2	1.65976E+06	10.39938	6158.94070	1.40751E+19
ZPPR_1_3	1.65207E+06	12.90408	6947.35293	1.50587E+19
ZPPR_1_4	1.94207E+06	7.32640	5484.14584	1.38157E+19
ZPPR_1_5	1.85420E+06	13.73022	7426.77208	1.60936E+19
ZPPR_2_1	2.00945E+06	7.60178	5643.95222	1.41607E+19
ZPPR_2_2	2.21157E+06	8.42792	6123.37137	1.51956E+19
ZPPR_2_3	1.66232E+06	9.56447	5896.13662	1.37473E+19
ZPPR_2_4	2.20389E+06	10.93262	6911.78361	1.61792E+19
ZPPR_2_5	1.94079E+06	7.74385	5615.54788	1.39796E+19
ZPPR_3_1	1.63286E+06	19.16583	8918.38352	1.75177E+19
ZPPR_3_2	1.64054E+06	16.66113	8129.97129	1.65341E+19
ZPPR_3_3	1.64567E+06	14.99133	7604.36313	1.58784E+19
ZPPR_3_4	1.69601E+06	9.70216	5976.03981	1.39198E+19
ZPPR_3_5	1.77235E+06	7.05539	5216.03192	1.31172E+19
ZPPR_4_1	1.66232E+06	9.56447	5896.13662	1.37473E+19
ZPPR_4_2	1.65976E+06	10.39938	6158.94070	1.40751E+19
ZPPR_4_3	1.77235E+06	7.05539	5216.03192	1.31172E+19
ZPPR_4_4	1.65207E+06	12.90408	6947.35293	1.50587E+19
ZPPR_4_5	2.04313E+06	7.73947	5723.85541	1.43332E+19
ZPPR_5_1	1.87469E+06	7.05101	5324.33945	1.34707E+19
ZPPR_5_2	1.70241E+06	7.61491	5319.02961	1.31001E+19
ZPPR_5_3	1.73738E+06	7.33515	5267.53076	1.31087E+19
ZPPR_5_4	1.66232E+06	9.56447	5896.13662	1.37473E+19
ZPPR_5_5	1.76595E+06	9.14265	5873.04211	1.39369E+19
ZPPR_6_1	1.65976E+06	10.39938	6158.94070	1.40751E+19
ZPPR_6_2	1.65207E+06	12.90408	6947.35293	1.50587E+19
ZPPR_6_3	1.69601E+06	9.70216	5976.03981	1.39198E+19
ZPPR_6_4	1.77235E+06	7.05539	5216.03192	1.31172E+19
ZPPR_6_5	1.73738E+06	7.33515	5267.53076	1.31087E+19

7. Conclusions and Recommendations

The ZPPR-15B as built base model, with 15-energy group cross section data, created in the deterministic REBUS/DIF3D nodal diffusion code system has been verified. Comparison with original experimental results and with the same model created in the Monte Carlo transport code MCNP using continuous energy cross sections showed very good agreement between all three data sets. The values of k-effective and reaction rate ratios across the radius of the core mid-plane were used for this benchmarking process. This indicates the ability to reliably use REBUS for modeling this type of reactor. The REBUS model was also demonstrated to behave linearly over an expected range of perturbations and also that as perturbation size is reduced the model converges to the linear result. This verifies that the ESM method is applicable to this analysis.

An ESM uncertainty quantification analysis was conducted on the ZPPR 15B base model k-effective value given cross section covariance information. The model k-effective had uncertainty of about ~0.86%. An ESM uncertainty quantification analysis was also conducted on the reaction rate ratios used to benchmark the ZPPR 15B model, and these values were compared to the experimental uncertainties and the Monte Carlo sampling uncertainties from MCNP. U-235 fission ratio uncertainties were on the same scale as the experimental uncertainties, i.e. about 1-1.5%. U-238 fission and capture ratio uncertainties were about 2.5-3% due to cross sections, but only about 1-1.5% due to experimental uncertainties and Monte Carlo sampling. While overall the uncertainty is low for each of the reaction rate ratios compared to the benchmark ratios, the uncertainty in the U-238 reaction

rate ratios due to cross section data uncertainty was about twice as high as for experimental uncertainties, implying the capability to obtain more accurate nuclear data.

Prior to the demonstration of the optimization methodology, an additional nine preliminary, or 0^{th} generation, variations of the ZPPR were created, gradually changing the layout and composition of the core from the as built experiment to a mock-up of an equilibrium ABTR. This method simulated a potential range of fast critical experiments with which to obtain data to adapt the REBUS model's 15-group cross section library to better simulate the ABTR, albeit that the mock-up variation is not always physically possible due to lack of fuel and radiation hazard. Each ZPPR variation was analyzed using the ESM method to propagate cross section uncertainties into reaction rates and integral parameters of the core. The results of these analyses agree with expectations. The minor actinide reaction rates showed the highest uncertainties. Uranium and plutonium reaction rates, and thus also k-effective and power related parameters, showed low uncertainties because of very accurately known cross sections. Void worth, Doppler reactivity coefficient and conversion ratio showed uncertainties on the scale of 2–16% and iron and sodium reaction rate uncertainties were on the order of 4%. Not surprisingly, when each of the ABTR models were also subjected to the ESM analysis using the same input cross section covariance information, similar magnitudes of uncertainties were seen on the corresponding ABTR parameters. Additional integral parameters in ABTR were examined and shown to have comparable magnitudes of uncertainties. The exception is the discharge isotopics, decay heat, and long term heat integrals from the ABTR equilibrium fuel. The uncertainties on

these parameters were shown to be exceptionally large due to the repeated recycling and irradiating of minor actinides whose input cross sections were considerably uncertain.

Given the sensitivity-singular vector products calculated by the ESM method, the representativity of the ZPPR-15B variations to the ABTR start-up and equilibrium cores was then computed for reaction rates and several integral parameters. Pu-239 fission, related power parameters, and the Doppler reactivity coefficient were shown to have overall low representativity for all of the ZPPR models. The Pu-239 fission representativity was low because the cross section is so accurate that the reaction rate is sensitive only to other factors which affect the flux spectrum, and are thus more core dependent. Reaction rates with high uncertainties were shown have high representativity because their sensitivity comes from the cross sections associated with specific reaction rates making their representativity more core independent. The Doppler reactivity coefficient was expected to have a low representativity because it is quite difficult for a room temperature reactor to simulate the much higher temperature of a power reactor core. Posteriori uncertainty reduction in parameters with low representativity is expected to rely mainly on correlation with other parameters with higher representativity.

Adaptive simulation was performed to obtain posteriori covariance data for the ATBR parameters selected in this study. Only reaction rates, k-effective, void worth and Doppler reactivity coefficient were used for adaption from the ZPPR models because these are directly measurable values. The optimization demonstration further reduced this data set by removing the void worth and Doppler coefficient from the adaption. The ZPPR experiments were used assuming a variety of experimental errors, the best being 0% error

and the most realistic being 1% error plus fission product yield, decay constant, and eigenvalue uncertainties. The latter is assumed to be most realistic because the average reaction rate error reported for the original experiments was approximately 1% due to counting statistics, sample impurities, detector positioning and repeatability.

The adpation results proved to be very positive, indicating the potential for great uncertainty reduction in the observed parameters, especially the minor actinide reaction rates and long term decay heat integral. However, even with adaption to the best ZPPR variations, one of the safety parameters never met its 95% target probability of not exceeding limits. Average reaction rate uncertainties were all around reduced. Integral parameter unertainties were also favorably reduced although void worth and the Doppler, axial expansion and radial expansion coefficients uncertainties could use further improvement. Of the 0^{th} generation ZPPR variations examined it was concluded that for both the ABTR-SU and ABTR-EQ core, the TRU v. 2 and 2-B variations were the least favorable. These models lumped TRU samples into the inner core of the ZPPR and placed all of the detectors into those samples. This detector lumping lost spatial distribution information which proved necessary for a good adaption, even though the plutonium and uranium reactions occurring in the ZPPR core outside the TRU center lump had low uncertainty. For the ABTR-SU core the best 0^{th} generation ZPPR variations tended to be TRU v. 1-C or the ZPPR-ABTR no matter which group of parameters were of interest. For the ABTR-EQ core, short of being able to use ABTR-SU for adaption, the best 0^{th} generation ZPPR variations were also ZPPR-ABTR and TRU v. 1-C, but also once TRU v. 3 depending upon which group of parameters was of most interest. The obvious overall conclusion is that the best way to capture ABTR physics would

be to mock-up the ABTR core. The other conclusion, which is more important to the optimization method developed herein, is that the aspects of the core design that are of interest influence which experiment is best suited to reduce uncertainties on those aspects. Overall the best adaption option is to load TRU samples into the inner most potion of the ZPPR core, where they will experience the irradiation conditions most like the ABTR and use an amount of them substantial enough to affect operating physics as well. Another option would be to distribute those same TRU samples about the inner and outer cores (TRU v. 3). One key observation is to radially and axially distribute the detectors when recording reaction rate data, thus giving the necessary spatial information.

Given the positive results for the preliminary work, the experiment optimization methodology developed in this work was tested. The 0^{th} generation ZPPR variations were assigned experimental cost and the posteriori information they provided used to perform an optimization of the ABTR design using the simulated annealing algorithm. The 0^{th} generation served to initialize the simulated algorithm to solve the optimization problem. The inner ABTR optimization perturbed six key design specifications and observed key safety and performance responses based upon core attributes. The outer, or overall, optimization of the experiment proceeded over six additional generations of ZPPR perturbations, or 30 total histories, with each perturbation requiring a separate ABTR optimization run.

The ABTR was optimized using a priori uncertainties which produced an ATBR cost of $1,494,951,800. The various ZPPR experiments had calculated costs between $355,944 and $4,045,160. The overall optimization problem arrived at ZPPR variation ZPPR_5_3 as

the optimized experiment. This variation placed the minimum number of detectors in the core and placed eight 1 x 2 groups of SNF and TRU drawers (4 of each) around the core at the inner-core/outer-core interface. Here SNF composition fuel and plain minor actinide targets received neutron flux spectra that would be expected in any average position in the ABTR core making it an ideal location for samples. The relatively low number of detectors and test drawers kept costs low and also preserved the overall behavior of a plutonium fueled fast reactor core with only small amounts of reprocessed LWR fuel, in essence the ABTR start-up core. When compared to the a priori optimized ABTR, the resulting posteriori optimized ABTR using data assimilated from ZPPR_5_3 showed that for only minor changes in fuel rod design and amount of control material, the plutonium requirements of the inner core could be reduced 2.0% and the TRU requirements of the middle core could be reduced 1.2% in exchange for a 3.5% increase in outer core enrichment. The experiment cost $740,712 and resulted in a net savings (overall objective function value) of $3,647,488. So for about three-quarters of a million dollars for an experiment the sponsor would be able to save about $3.65 million. While this is only about a quarter of a percent of the ABTR cost, it is almost five times the cost of the experiment so the benefit of doing the experiment outweighs the cost. Note that this conclusion is based upon assumed cost data that may be shown to not be realistic. Further a change in the selected objective function could also change the results.

This demonstration shows the effectiveness of the methodology developed in this work. Preliminary work using experiments based on engineering judgment readily showed that the ZPPR platform had the potential to reduce posteriori uncertainties on the ABTR

design and thus allow for an optimization of ABTR. Using the optimization method developed, a simultaneous optimization of the experiment and the reactor design was completed. ZPPR_5_3 is specifically designed to allow for the design of the optimized ABTR core associated with it. The method demonstrates a logical, mathematical path to follow to optimize the experiment to fit an optimized reactor design concept. The final experiment balanced experimental cost and final ATBR cost to get the best net savings possible. The final experiment was also highly representative of the ABTR core as evidenced by the representativity factors calculated. This method therefore not only allowed for obtaining the greatest return on the investment in the experiment, but also preserved as expected an experiment that captured key physics needed for the ABTR design. This satisfies both economic and scientific desires for the experiment.

Finally, consideration was given to the feasibility for an experiment. An experiment must be physically possible and economically attractive if it is likely to be funded and conducted. The feasibility is limited by radiological safety and availability of the necessary facilities, since it has been shown that experiments can be designed that are economically attractive to perform in support of a reactor design concept and that indeed future experimentation would be beneficial to fast reactor design.

Future Generation IV fast reactors need more accurate information in order to more economically operate. Considerably more accurate information is needed for minor actinides reactions and affects, especially in burner-recycle type reactors which aim to progress to an all SNF equilibrium core. There is great potential for reducing these key uncertainties to improve Generation IV reactor operation. This work provided a methodology for optimizing

an experiment based on the designers objectives and chosen constraints. The experiment will be specifically designed to permit, via data assimilation, the reduction of required margin and thus the expansion of design space to allow for an optimized reactor concept based upon changes in the specifications chosen by the designer.

This method has the potential to become a powerful tool in the optimization of experiments that support nuclear designs. As such there is much room for future development of this methodology. In particular, it was seen that there is a lack of published, contemporary economic data for fast reactor design or for reprocessing. Monetary values developed for this work relied on relatively few sources, expert opinions, and engineering judgment. If Generation IV reactors are to become economically attractive, more work needs to be done on deeply analyzing their economics and fuel cycle necessary to fuel these reactors, and that work needs to be published for designers to have available to them.

A second very open area for future work is refining the design specifications and penalties applied in this work. Since this work was to demonstrate the methodology, only six general design specifications were perturbed and only by relative amounts. The penalties applied were developed on the most basic kinds of limits, e.g. safety parameter violations. Refining and expanding the design specifications and the penalty factors would make the method much more robust and potentially realize greater savings. The choice of decision variables and the development of penalties may also make the problem more design specific.

The method could also be adapted in future work to support a multi-experiment program optimization. The method demonstrated here optimized a single experiment primarily for neutronic considerations, but it is more common for a program of many

experiments, multi-physics in nature, to be conducted to support a reactor design. This method could be adapted to support the optimization of a program of multi-physics experiments to optimize a reactor design.

Finally, the methodology encountered issues with computational time requirements. Simulated annealing algorithms have the capability to be parallelized. Parallelization could be used to reduce run times and permit even more experiment variations to be analyzed. Improved economic information, decision variable and penalty refinements, and runtime improvements are only a few of the possibilities for the future study in this methodology and the potential to realize even greater savings and even better optimized experiments.

References

[1] LeSage, L. G., "An Overview of the Argonne National Laboratory Fast Critical Experiments 1963 – 1990," ANL-NT-175, Argonne National Lab, Argonne, IL, April 2001.

[2] Chang, Y. I., et. al., "Advanced Burner Test Reactor Preconceptual Design Report," Argonne National Laboraotry, Sept. 2006.

[3] Usachev, L.M., Bobkov, Y.G., "Mathematical Theory of Experiment and Generalized Perturbation Theory - An Effective Approach to Reactor Physics Investigations," INDC(CCP) - 33/L, IAEA, Vienna, 1973.

[4] Aliberti, G., Palmiotti, G., Salvatores, M., "Representativity Studies for Sodium and Gas-Cooled Reactors," Transactions of the American Nuclear Society, v. 95, 2006.

[5] Abdel-Khalik, H., "Adaptive Core Simulation," Doctoral Dissertation, Master of Science Thesis, North Carolina State University, 2002 and 2004.

[6] Abdel-Khalik, H., Turinsky, P., Jessee, M., "Efficient Subspace Methods-based Algorithms for Performing Sensitivity, Uncertainty, and Adaptive Simulation of Large-Scale Computational Models," Nuclear Science and Engineering, v. 159, n 3, July 2008

[7] Iqbal, M., et. al., "Adaptive Simulation for a Model of the ZPR6-7 Fast Critical Reactor," Transactions of the American Nuclear Society, v 98, 2008.

[8] Elkins, J., Abdel-Khalik, H., Turinsky, P., "Toward More Efficient Uncertainty Quantification, Part I: Theory," Transactions of the American Nuclear Society, v 98, 2008.

[9] Elkins, J., Abdel-Khalik, H., Turinsky, P., "Toward More Efficient Uncertainty Quantification, Part II: Numerical Results," Transactions of the American Nuclear Society, v 98, 2008.

[10] H. Abdel-Khalik, P. Turinsky, M. Jessee, J. Elkins, T. Stover, and M. Iqbal, "Uncertainty Quantification, Sensitivity Analysis, and Data Assimilation for Nuclear Systems Simulation," Proceedings from meeting at Brookhaven National Lab, 2008.

[11] Jessee, M.A., "Cross-Section Adjustment Techniques for BWR Adaptive Simulation," Doctoral Dissertation, North Carolina State University, 2008.

[12] A. N. Tikhonov, Numerical Methods for the Solution of Ill-Posed Problems, Kluwer Academic Publishers (1995).

[13] Wade, D. and Fujita, E., "Trends versus Reactor Size of Passive Reactivity Shutdown and Control Performance," Nuclear Science and Engineering, v. 103, 1989.

[14] Aliberti, G., et. al., "Nuclear Data Sensitivity, Uncertainty, and Target Accuracy Assessment for Future Nuclear Systems," Annals of Nuclear Energy, v. 33, n 6, May 2006.

[15] Private communication with Terry Jensen of Idaho National Laboratory.

[16] Hins, A. G., "Manufacture of Clad Fissionable Foils for ZPR Measurements," Nuclear Instruments and Methods, v. 102, 1972.

[17] Lell, R. M., "ZPR-6 Assembly 7 High Pu-240 Core: A Cylindrical Assembly with Mixed Oxide Fuel and a Central High Pu-240 Zone," Handbook of Evaluated Criticality Benchmark Experiments, Nuclear Energy Agency, 2007.

[18] Brumbach, S. B. and Collins, P. J., "ZPPR Progress Report for April, May, and June as of June 30, 1986," ZPR Technical Memo Series No. 470, ZPR-TM-470, Argonne National Laboratory, June 1986.

[19] Hilton, B., Porter, D., and Hayes, S., "ACF-1 Transmutation Fuels Post-Irradiation Hot-Cell Examination 4 to 8 at. % Final Report," Idaho National Laboratory, Sept. 2006.

[20] Nuclear Energy Agency, Handbook of Evaluated Criticality Benchmark Experiments, 2007.

[21] Nuclear Energy Agency, Handbook of Evaluated Reactor Physics Benchmark Experiments, 2006.

[22] Smith, M.A., et. al., "ZPR-6 Assembly 7: A Cylindrical Assembly with Mixed Oxide Fuel and Sodium with A Thick Depleted Uranium Reflector," Handbook of Evaluated Criticality Benchmark Experiments, Nuclear Energy Agency, 2007.

[23] Carpenter, S. G., et. al., "Interim Reactivity Measurements for Control and Fuel Materials for ZPPR Assembly 2," ZPR Technical Memo Series No. 22, ZPR-TM-22, Argonne National Lab, Argonne, IL, June 1970.

[24] Daughtry, J. W., et. al., "ZPR-9 Assembly 27: The Fast Test Reactor Engineering Mockup Critical (FTR-EMC)," ZPR Technical Memo Series No. 103, ZPR-TM-103, Argonne National Laboratory, April 1972.

[25] Davey, W. G., "ZPPR 3, Monthly Report for April 1972 as of April 30, 1972," ZPR Technical Memo Series No. 105, ZPR-TM-105, Argonne National Laboratory, May 1972.

[26] Amundson, P. I., "ZPPR-6 Monthly Report for February 1976 As of February 27, 1976," ZPR Technical Memo Series No. 228, ZPR-TM-228, Argonne National Laboratory, March 1976.

[27] Amundson, P. I., "ZPPR-9 Monthly Report for November 1978," ZPR Technical Memo Series No. 331, ZPR-TM-331, Argonne National Lab, Argonne, IL, November 1978.

[28] Brumbach, S. B. and Collins, P. J., "ZPPR Progress Report for August and Septermber as of Sept. 30, 1985," ZPR Technical Memo Series No. 465, ZPR-TM-465, Argonne National Laboratory, September 1985.

[29] Brumbach, S. B. and Collins, P. J., "ZPPR Progress Report for January, February and March as of March 31, 1986," ZPR Technical Memo Series No. 469, ZPR-TM-469, Argonne National Laboratory, March 1986.

[30] Bendat, J., and A. Piersol. Random Data: Analysis and Measurement Procedures, 2nd Ed. Hoboken, NJ. John Wiley & Sons, Inc., 1986.

[31] Ronen, Yigal. Uncertainty Analysis. Boca Raton, FL. CRC Press Inc., 1988.

[32] Cacuci, Dan. Sensitivity and Uncertainty Analysis, Volume I. Chapman & Hall/CRC Press, 2005.

[33] Stover, T., Abdel -Khalik, H., Turinsky, P., "Quantification of Back End Fuel Cycle Metrics Uncertainties," Transactions of the American Nuclear Society, v 96, 2007.

[34] Elkins, J. R., "Efficient Uncertainty Quantification for a Fast-Spectrum Generation IV Reactor System," Master of Science Thesis, North Carolina State University, 2008.

[35] Stover, T. E., "Quantification of Back End Fuel Cycle Metrics Uncertainties Due to Cross Sections," Master of Science Thesis, North Carolina State University, 2007.

[36] De Saint Jean, C., et. al., "A Monte Carlo Approach to Nuclear Model Parameter Uncertainties Propagation," Nuclear Science and Engineering, v. 161, 2009.

[37] Toppel, B. J., "REBUS-3/VARIANT8.0: Code System for Analysis of Fast Reactor Fuel Cycles," Argonne National Laboraotry, April 2001.

[38] Henryson, H., et. al., "MC2-2: Code System for Calculating Fast Neutron Spectra and Multigroup Cross Sections," Argonne National Laboratory, Dec. 2000.

[39] Rochman, D., et. al., "Preliminary Cross Section and nu-bar Covariances for WPEC Subgroup 26," BNL-77407-2007-IR, Brookhaven National Laboratory, Jan. 2007.

[40] X-5 Monte Carlo Team, "MCNP – A General Monte Carlo N-Particle Transport Code, Version 5," LA-UR-03-1987, Los Alamos National Laboratory, April 2003.

[41] Private discussion with Dr. Paul Turinsky of North Carolina State University.

[42] Evaluated Nuclear Data File B Version VII, available at www.nndc.bnl.gov/endf/

[43] Chart of the Nuclides, available at www.nndc.bnl.gov/chart/

[44] Zheng, Yun, "Application research of genetic algorithm in wind tunnel experiment optimization", Journal of Experimental Fluid Mechanics, v. 21, n 3, p58-61, Sept. 2007

[45] Thongdaeng, Rutsuda, "Deisgn of experiment optimization of erbium-doped fiber to single mode fiber splices", Proceedings of SPIE - The International Society for Optical Engineering, v 7386, 2009, Photonics North 2009

[46] Moroz, Leonid; Govoruschenko, Yuri; Pagur, Petr, "Axial turbine stages design: 1D/2D/3D simulation, experiment, optimization - Design of single stage test air turbine models and validation of 1D/2D/3D aerodynamic computation results against test data", Proceedings of the ASME Turbo Expo, v 6 PART B, p 1137-1146, 2005, Proceedings of the ASME Turbo Expo 2005

[47] Anderson, Corby G.,"The design-of-experiment optimization and development of cobaltite ore mineral processing", JOM, v 58, n 10, p 43-46, October 2006

[48] Molina, Mary A.; Zhao, Weixiang; Sankaran, Shankar; Schivo, Michael; Kenyon, Nicholas J.; Davis, Cristina E., "Design-of-experiment optimization of exhaled breath condensate analysis using a miniature differential mobility spectrometer (DMS)", Analytica Chimica Acta, v 628, n 2, p 155-161, November 3, 2008

[49] Zhu, Lei; Li, Jianjun; Hu, Han, "Optimization experiment of coagulation mixing energy consumption allocation program", 2010 4th International Conference on Bioinformatics and Biomedical Engineering, iCBBE 2010, 2010, 2010 4th International Conference on Bioinformatics and Biomedical Engineering, iCBBE 2010

[50] Hsu, C.; Mumaw, J.; Thomas, J.; Maria, P., "Robotic stud welding process optimization with designed experiment", Source: Welding Journal (Miami, Fla), v 87, n 10, p 265s-272s, October 2008

[51] van Laarhove, P. J. M. and Aarts, E. H. L., Simulated Annealing: Theory and Applications, Kulwar Academic Publishing, Norwell, MA, 1987

[52] Kropaczek, David J., Turinsky, Paul J., "In-core nuclear fuel management optimization for pressurized water reactors utilizing simulated annealing.", Nuclear Technology, v 95, n 1, p 9-32, Jul 1991

[53] Moore, Brian R., “Higher Order Generalized Perturbation Theory for BWR In-Core Nuclear Fuel Management Optimization”, Doctoral Dissertation, North Carolina State University, 1996

[54] Hays, Ross D., “Boiling Water Reactor In-Core Fuel Management Through Parallel Simulated Annealing in FORMOSA-B”, M.S. Thesis, North Carolina State University, 2009

[55] Du, Shuang, “Implementation of Genetic Algorithms and Parallel Simulated Annealing in OCEON-P”, M.S. Thesis, 2008

[56] Ye, Jianqing, “Optimal Core Control for Pressurized Water Reactors Utilizing Simulated Annealing”, M.S. Thesis, 1995

[57] D'Angelo, A. and Rowlands, J. L., "Conclusions Concerning the Delayed Neutron Data for Major Actinides", Progress in Nuclear Engineering, Vol. 41, No. 1-4, 2002

[58] Williams, M. L., "Sensitivty and Uncertainty Analysis for Eigenvalue-Difference Responses", Nuclear Science and Engineering, Vol. 155, pp. 18-36, 2007

[59] Salvatores, M., "Uncertainty and Target Accuracy Assessment for Innovative Systems Using Recent Covariance Data Evaluations", International Evaluation Co-operation of the NEA Nuclear Science Committee, NEA/WPEC-26, Nuclear Engergy Agency, 2008

[60] Greebler, P., Hutchins, B., Linford, R., "Sensitivity of Fast Reactor Economics to Uncertainties in Nuclear Data", Nuclear Applications, v. 4, May 1968

[61] Salvatores, M. and Palmiotti, G., "LMFBR Deisgn Parameter Uncertainty and Target Accuracies", Annals of Nuclear Energy, v. 12, n. 6, 1985

[62] Konomura, M. and Ichimiya, M., "Design Challenges for Sodium Cooled Fast Reactors", Journal of Nuclear Materials, v. 371m p 250-269, 2007

[63] Aliberti, G., Palmiotti, G., Salvatores, M., Kim, T., Taiwo, T., "Sensitivity and Uncertainty Assessment of Coolant Void Reactivity Coefficients for Liquid Salt Cooled VHTR", Transactions of the American Nuclear Society, v. 93, 2005, p 972-4

[64] Salvatores, M., Aliberti, G., Palmiotti, G., "Nuclear Data Validation and Fast Reactor Design Performances Uncertainty Reduction", Transactions of the American Nuclear Society, v. 96, p 519-22, 2007

[65] Aliberti, G., Palmiotti, G., Taiwo, T., Khalil, H., "Sensitivity Studies of Experimental Configurations Reprsentative of Gas-COoled Fast Reactors", Transactions of the American Nuclear Society, v. 96, 2007, p. 613-17

[66] Tarantola, A., Inverse Problem Theory and Methods for Parameter Estimation, Society for Industrial and Applied Mathematics, Philadelphia, PA, 2005

[67] Chow, B. G., "Comparative Economics of the Breeder and Light Water Reactor", Energy Policy, Dec. 1980.

[68] Bunn, M., et. al., "The Economics of Reprocessing vs. Direct Disposal of Spent Nuclear Fuel", Project on Managing the Atom, Harvard University, Dec. 2003.

[69] "The Economics of Nuclear Power". *Information and Issue Briefs*. World Nuclear Association. 2009. http://www.world-nuclear.org/info/inf02.html. April 1, 2009.

[70] Fanning, T. H. (Argonne National Laboratory), "Sodium as a Fast Reactor Coolant", topical seminar presented to U.S. DOE, May 3, 2007.

[71] Private Discussion with Peter Harder of Westinghouse Electric Company.

[72] Mukerjee, R. and Wu, C., A Modern Theory of Factorial Designs, Springer Science and Business Media, Inc., 2006

[73] H. W. Engl and W. Grever, "Using the L-Curve for determining optimal regularization parameters," Numerische Mathematik, 69, 25 (1994).

Appendices

Appendix A: ZPPR-15B Model Verification and Validation

Verification of the ZPPR-15B models were based on k-effective value and the reaction rate ratios in 17 drawers extending radially outward from the center of the core, along the midplane to the outer core / blanket interface. These coordinates were selected because the reaction rate ratios in each were explicitly measured by the original experiment and that data is available [29]. The tables that follow appear in groups of 3 for each parameter. The first table will present the nominal values of the parameter, the second will present the relative (fractional) uncertainty and the third will present the C/E values. The original calculations were preformed in 2-D rz geometry with appropriate transport corrections made by the analysts. The experimental uncertainties include positioning, isotopic impurities in the sample, and counting statistics, of which the latter is assumed to dominate. The REBUS uncertainties are due to the uncertainties on the input cross sections. The MCNP uncertainties are due to the random Monte Carlo sampling of a finite number of histories and do not include uncertainties on the input cross sections. All uncertainties represent one standard deviation. Tables A-1 –A-3 show the values for k-effective. Tables A-4 – A-6 show the values for U-235 fission to Pu-239 fission. Table A-7 – A-9 show the values for U-238 capture to Pu-239 fission. Tables A-10 – A-12 show the values for U-238 fission to Pu-239 fission.

The calculated k-effectives are very close to unity, leading to a C/E value that is even better than the original reported C/E. The cross section induced uncertainty was only 0.86% which is comparable to other work [14]. The standard deviation of the MCNP samples was

even less, 0.02%. In examining the U-235 ratios, it is seen that both the REBUS and MCNP values are typically <1% from the experimental value, with MCNP being marginally closer to the experimental and original C/E value. The U-235 reaction ratio uncertainties are on the order of 1 to 1.5% for the experimental as well as the MCNP and REBUS results, i.e. calculation uncertainties dues to cross section uncertainty and Monte Carlo sampling are both on the same order as the experimental uncertainty, which itself is low. In examining the U-238 capture ratios, it is seen that all the calculated values are typically higher than the experimental ratios, with the MCNP and the original results having an average C/E of 1.025 and the REBUS results having an average C/E of 1.042. The U-238 capture ratio uncertainties are about 1.1% for the experiment and 1.7% for MCNP, but 2.2% for REBUS. This means that for U-238 capture, the cross sections are causing twice as much uncertainty as the experimental procedure, although both are still very low. Finally, in examining the U-238 fission ratio, deterministic calculations consistently under predicted the experimental values but this under-prediction is only in terms of C/E about 0.025 for the original calculations and <0.01 for the REBUS calculations. MCNP both under- and over-predicted the U-238 fission ratio, depending on position, with an average C/E of 1.008. As for the U-238 capture reaction, the uncertainty for the fission reaction is also about twice the experimental uncertainty, in this case, for both REBUS and MCNP, specifically 1.7% experimental uncertainty to 2.8% from cross sections and 3.0% from Monte Carlo sampling.

Overall, there is very good agreement between REBUS, MCNP, and the experimental results. Uncertainty is generally low for all cases, with cross section induced uncertainty tending to dominate over experimental induced uncertainty. This serves to both verify and

validate the capabilities of REBUS, and thus allow the analysis to proceed to the next stage of uncertainty analysis and representativity.

Table A-1 : K-effective calculated values.

Parameter	Location	Experimental	REBUS	MCNP
k-eff	---	1.00060	1.000403	1.000420

Table A-2 : K-effective relative uncertainties.

Parameter	Location	Exp. Uncer. (rel.)	REBUS Uncer. (rel.)	MCNP Uncer. (rel.)
k-eff	---	---	0.0086	0.00022

Table A-3 : K-effective C/E values.

Parameter	Location	Reported C/E	REBUS C/E	MCNP C/E
k-eff	---	0.99184	0.99980	0.99982

Table A-4 : U-235 fission ratio calculated values.

Parameter	Location (cm from center)	Experimental	REBUS	MCNP
U-235 Fission /	5.5245	0.989	1.0054	1.0062
Pu-239 Fission	11.049	1.01400	1.0053	1.0030
	16.5735	1.02300	1.0051	1.0168
	22.098	1.02300	1.0048	1.0146
	27.6225	1.02300	1.0043	1.0148
	33.147	1.01300	1.0035	1.0099
	38.6715	1.01500	1.0023	1.0109
	44.196	1.01400	1.0003	1.0082
	49.7205	1.00200	0.9973	1.0018
	55.245	---	0.9928	0.9906
	60.7695	0.99400	0.9857	0.9863
	66.294	0.97900	0.9747	0.9797
	71.8185	0.97600	0.9539	0.9671
	77.343	0.97400	0.9590	0.9569
	82.8675	0.96800	0.9514	0.9596
	88.392	0.97400	0.9640	0.9665
	93.9165	0.97000	0.9653	0.9722
Average	---	*0.9969*	*0.9868*	*0.9921*

Table A-5 : U-235 fission ratio relative uncertainties.

Parameter	Location (cm from center)	Exp. Uncer. (rel)	REBUS Uncer (rel.)	MCNP Uncer (rel.)
U-235 Fission /	5.5245	---	0.0139	0.0132
Pu-239 Fission	11.049	0.0109	0.0138	0.0133
	16.5735	0.0117	0.0138	0.0130
	22.098	0.0098	0.0139	0.0132
	27.6225	0.0050	0.0138	0.0134
	33.147	0.0096	0.0139	0.0134
	38.6715	0.0101	0.0140	0.0133
	44.196	0.0101	0.0141	0.0135
	49.7205	0.0115	0.0144	0.0135
	55.245	---	0.0148	0.0133
	60.7695	0.0109	0.0152	0.0139
	66.294	0.0112	0.0158	0.0137
	71.8185	0.0105	0.0165	0.0140
	77.343	0.0110	0.0169	0.0149
	82.8675	0.0111	0.0165	0.0151
	88.392	0.0112	0.0158	0.0174
	93.9165	0.0136	0.0146	0.0187
Average	---	*0.0105*	*0.0148*	*0.0142*

Table A-6 : U-235 fission ratio C/E values.

Parameter	Location (cm from center)	Reported C/E	REBUS C/E	MCNP C/E
U-235 Fission /	5.5245	1.0120	1.017	1.017
Pu-239 Fission	11.049	1.0010	0.991	0.989
	16.5735	0.9920	0.983	0.994
	22.098	0.9910	0.982	0.992
	27.6225	0.9910	0.982	0.992
	33.147	1.0000	0.991	0.997
	38.6715	0.9970	0.987	0.996
	44.196	0.9960	0.987	0.994
	49.7205	1.0020	0.995	1.000
	55.245	---	---	---
	60.7695	0.9960	0.992	0.992
	66.294	0.9980	0.996	1.001
	71.8185	0.9950	0.977	0.991
	77.343	0.9820	0.985	0.982
	82.8675	0.9960	0.983	0.991
	88.392	0.9870	0.990	0.992
	93.9165	1.0070	0.995	1.002
Average	---	*0.9964*	*0.9895*	*0.9952*

Table A-7 : U-238 capture ration calculated values.

Parameter	Location (cm from center)	Experimental	REBUS	MCNP
U-238 Capture /	5.5245	0.1282	0.1370	0.1366
Pu-239 Fission	11.049	0.13090	0.1370	0.1334
	16.5735	0.13180	0.1369	0.1339
	22.098	0.13160	0.1369	0.1343
	27.6225	0.13130	0.1367	0.1333
	33.147	0.13030	0.1365	0.1330
	38.6715	0.12920	0.1362	0.1345
	44.196	0.13140	0.1356	0.1334
	49.7205	0.12950	0.1348	0.1335
	55.245	0.12940	0.1335	0.1308
	60.7695	0.12760	0.1315	0.1284
	66.294	0.12380	0.1284	0.1265
	71.8185	0.11950	0.1227	0.1225
	77.343	0.11940	0.1240	0.1216
	82.8675	0.11830	0.1220	0.1220
	88.392	0.11960	0.1256	0.1244
	93.9165	0.11970	0.1265	0.1256
Average	---	*0.12656*	*0.1319*	*0.1299*

Table A-8: U-238 capture ratio relative uncertainty values.

Parameter	Location (cm from center)	Exp. Uncer. (rel)	REBUS Uncer (rel.)	MCNP Uncer (rel.)
U-238 Capture /	5.5245	---	0.0204	0.0161
Pu-239 Fission	11.049	0.0108	0.0204	0.0165
	16.5735	0.0122	0.0205	0.0151
	22.098	0.0103	0.0207	0.0153
	27.6225	0.0055	0.0209	0.0155
	33.147	0.0102	0.0211	0.0153
	38.6715	0.0108	0.0214	0.0155
	44.196	0.0105	0.0219	0.0154
	49.7205	0.0120	0.0223	0.0160
	55.245	0.0107	0.0229	0.0160
	60.7695	0.0118	0.0235	0.0163
	66.294	0.0113	0.0242	0.0166
	71.8185	0.0110	0.0251	0.0167
	77.343	0.0111	0.0253	0.0172
	82.8675	0.0116	0.0249	0.0183
	88.392	0.0114	0.0236	0.0216
	93.9165	0.0142	0.0219	0.0215
Average	---	*0.0110*	*0.0224*	*0.0168*

Table A-9: U-238 capture ratio C/E values.

Parameter	Location (cm from center)	Reported C/E	REBUS C/E	MCNP C/E
U-238 Capture /	5.5245	1.0400	1.069	1.065
Pu-239 Fission	11.049	1.0260	1.047	1.019
	16.5735	1.0190	1.039	1.016
	22.098	1.0200	1.040	1.021
	27.6225	1.0210	1.041	1.015
	33.147	1.0280	1.048	1.021
	38.6715	1.0340	1.054	1.041
	44.196	1.0120	1.032	1.015
	49.7205	1.0210	1.041	1.031
	55.245	1.0120	1.031	1.011
	60.7695	1.0100	1.031	1.006
	66.294	1.0160	1.037	1.021
	71.8185	1.0360	1.027	1.025
	77.343	1.0170	1.038	1.019
	82.8675	1.0340	1.031	1.031
	88.392	1.0300	1.050	1.040
	93.9165	1.0520	1.057	1.049
Average	---	*1.0252*	*1.0420*	*1.0263*

Table A-10: U-238 fission ratio calculated values.

Parameter	Location (cm from center)	Experimental	REBUS	MCNP
U-238 Fission /	5.5245	0.02058	0.0210	0.0194
Pu-239 Fission	11.049	0.02142	0.0210	0.0207
	16.5735	0.02112	0.0210	0.0209
	22.098	0.02121	0.0210	0.0215
	27.6225	0.02137	0.0210	0.0219
	33.147	0.02139	0.0210	0.0218
	38.6715	0.02114	0.0211	0.0215
	44.196	0.02085	0.0212	0.0212
	49.7205	0.02075	0.0214	0.0215
	55.245	0.02156	0.0219	0.0232
	60.7695	0.02230	0.0228	0.0225
	66.294	0.02414	0.0246	0.0251
	71.8185	0.02869	0.0285	0.0291
	77.343	0.02748	0.0272	0.0279
	82.8675	0.02986	0.0287	0.0287
	88.392	0.02682	0.0263	0.0272
	93.9165	0.02697	0.0258	0.0266
Average	---	*0.0234*	*0.0233*	*0.0236*

Table A-11: U-238 fission ratio relative uncertainty values.

Parameter	Location (cm from center)	Exp. Uncer. (rel)	REBUS Uncer (rel.)	MCNP Uncer (rel.)
U-238 Fission /	5.5245	---	0.0297	0.0293
Pu-239 Fission	11.049	0.0163	0.0296	0.0294
	16.5735	0.0183	0.0296	0.0290
	22.098	0.0166	0.0295	0.0286
	27.6225	0.0112	0.0293	0.0290
	33.147	0.0160	0.0293	0.0294
	38.6715	0.0167	0.0291	0.0289
	44.196	0.0176	0.0291	0.0293
	49.7205	0.0183	0.0291	0.0294
	55.245	0.0170	0.0292	0.0290
	60.7695	0.0175	0.0286	0.0297
	66.294	0.0177	0.0270	0.0291
	71.8185	0.0171	0.0248	0.0274
	77.343	0.0177	0.0260	0.0291
	82.8675	0.0179	0.0247	0.0305
	88.392	0.0188	0.0262	0.0341
	93.9165	0.0232	0.0259	0.0376
Average	---	*0.0174*	*0.0280*	*0.0299*

Table A-12: U-238 fission ratio C/E values.

Parameter	Location (cm from center)	Reported C/E	REBUS C/E	MCNP C/E
U-238 Fission /	5.5245	0.9870	1.020	0.942
Pu-239 Fission	11.049	0.9550	0.980	0.965
	16.5735	0.9700	0.994	0.990
	22.098	0.9650	0.990	1.012
	27.6225	0.9580	0.983	1.024
	33.147	0.9580	0.983	1.020
	38.6715	0.9710	0.997	1.019
	44.196	0.9890	1.016	1.016
	49.7205	1.0040	1.032	1.038
	55.245	0.9870	1.014	1.074
	60.7695	0.9950	1.021	1.010
	66.294	0.9980	1.018	1.039
	71.8185	0.9530	0.995	1.016
	77.343	0.9900	0.991	1.016
	82.8675	0.9510	0.962	0.960
	88.392	0.9810	0.979	1.013
	93.9165	0.9640	0.957	0.987
Average	---	*0.9751*	*0.9960*	*1.0082*

Appendix B: REBUS Linearity

As indicated in the discussion on methodology, for the ESM to be applicable to this problem the core simulator REBUS must behave linearly over some range of expected perturbations. This is required such that the higher order non-linear terms of the uncertainty propagation can be neglected due to their small magnitude. Elkins showed that indeed the REBUS simulator does behave linearly for the application that it was used for in his work, the ABTR model [34]. However, showing REBUS linearity also serves as further verification of the analysis capabilities.

Verification of the analysis capabilities could be partially completed by utilizing an alternate methodology such as using Generalized Perturbation Theory to obtain sensitivity coefficients. It could also be completed by solving for multiple responses for various perturbations of the cross section values by the capabilities being utilized, e.g. ESM, and comparing results with a forward solution approach. This indeed is what has been done to show that assuming linearity of the responses with respect to the cross sections is an acceptable assumption for the application at hand. As the perturbation size is reduced, the linear and forward solution responses should converge. This is the approach that will be utilized in support of completing the verification of the analysis capabilities.

To demonstrate linearity an approach similar to the one used by Elkins is applied to the REBUS code using the ZPPR-15B base model (Elkins already showed linearity using the ABTR model). A random perturbation of the cross sections that are input to the ZPPR model was generated. The perturbations were drawn from a Gaussian distribution with a standard

deviation of 5% from nominal. This randomized vector was then scaled from 0 to 5 such that the sample with a scaling factor of 0 is unperturbed, a scaling factor of 1 is the initial 5% Gaussian perturbation, and a scaling factor of 5 perturbs up to a 25% Gaussian which is far beyond the range of cross section perturbations in this work. The 5% was chosen because many of the most heavily concentrated isotopes' cross sections, within the dominant portion of the flux spectrum, have a priori uncertainties between 1 and 15%.

With each scaling the cross sections were input to the ZPPR model and the model executed. Tables B-1 though B-6 show the results of the study on several important ZPPR observables – k-effective, conversion ratio, peaking factor, Pu-239 and Am-241 fission, and U-238 neutron capture. A linear fit is then applied to the data using the results from the runs with scaling factors of 1 and 0. This fit is used to extrapolate linearly the expected perturbations in the observables.

As can be seen there is good agreement between the linearly extrapolated values and the calculated values over the range of expected perturbations, i.e. 0 to 15%, and in most cases even beyond this point. The only exceptions to this are the Pu-239 fission and U-238 capture reaction rates whose linearity begins to breakdown near scaling factors of 2 to 2.5. This will not affect this work, even though these are key driving reactions of the reactor, as these reactions are very well understood and therefore the a priori uncertainty on U-238 capture is < 5% and the a priori uncertainty on Pu-239 fission is < 1%.

Tables B-1 though B-6 also support the requirement that as perturbation size is reduced that the forward and linear solutions do indeed approach each other and converge when the perturbation is very near zero. Elkins performed a similar linearity study on the

ABTR using REBUS models and came to the same conclusions, though more quantitatively evaluated. This demonstration serves to further verify the capability of the ESM method applied to this analysis. It also reaffirms the linearity conclusions made in Elkins' work by using a different reactor model input and different cross sections.

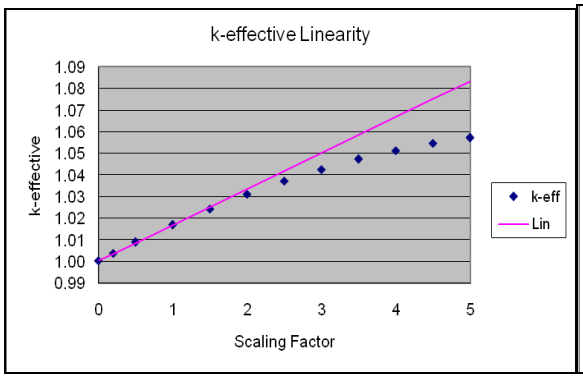

Figure B-1: K-effective linearity.

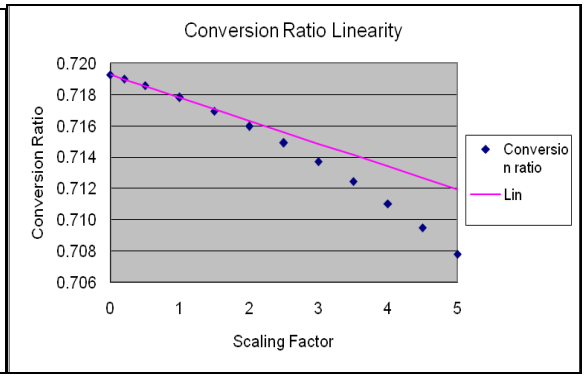

Figure B-2: Conversion ratio linearity.

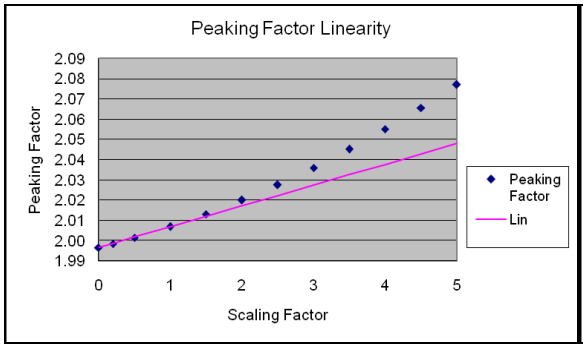

Figure B-3: Peaking factor linearity.

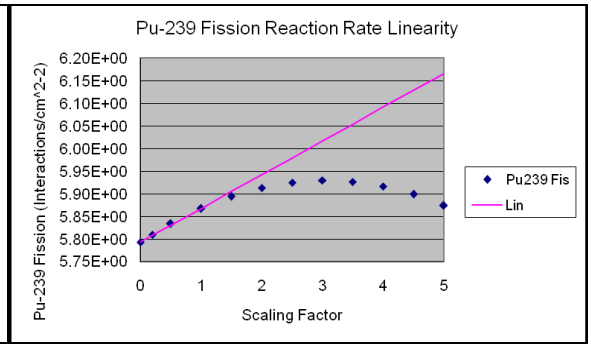

Figure B-4: Pu-239 fission rate linearity.

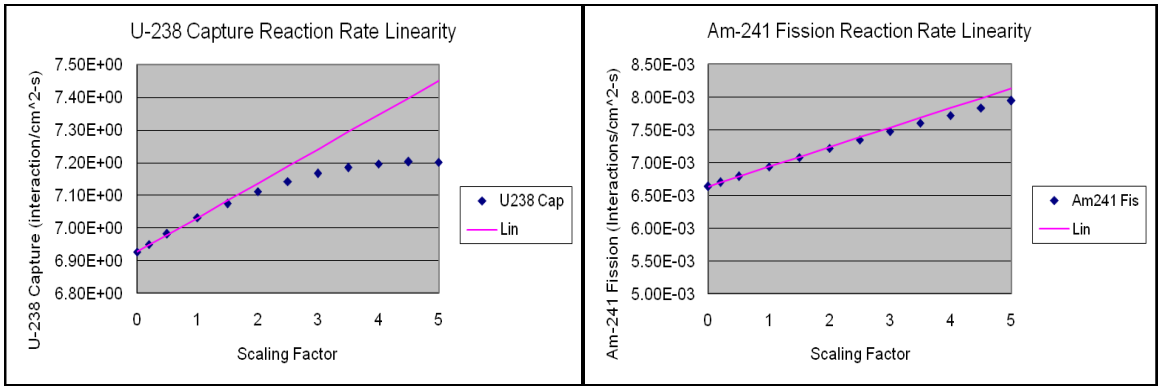

Figure B-5: U-238 fission rate linearity. **Figure B-6: Am-241 fission rate linearity.**

Appendix C: ZPPR Variations for Optimization Problem

The optimization method demonstrated in this work examined, in addition to the 0^{th} generation ZPPR experiment, 30 ZPPR variations. The few 0^{th} generation variations were described and pictured in detail in Chapter 4. The subsequent variations were too numerous to be included in similar detail in the main body of this work. This appendix shows each variation of the ZPPR experiment in quarter core format using the same coloring scheme as Chapter 4. Detector locations are marked with a red X. Table C.1 lists the number of SNF and TRU drawers each variation contains, the number of detectors, and the calculated cost of the experiment. Applicable 0^{th} generation values are also presented in Table C.1 for comparison. The balance of Appendix C is Figures C.1 through C.20 that show each variation.

Table C.1: Design specifications of each ZPPR variations used in the optimization.

Experiment	Number of SNF Drawers	Number of TRU Drawers	Number of Detectors	Cost
TRU 1, 2	0	16	4	$335,944
TRU 1B, 1C, 2B	0	32	4	$354,888
TRU 3	0	32	4	$354,888
SNF	72	0	4	$4,045,160
ZPPR_1_1	24	0	4	$1,559,720
ZPPR_1_2	0	40	4	$364,360
ZPPR_1_3	0	64	4	$392,776
ZPPR_1_4	32	0	4	$1,973,960
ZPPR_1_5	24	64	4	$1,635,496
ZPPR_2_1	40	0	4	$2,388,200
ZPPR_2_2	64	0	4	$3,630,920
ZPPR_2_3	0	32	4	$354,888
ZPPR_2_4	64	24	4	$3,659,336
ZPPR_2_5	32	4	4	$1,978,696
ZPPR_3_1	0	124	4	$463,816
ZPPR_3_2	0	100	4	$435,400
ZPPR_3_3	0	84	4	$416,456
ZPPR_3_4	4	32	4	$562,008
ZPPR_3_5	12	4	4	$943,096
ZPPR_4_1	0	32	6	$360,288
ZPPR_4_2	0	40	5	$367,060
ZPPR_4_3	12	4	5	$945,796
ZPPR_4_4	0	64	5	$395,476
ZPPR_4_5	44	0	4	$2,595,320
ZPPR_5_1	24	0	4	$1,559,720
ZPPR_5_2	4	12	4	$943,096
ZPPR_5_3	8	8	4	$740,712
ZPPR_5_4	0	32	7	$362,988
ZPPR_5_5	12	24	4	$966,776
ZPPR_6_1	0	40	6	$1,559,720
ZPPR_6_2	0	64	6	$943,096
ZPPR_6_3	4	32	6	$740,712
ZPPR_6_4	12	4	6	$362,988
ZPPR_6_5	8	8	6	$966,776

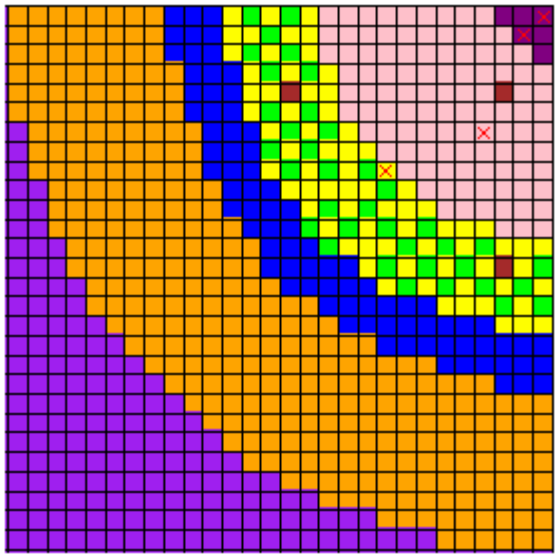

Figure C.1: ZPPR_1_1.

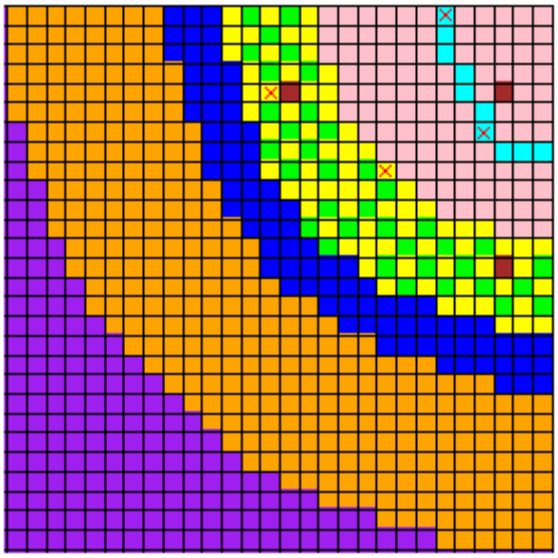

Figure C.2: ZPPR_1_2.

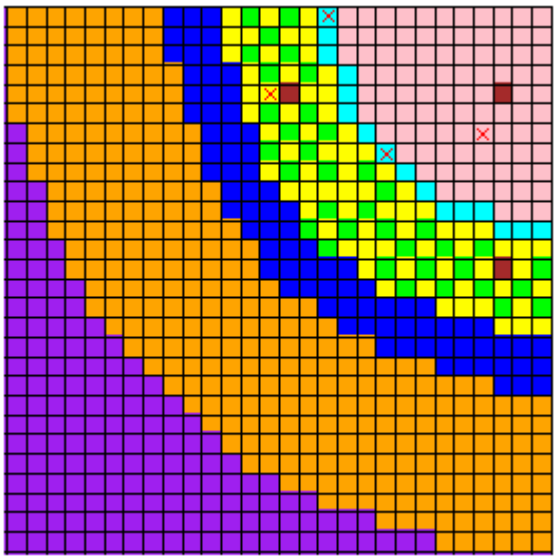

Figure C.3: ZPPR_1_3.

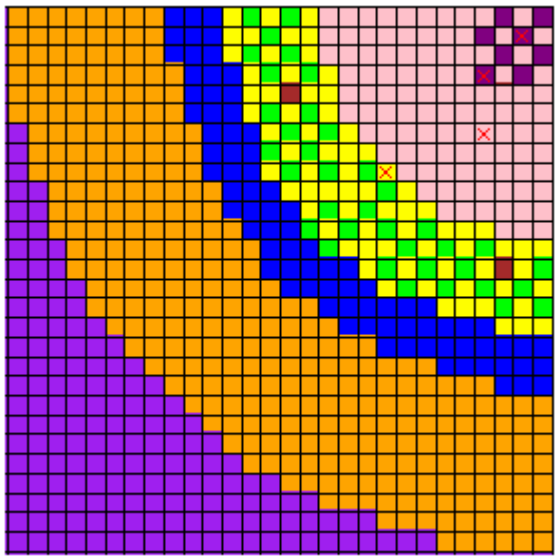

Figure C.4: ZPPR_1_4.

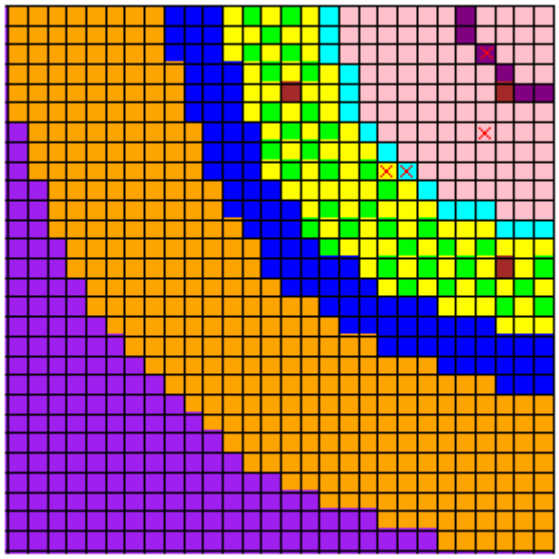

Figure C.5: ZPPR_1_5.

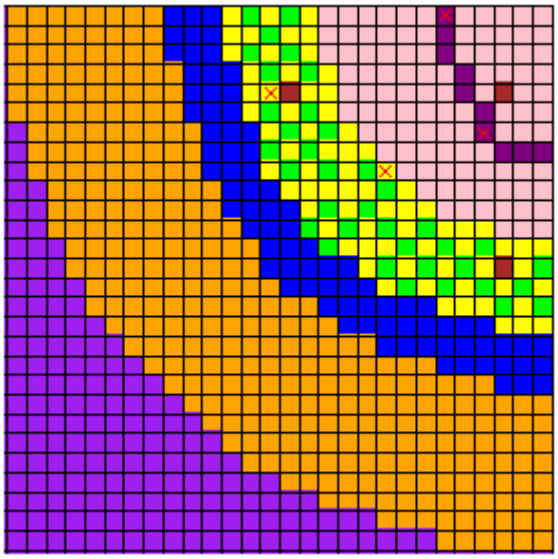

Figure C.6: ZPPR_2_1.

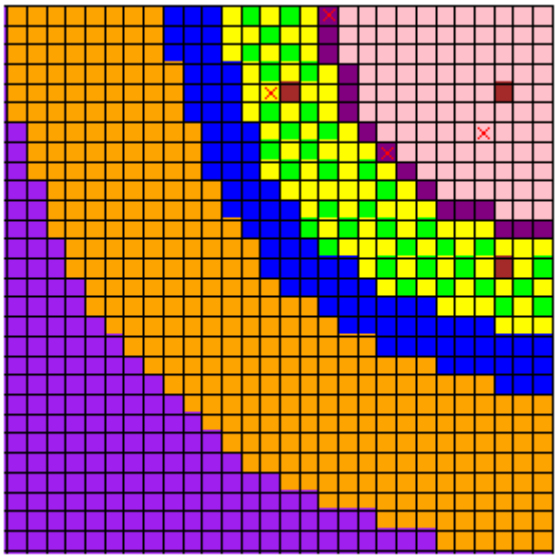

Figure C.7: ZPPR_2_2.

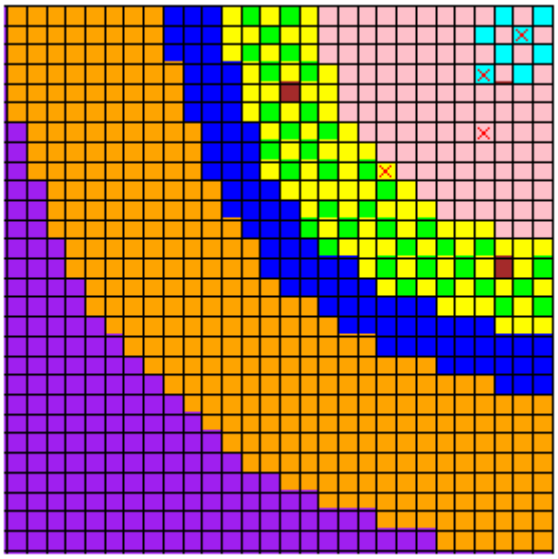

Figure C.8: ZPPR_2_3.

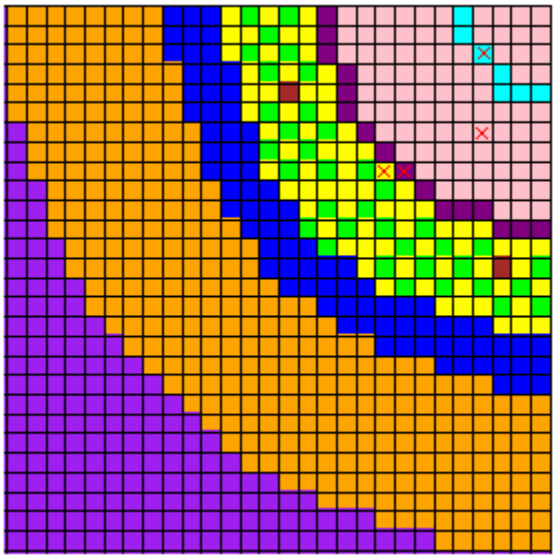

Figure C.9: ZPPR_2_4.

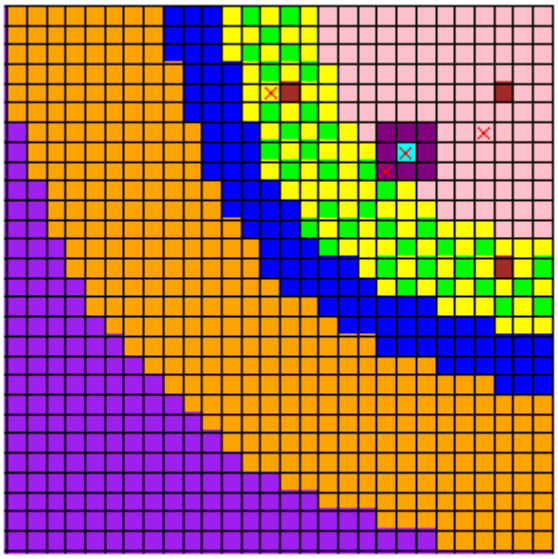

Figure C.10: ZPPR_2_5.

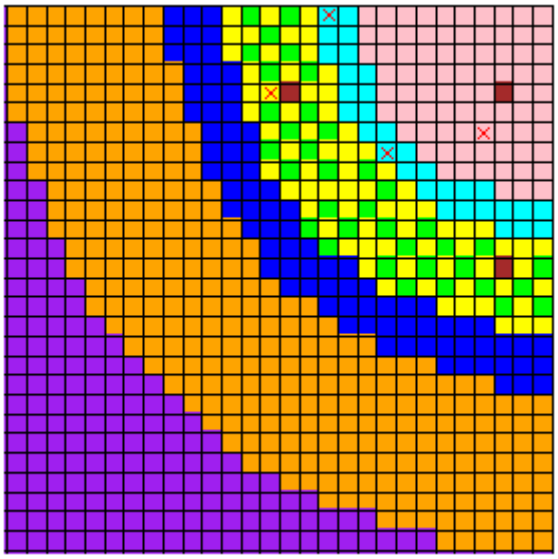

Figure C.11: ZPPR_3_1.

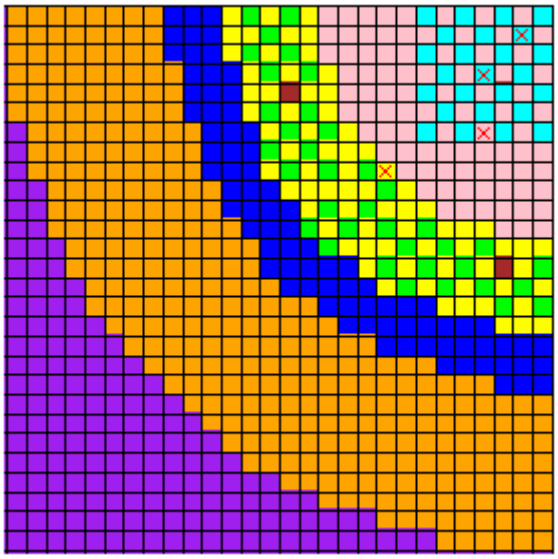

Figure C.12: ZPPR_3_2.

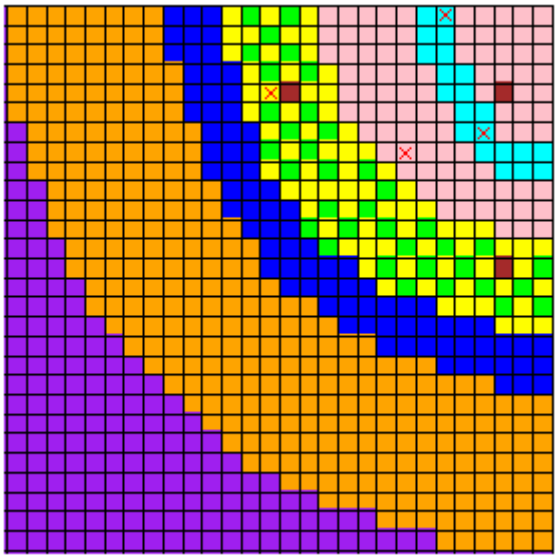

Figure C.13: ZPPR_3_3.

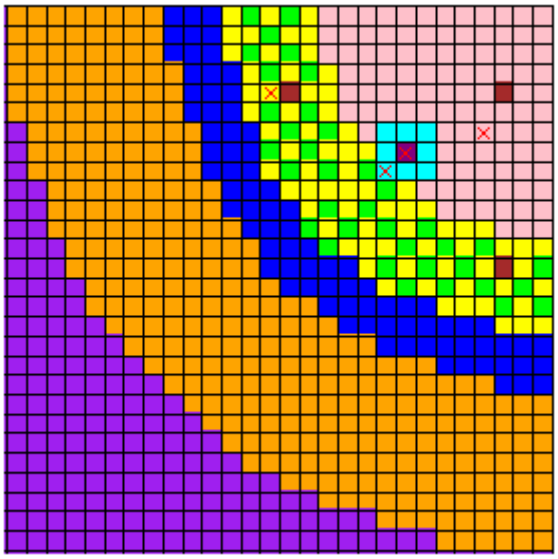

Figure C.14: ZPPR_3_4.

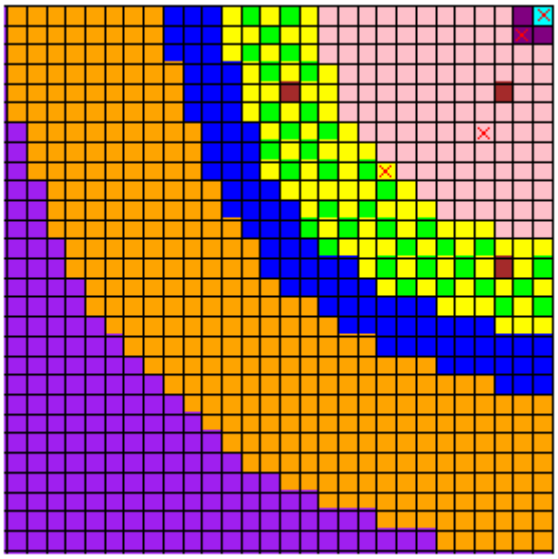

Figure C.15: ZPPR_3_5.

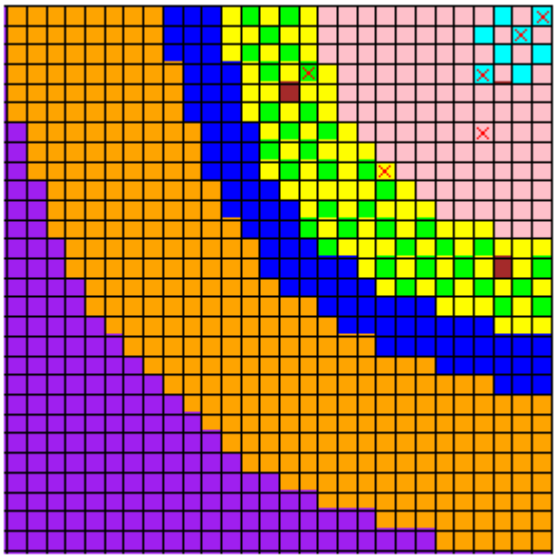

Figure C.16: ZPPR_4_1.

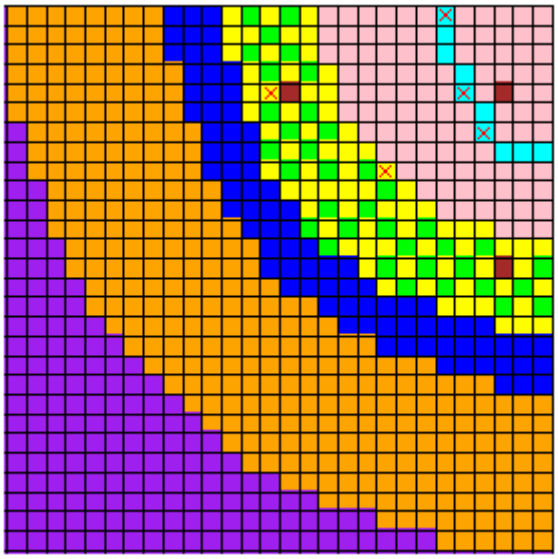

Figure C.17: ZPPR_4_2.

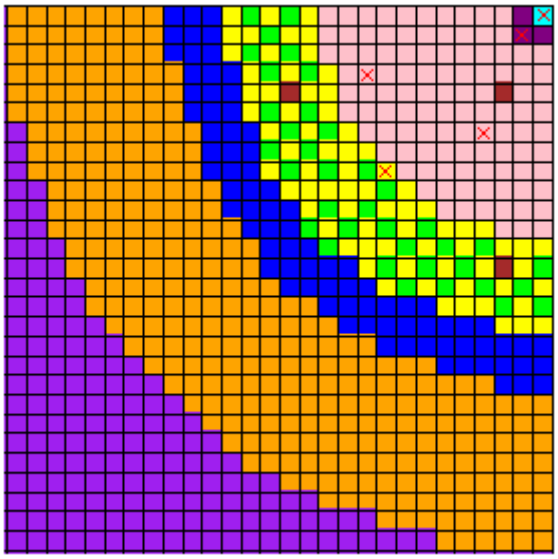

Figure C.18: ZPPR_4_3.

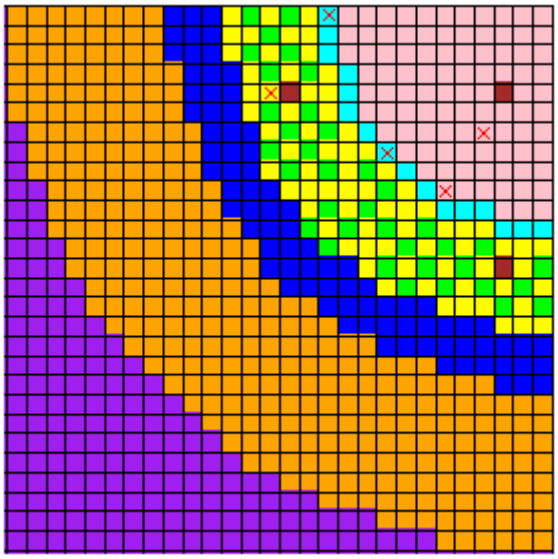

Figure C.19: ZPPR_4_4.

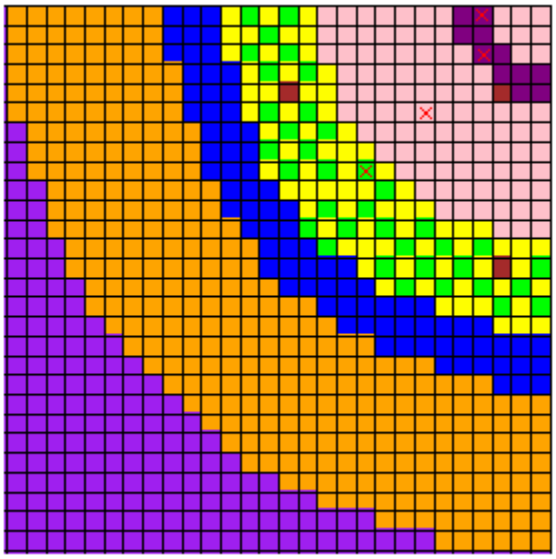

Figure C.20: ZPPR_4_5.

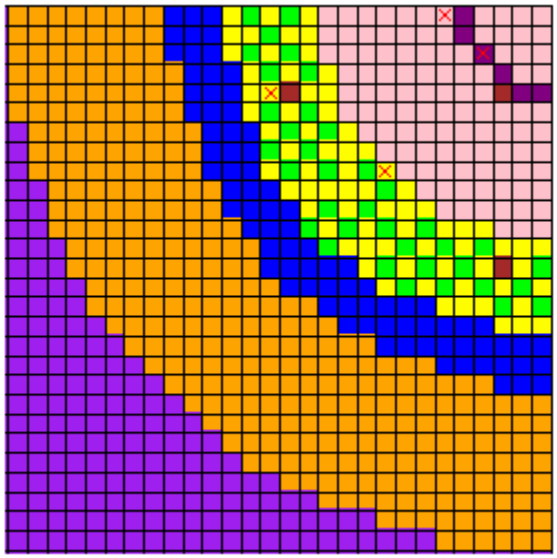

Figure C.21: ZPPR_5_1.

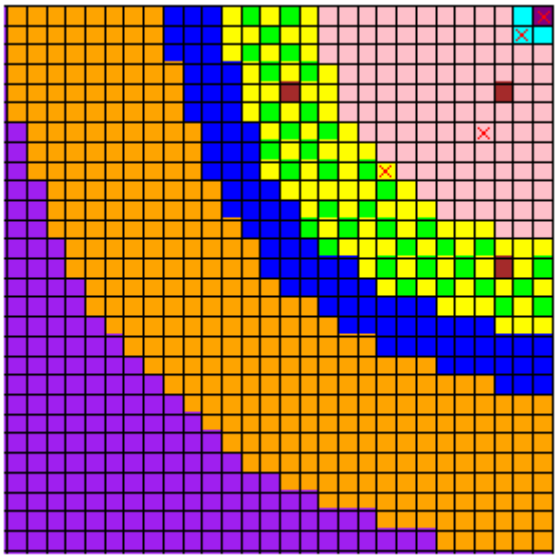

Figure C.22: ZPPR_5_2.

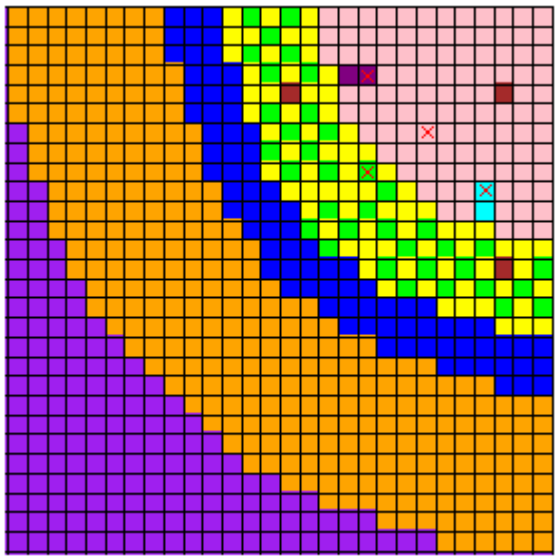

Figure C.23: ZPPR_5_3.

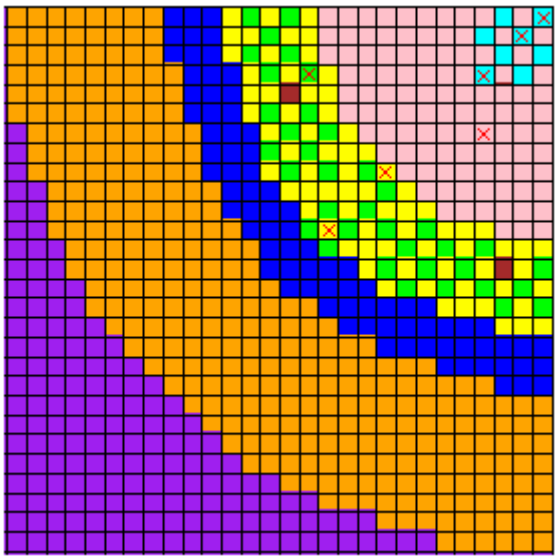

Figure C.24: ZPPR_5_4.

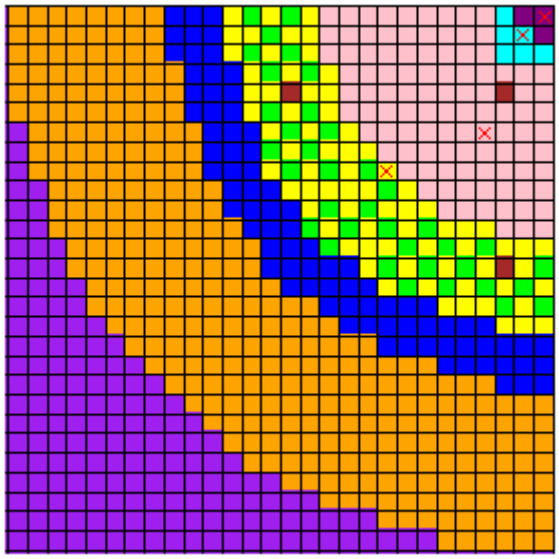

Figure C.25: ZPPR_5_5.

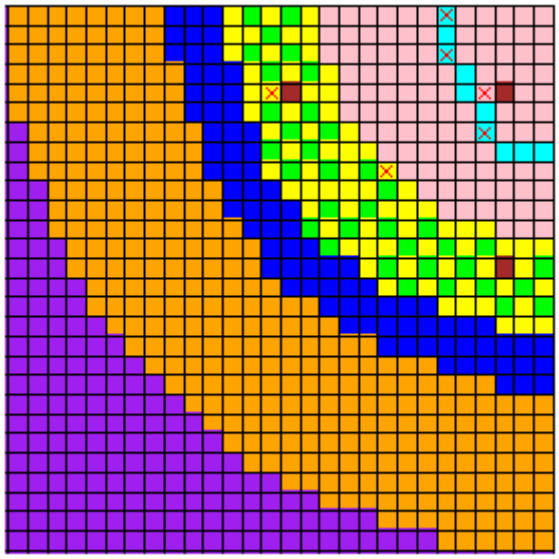

Figure C.26: ZPPR_6_1.

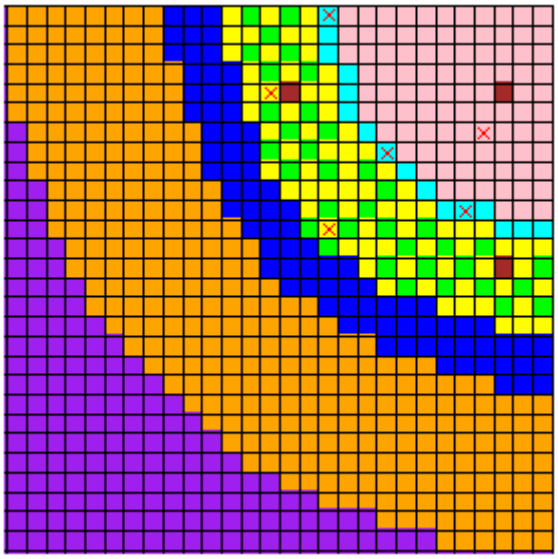

Figure C.27: ZPPR_6_2.

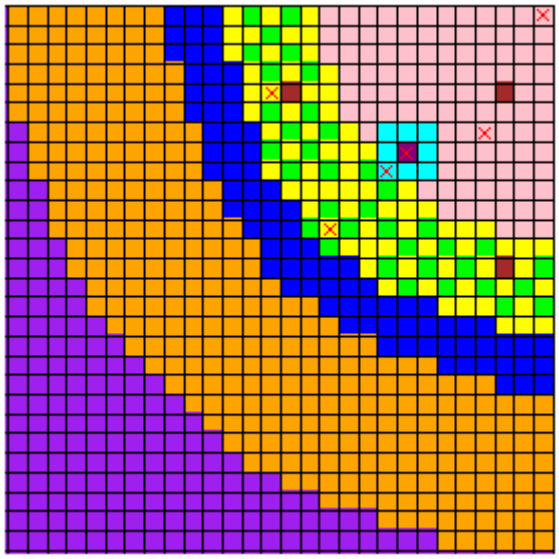

Figure C.28: ZPPR_6_3.

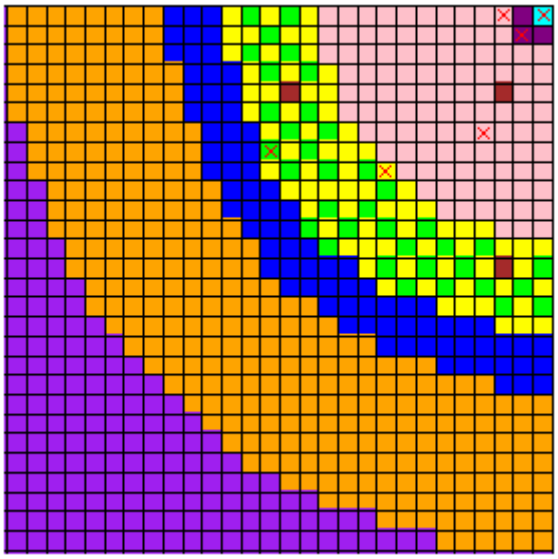

Figure C.29: ZPPR_6_4.

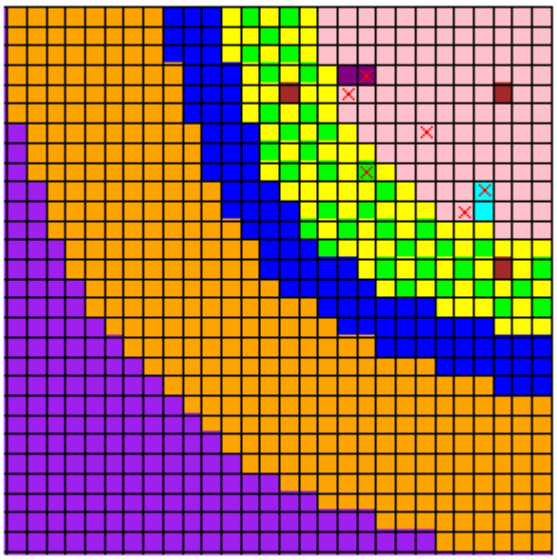

Figure C.30: ZPPR_6_5.

Appendix D: Additional Adaption Results

The following pages contain tables of data from the various adaptive simulation experiments that were deemed not prudent to be placed in the main body of this work. These include the minor actinide capture reaction rates, sodium and iron elastic scatter, end of cycle isotopics, and for the equilibrium core discharge isotopics as well. The results tables are presented in the same order that their corresponding tables of more important data as appeared in the main body of the work. The following tables are presented in this Appendix:

Table D.1: Posteriori uncertainties for ABTR-SU adapted to ZPPR-15B.

Parameter	Nominal Values	A Priori	0%	1%	1% + FPY	7.50%
Average Reaction Rates						
U-235 Capture	1.36070E+10	**1.5221**	0.1122	0.3464	0.3478	0.8163
Np-237 Capture	1.15415E+11	**3.0851**	2.4425	2.4884	2.4887	2.6496
Pu-238 Capture	2.83738E+10	**11.8061**	0.3149	0.7983	0.8000	1.9602
Pu-239 Capture	1.02875E+12	**4.6378**	0.1505	0.5681	0.5693	1.8446
Pu-240 Capture	3.13125E+11	**10.9878**	0.1678	0.5034	0.5046	1.9126
Pu-241 Capture	5.72420E+10	**10.8240**	0.1500	0.6477	0.6563	2.4122
Pu-242 Capture	3.82369E+10	**19.7742**	0.6730	1.3794	1.3819	3.0628
Am-241 Capture	1.53269E+11	**4.7001**	0.1268	0.5615	0.5650	1.7214
Am-242m Capture	7.66985E+08	**14.2233**	13.9313	13.9600	13.9603	14.0257
Am-243 Capture	2.27687E+10	**5.1920**	4.1619	4.2167	4.2171	4.3456
Cm-242 Capture	7.23472E+08	**15.6376**	15.2195	15.2428	15.2430	15.3125
Cm-244 Capture	4.03373E+09	**14.0488**	13.9025	13.9148	13.9150	13.9513
Cm-245 Capture	1.44377E+08	**12.3336**	12.1425	12.1621	12.1623	12.2129
Fe (n,el)	1.64649E+09	**3.1362**	0.3087	0.5779	0.5806	1.2074
Na-23 (n,el)	1.57721E+09	**3.2893**	0.3377	0.6014	0.6042	1.2385
End of Cycle Masses						
EOC U-234 Mass (kg, 1/3 core)	7.5899E-03	**0.3596**	*0.3546*	*0.3554*	*0.3554*	*0.3560*
EOC U-235 Mass (kg, 1/3 core)	1.6698E+00	**0.0524**	*0.0028*	*0.0089*	*0.0090*	*0.0270*
EOC U-236 Mass (kg, 1/3 core)	1.1398E-01	**0.2421**	*0.1062*	*0.1166*	*0.1169*	*0.1643*
EOC U-238 Mass (kg, 1/3 core)	1.0820E+03	**0.0100**	*0.0009*	*0.0024*	*0.0025*	*0.0065*
EOC NP237 Mass (kg, 1/3 core)	1.2497E+00	**0.1893**	*0.1399*	*0.1448*	*0.1448*	*0.1522*
EOC PU236 Mass (kg, 1/3 core)	8.6229E-06	**2.4712**	*2.3186*	*2.3223*	*2.3223*	*2.3393*
EOC PU238 Mass (kg, 1/3 core)	5.8723E-01	**0.5148**	*0.1464*	*0.1623*	*0.1643*	*0.1940*
EOC PU239 Mass (kg, 1/3 core)	2.1251E+02	**0.0580**	*0.0019*	*0.0081*	*0.0085*	*0.0338*
EOC PU240 Mass (kg, 1/3 core)	2.7814E+01	**0.2461**	*0.0080*	*0.0235*	*0.0236*	*0.0899*
EOC PU241 Mass (kg, 1/3 core)	3.0264E+00	**1.0211**	*0.0167*	*0.0484*	*0.0643*	*0.1770*
EOC PU242 Mass (kg, 1/3 core)	1.3785E+00	**0.2957**	*0.0037*	*0.0131*	*0.0146*	*0.0504*
EOC AM241 Mass (kg, 1/3 core)	1.3285E+00	**0.1766**	*0.0034*	*0.0201*	*0.0202*	*0.0608*
EOC AM242 Mass (kg, 1/3 core)	3.9258E-02	**1.4299**	*1.0306*	*1.0381*	*1.0382*	*1.0982*
EOC AM243 Mass (kg, 1/3 core)	2.6104E-01	**0.8554**	*0.1124*	*0.1173*	*0.1174*	*0.1619*
EOC CM242 Mass (kg, 1/3 core)	4.8115E-02	**2.2253**	*0.1500*	*0.3078*	*0.3094*	*0.8383*
EOC CM243 Mass (kg, 1/3 core)	1.3710E-03	**2.9256**	*2.9065*	*2.9076*	*2.9076*	*2.9116*
EOC CM244 Mass (kg, 1/3 core)	6.6660E-02	**0.7652**	*0.7507*	*0.7525*	*0.7525*	*0.7555*
EOC CM245 Mass (kg, 1/3 core)	6.2128E-03	**3.1718**	*3.1636*	*3.1651*	*3.1651*	*3.1670*
EOC CM246 Mass (kg, 1/3 core)	4.2967E-04	**1.0307**	*1.0178*	*1.0192*	*1.0192*	*1.0225*

Table D.2: Posteriori uncertainties for ABTR-SU adapted to ZPPR-15B w/ TRU.

Parameter	Nominal Values	A Priori	0%	1%	1% + FPY	7.50%
Average Reaction Rates						
U-235 Capture	1.36070E+10	**1.5221**	0.1040	0.3365	0.3393	0.7711
Np-237 Capture	1.15415E+11	**3.0851**	0.2843	0.5434	0.5459	1.3874
Pu-238 Capture	2.83738E+10	**11.8061**	0.2366	0.7705	0.7734	1.9477
Pu-239 Capture	1.02875E+12	**4.6378**	0.1412	0.5627	0.5650	1.8422
Pu-240 Capture	3.13125E+11	**10.9878**	0.1591	0.4972	0.4994	1.9099
Pu-241 Capture	5.72420E+10	**10.8240**	0.1418	0.6438	0.6530	2.4104
Pu-242 Capture	3.82369E+10	**19.7742**	0.6525	1.3669	1.3710	3.0579
Am-241 Capture	1.53269E+11	**4.7001**	0.1189	0.5580	0.5621	1.7196
Am-242m Capture	7.66985E+08	**14.2233**	0.2513	0.8811	0.8920	2.9101
Am-243 Capture	2.27687E+10	**5.1920**	0.3204	1.2151	1.4001	2.2315
Cm-242 Capture	7.23472E+08	**15.6376**	0.2543	0.9815	0.9852	2.8680
Cm-244 Capture	4.03373E+09	**14.0488**	0.1717	0.6826	0.7161	2.2663
Cm-245 Capture	1.44377E+08	**12.3336**	0.1557	0.6943	0.7128	2.5012
Fe (n,el)	1.64649E+09	**3.1362**	0.2950	0.5719	0.5764	1.2047
Na-23 (n,el)	1.57721E+09	**3.2893**	0.3235	0.5955	0.5999	1.2353
End of Cycle Masses						
EOC U-234 Mass (kg, 1/3 core)	7.5899E-03	**0.3596**	*0.3542*	*0.3550*	*0.3551*	*0.3557*
EOC U-235 Mass (kg, 1/3 core)	1.6698E+00	**0.0524**	*0.0026*	*0.0088*	*0.0089*	*0.0257*
EOC U-236 Mass (kg, 1/3 core)	1.1398E-01	**0.2421**	*0.1059*	*0.1152*	*0.1158*	*0.1605*
EOC U-238 Mass (kg, 1/3 core)	1.0820E+03	**0.0100**	*0.0009*	*0.0024*	*0.0025*	*0.0064*
EOC NP237 Mass (kg, 1/3 core)	1.2497E+00	**0.1893**	*0.0952*	*0.1038*	*0.1039*	*0.1183*
EOC PU236 Mass (kg, 1/3 core)	8.6229E-06	**2.4712**	*2.3183*	*2.3222*	*2.3222*	*2.3392*
EOC PU238 Mass (kg, 1/3 core)	5.8723E-01	**0.5148**	*0.0341*	*0.0783*	*0.0826*	*0.1403*
EOC PU239 Mass (kg, 1/3 core)	2.1251E+02	**0.0580**	*0.0018*	*0.0081*	*0.0084*	*0.0332*
EOC PU240 Mass (kg, 1/3 core)	2.7814E+01	**0.2461**	*0.0077*	*0.0233*	*0.0234*	*0.0898*
EOC PU241 Mass (kg, 1/3 core)	3.0264E+00	**1.0211**	*0.0160*	*0.0478*	*0.0640*	*0.1769*
EOC PU242 Mass (kg, 1/3 core)	1.3785E+00	**0.2957**	*0.0035*	*0.0131*	*0.0146*	*0.0504*
EOC AM241 Mass (kg, 1/3 core)	1.3285E+00	**0.1766**	*0.0032*	*0.0200*	*0.0202*	*0.0608*
EOC AM242 Mass (kg, 1/3 core)	3.9258E-02	**1.4299**	*0.0128*	*0.1289*	*0.1457*	*0.4201*
EOC AM243 Mass (kg, 1/3 core)	2.6104E-01	**0.8554**	*0.0108*	*0.0420*	*0.0462*	*0.1271*
EOC CM242 Mass (kg, 1/3 core)	4.8115E-02	**2.2253**	*0.0345*	*0.2703*	*0.2722*	*0.8251*
EOC CM243 Mass (kg, 1/3 core)	1.3710E-03	**2.9256**	*1.9385*	*1.9474*	*1.9475*	*1.9909*
EOC CM244 Mass (kg, 1/3 core)	6.6660E-02	**0.7652**	*0.0098*	*0.1005*	*0.1223*	*0.2022*
EOC CM245 Mass (kg, 1/3 core)	6.2128E-03	**3.1718**	*0.0139*	*0.1149*	*0.1272*	*0.4268*
EOC CM246 Mass (kg, 1/3 core)	4.2967E-04	**1.0307**	*0.0082*	*0.0629*	*0.0647*	*0.2334*

Table D.3: Posteriori uncertainties for ABTR-SU adapted to TRU v. 1.

Parameter	Nominal Values	A Priori	0%	1%	1% + FPY	7.50%
Average Reaction Rates						
U-235 Capture	1.36070E+10	**1.5221**	0.0965	0.3125	0.3160	0.7940
Np-237 Capture	1.15415E+11	**3.0851**	0.2780	0.5531	0.5555	1.3968
Pu-238 Capture	2.83738E+10	**11.8061**	0.2646	0.7812	0.7852	2.1180
Pu-239 Capture	1.02875E+12	**4.6378**	0.1317	0.5955	0.5976	1.9986
Pu-240 Capture	3.13125E+11	**10.9878**	0.1495	0.5220	0.5243	2.0509
Pu-241 Capture	5.72420E+10	**10.8240**	0.1294	0.6324	0.6426	2.8706
Pu-242 Capture	3.82369E+10	**19.7742**	0.6236	1.2849	1.2887	3.3621
Am-241 Capture	1.53269E+11	**4.7001**	0.1121	0.5625	0.5676	1.8604
Am-242m Capture	7.66985E+08	**14.2233**	0.2319	0.8404	0.8514	3.2595
Am-243 Capture	2.27687E+10	**5.1920**	0.3036	1.1255	1.3524	2.3626
Cm-242 Capture	7.23472E+08	**15.6376**	0.2274	0.9200	0.9241	3.2737
Cm-244 Capture	4.03373E+09	**14.0488**	0.1629	0.6786	0.7173	2.6317
Cm-245 Capture	1.44377E+08	**12.3336**	0.1460	0.6804	0.7000	2.9229
Fe (n,el)	1.64649E+09	**3.1362**	0.2451	0.5482	0.5534	1.1479
Na-23 (n,el)	1.57721E+09	**3.2893**	0.2669	0.5822	0.5870	1.1961
End of Cycle Masses						
EOC U-234 Mass (kg, 1/3 core)	7.5899E-03	**0.3596**	*0.3544*	*0.3552*	*0.3552*	*0.3557*
EOC U-235 Mass (kg, 1/3 core)	1.6698E+00	**0.0524**	*0.0025*	*0.0089*	*0.0090*	*0.0266*
EOC U-236 Mass (kg, 1/3 core)	1.1398E-01	**0.2421**	*0.1057*	*0.1141*	*0.1151*	*0.1665*
EOC U-238 Mass (kg, 1/3 core)	1.0820E+03	**0.0100**	*0.0009*	*0.0023*	*0.0024*	*0.0064*
EOC NP237 Mass (kg, 1/3 core)	1.2497E+00	**0.1893**	*0.0955*	*0.1038*	*0.1039*	*0.1190*
EOC PU236 Mass (kg, 1/3 core)	8.6229E-06	**2.4712**	*2.2312*	*2.3228*	*2.3228*	*2.3372*
EOC PU238 Mass (kg, 1/3 core)	5.8723E-01	**0.5148**	*0.0425*	*0.0790*	*0.0850*	*0.1495*
EOC PU239 Mass (kg, 1/3 core)	2.1251E+02	**0.0580**	*0.0016*	*0.0091*	*0.0095*	*0.0331*
EOC PU240 Mass (kg, 1/3 core)	2.7814E+01	**0.2461**	*0.0075*	*0.0260*	*0.0262*	*0.0967*
EOC PU241 Mass (kg, 1/3 core)	3.0264E+00	**1.0211**	*0.0152*	*0.0492*	*0.0716*	*0.1946*
EOC PU242 Mass (kg, 1/3 core)	1.3785E+00	**0.2957**	*0.0035*	*0.0133*	*0.0156*	*0.0593*
EOC AM241 Mass (kg, 1/3 core)	1.3285E+00	**0.1766**	*0.0031*	*0.0202*	*0.0204*	*0.0666*
EOC AM242 Mass (kg, 1/3 core)	3.9258E-02	**1.4299**	*0.0108*	*0.1290*	*0.1473*	*0.4671*
EOC AM243 Mass (kg, 1/3 core)	2.6104E-01	**0.8554**	*0.0104*	*0.0397*	*0.0445*	*0.1435*
EOC CM242 Mass (kg, 1/3 core)	4.8115E-02	**2.2253**	*0.0302*	*0.2712*	*0.2735*	*0.9025*
EOC CM243 Mass (kg, 1/3 core)	1.3710E-03	**2.9256**	*1.9396*	*1.9497*	*1.9498*	*2.0042*
EOC CM244 Mass (kg, 1/3 core)	6.6660E-02	**0.7652**	*0.0090*	*0.0928*	*0.1190*	*0.2179*
EOC CM245 Mass (kg, 1/3 core)	6.2128E-03	**3.1718**	*0.0132*	*0.1138*	*0.1270*	*0.5015*
EOC CM246 Mass (kg, 1/3 core)	4.2967E-04	**1.0307**	*0.0070*	*0.0600*	*0.0618*	*0.2716*

Table D.4: Posteriori uncertainties for ABTR-SU adapted to TRU v. 1-B.

Parameter	Nominal Values	A Priori	0%	1%	1% + FPY	7.50%
Average Reaction Rates						
U-235 Capture	1.36070E+10	**1.5221**	0.0944	0.3116	0.3154	0.8008
Np-237 Capture	1.15415E+11	**3.0851**	0.2802	0.5523	0.5548	1.4016
Pu-238 Capture	2.83738E+10	**11.8061**	0.2495	0.7500	0.7534	2.1654
Pu-239 Capture	1.02875E+12	**4.6378**	0.1303	0.5781	0.5802	2.0411
Pu-240 Capture	3.13125E+11	**10.9878**	0.1453	0.5215	0.5238	2.0956
Pu-241 Capture	5.72420E+10	**10.8240**	0.1285	0.5932	0.6033	2.9320
Pu-242 Capture	3.82369E+10	**19.7742**	0.6211	1.2293	1.2332	3.3693
Am-241 Capture	1.53269E+11	**4.7001**	0.1090	0.5374	0.5425	1.9060
Am-242m Capture	7.66985E+08	**14.2233**	0.2261	0.7998	0.8103	3.2523
Am-243 Capture	2.27687E+10	**5.1920**	0.2986	1.0594	1.2869	2.3889
Cm-242 Capture	7.23472E+08	**15.6376**	0.2217	0.8732	0.8776	3.3235
Cm-244 Capture	4.03373E+09	**14.0488**	0.1579	0.6391	0.6764	2.7006
Cm-245 Capture	1.44377E+08	**12.3336**	0.1434	0.6360	0.6545	2.9724
Fe (n,el)	1.64649E+09	**3.1362**	0.2444	0.5449	0.5498	1.1587
Na-23 (n,el)	1.57721E+09	**3.2893**	0.2646	0.5834	0.5880	1.2160
End of Cycle Masses						
EOC U-234 Mass (kg, 1/3 core)	7.5899E-03	**0.3596**	*0.3548*	*0.3552*	*0.3552*	*0.3557*
EOC U-235 Mass (kg, 1/3 core)	1.6698E+00	**0.0524**	*0.0026*	*0.0089*	*0.0090*	*0.0269*
EOC U-236 Mass (kg, 1/3 core)	1.1398E-01	**0.2421**	*0.1057*	*0.1149*	*0.1155*	*0.1662*
EOC U-238 Mass (kg, 1/3 core)	1.0820E+03	**0.0100**	*0.0009*	*0.0023*	*0.0024*	*0.0063*
EOC NP237 Mass (kg, 1/3 core)	1.2497E+00	**0.1893**	*0.0982*	*0.1039*	*0.1041*	*0.1197*
EOC PU236 Mass (kg, 1/3 core)	8.6229E-06	**2.4712**	*2.1065*	*2.3226*	*2.3226*	*2.3380*
EOC PU238 Mass (kg, 1/3 core)	5.8723E-01	**0.5148**	*0.0390*	*0.0784*	*0.0836*	*0.1517*
EOC PU239 Mass (kg, 1/3 core)	2.1251E+02	**0.0580**	*0.0017*	*0.0093*	*0.0097*	*0.0329*
EOC PU240 Mass (kg, 1/3 core)	2.7814E+01	**0.2461**	*0.0077*	*0.0257*	*0.0258*	*0.0988*
EOC PU241 Mass (kg, 1/3 core)	3.0264E+00	**1.0211**	*0.0150*	*0.0488*	*0.0709*	*0.2000*
EOC PU242 Mass (kg, 1/3 core)	1.3785E+00	**0.2957**	*0.0035*	*0.0126*	*0.0152*	*0.0606*
EOC AM241 Mass (kg, 1/3 core)	1.3285E+00	**0.1766**	*0.0029*	*0.0190*	*0.0192*	*0.0683*
EOC AM242 Mass (kg, 1/3 core)	3.9258E-02	**1.4299**	*0.0110*	*0.1210*	*0.1381*	*0.4792*
EOC AM243 Mass (kg, 1/3 core)	2.6104E-01	**0.8554**	*0.0104*	*0.0366*	*0.0415*	*0.1443*
EOC CM242 Mass (kg, 1/3 core)	4.8115E-02	**2.2253**	*0.0296*	*0.2545*	*0.2568*	*0.9260*
EOC CM243 Mass (kg, 1/3 core)	1.3710E-03	**2.9256**	*1.9435*	*1.9501*	*1.9502*	*2.0059*
EOC CM244 Mass (kg, 1/3 core)	6.6660E-02	**0.7652**	*0.0089*	*0.0858*	*0.1119*	*0.2212*
EOC CM245 Mass (kg, 1/3 core)	6.2128E-03	**3.1718**	*0.0131*	*0.1041*	*0.1165*	*0.5132*
EOC CM246 Mass (kg, 1/3 core)	4.2967E-04	**1.0307**	*0.0071*	*0.0546*	*0.0563*	*0.2742*

Table D.5: Posteriori uncertainties for ABTR-SU adapted to TRU v. 1-C.

Parameter	Nominal Values	A Priori	0%	1%	1% + FPY	7.50%
Average Reaction Rates						
U-235 Capture	1.36070E+10	**1.5221**	0.0909	0.3001	0.3038	0.7753
Np-237 Capture	1.15415E+11	**3.0851**	0.2775	0.5181	0.5207	1.3881
Pu-238 Capture	2.83738E+10	**11.8061**	0.2382	0.6719	0.6748	1.9996
Pu-239 Capture	1.02875E+12	**4.6378**	0.1261	0.5013	0.5037	1.8951
Pu-240 Capture	3.13125E+11	**10.9878**	0.1425	0.4685	0.4711	1.9647
Pu-241 Capture	5.72420E+10	**10.8240**	0.1250	0.5083	0.5168	2.4766
Pu-242 Capture	3.82369E+10	**19.7742**	0.6152	1.1651	1.1689	3.0150
Am-241 Capture	1.53269E+11	**4.7001**	0.1057	0.4666	0.4714	1.7747
Am-242m Capture	7.66985E+08	**14.2233**	0.2231	0.7259	0.7346	2.8266
Am-243 Capture	2.27687E+10	**5.1920**	0.2922	0.9863	1.1851	2.2602
Cm-242 Capture	7.23472E+08	**15.6376**	0.2161	0.8033	0.8077	2.9131
Cm-244 Capture	4.03373E+09	**14.0488**	0.1540	0.5586	0.5891	2.3374
Cm-245 Capture	1.44377E+08	**12.3336**	0.1398	0.5475	0.5626	2.5404
Fe (n,el)	1.64649E+09	**3.1362**	0.2200	0.5369	0.5421	1.1193
Na-23 (n,el)	1.57721E+09	**3.2893**	0.2375	0.5709	0.5757	1.1696
End of Cycle Masses						
EOC U-234 Mass (kg, 1/3 core)	7.5899E-03	**0.3596**	*0.3547*	*0.3552*	*0.3552*	*0.3557*
EOC U-235 Mass (kg, 1/3 core)	1.6698E+00	**0.0524**	*0.0025*	*0.0086*	*0.0086*	*0.0260*
EOC U-236 Mass (kg, 1/3 core)	1.1398E-01	**0.2421**	*0.1056*	*0.1131*	*0.1138*	*0.1635*
EOC U-238 Mass (kg, 1/3 core)	1.0820E+03	**0.0100**	*0.0009*	*0.0023*	*0.0024*	*0.0062*
EOC NP237 Mass (kg, 1/3 core)	1.2497E+00	**0.1893**	*0.0973*	*0.1037*	*0.1038*	*0.1186*
EOC PU236 Mass (kg, 1/3 core)	8.6229E-06	**2.4712**	*2.2433*	*2.3225*	*2.3226*	*2.3368*
EOC PU238 Mass (kg, 1/3 core)	5.8723E-01	**0.5148**	*0.0366*	*0.0752*	*0.0789*	*0.1420*
EOC PU239 Mass (kg, 1/3 core)	2.1251E+02	**0.0580**	*0.0016*	*0.0082*	*0.0085*	*0.0322*
EOC PU240 Mass (kg, 1/3 core)	2.7814E+01	**0.2461**	*0.0074*	*0.0220*	*0.0222*	*0.0923*
EOC PU241 Mass (kg, 1/3 core)	3.0264E+00	**1.0211**	*0.0149*	*0.0429*	*0.0600*	*0.1832*
EOC PU242 Mass (kg, 1/3 core)	1.3785E+00	**0.2957**	*0.0033*	*0.0107*	*0.0128*	*0.0517*
EOC AM241 Mass (kg, 1/3 core)	1.3285E+00	**0.1766**	*0.0029*	*0.0163*	*0.0164*	*0.0631*
EOC AM242 Mass (kg, 1/3 core)	3.9258E-02	**1.4299**	*0.0111*	*0.1011*	*0.1149*	*0.4354*
EOC AM243 Mass (kg, 1/3 core)	2.6104E-01	**0.8554**	*0.0104*	*0.0323*	*0.0367*	*0.1262*
EOC CM242 Mass (kg, 1/3 core)	4.8115E-02	**2.2253**	*0.0298*	*0.2153*	*0.2174*	*0.8552*
EOC CM243 Mass (kg, 1/3 core)	1.3710E-03	**2.9256**	*1.9429*	*1.9494*	*1.9495*	*1.9923*
EOC CM244 Mass (kg, 1/3 core)	6.6660E-02	**0.7652**	*0.0085*	*0.0774*	*0.1007*	*0.2066*
EOC CM245 Mass (kg, 1/3 core)	6.2128E-03	**3.1718**	*0.0129*	*0.0862*	*0.0961*	*0.4389*
EOC CM246 Mass (kg, 1/3 core)	4.2967E-04	**1.0307**	*0.0070*	*0.0459*	*0.0472*	*0.2340*

Table D.6: Posteriori uncertainties for ABTR-SU adapted to TRU v. 2.

Parameter	Nominal Values	A Priori	0%	1%	1% + FPY	7.50%
Average Reaction Rates						
U-235 Capture	1.36070E+10	**1.5221**	0.1265	0.3700	0.3725	0.8613
Np-237 Capture	1.15415E+11	**3.0851**	0.3112	0.6782	0.6802	1.4626
Pu-238 Capture	2.83738E+10	**11.8061**	0.3172	1.4951	1.4999	2.4220
Pu-239 Capture	1.02875E+12	**4.6378**	0.1850	1.2094	1.2132	2.2921
Pu-240 Capture	3.13125E+11	**10.9878**	0.1992	0.7593	0.7612	2.3065
Pu-241 Capture	5.72420E+10	**10.8240**	0.1873	2.4630	2.4842	4.2685
Pu-242 Capture	3.82369E+10	**19.7742**	0.6893	2.7044	2.7110	4.3720
Am-241 Capture	1.53269E+11	**4.7001**	0.1524	1.3148	1.3187	2.1184
Am-242m Capture	7.66985E+08	**14.2233**	0.4281	3.4158	3.4397	4.8447
Am-243 Capture	2.27687E+10	**5.1920**	0.3671	2.0802	2.1409	2.6240
Cm-242 Capture	7.23472E+08	**15.6376**	0.4451	3.4169	3.4184	4.5935
Cm-244 Capture	4.03373E+09	**14.0488**	0.2244	2.0696	2.1349	3.5593
Cm-245 Capture	1.44377E+08	**12.3336**	0.1875	2.3870	2.4366	4.1327
Fe (n,el)	1.64649E+09	**3.1362**	0.3261	0.8129	0.8190	1.2955
Na-23 (n,el)	1.57721E+09	**3.2893**	0.3538	0.8704	0.8752	1.3524
End of Cycle Masses						
EOC U-234 Mass (kg, 1/3 core)	7.5899E-03	**0.3596**	*0.3546*	*0.3553*	*0.3554*	*0.3559*
EOC U-235 Mass (kg, 1/3 core)	1.6698E+00	**0.0524**	*0.0033*	*0.0108*	*0.0109*	*0.0295*
EOC U-236 Mass (kg, 1/3 core)	1.1398E-01	**0.2421**	*0.1062*	*0.1186*	*0.1199*	*0.1735*
EOC U-238 Mass (kg, 1/3 core)	1.0820E+03	**0.0100**	*0.0011*	*0.0025*	*0.0026*	*0.0068*
EOC NP237 Mass (kg, 1/3 core)	1.2497E+00	**0.1893**	*0.0966*	*0.1077*	*0.1079*	*0.1219*
EOC PU236 Mass (kg, 1/3 core)	8.6229E-06	**2.4712**	*2.1927*	*2.3282*	*2.3283*	*2.3421*
EOC PU238 Mass (kg, 1/3 core)	5.8723E-01	**0.5148**	*0.0454*	*0.1031*	*0.1228*	*0.1745*
EOC PU239 Mass (kg, 1/3 core)	2.1251E+02	**0.0580**	*0.0022*	*0.0131*	*0.0134*	*0.0353*
EOC PU240 Mass (kg, 1/3 core)	2.7814E+01	**0.2461**	*0.0092*	*0.0527*	*0.0529*	*0.1088*
EOC PU241 Mass (kg, 1/3 core)	3.0264E+00	**1.0211**	*0.0203*	*0.1091*	*0.1312*	*0.2293*
EOC PU242 Mass (kg, 1/3 core)	1.3785E+00	**0.2957**	*0.0043*	*0.0488*	*0.0502*	*0.0852*
EOC AM241 Mass (kg, 1/3 core)	1.3285E+00	**0.1766**	*0.0041*	*0.0498*	*0.0500*	*0.0779*
EOC AM242 Mass (kg, 1/3 core)	3.9258E-02	**1.4299**	*0.0216*	*0.3666*	*0.4004*	*0.5667*
EOC AM243 Mass (kg, 1/3 core)	2.6104E-01	**0.8554**	*0.0119*	*0.1148*	*0.1161*	*0.1918*
EOC CM242 Mass (kg, 1/3 core)	4.8115E-02	**2.2253**	*0.0492*	*0.6817*	*0.6835*	*1.0375*
EOC CM243 Mass (kg, 1/3 core)	1.3710E-03	**2.9256**	*1.9425*	*2.0119*	*2.0119*	*2.0595*
EOC CM244 Mass (kg, 1/3 core)	6.6660E-02	**0.7652**	*0.0144*	*0.1961*	*0.2039*	*0.2473*
EOC CM245 Mass (kg, 1/3 core)	6.2128E-03	**3.1718**	*0.0234*	*0.4075*	*0.4350*	*0.6906*
EOC CM246 Mass (kg, 1/3 core)	4.2967E-04	**1.0307**	*0.0099*	*0.2276*	*0.2321*	*0.3845*

Table D.7: Posteriori uncertainties for ABTR-SU adapted to TRU v. 2-B.

Parameter	Nominal Values	A Priori	0%	1%	1% + FPY	7.50%
Average Reaction Rates						
U-235 Capture	1.36070E+10	**1.5221**	0.1286	0.3985	0.4009	0.8885
Np-237 Capture	1.15415E+11	**3.0851**	0.3174	0.7311	0.7329	1.4940
Pu-238 Capture	2.83738E+10	**11.8061**	0.3176	1.7379	1.7410	2.5959
Pu-239 Capture	1.02875E+12	**4.6378**	0.1894	1.4342	1.4368	2.4383
Pu-240 Capture	3.13125E+11	**10.9878**	0.2051	0.8693	0.8710	2.4552
Pu-241 Capture	5.72420E+10	**10.8240**	0.1977	3.2667	3.2903	4.9975
Pu-242 Capture	3.82369E+10	**19.7742**	0.7008	3.1706	3.1778	4.7831
Am-241 Capture	1.53269E+11	**4.7001**	0.1578	1.5380	1.5423	2.2689
Am-242m Capture	7.66985E+08	**14.2233**	0.4497	4.2341	4.2554	5.3492
Am-243 Capture	2.27687E+10	**5.1920**	0.3796	2.2523	2.2951	2.7373
Cm-242 Capture	7.23472E+08	**15.6376**	0.4517	4.0957	4.0972	5.1378
Cm-244 Capture	4.03373E+09	**14.0488**	0.2289	2.6263	2.6973	4.0651
Cm-245 Capture	1.44377E+08	**12.3336**	0.1909	3.0436	3.0980	4.7059
Fe (n,el)	1.64649E+09	**3.1362**	0.3770	0.9710	0.9751	1.3690
Na-23 (n,el)	1.57721E+09	**3.2893**	0.4078	1.0509	1.0543	1.4432
End of Cycle Masses						
EOC U-234 Mass (kg, 1/3 core)	7.5899E-03	**0.3596**	*0.3549*	*0.3553*	*0.3554*	*0.3560*
EOC U-235 Mass (kg, 1/3 core)	1.6698E+00	**0.0524**	*0.0036*	*0.0116*	*0.0117*	*0.0304*
EOC U-236 Mass (kg, 1/3 core)	1.1398E-01	**0.2421**	*0.1062*	*0.1193*	*0.1199*	*0.1731*
EOC U-238 Mass (kg, 1/3 core)	1.0820E+03	**0.0100**	*0.0011*	*0.0027*	*0.0028*	*0.0068*
EOC NP237 Mass (kg, 1/3 core)	1.2497E+00	**0.1893**	*0.0964*	*0.1106*	*0.1108*	*0.1245*
EOC PU236 Mass (kg, 1/3 core)	8.6229E-06	**2.4712**	*2.0997*	*2.3315*	*2.3316*	*2.3457*
EOC PU238 Mass (kg, 1/3 core)	5.8723E-01	**0.5148**	*0.0451*	*0.1182*	*0.1445*	*0.1969*
EOC PU239 Mass (kg, 1/3 core)	2.1251E+02	**0.0580**	*0.0028*	*0.0149*	*0.0151*	*0.0355*
EOC PU240 Mass (kg, 1/3 core)	2.7814E+01	**0.2461**	*0.0099*	*0.0638*	*0.0640*	*0.1157*
EOC PU241 Mass (kg, 1/3 core)	3.0264E+00	**1.0211**	*0.0214*	*0.1365*	*0.1604*	*0.2535*
EOC PU242 Mass (kg, 1/3 core)	1.3785E+00	**0.2957**	*0.0047*	*0.0640*	*0.0658*	*0.0991*
EOC AM241 Mass (kg, 1/3 core)	1.3285E+00	**0.1766**	*0.0044*	*0.0580*	*0.0582*	*0.0838*
EOC AM242 Mass (kg, 1/3 core)	3.9258E-02	**1.4299**	*0.0245*	*0.4432*	*0.4801*	*0.6256*
EOC AM243 Mass (kg, 1/3 core)	2.6104E-01	**0.8554**	*0.0124*	*0.1382*	*0.1393*	*0.2114*
EOC CM242 Mass (kg, 1/3 core)	4.8115E-02	**2.2253**	*0.0534*	*0.7905*	*0.7925*	*1.1128*
EOC CM243 Mass (kg, 1/3 core)	1.3710E-03	**2.9256**	*1.9451*	*2.0406*	*2.0408*	*2.0863*
EOC CM244 Mass (kg, 1/3 core)	6.6660E-02	**0.7652**	*0.0164*	*0.2158*	*0.2229*	*0.2625*
EOC CM245 Mass (kg, 1/3 core)	6.2128E-03	**3.1718**	*0.0246*	*0.5163*	*0.5478*	*0.7924*
EOC CM246 Mass (kg, 1/3 core)	4.2967E-04	**1.0307**	*0.0105*	*0.2862*	*0.2910*	*0.4341*

Table D.8: Posteriori uncertainties for ABTR-SU adapted to TRU v. 3.

Parameter	Nominal Values	A Priori	0%	1%	1% + FPY	7.50%
Average Reaction Rates						
U-235 Capture	1.36070E+10	**1.5221**	0.0973	0.2990	0.3020	0.7681
Np-237 Capture	1.15415E+11	**3.0851**	0.2789	0.5358	0.5381	1.3844
Pu-238 Capture	2.83738E+10	**11.8061**	0.2506	0.7891	0.7925	2.0055
Pu-239 Capture	1.02875E+12	**4.6378**	0.1311	0.5890	0.5917	1.9049
Pu-240 Capture	3.13125E+11	**10.9878**	0.1467	0.5028	0.5051	1.9644
Pu-241 Capture	5.72420E+10	**10.8240**	0.1316	0.6727	0.6830	2.6182
Pu-242 Capture	3.82369E+10	**19.7742**	0.5772	1.3383	1.3424	3.1827
Am-241 Capture	1.53269E+11	**4.7001**	0.1122	0.5749	0.5796	1.7689
Am-242m Capture	7.66985E+08	**14.2233**	0.2314	0.8884	0.9001	3.1084
Am-243 Capture	2.27687E+10	**5.1920**	0.2855	1.2100	1.4158	2.2838
Cm-242 Capture	7.23472E+08	**15.6376**	0.2329	0.9923	0.9961	3.0907
Cm-244 Capture	4.03373E+09	**14.0488**	0.1651	0.7052	0.7425	2.3999
Cm-245 Capture	1.44377E+08	**12.3336**	0.1486	0.7185	0.7388	2.6783
Fe (n,el)	1.64649E+09	**3.1362**	0.2514	0.5524	0.5577	1.1416
Na-23 (n,el)	1.57721E+09	**3.2893**	0.2718	0.5755	0.5807	1.1810
End of Cycle Masses						
EOC U-234 Mass (kg, 1/3 core)	7.5899E-03	**0.3596**	*0.3551*	*0.3553*	*0.3553*	*0.3557*
EOC U-235 Mass (kg, 1/3 core)	1.6698E+00	**0.0524**	*0.0025*	*0.0088*	*0.0089*	*0.0256*
EOC U-236 Mass (kg, 1/3 core)	1.1398E-01	**0.2421**	*0.1057*	*0.1144*	*0.1154*	*0.1650*
EOC U-238 Mass (kg, 1/3 core)	1.0820E+03	**0.0100**	*0.0009*	*0.0023*	*0.0024*	*0.0063*
EOC NP237 Mass (kg, 1/3 core)	1.2497E+00	**0.1893**	*0.0967*	*0.1039*	*0.1040*	*0.1184*
EOC PU236 Mass (kg, 1/3 core)	8.6229E-06	**2.4712**	*2.2484*	*2.3228*	*2.3229*	*2.3369*
EOC PU238 Mass (kg, 1/3 core)	5.8723E-01	**0.5148**	*0.0397*	*0.0792*	*0.0849*	*0.1444*
EOC PU239 Mass (kg, 1/3 core)	2.1251E+02	**0.0580**	*0.0015*	*0.0086*	*0.0089*	*0.0328*
EOC PU240 Mass (kg, 1/3 core)	2.7814E+01	**0.2461**	*0.0075*	*0.0249*	*0.0251*	*0.0926*
EOC PU241 Mass (kg, 1/3 core)	3.0264E+00	**1.0211**	*0.0138*	*0.0492*	*0.0686*	*0.1837*
EOC PU242 Mass (kg, 1/3 core)	1.3785E+00	**0.2957**	*0.0033*	*0.0140*	*0.0158*	*0.0544*
EOC AM241 Mass (kg, 1/3 core)	1.3285E+00	**0.1766**	*0.0031*	*0.0210*	*0.0211*	*0.0628*
EOC AM242 Mass (kg, 1/3 core)	3.9258E-02	**1.4299**	*0.0103*	*0.1367*	*0.1555*	*0.4390*
EOC AM243 Mass (kg, 1/3 core)	2.6104E-01	**0.8554**	*0.0096*	*0.0431*	*0.0475*	*0.1344*
EOC CM242 Mass (kg, 1/3 core)	4.8115E-02	**2.2253**	*0.0296*	*0.2828*	*0.2850*	*0.8533*
EOC CM243 Mass (kg, 1/3 core)	1.3710E-03	**2.9256**	*1.9468*	*1.9514*	*1.9515*	*1.9988*
EOC CM244 Mass (kg, 1/3 core)	6.6660E-02	**0.7652**	*0.0086*	*0.1021*	*0.1259*	*0.2091*
EOC CM245 Mass (kg, 1/3 core)	6.2128E-03	**3.1718**	*0.0135*	*0.1216*	*0.1352*	*0.4564*
EOC CM246 Mass (kg, 1/3 core)	4.2967E-04	**1.0307**	*0.0070*	*0.0657*	*0.0677*	*0.2508*

Table D.9: Posteriori uncertainties for ABTR-SU adapted to ZPPR-SNF.

Parameter	Nominal Values	A Priori	0%	1%	1% + FPY	7.50%
Average Reaction Rates						
U-235 Capture	1.36070E+10	**1.5221**	0.1030	0.3134	0.3166	0.7696
Np-237 Capture	1.15415E+11	**3.0851**	0.2804	0.5419	0.5443	1.3881
Pu-238 Capture	2.83738E+10	**11.8061**	0.2497	0.8022	0.8060	1.9864
Pu-239 Capture	1.02875E+12	**4.6378**	0.1385	0.5991	0.6016	1.8898
Pu-240 Capture	3.13125E+11	**10.9878**	0.1508	0.5042	0.5066	1.9413
Pu-241 Capture	5.72420E+10	**10.8240**	0.1353	0.6928	0.7035	2.5495
Pu-242 Capture	3.82369E+10	**19.7742**	0.5813	1.3927	1.3970	3.1693
Am-241 Capture	1.53269E+11	**4.7001**	0.1166	0.5892	0.5940	1.7521
Am-242m Capture	7.66985E+08	**14.2233**	0.2375	0.9198	0.9317	3.0603
Am-243 Capture	2.27687E+10	**5.1920**	0.2915	1.2506	1.4446	2.2685
Cm-242 Capture	7.23472E+08	**15.6376**	0.2455	1.0295	1.0332	3.0308
Cm-244 Capture	4.03373E+09	**14.0488**	0.1724	0.7252	0.7618	2.3607
Cm-245 Capture	1.44377E+08	**12.3336**	0.1541	0.7454	0.7659	2.6325
Fe (n,el)	1.64649E+09	**3.1362**	0.2659	0.5720	0.5774	1.1707
Na-23 (n,el)	1.57721E+09	**3.2893**	0.2894	0.5955	0.6004	1.2025
End of Cycle Masses						
EOC U-234 Mass (kg, 1/3 core)	7.5899E-03	**0.3596**	*0.3551*	*0.3553*	*0.3553*	*0.3557*
EOC U-235 Mass (kg, 1/3 core)	1.6698E+00	**0.0524**	*0.0026*	*0.0088*	*0.0089*	*0.0258*
EOC U-236 Mass (kg, 1/3 core)	1.1398E-01	**0.2421**	*0.1057*	*0.1134*	*0.1143*	*0.1636*
EOC U-238 Mass (kg, 1/3 core)	1.0820E+03	**0.0100**	*0.0009*	*0.0023*	*0.0024*	*0.0063*
EOC NP237 Mass (kg, 1/3 core)	1.2497E+00	**0.1893**	*0.0959*	*0.1041*	*0.1042*	*0.1184*
EOC PU236 Mass (kg, 1/3 core)	8.6229E-06	**2.4712**	*2.2966*	*2.3229*	*2.3229*	*2.3379*
EOC PU238 Mass (kg, 1/3 core)	5.8723E-01	**0.5148**	*0.0393*	*0.0789*	*0.0843*	*0.1423*
EOC PU239 Mass (kg, 1/3 core)	2.1251E+02	**0.0580**	*0.0015*	*0.0083*	*0.0086*	*0.0330*
EOC PU240 Mass (kg, 1/3 core)	2.7814E+01	**0.2461**	*0.0076*	*0.0250*	*0.0252*	*0.0919*
EOC PU241 Mass (kg, 1/3 core)	3.0264E+00	**1.0211**	*0.0139*	*0.0495*	*0.0672*	*0.1813*
EOC PU242 Mass (kg, 1/3 core)	1.3785E+00	**0.2957**	*0.0032*	*0.0143*	*0.0158*	*0.0531*
EOC AM241 Mass (kg, 1/3 core)	1.3285E+00	**0.1766**	*0.0030*	*0.0214*	*0.0216*	*0.0621*
EOC AM242 Mass (kg, 1/3 core)	3.9258E-02	**1.4299**	*0.0104*	*0.1399*	*0.1585*	*0.4326*
EOC AM243 Mass (kg, 1/3 core)	2.6104E-01	**0.8554**	*0.0098*	*0.0447*	*0.0488*	*0.1332*
EOC CM242 Mass (kg, 1/3 core)	4.8115E-02	**2.2253**	*0.0304*	*0.2909*	*0.2930*	*0.8437*
EOC CM243 Mass (kg, 1/3 core)	1.3710E-03	**2.9256**	*1.9467*	*1.9518*	*1.9518*	*1.9968*
EOC CM244 Mass (kg, 1/3 core)	6.6660E-02	**0.7652**	*0.0087*	*0.1054*	*0.1279*	*0.2066*
EOC CM245 Mass (kg, 1/3 core)	6.2128E-03	**3.1718**	*0.0140*	*0.1255*	*0.1391*	*0.4478*
EOC CM246 Mass (kg, 1/3 core)	4.2967E-04	**1.0307**	*0.0071*	*0.0687*	*0.0707*	*0.2466*

Table D.10: Posteriori uncertainties for ABTR-SU adapted to ZPPR-ABTR.

Parameter	Nominal Values	A Priori	0%	1%	1% + FPY	7.50%
Average Reaction Rates						
U-235 Capture	1.36070E+10	**1.5221**	0.0737	0.3680	0.3763	0.9026
Np-237 Capture	1.15415E+11	**3.0851**	0.2709	0.5480	0.5553	1.5848
Pu-238 Capture	2.83738E+10	**11.8061**	0.2528	0.5727	0.5786	1.7858
Pu-239 Capture	1.02875E+12	**4.6378**	0.1278	0.4929	0.5022	1.6530
Pu-240 Capture	3.13125E+11	**10.9878**	0.1217	0.4643	0.4731	1.7496
Pu-241 Capture	5.72420E+10	**10.8240**	0.0963	0.4156	0.4236	1.7826
Pu-242 Capture	3.82369E+10	**19.7742**	0.5482	1.1233	1.1337	2.3549
Am-241 Capture	1.53269E+11	**4.7001**	0.0884	0.3985	0.4065	1.6244
Am-242m Capture	7.66985E+08	**14.2233**	0.2183	0.7516	0.7652	2.1568
Am-243 Capture	2.27687E+10	**5.1920**	0.2569	0.7776	0.8665	1.9417
Cm-242 Capture	7.23472E+08	**15.6376**	0.1826	0.7302	0.7448	2.1480
Cm-244 Capture	4.03373E+09	**14.0488**	0.1305	0.4899	0.5105	1.8391
Cm-245 Capture	1.44377E+08	**12.3336**	0.1259	0.5086	0.5230	1.9049
Fe (n,el)	1.64649E+09	**3.1362**	0.1449	0.5756	0.5795	1.3454
Na-23 (n,el)	1.57721E+09	**3.2893**	0.1600	0.6226	0.6262	1.4315
End of Cycle Masses						
EOC U-234 Mass (kg, 1/3 core)	7.5899E-03	**0.3596**	*0.1658*	*0.3527*	*0.3530*	*0.3548*
EOC U-235 Mass (kg, 1/3 core)	1.6698E+00	**0.0524**	*0.0022*	*0.0093*	*0.0095*	*0.0296*
EOC U-236 Mass (kg, 1/3 core)	1.1398E-01	**0.2421**	*0.0842*	*0.1174*	*0.1183*	*0.1633*
EOC U-238 Mass (kg, 1/3 core)	1.0820E+03	**0.0100**	*0.0010*	*0.0025*	*0.0025*	*0.0067*
EOC NP237 Mass (kg, 1/3 core)	1.2497E+00	**0.1893**	*0.0977*	*0.1063*	*0.1064*	*0.1249*
EOC PU236 Mass (kg, 1/3 core)	8.6229E-06	**2.4712**	*2.2716*	*2.3227*	*2.3228*	*2.3477*
EOC PU238 Mass (kg, 1/3 core)	5.8723E-01	**0.5148**	*0.0452*	*0.0758*	*0.0775*	*0.1308*
EOC PU239 Mass (kg, 1/3 core)	2.1251E+02	**0.0580**	*0.0023*	*0.0084*	*0.0088*	*0.0347*
EOC PU240 Mass (kg, 1/3 core)	2.7814E+01	**0.2461**	*0.0070*	*0.0253*	*0.0258*	*0.0810*
EOC PU241 Mass (kg, 1/3 core)	3.0264E+00	**1.0211**	*0.0119*	*0.0376*	*0.0454*	*0.1514*
EOC PU242 Mass (kg, 1/3 core)	1.3785E+00	**0.2957**	*0.0028*	*0.0089*	*0.0106*	*0.0374*
EOC AM241 Mass (kg, 1/3 core)	1.3285E+00	**0.1766**	*0.0024*	*0.0115*	*0.0118*	*0.0558*
EOC AM242 Mass (kg, 1/3 core)	3.9258E-02	**1.4299**	*0.0091*	*0.0643*	*0.0711*	*0.3592*
EOC AM243 Mass (kg, 1/3 core)	2.6104E-01	**0.8554**	*0.0093*	*0.0239*	*0.0258*	*0.0847*
EOC CM242 Mass (kg, 1/3 core)	4.8115E-02	**2.2253**	*0.0247*	*0.1503*	*0.1537*	*0.7464*
EOC CM243 Mass (kg, 1/3 core)	1.3710E-03	**2.9256**	*0.7555*	*1.9354*	*1.9368*	*1.9584*
EOC CM244 Mass (kg, 1/3 core)	6.6660E-02	**0.7652**	*0.0079*	*0.0495*	*0.0606*	*0.1657*
EOC CM245 Mass (kg, 1/3 core)	6.2128E-03	**3.1718**	*0.0115*	*0.0563*	*0.0615*	*0.3035*
EOC CM246 Mass (kg, 1/3 core)	4.2967E-04	**1.0307**	*0.0061*	*0.0349*	*0.0359*	*0.1540*

Table D.11: Posteriori uncertainties for ABTR-EQ adapted to ZPPR-15B.

Parameter	Nominal Values	A Priori	0%	1%	1% + FPY	7.50%
Average Reaction Rates						
U-235 Capture	1.50418E+10	**1.7741**	0.2544	0.4257	0.4288	0.8552
Np-237 Capture	1.29109E+11	**3.0616**	2.3290	2.3735	2.3741	2.5312
Pu-238 Capture	9.24364E+10	**11.9504**	0.2727	0.7570	0.7607	1.9977
Pu-239 Capture	8.96572E+11	**4.9738**	0.2903	0.7261	0.7286	2.0205
Pu-240 Capture	6.56849E+11	**11.4211**	0.2729	0.5597	0.5622	1.9907
Pu-241 Capture	8.06078E+10	**11.3481**	0.2793	0.8085	0.8220	2.7377
Pu-242 Capture	1.07587E+11	**21.0632**	0.2870	0.8969	0.9014	3.0333
Am-241 Capture	2.78575E+11	**4.8517**	0.2536	0.7134	0.7191	1.8590
Am-242m Capture	3.13909E+09	**14.3345**	14.0992	14.1301	14.1304	14.1835
Am-243 Capture	1.01034E+11	**4.6468**	4.2011	4.2211	4.2215	4.3025
Cm-242 Capture	1.15857E+09	**16.6336**	16.2367	16.2586	16.2588	16.3155
Cm-244 Capture	3.26601E+10	**14.4697**	14.3340	14.3444	14.3445	14.3717
Cm-245 Capture	2.81558E+09	**12.1820**	12.0114	12.0265	12.0267	12.0620
Fe (n,el)	1.41214E+09	**2.7838**	0.4569	0.7661	0.7690	1.1926
Na-23 (n,el)	1.55294E+09	**2.8903**	0.4981	0.8107	0.8134	1.2204
End of Cycle Masses						
EOC U-235 Mass (kg, 1/3 core)	1.9941E+00	**0.0611**	*0.0110*	*0.0137*	*0.0138*	*0.0274*
EOC U-238 Mass (kg, 1/3 core)	1.2944E+03	**0.0101**	*0.0013*	*0.0024*	*0.0025*	*0.0059*
EOC NP237 Mass (kg, 1/3 core)	5.9906E+00	**0.0969**	*0.0841*	*0.0850*	*0.0850*	*0.0875*
EOC PU238 Mass (kg, 1/3 core)	9.9789E+00	**0.3575**	*0.0336*	*0.0364*	*0.0403*	*0.0648*
EOC PU239 Mass (kg, 1/3 core)	1.6923E+02	**0.0753**	*0.0052*	*0.0130*	*0.0134*	*0.0455*
EOC PU240 Mass (kg, 1/3 core)	1.0233E+02	**0.1024**	*0.0081*	*0.0133*	*0.0133*	*0.0302*
EOC PU241 Mass (kg, 1/3 core)	1.3555E+01	**0.8082**	*0.0075*	*0.0313*	*0.0466*	*0.1358*
EOC PU242 Mass (kg, 1/3 core)	2.0207E+01	**0.1803**	*0.0017*	*0.0058*	*0.0072*	*0.0230*
EOC AM241 Mass (kg, 1/3 core)	1.3043E+01	**0.1339**	*0.0069*	*0.0145*	*0.0146*	*0.0450*
EOC AM242 Mass (kg, 1/3 core)	9.3048E-01	**0.8624**	*0.8040*	*0.8050*	*0.8050*	*0.8133*
EOC AM243 Mass (kg, 1/3 core)	6.5145E+00	**0.4022**	*0.0855*	*0.0864*	*0.0864*	*0.0982*
EOC CM242 Mass (kg, 1/3 core)	3.8436E-01	**2.1191**	*0.1533*	*0.2686*	*0.2706*	*0.7616*
EOC CM244 Mass (kg, 1/3 core)	3.0155E+00	**0.5141**	*0.5098*	*0.5110*	*0.5110*	*0.5120*
EOC CM245 Mass (kg, 1/3 core)	7.1012E-01	**1.7686**	*1.7645*	*1.7670*	*1.7670*	*1.7683*
Discharge Masses						
DIS U-235 Mass (kg, 1/3 core)	9.5694E-02	**7.3322**	*0.5833*	*1.2561*	*1.6387*	*2.2144*
DIS U-238 Mass (kg, 1/3 core)	8.1533E+01	**10.0496**	*1.2745*	*2.1503*	*2.5283*	*3.1773*
DIS NP237 Mass (kg, 1/3 core)	2.7183E-01	**73.4646**	*9.6771*	*16.8392*	*21.5153*	*26.5675*
DIS PU238 Mass (kg, 1/3 core)	1.3071E+00	**21.4872**	*5.6636*	*7.8818*	*8.0331*	*8.9210*
DIS PU239 Mass (kg, 1/3 core)	1.3642E+01	**16.8644**	*1.3278*	*3.0469*	*4.1480*	*5.4187*
DIS PU240 Mass (kg, 1/3 core)	1.2759E+01	**31.8332**	*3.4175*	*6.3530*	*7.9313*	*10.1453*
DIS PU241 Mass (kg, 1/3 core)	2.1243E+00	**35.1597**	*3.3083*	*6.2891*	*7.3207*	*9.5258*
DIS PU242 Mass (kg, 1/3 core)	3.0327E+00	**80.3409**	*7.0048*	*14.3394*	*18.2240*	*23.8359*
DIS AM241 Mass (kg, 1/3 core)	1.3990E+00	**44.2526**	*5.9531*	*9.7693*	*11.0456*	*13.9075*
DIS AM242 Mass (kg, 1/3 core)	1.1967E-01	**48.9414**	*10.3311*	*13.1520*	*14.4000*	*16.8128*
DIS AM243 Mass (kg, 1/3 core)	9.9116E-01	**99.3120**	*9.2678*	*18.1087*	*23.2499*	*29.9826*
DIS CM242 Mass (kg, 1/3 core)	6.0048E-02	**38.2103**	*4.3134*	*7.5417*	*8.7162*	*11.0510*
DIS CM244 Mass (kg, 1/3 core)	7.1269E-01	**118.1987**	*11.7057*	*21.7914*	*28.1601*	*36.1961*
DIS CM245 Mass (kg, 1/3 core)	2.1995E-01	**140.3874**	*22.1672*	*31.0582*	*37.7136*	*46.3599*

Table D.12: Posteriori uncertainties for ABTR-EQ adapted to ZPPR-15B w/ TRU.

Parameter	Nominal Values	A Priori	0%	1%	1% + FPY	7.50%
Average Reaction Rates						
U-235 Capture	1.50418E+10	**1.7741**	0.1422	0.3656	0.3705	0.7969
Np-237 Capture	1.29109E+11	**3.0616**	0.1722	0.5022	0.5060	1.3187
Pu-238 Capture	9.24364E+10	**11.9504**	0.1656	0.7232	0.7275	1.9849
Pu-239 Capture	8.96572E+11	**4.9738**	0.1850	0.6886	0.6921	2.0061
Pu-240 Capture	6.56849E+11	**11.4211**	0.1617	0.5127	0.5163	1.9750
Pu-241 Capture	8.06078E+10	**11.3481**	0.1711	0.7753	0.7897	2.7266
Pu-242 Capture	1.07587E+11	**21.0632**	0.1835	0.8646	0.8698	3.0243
Am-241 Capture	2.78575E+11	**4.8517**	0.1394	0.6789	0.6856	1.8461
Am-242m Capture	3.13909E+09	**14.3345**	0.2664	1.0788	1.0940	3.6831
Am-243 Capture	1.01034E+11	**4.6468**	0.1778	1.1777	1.4146	2.2425
Cm-242 Capture	1.15857E+09	**16.6336**	0.3086	1.2402	1.2454	3.4456
Cm-244 Capture	3.26601E+10	**14.4697**	0.1720	0.7564	0.7920	2.5230
Cm-245 Capture	2.81558E+09	**12.1820**	0.1603	0.7999	0.8234	2.8147
Fe (n,el)	1.41214E+09	**2.7838**	0.4162	0.7472	0.7514	1.1810
Na-23 (n,el)	1.55294E+09	**2.8903**	0.4588	0.7937	0.7975	1.2095
End of Cycle Masses						
EOC U-235 Mass (kg, 1/3 core)	1.9941E+00	**0.0611**	*0.0077*	*0.0112*	*0.0114*	*0.0256*
EOC U-238 Mass (kg, 1/3 core)	1.2944E+03	**0.0101**	*0.0010*	*0.0023*	*0.0024*	*0.0058*
EOC NP237 Mass (kg, 1/3 core)	5.9906E+00	**0.0969**	*0.0242*	*0.0275*	*0.0276*	*0.0433*
EOC PU238 Mass (kg, 1/3 core)	9.9789E+00	**0.3575**	*0.0033*	*0.0144*	*0.0225*	*0.0566*
EOC PU239 Mass (kg, 1/3 core)	1.6923E+02	**0.0753**	*0.0048*	*0.0129*	*0.0133*	*0.0448*
EOC PU240 Mass (kg, 1/3 core)	1.0233E+02	**0.1024**	*0.0042*	*0.0113*	*0.0114*	*0.0294*
EOC PU241 Mass (kg, 1/3 core)	1.3555E+01	**0.8082**	*0.0073*	*0.0312*	*0.0465*	*0.1358*
EOC PU242 Mass (kg, 1/3 core)	2.0207E+01	**0.1803**	*0.0016*	*0.0057*	*0.0072*	*0.0229*
EOC AM241 Mass (kg, 1/3 core)	1.3043E+01	**0.1339**	*0.0026*	*0.0130*	*0.0132*	*0.0446*
EOC AM242 Mass (kg, 1/3 core)	9.3048E-01	**0.8624**	*0.0090*	*0.0461*	*0.0644*	*0.1790*
EOC AM243 Mass (kg, 1/3 core)	6.5145E+00	**0.4022**	*0.0029*	*0.0210*	*0.0246*	*0.0600*
EOC CM242 Mass (kg, 1/3 core)	3.8436E-01	**2.1191**	*0.0562*	*0.2265*	*0.2291*	*0.7479*
EOC CM244 Mass (kg, 1/3 core)	3.0155E+00	**0.5141**	*0.0064*	*0.0398*	*0.0480*	*0.0861*
EOC CM245 Mass (kg, 1/3 core)	7.1012E-01	**1.7686**	*0.0072*	*0.0359*	*0.0455*	*0.1524*
Discharge Masses						
DIS U-235 Mass (kg, 1/3 core)	9.5694E-02	**7.3322**	*0.5170*	*1.2384*	*1.6271*	*2.1998*
DIS U-238 Mass (kg, 1/3 core)	8.1533E+01	**10.0496**	*1.0569*	*2.0634*	*2.4564*	*3.1404*
DIS NP237 Mass (kg, 1/3 core)	2.7183E-01	**73.4646**	*7.5824*	*15.9472*	*20.8677*	*26.1289*
DIS PU238 Mass (kg, 1/3 core)	1.3071E+00	**21.4872**	*4.5634*	*7.3062*	*7.4756*	*8.6336*
DIS PU239 Mass (kg, 1/3 core)	1.3642E+01	**16.8644**	*1.1891*	*3.0203*	*4.1336*	*5.4080*
DIS PU240 Mass (kg, 1/3 core)	1.2759E+01	**31.8332**	*2.8747*	*6.1669*	*7.7881*	*10.0613*
DIS PU241 Mass (kg, 1/3 core)	2.1243E+00	**35.1597**	*2.8258*	*6.1325*	*7.1907*	*9.4465*
DIS PU242 Mass (kg, 1/3 core)	3.0327E+00	**80.3409**	*6.1674*	*14.1246*	*18.0660*	*23.7296*
DIS AM241 Mass (kg, 1/3 core)	1.3990E+00	**44.2526**	*4.9468*	*9.3604*	*10.6863*	*13.7262*
DIS AM242 Mass (kg, 1/3 core)	1.1967E-01	**48.9414**	*5.0867*	*9.9245*	*11.7559*	*15.2060*
DIS AM243 Mass (kg, 1/3 core)	9.9116E-01	**99.3120**	*7.3219*	*17.3892*	*22.7251*	*29.7321*
DIS CM242 Mass (kg, 1/3 core)	6.0048E-02	**38.2103**	*3.6259*	*7.2852*	*8.4991*	*10.9336*
DIS CM244 Mass (kg, 1/3 core)	7.1269E-01	**118.1987**	*8.1030*	*20.2857*	*27.0416*	*35.3760*
DIS CM245 Mass (kg, 1/3 core)	2.1995E-01	**140.3874**	*9.3539*	*23.9299*	*32.1599*	*42.1061*

Table D.13: Posteriori uncertainties for ABTR-EQ adapted to TRU v. 1.

Parameter	Nominal Values	A Priori	0%	1%	1% + FPY	7.50%
Average Reaction Rates						
U-235 Capture	1.50418E+10	**1.7741**	0.1097	0.3453	0.3526	0.8038
Np-237 Capture	1.29109E+11	**3.0616**	0.1338	0.5168	0.5216	1.3206
Pu-238 Capture	9.24364E+10	**11.9504**	0.1334	0.7243	0.7292	2.1685
Pu-239 Capture	8.96572E+11	**4.9738**	0.1441	0.7066	0.7103	2.1735
Pu-240 Capture	6.56849E+11	**11.4211**	0.1251	0.5502	0.5546	2.1232
Pu-241 Capture	8.06078E+10	**11.3481**	0.1354	0.7284	0.7449	3.2145
Pu-242 Capture	1.07587E+11	**21.0632**	0.1461	0.8206	0.8258	3.4119
Am-241 Capture	2.78575E+11	**4.8517**	0.1085	0.6540	0.6622	2.0039
Am-242m Capture	3.13909E+09	**14.3345**	0.2090	0.9775	0.9919	3.9815
Am-243 Capture	1.01034E+11	**4.6468**	0.1419	1.0784	1.3626	2.3879
Cm-242 Capture	1.15857E+09	**16.6336**	0.2394	1.1146	1.1207	3.8719
Cm-244 Capture	3.26601E+10	**14.4697**	0.1399	0.7309	0.7690	2.9207
Cm-245 Capture	2.81558E+09	**12.1820**	0.1224	0.7524	0.7761	3.2394
Fe (n,el)	1.41214E+09	**2.7838**	0.2659	0.7331	0.7372	1.1380
Na-23 (n,el)	1.55294E+09	**2.8903**	0.2945	0.7858	0.7895	1.1866
End of Cycle Masses						
EOC U-235 Mass (kg, 1/3 core)	1.9941E+00	**0.0611**	*0.0075*	*0.0112*	*0.0115*	*0.0261*
EOC U-238 Mass (kg, 1/3 core)	1.2944E+03	**0.0101**	*0.0010*	*0.0023*	*0.0024*	*0.0058*
EOC NP237 Mass (kg, 1/3 core)	5.9906E+00	**0.0969**	*0.0241*	*0.0278*	*0.0280*	*0.0435*
EOC PU238 Mass (kg, 1/3 core)	9.9789E+00	**0.3575**	*0.0031*	*0.0154*	*0.0257*	*0.0665*
EOC PU239 Mass (kg, 1/3 core)	1.6923E+02	**0.0753**	*0.0034*	*0.0138*	*0.0143*	*0.0452*
EOC PU240 Mass (kg, 1/3 core)	1.0233E+02	**0.1024**	*0.0037*	*0.0114*	*0.0115*	*0.0310*
EOC PU241 Mass (kg, 1/3 core)	1.3555E+01	**0.8082**	*0.0069*	*0.0345*	*0.0549*	*0.1509*
EOC PU242 Mass (kg, 1/3 core)	2.0207E+01	**0.1803**	*0.0015*	*0.0059*	*0.0081*	*0.0264*
EOC AM241 Mass (kg, 1/3 core)	1.3043E+01	**0.1339**	*0.0026*	*0.0137*	*0.0139*	*0.0483*
EOC AM242 Mass (kg, 1/3 core)	9.3048E-01	**0.8624**	*0.0063*	*0.0480*	*0.0689*	*0.2060*
EOC AM243 Mass (kg, 1/3 core)	6.5145E+00	**0.4022**	*0.0029*	*0.0203*	*0.0245*	*0.0678*
EOC CM242 Mass (kg, 1/3 core)	3.8436E-01	**2.1191**	*0.0449*	*0.2342*	*0.2373*	*0.8094*
EOC CM244 Mass (kg, 1/3 core)	3.0155E+00	**0.5141**	*0.0053*	*0.0375*	*0.0476*	*0.0939*
EOC CM245 Mass (kg, 1/3 core)	7.1012E-01	**1.7686**	*0.0067*	*0.0382*	*0.0491*	*0.1822*
Discharge Masses						
DIS U-235 Mass (kg, 1/3 core)	9.5694E-02	**7.3322**	*0.5251*	*1.1850*	*1.5917*	*2.3779*
DIS U-238 Mass (kg, 1/3 core)	8.1533E+01	**10.0496**	*0.8194*	*2.0050*	*2.4290*	*3.3717*
DIS NP237 Mass (kg, 1/3 core)	2.7183E-01	**73.4646**	*6.0719*	*14.7782*	*19.7432*	*27.8184*
DIS PU238 Mass (kg, 1/3 core)	1.3071E+00	**21.4872**	*2.9188*	*7.2107*	*7.4324*	*8.7883*
DIS PU239 Mass (kg, 1/3 core)	1.3642E+01	**16.8644**	*1.1507*	*2.7975*	*3.9326*	*5.8029*
DIS PU240 Mass (kg, 1/3 core)	1.2759E+01	**31.8332**	*2.3968*	*5.8838*	*7.5809*	*10.8301*
DIS PU241 Mass (kg, 1/3 core)	2.1243E+00	**35.1597**	*2.4254*	*6.0913*	*7.3005*	*10.2706*
DIS PU242 Mass (kg, 1/3 core)	3.0327E+00	**80.3409**	*5.5561*	*13.6178*	*17.7664*	*25.6552*
DIS AM241 Mass (kg, 1/3 core)	1.3990E+00	**44.2526**	*3.6788*	*9.1394*	*10.6234*	*14.5864*
DIS AM242 Mass (kg, 1/3 core)	1.1967E-01	**48.9414**	*3.8916*	*9.6823*	*11.5538*	*16.0867*
DIS AM243 Mass (kg, 1/3 core)	9.9116E-01	**99.3120**	*6.8254*	*16.6421*	*22.2212*	*32.2565*
DIS CM242 Mass (kg, 1/3 core)	6.0048E-02	**38.2103**	*2.8862*	*7.2021*	*8.5575*	*11.8121*
DIS CM244 Mass (kg, 1/3 core)	7.1269E-01	**118.1987**	*7.9240*	*19.2922*	*26.3283*	*38.4407*
DIS CM245 Mass (kg, 1/3 core)	2.1995E-01	**140.3874**	*9.3049*	*22.6640*	*31.1981*	*45.6798*

Table D.14: Posteriori uncertainties for ABTR-EQ adapted to TRU v. 1-B.

Parameter	Nominal Values	A Priori	0%	1%	1% + FPY	7.50%
Average Reaction Rates						
U-235 Capture	1.50418E+10	**1.7741**	0.1108	0.3461	0.3540	0.8092
Np-237 Capture	1.29109E+11	**3.0616**	0.1338	0.5148	0.5202	1.3255
Pu-238 Capture	9.24364E+10	**11.9504**	0.1415	0.6775	0.6828	2.2229
Pu-239 Capture	8.96572E+11	**4.9738**	0.1484	0.6799	0.6839	2.2182
Pu-240 Capture	6.56849E+11	**11.4211**	0.1262	0.5506	0.5554	2.1711
Pu-241 Capture	8.06078E+10	**11.3481**	0.1398	0.6732	0.6898	3.2623
Pu-242 Capture	1.07587E+11	**21.0632**	0.1476	0.7530	0.7583	3.4119
Am-241 Capture	2.78575E+11	**4.8517**	0.1091	0.6142	0.6226	2.0529
Am-242m Capture	3.13909E+09	**14.3345**	0.2099	0.9143	0.9280	3.9179
Am-243 Capture	1.01034E+11	**4.6468**	0.1436	0.9987	1.2828	2.4194
Cm-242 Capture	1.15857E+09	**16.6336**	0.2371	1.0450	1.0518	3.9055
Cm-244 Capture	3.26601E+10	**14.4697**	0.1393	0.6751	0.7108	2.9813
Cm-245 Capture	2.81558E+09	**12.1820**	0.1245	0.6898	0.7119	3.2651
Fe (n,el)	1.41214E+09	**2.7838**	0.2649	0.7294	0.7334	1.1470
Na-23 (n,el)	1.55294E+09	**2.8903**	0.2881	0.7850	0.7889	1.2027
End of Cycle Masses						
EOC U-235 Mass (kg, 1/3 core)	1.9941E+00	**0.0611**	*0.0075*	*0.0112*	*0.0115*	*0.0263*
EOC U-238 Mass (kg, 1/3 core)	1.2944E+03	**0.0101**	*0.0011*	*0.0023*	*0.0024*	*0.0058*
EOC NP237 Mass (kg, 1/3 core)	5.9906E+00	**0.0969**	*0.0248*	*0.0279*	*0.0281*	*0.0437*
EOC PU238 Mass (kg, 1/3 core)	9.9789E+00	**0.3575**	*0.0029*	*0.0146*	*0.0247*	*0.0689*
EOC PU239 Mass (kg, 1/3 core)	1.6923E+02	**0.0753**	*0.0036*	*0.0141*	*0.0146*	*0.0449*
EOC PU240 Mass (kg, 1/3 core)	1.0233E+02	**0.1024**	*0.0034*	*0.0115*	*0.0116*	*0.0315*
EOC PU241 Mass (kg, 1/3 core)	1.3555E+01	**0.8082**	*0.0074*	*0.0337*	*0.0543*	*0.1556*
EOC PU242 Mass (kg, 1/3 core)	2.0207E+01	**0.1803**	*0.0014*	*0.0056*	*0.0081*	*0.0270*
EOC AM241 Mass (kg, 1/3 core)	1.3043E+01	**0.1339**	*0.0025*	*0.0131*	*0.0133*	*0.0496*
EOC AM242 Mass (kg, 1/3 core)	9.3048E-01	**0.8624**	*0.0069*	*0.0453*	*0.0652*	*0.2118*
EOC AM243 Mass (kg, 1/3 core)	6.5145E+00	**0.4022**	*0.0029*	*0.0188*	*0.0231*	*0.0688*
EOC CM242 Mass (kg, 1/3 core)	3.8436E-01	**2.1191**	*0.0453*	*0.2256*	*0.2287*	*0.8307*
EOC CM244 Mass (kg, 1/3 core)	3.0155E+00	**0.5141**	*0.0054*	*0.0350*	*0.0451*	*0.0956*
EOC CM245 Mass (kg, 1/3 core)	7.1012E-01	**1.7686**	*0.0065*	*0.0357*	*0.0461*	*0.1879*
Discharge Masses						
DIS U-235 Mass (kg, 1/3 core)	9.5694E-02	**7.3322**	*0.5754*	*1.1609*	*1.5182*	*2.3974*
DIS U-238 Mass (kg, 1/3 core)	8.1533E+01	**10.0496**	*0.9051*	*1.9780*	*2.3517*	*3.4033*
DIS NP237 Mass (kg, 1/3 core)	2.7183E-01	**73.4646**	*6.3491*	*14.3206*	*18.5942*	*27.8429*
DIS PU238 Mass (kg, 1/3 core)	1.3071E+00	**21.4872**	*3.0403*	*7.1441*	*7.3588*	*8.8060*
DIS PU239 Mass (kg, 1/3 core)	1.3642E+01	**16.8644**	*1.2645*	*2.7135*	*3.7038*	*5.8181*
DIS PU240 Mass (kg, 1/3 core)	1.2759E+01	**31.8332**	*2.6792*	*5.7684*	*7.2500*	*10.9092*
DIS PU241 Mass (kg, 1/3 core)	2.1243E+00	**35.1597**	*2.7480*	*6.0415*	*7.1399*	*10.4295*
DIS PU242 Mass (kg, 1/3 core)	3.0327E+00	**80.3409**	*6.2583*	*13.3722*	*17.0233*	*25.8715*
DIS AM241 Mass (kg, 1/3 core)	1.3990E+00	**44.2526**	*4.0635*	*9.0303*	*10.3602*	*14.7036*
DIS AM242 Mass (kg, 1/3 core)	1.1967E-01	**48.9414**	*4.3220*	*9.5500*	*11.2002*	*16.1667*
DIS AM243 Mass (kg, 1/3 core)	9.9116E-01	**99.3120**	*7.6876*	*16.3044*	*21.2021*	*32.5304*
DIS CM242 Mass (kg, 1/3 core)	6.0048E-02	**38.2103**	*3.2372*	*7.1319*	*8.3508*	*11.9617*
DIS CM244 Mass (kg, 1/3 core)	7.1269E-01	**118.1987**	*8.9175*	*18.8581*	*25.0293*	*38.7558*
DIS CM245 Mass (kg, 1/3 core)	2.1995E-01	**140.3874**	*10.4432*	*22.1198*	*29.5971*	*46.0186*

Table D.15: Posteriori uncertainties for ABTR-EQ adapted to TRU v. 1-C.

Parameter	Nominal Values	A Priori	0%	1%	1% + FPY	7.50%
Average Reaction Rates						
U-235 Capture	1.50418E+10	**1.7741**	0.1071	0.3374	0.3438	0.7894
Np-237 Capture	1.29109E+11	**3.0616**	0.1310	0.4780	0.4826	1.3156
Pu-238 Capture	9.24364E+10	**11.9504**	0.1393	0.5874	0.5921	2.0486
Pu-239 Capture	8.96572E+11	**4.9738**	0.1426	0.5998	0.6035	2.0593
Pu-240 Capture	6.56849E+11	**11.4211**	0.1228	0.4921	0.4965	2.0332
Pu-241 Capture	8.06078E+10	**11.3481**	0.1372	0.5854	0.5987	2.7659
Pu-242 Capture	1.07587E+11	**21.0632**	0.1444	0.6587	0.6634	2.9573
Am-241 Capture	2.78575E+11	**4.8517**	0.1051	0.5389	0.5463	1.9043
Am-242m Capture	3.13909E+09	**14.3345**	0.2054	0.8423	0.8536	3.4553
Am-243 Capture	1.01034E+11	**4.6468**	0.1364	0.9148	1.1676	2.2803
Cm-242 Capture	1.15857E+09	**16.6336**	0.2300	0.9806	0.9866	3.4515
Cm-244 Capture	3.26601E+10	**14.4697**	0.1350	0.5874	0.6159	2.5768
Cm-245 Capture	2.81558E+09	**12.1820**	0.1208	0.5971	0.6150	2.8046
Fe (n,el)	1.41214E+09	**2.7838**	0.2454	0.7262	0.7305	1.1207
Na-23 (n,el)	1.55294E+09	**2.8903**	0.2668	0.7790	0.7829	1.1697
End of Cycle Masses						
EOC U-235 Mass (kg, 1/3 core)	1.9941E+00	**0.0611**	*0.0075*	*0.0110*	*0.0112*	*0.0256*
EOC U-238 Mass (kg, 1/3 core)	1.2944E+03	**0.0101**	*0.0009*	*0.0023*	*0.0023*	*0.0057*
EOC NP237 Mass (kg, 1/3 core)	5.9906E+00	**0.0969**	*0.0245*	*0.0275*	*0.0277*	*0.0434*
EOC PU238 Mass (kg, 1/3 core)	9.9789E+00	**0.3575**	*0.0028*	*0.0123*	*0.0201*	*0.0597*
EOC PU239 Mass (kg, 1/3 core)	1.6923E+02	**0.0753**	*0.0035*	*0.0129*	*0.0133*	*0.0439*
EOC PU240 Mass (kg, 1/3 core)	1.0233E+02	**0.1024**	*0.0039*	*0.0108*	*0.0109*	*0.0300*
EOC PU241 Mass (kg, 1/3 core)	1.3555E+01	**0.8082**	*0.0074*	*0.0285*	*0.0448*	*0.1414*
EOC PU242 Mass (kg, 1/3 core)	2.0207E+01	**0.1803**	*0.0014*	*0.0048*	*0.0068*	*0.0235*
EOC AM241 Mass (kg, 1/3 core)	1.3043E+01	**0.1339**	*0.0024*	*0.0112*	*0.0113*	*0.0461*
EOC AM242 Mass (kg, 1/3 core)	9.3048E-01	**0.8624**	*0.0068*	*0.0374*	*0.0531*	*0.1860*
EOC AM243 Mass (kg, 1/3 core)	6.5145E+00	**0.4022**	*0.0029*	*0.0163*	*0.0202*	*0.0609*
EOC CM242 Mass (kg, 1/3 core)	3.8436E-01	**2.1191**	*0.0426*	*0.1938*	*0.1966*	*0.7736*
EOC CM244 Mass (kg, 1/3 core)	3.0155E+00	**0.5141**	*0.0051*	*0.0315*	*0.0403*	*0.0885*
EOC CM245 Mass (kg, 1/3 core)	7.1012E-01	**1.7686**	*0.0064*	*0.0291*	*0.0373*	*0.1593*
Discharge Masses						
DIS U-235 Mass (kg, 1/3 core)	9.5694E-02	**7.3322**	*0.5070*	*1.1244*	*1.4215*	*2.2020*
DIS U-238 Mass (kg, 1/3 core)	8.1533E+01	**10.0496**	*0.8094*	*1.9363*	*2.2391*	*3.1579*
DIS NP237 Mass (kg, 1/3 core)	2.7183E-01	**73.4646**	*5.9058*	*14.0462*	*17.7161*	*25.8513*
DIS PU238 Mass (kg, 1/3 core)	1.3071E+00	**21.4872**	*2.9892*	*7.1201*	*7.2844*	*8.5965*
DIS PU239 Mass (kg, 1/3 core)	1.3642E+01	**16.8644**	*1.1031*	*2.6299*	*3.4742*	*5.3418*
DIS PU240 Mass (kg, 1/3 core)	1.2759E+01	**31.8332**	*2.3285*	*5.6256*	*6.8610*	*10.0762*
DIS PU241 Mass (kg, 1/3 core)	2.1243E+00	**35.1597**	*2.4281*	*5.8915*	*6.7463*	*9.5968*
DIS PU242 Mass (kg, 1/3 core)	3.0327E+00	**80.3409**	*5.4030*	*12.9830*	*15.9980*	*23.7684*
DIS AM241 Mass (kg, 1/3 core)	1.3990E+00	**44.2526**	*3.6849*	*8.8777*	*9.9242*	*13.7617*
DIS AM242 Mass (kg, 1/3 core)	1.1967E-01	**48.9414**	*3.8779*	*9.3637*	*10.7051*	*15.1196*
DIS AM243 Mass (kg, 1/3 core)	9.9116E-01	**99.3120**	*6.5889*	*15.7987*	*19.8831*	*29.8108*
DIS CM242 Mass (kg, 1/3 core)	6.0048E-02	**38.2103**	*2.8888*	*6.9757*	*7.9344*	*11.0581*
DIS CM244 Mass (kg, 1/3 core)	7.1269E-01	**118.1987**	*7.5974*	*18.2350*	*23.4171*	*35.4429*
DIS CM245 Mass (kg, 1/3 core)	2.1995E-01	**140.3874**	*8.8844*	*21.3796*	*27.6858*	*42.1090*

Table D.16: Posteriori uncertainties for ABTR-EQ adapted to TRU v. 2.

Parameter	Nominal Values	A Priori	0%	1%	1% + FPY	7.50%
Average Reaction Rates						
U-235 Capture	1.50418E+10	**1.7741**	0.1513	0.4041	0.4123	0.8509
Np-237 Capture	1.29109E+11	**3.0616**	0.1936	0.6554	0.6604	1.3588
Pu-238 Capture	9.24364E+10	**11.9504**	0.2014	1.5905	1.5970	2.4821
Pu-239 Capture	8.96572E+11	**4.9738**	0.2206	1.4150	1.4203	2.4744
Pu-240 Capture	6.56849E+11	**11.4211**	0.1896	0.8048	0.8098	2.3750
Pu-241 Capture	8.06078E+10	**11.3481**	0.2013	2.8225	2.8499	4.7459
Pu-242 Capture	1.07587E+11	**21.0632**	0.2139	2.6628	2.6728	4.6834
Am-241 Capture	2.78575E+11	**4.8517**	0.1679	1.5483	1.5558	2.2767
Am-242m Capture	3.13909E+09	**14.3345**	0.4757	4.2549	4.2856	5.8474
Am-243 Capture	1.01034E+11	**4.6468**	0.2132	2.1724	2.2422	2.6440
Cm-242 Capture	1.15857E+09	**16.6336**	0.5195	4.2063	4.2093	5.3736
Cm-244 Capture	3.26601E+10	**14.4697**	0.2197	2.3716	2.4496	3.9430
Cm-245 Capture	2.81558E+09	**12.1820**	0.1714	2.7023	2.7597	4.5433
Fe (n,el)	1.41214E+09	**2.7838**	0.4172	0.8867	0.8938	1.2358
Na-23 (n,el)	1.55294E+09	**2.8903**	0.4616	0.9555	0.9612	1.2934
End of Cycle Masses						
EOC U-235 Mass (kg, 1/3 core)	1.9941E+00	**0.0611**	*0.0079*	*0.0131*	*0.0137*	*0.0279*
EOC U-238 Mass (kg, 1/3 core)	1.2944E+03	**0.0101**	*0.0012*	*0.0025*	*0.0026*	*0.0060*
EOC NP237 Mass (kg, 1/3 core)	5.9906E+00	**0.0969**	*0.0247*	*0.0298*	*0.0300*	*0.0446*
EOC PU238 Mass (kg, 1/3 core)	9.9789E+00	**0.3575**	*0.0040*	*0.0455*	*0.0650*	*0.0933*
EOC PU239 Mass (kg, 1/3 core)	1.6923E+02	**0.0753**	*0.0045*	*0.0187*	*0.0191*	*0.0481*
EOC PU240 Mass (kg, 1/3 core)	1.0233E+02	**0.1024**	*0.0044*	*0.0177*	*0.0178*	*0.0338*
EOC PU241 Mass (kg, 1/3 core)	1.3555E+01	**0.8082**	*0.0120*	*0.0864*	*0.1058*	*0.1805*
EOC PU242 Mass (kg, 1/3 core)	2.0207E+01	**0.1803**	*0.0020*	*0.0198*	*0.0212*	*0.0360*
EOC AM241 Mass (kg, 1/3 core)	1.3043E+01	**0.1339**	*0.0036*	*0.0336*	*0.0339*	*0.0551*
EOC AM242 Mass (kg, 1/3 core)	9.3048E-01	**0.8624**	*0.0150*	*0.1681*	*0.2035*	*0.2759*
EOC AM243 Mass (kg, 1/3 core)	6.5145E+00	**0.4022**	*0.0037*	*0.0549*	*0.0560*	*0.0879*
EOC CM242 Mass (kg, 1/3 core)	3.8436E-01	**2.1191**	*0.0646*	*0.5678*	*0.5710*	*0.9163*
EOC CM244 Mass (kg, 1/3 core)	3.0155E+00	**0.5141**	*0.0078*	*0.0807*	*0.0854*	*0.1104*
EOC CM245 Mass (kg, 1/3 core)	7.1012E-01	**1.7686**	*0.0100*	*0.1436*	*0.1669*	*0.2596*
Discharge Masses						
DIS U-235 Mass (kg, 1/3 core)	9.5694E-02	**7.3322**	*0.6834*	*2.0118*	*2.4404*	*2.8584*
DIS U-238 Mass (kg, 1/3 core)	8.1533E+01	**10.0496**	*1.0171*	*2.9253*	*3.4398*	*3.9728*
DIS NP237 Mass (kg, 1/3 core)	2.7183E-01	**73.4646**	*7.5849*	*24.8389*	*29.6490*	*33.1074*
DIS PU238 Mass (kg, 1/3 core)	1.3071E+00	**21.4872**	*3.2917*	*7.8892*	*8.2935*	*9.4381*
DIS PU239 Mass (kg, 1/3 core)	1.3642E+01	**16.8644**	*1.5374*	*5.0554*	*6.1478*	*7.0566*
DIS PU240 Mass (kg, 1/3 core)	1.2759E+01	**31.8332**	*3.0274*	*9.3989*	*11.2411*	*12.8993*
DIS PU241 Mass (kg, 1/3 core)	2.1243E+00	**35.1597**	*3.2148*	*8.7462*	*10.3487*	*12.2307*
DIS PU242 Mass (kg, 1/3 core)	3.0327E+00	**80.3409**	*7.3308*	*22.2312*	*26.7642*	*30.8573*
DIS AM241 Mass (kg, 1/3 core)	1.3990E+00	**44.2526**	*4.5508*	*12.5493*	*14.5373*	*16.9742*
DIS AM242 Mass (kg, 1/3 core)	1.1967E-01	**48.9414**	*4.8561*	*13.7969*	*16.2167*	*18.8239*
DIS AM243 Mass (kg, 1/3 core)	9.9116E-01	**99.3120**	*9.0444*	*28.0550*	*33.9221*	*38.9469*
DIS CM242 Mass (kg, 1/3 core)	6.0048E-02	**38.2103**	*3.7000*	*10.1977*	*11.9726*	*13.9837*
DIS CM244 Mass (kg, 1/3 core)	7.1269E-01	**118.1987**	*10.6041*	*33.5219*	*40.7080*	*46.5898*
DIS CM245 Mass (kg, 1/3 core)	2.1995E-01	**140.3874**	*12.4792*	*39.8393*	*48.4420*	*55.3565*

Table D.17: Posteriori uncertainties for ABTR-EQ adapted to TRU v. 2-B.

Parameter	Nominal Values	A Priori	0%	1%	1% + FPY	7.50%
Average Reaction Rates						
U-235 Capture	1.50418E+10	**1.7741**	0.1551	0.4456	0.4560	0.8808
Np-237 Capture	1.29109E+11	**3.0616**	0.2020	0.7172	0.7237	1.3891
Pu-238 Capture	9.24364E+10	**11.9504**	0.2089	1.8652	1.8730	2.6723
Pu-239 Capture	8.96572E+11	**4.9738**	0.2260	1.6596	1.6644	2.6297
Pu-240 Capture	6.56849E+11	**11.4211**	0.1986	0.9338	0.9398	2.5302
Pu-241 Capture	8.06078E+10	**11.3481**	0.2144	3.6803	3.7103	5.5110
Pu-242 Capture	1.07587E+11	**21.0632**	0.2151	3.2610	3.2722	5.1724
Am-241 Capture	2.78575E+11	**4.8517**	0.1757	1.7829	1.7909	2.4367
Am-242m Capture	3.13909E+09	**14.3345**	0.4954	5.1683	5.1955	6.3543
Am-243 Capture	1.01034E+11	**4.6468**	0.2329	2.3595	2.4080	2.7577
Cm-242 Capture	1.15857E+09	**16.6336**	0.5272	4.9527	4.9561	5.9573
Cm-244 Capture	3.26601E+10	**14.4697**	0.2203	2.9738	3.0575	4.4761
Cm-245 Capture	2.81558E+09	**12.1820**	0.1755	3.3885	3.4507	5.1192
Fe (n,el)	1.41214E+09	**2.7838**	0.4466	0.9991	1.0051	1.2951
Na-23 (n,el)	1.55294E+09	**2.8903**	0.4922	1.0837	1.0885	1.3663
End of Cycle Masses						
EOC U-235 Mass (kg, 1/3 core)	1.9941E+00	**0.0611**	*0.0080*	*0.0145*	*0.0151*	*0.0291*
EOC U-238 Mass (kg, 1/3 core)	1.2944E+03	**0.0101**	*0.0012*	*0.0027*	*0.0027*	*0.0061*
EOC NP237 Mass (kg, 1/3 core)	5.9906E+00	**0.0969**	*0.0245*	*0.0311*	*0.0313*	*0.0456*
EOC PU238 Mass (kg, 1/3 core)	9.9789E+00	**0.3575**	*0.0043*	*0.0615*	*0.0859*	*0.1139*
EOC PU239 Mass (kg, 1/3 core)	1.6923E+02	**0.0753**	*0.0043*	*0.0207*	*0.0211*	*0.0485*
EOC PU240 Mass (kg, 1/3 core)	1.0233E+02	**0.1024**	*0.0041*	*0.0205*	*0.0206*	*0.0355*
EOC PU241 Mass (kg, 1/3 core)	1.3555E+01	**0.8082**	*0.0135*	*0.1103*	*0.1309*	*0.2015*
EOC PU242 Mass (kg, 1/3 core)	2.0207E+01	**0.1803**	*0.0022*	*0.0255*	*0.0273*	*0.0413*
EOC AM241 Mass (kg, 1/3 core)	1.3043E+01	**0.1339**	*0.0038*	*0.0398*	*0.0401*	*0.0593*
EOC AM242 Mass (kg, 1/3 core)	9.3048E-01	**0.8624**	*0.0162*	*0.2158*	*0.2537*	*0.3177*
EOC AM243 Mass (kg, 1/3 core)	6.5145E+00	**0.4022**	*0.0042*	*0.0654*	*0.0664*	*0.0968*
EOC CM242 Mass (kg, 1/3 core)	3.8436E-01	**2.1191**	*0.0684*	*0.6713*	*0.6748*	*0.9842*
EOC CM244 Mass (kg, 1/3 core)	3.0155E+00	**0.5141**	*0.0085*	*0.0916*	*0.0969*	*0.1207*
EOC CM245 Mass (kg, 1/3 core)	7.1012E-01	**1.7686**	*0.0105*	*0.1886*	*0.2164*	*0.3070*
Discharge Masses						
DIS U-235 Mass (kg, 1/3 core)	9.5694E-02	**7.3322**	*0.7627*	*2.3009*	*2.7316*	*3.1307*
DIS U-238 Mass (kg, 1/3 core)	8.1533E+01	**10.0496**	*1.1096*	*3.2842*	*3.8139*	*4.3233*
DIS NP237 Mass (kg, 1/3 core)	2.7183E-01	**73.4646**	*8.2649*	*27.7844*	*32.5455*	*35.8600*
DIS PU238 Mass (kg, 1/3 core)	1.3071E+00	**21.4872**	*3.2309*	*8.2182*	*8.7031*	*9.8396*
DIS PU239 Mass (kg, 1/3 core)	1.3642E+01	**16.8644**	*1.7409*	*5.7543*	*6.8349*	*7.7011*
DIS PU240 Mass (kg, 1/3 core)	1.2759E+01	**31.8332**	*3.3806*	*10.6243*	*12.4761*	*14.0576*
DIS PU241 Mass (kg, 1/3 core)	2.1243E+00	**35.1597**	*3.5111*	*9.9623*	*11.6534*	*13.4596*
DIS PU242 Mass (kg, 1/3 core)	3.0327E+00	**80.3409**	*8.2459*	*25.3329*	*29.9116*	*33.7965*
DIS AM241 Mass (kg, 1/3 core)	1.3990E+00	**44.2526**	*4.8850*	*13.9664*	*16.0651*	*18.4035*
DIS AM242 Mass (kg, 1/3 core)	1.1967E-01	**48.9414**	*5.2764*	*15.4025*	*17.8911*	*20.3894*
DIS AM243 Mass (kg, 1/3 core)	9.9116E-01	**99.3120**	*10.2466*	*32.0278*	*37.9141*	*42.6952*
DIS CM242 Mass (kg, 1/3 core)	6.0048E-02	**38.2103**	*4.0178*	*11.5092*	*13.3748*	*15.3031*
DIS CM244 Mass (kg, 1/3 core)	7.1269E-01	**118.1987**	*12.0727*	*38.3392*	*45.5140*	*51.1156*
DIS CM245 Mass (kg, 1/3 core)	2.1995E-01	**140.3874**	*14.2325*	*45.5468*	*54.1122*	*60.6955*

Table D.18: Posteriori uncertainties for ABTR-EQ adapted to TRU v. 3.

Parameter	Nominal Values	A Priori	0%	1%	1% + FPY	7.50%
Average Reaction Rates						
U-235 Capture	1.50418E+10	**1.7741**	0.1070	0.3300	0.3370	0.7920
Np-237 Capture	1.29109E+11	**3.0616**	0.1288	0.4968	0.5017	1.3157
Pu-238 Capture	9.24364E+10	**11.9504**	0.1225	0.7510	0.7560	2.0518
Pu-239 Capture	8.96572E+11	**4.9738**	0.1412	0.7071	0.7114	2.0763
Pu-240 Capture	6.56849E+11	**11.4211**	0.1230	0.5249	0.5295	2.0361
Pu-241 Capture	8.06078E+10	**11.3481**	0.1310	0.7984	0.8145	2.9586
Pu-242 Capture	1.07587E+11	**21.0632**	0.1410	0.8875	0.8931	3.2060
Am-241 Capture	2.78575E+11	**4.8517**	0.1061	0.6918	0.6999	1.9046
Am-242m Capture	3.13909E+09	**14.3345**	0.2023	1.0734	1.0895	3.8951
Am-243 Capture	1.01034E+11	**4.6468**	0.1378	1.1851	1.4446	2.3063
Cm-242 Capture	1.15857E+09	**16.6336**	0.2441	1.2357	1.2415	3.6971
Cm-244 Capture	3.26601E+10	**14.4697**	0.1391	0.7799	0.8194	2.6774
Cm-245 Capture	2.81558E+09	**12.1820**	0.1193	0.8225	0.8483	3.0097
Fe (n,el)	1.41214E+09	**2.7838**	0.3180	0.7243	0.7293	1.1392
Na-23 (n,el)	1.55294E+09	**2.8903**	0.3463	0.7692	0.7743	1.1798
End of Cycle Masses						
EOC U-235 Mass (kg, 1/3 core)	1.9941E+00	**0.0611**	*0.0075*	*0.0112*	*0.0114*	*0.0256*
EOC U-238 Mass (kg, 1/3 core)	1.2944E+03	**0.0101**	*0.0009*	*0.0023*	*0.0023*	*0.0058*
EOC NP237 Mass (kg, 1/3 core)	5.9906E+00	**0.0969**	*0.0243*	*0.0276*	*0.0278*	*0.0433*
EOC PU238 Mass (kg, 1/3 core)	9.9789E+00	**0.3575**	*0.0028*	*0.0155*	*0.0252*	*0.0607*
EOC PU239 Mass (kg, 1/3 core)	1.6923E+02	**0.0753**	*0.0027*	*0.0131*	*0.0136*	*0.0447*
EOC PU240 Mass (kg, 1/3 core)	1.0233E+02	**0.1024**	*0.0037*	*0.0115*	*0.0117*	*0.0300*
EOC PU241 Mass (kg, 1/3 core)	1.3555E+01	**0.8082**	*0.0060*	*0.0338*	*0.0514*	*0.1416*
EOC PU242 Mass (kg, 1/3 core)	2.0207E+01	**0.1803**	*0.0015*	*0.0061*	*0.0078*	*0.0244*
EOC AM241 Mass (kg, 1/3 core)	1.3043E+01	**0.1339**	*0.0025*	*0.0138*	*0.0140*	*0.0459*
EOC AM242 Mass (kg, 1/3 core)	9.3048E-01	**0.8624**	*0.0072*	*0.0498*	*0.0706*	*0.1903*
EOC AM243 Mass (kg, 1/3 core)	6.5145E+00	**0.4022**	*0.0027*	*0.0218*	*0.0257*	*0.0633*
EOC CM242 Mass (kg, 1/3 core)	3.8436E-01	**2.1191**	*0.0430*	*0.2379*	*0.2411*	*0.7705*
EOC CM244 Mass (kg, 1/3 core)	3.0155E+00	**0.5141**	*0.0051*	*0.0405*	*0.0497*	*0.0894*
EOC CM245 Mass (kg, 1/3 core)	7.1012E-01	**1.7686**	*0.0069*	*0.0394*	*0.0502*	*0.1642*
Discharge Masses						
DIS U-235 Mass (kg, 1/3 core)	9.5694E-02	**7.3322**	*0.5188*	*1.2357*	*1.6582*	*2.2765*
DIS U-238 Mass (kg, 1/3 core)	8.1533E+01	**10.0496**	*0.8406*	*2.0467*	*2.4873*	*3.2355*
DIS NP237 Mass (kg, 1/3 core)	2.7183E-01	**73.4646**	*5.9518*	*15.6135*	*20.9429*	*26.9609*
DIS PU238 Mass (kg, 1/3 core)	1.3071E+00	**21.4872**	*2.9400*	*7.1865*	*7.4042*	*8.6917*
DIS PU239 Mass (kg, 1/3 core)	1.3642E+01	**16.8644**	*1.1387*	*2.9726*	*4.1642*	*5.5857*
DIS PU240 Mass (kg, 1/3 core)	1.2759E+01	**31.8332**	*2.4738*	*6.1132*	*7.8951*	*10.3950*
DIS PU241 Mass (kg, 1/3 core)	2.1243E+00	**35.1597**	*2.4156*	*6.1439*	*7.3476*	*9.7733*
DIS PU242 Mass (kg, 1/3 core)	3.0327E+00	**80.3409**	*5.6729*	*14.1096*	*18.4156*	*24.5731*
DIS AM241 Mass (kg, 1/3 core)	1.3990E+00	**44.2526**	*3.7619*	*9.2964*	*10.8017*	*14.0787*
DIS AM242 Mass (kg, 1/3 core)	1.1967E-01	**48.9414**	*3.9663*	*9.8626*	*11.8566*	*15.5867*
DIS AM243 Mass (kg, 1/3 core)	9.9116E-01	**99.3120**	*6.9820*	*17.3527*	*23.1592*	*30.8449*
DIS CM242 Mass (kg, 1/3 core)	6.0048E-02	**38.2103**	*2.9208*	*7.2805*	*8.6520*	*11.2904*
DIS CM244 Mass (kg, 1/3 core)	7.1269E-01	**118.1987**	*8.0663*	*20.2332*	*27.5602*	*36.7424*
DIS CM245 Mass (kg, 1/3 core)	2.1995E-01	**140.3874**	*9.4603*	*23.8473*	*32.7567*	*43.7160*

Table D.19: Posteriori uncertainties for ABTR-EQ adapted to ZPPR-SNF.

Parameter	Nominal Values	A Priori	0%	1%	1% + FPY	7.50%
Average Reaction Rates						
U-235 Capture	1.50418E+10	**1.7741**	0.1084	0.3436	0.3509	0.7918
Np-237 Capture	1.29109E+11	**3.0616**	0.1304	0.5026	0.5075	1.3170
Pu-238 Capture	9.24364E+10	**11.9504**	0.1219	0.7671	0.7719	2.0286
Pu-239 Capture	8.96572E+11	**4.9738**	0.1436	0.7249	0.7284	2.0598
Pu-240 Capture	6.56849E+11	**11.4211**	0.1249	0.5216	0.5262	2.0071
Pu-241 Capture	8.06078E+10	**11.3481**	0.1309	0.8307	0.8467	2.8840
Pu-242 Capture	1.07587E+11	**21.0632**	0.1434	0.9215	0.9273	3.1786
Am-241 Capture	2.78575E+11	**4.8517**	0.1074	0.7157	0.7235	1.8840
Am-242m Capture	3.13909E+09	**14.3345**	0.2017	1.1263	1.1426	3.8590
Am-243 Capture	1.01034E+11	**4.6468**	0.1378	1.2251	1.4704	2.2838
Cm-242 Capture	1.15857E+09	**16.6336**	0.2467	1.2943	1.2994	3.6332
Cm-244 Capture	3.26601E+10	**14.4697**	0.1424	0.8079	0.8472	2.6339
Cm-245 Capture	2.81558E+09	**12.1820**	0.1204	0.8595	0.8854	2.9632
Fe (n,el)	1.41214E+09	**2.7838**	0.3912	0.7453	0.7497	1.1560
Na-23 (n,el)	1.55294E+09	**2.8903**	0.4269	0.7931	0.7971	1.1881
End of Cycle Masses						
EOC U-235 Mass (kg, 1/3 core)	1.9941E+00	**0.0611**	*0.0075*	*0.0111*	*0.0114*	*0.0256*
EOC U-238 Mass (kg, 1/3 core)	1.2944E+03	**0.0101**	*0.0009*	*0.0023*	*0.0023*	*0.0058*
EOC NP237 Mass (kg, 1/3 core)	5.9906E+00	**0.0969**	*0.0243*	*0.0276*	*0.0278*	*0.0433*
EOC PU238 Mass (kg, 1/3 core)	9.9789E+00	**0.3575**	*0.0031*	*0.0156*	*0.0247*	*0.0589*
EOC PU239 Mass (kg, 1/3 core)	1.6923E+02	**0.0753**	*0.0029*	*0.0127*	*0.0132*	*0.0447*
EOC PU240 Mass (kg, 1/3 core)	1.0233E+02	**0.1024**	*0.0036*	*0.0112*	*0.0114*	*0.0298*
EOC PU241 Mass (kg, 1/3 core)	1.3555E+01	**0.8082**	*0.0055*	*0.0334*	*0.0496*	*0.1392*
EOC PU242 Mass (kg, 1/3 core)	2.0207E+01	**0.1803**	*0.0015*	*0.0062*	*0.0077*	*0.0239*
EOC AM241 Mass (kg, 1/3 core)	1.3043E+01	**0.1339**	*0.0025*	*0.0139*	*0.0141*	*0.0454*
EOC AM242 Mass (kg, 1/3 core)	9.3048E-01	**0.8624**	*0.0068*	*0.0508*	*0.0712*	*0.1864*
EOC AM243 Mass (kg, 1/3 core)	6.5145E+00	**0.4022**	*0.0028*	*0.0225*	*0.0261*	*0.0626*
EOC CM242 Mass (kg, 1/3 core)	3.8436E-01	**2.1191**	*0.0445*	*0.2415*	*0.2446*	*0.7621*
EOC CM244 Mass (kg, 1/3 core)	3.0155E+00	**0.5141**	*0.0052*	*0.0416*	*0.0503*	*0.0881*
EOC CM245 Mass (kg, 1/3 core)	7.1012E-01	**1.7686**	*0.0072*	*0.0401*	*0.0508*	*0.1603*
Discharge Masses						
DIS U-235 Mass (kg, 1/3 core)	9.5694E-02	**7.3322**	*0.4693*	*1.2634*	*1.6638*	*2.2579*
DIS U-238 Mass (kg, 1/3 core)	8.1533E+01	**10.0496**	*0.7427*	*2.0761*	*2.4979*	*3.2136*
DIS NP237 Mass (kg, 1/3 core)	2.7183E-01	**73.4646**	*5.2679*	*16.0870*	*20.9321*	*26.7077*
DIS PU238 Mass (kg, 1/3 core)	1.3071E+00	**21.4872**	*2.6826*	*7.2483*	*7.4655*	*8.6893*
DIS PU239 Mass (kg, 1/3 core)	1.3642E+01	**16.8644**	*1.0075*	*3.0646*	*4.1603*	*5.5291*
DIS PU240 Mass (kg, 1/3 core)	1.2759E+01	**31.8332**	*2.1559*	*6.2365*	*7.9256*	*10.3132*
DIS PU241 Mass (kg, 1/3 core)	2.1243E+00	**35.1597**	*2.1246*	*6.1832*	*7.3614*	*9.6842*
DIS PU242 Mass (kg, 1/3 core)	3.0327E+00	**80.3409**	*4.9989*	*14.3629*	*18.4196*	*24.3382*
DIS AM241 Mass (kg, 1/3 core)	1.3990E+00	**44.2526**	*3.3299*	*9.3956*	*10.8527*	*13.9938*
DIS AM242 Mass (kg, 1/3 core)	1.1967E-01	**48.9414**	*3.5030*	*9.9868*	*11.9307*	*15.4976*
DIS AM243 Mass (kg, 1/3 core)	9.9116E-01	**99.3120**	*6.1230*	*17.7056*	*23.1519*	*30.5298*
DIS CM242 Mass (kg, 1/3 core)	6.0048E-02	**38.2103**	*2.5806*	*7.3453*	*8.6751*	*11.1960*
DIS CM244 Mass (kg, 1/3 core)	7.1269E-01	**118.1987**	*7.0635*	*20.6868*	*27.5419*	*36.3534*
DIS CM245 Mass (kg, 1/3 core)	2.1995E-01	**140.3874**	*8.2815*	*24.4088*	*32.7413*	*43.2599*

Table D.20: Posteriori uncertainties for ABTR-EQ adapted to ZPPR-ABTR.

Parameter	Nominal Values	A Priori	0%	1%	1% + FPY	7.50%
Average Reaction Rates						
U-235 Capture	1.50418E+10	**1.7741**	0.0534	0.3061	0.3097	0.8489
Np-237 Capture	1.29109E+11	**3.0616**	0.0722	0.3680	0.3713	1.4409
Pu-238 Capture	9.24364E+10	**11.9504**	0.0596	0.3434	0.3459	1.7081
Pu-239 Capture	8.96572E+11	**4.9738**	0.0908	0.4017	0.4048	1.6769
Pu-240 Capture	6.56849E+11	**11.4211**	0.0607	0.3433	0.3460	1.7289
Pu-241 Capture	8.06078E+10	**11.3481**	0.0664	0.3534	0.3593	1.8155
Pu-242 Capture	1.07587E+11	**21.0632**	0.0826	0.4052	0.4087	1.8904
Am-241 Capture	2.78575E+11	**4.8517**	0.0516	0.3293	0.3329	1.6036
Am-242m Capture	3.13909E+09	**14.3345**	0.1296	0.5150	0.5220	1.9714
Am-243 Capture	1.01034E+11	**4.6468**	0.0824	0.5545	0.6850	1.8179
Cm-242 Capture	1.15857E+09	**16.6336**	0.1189	0.5262	0.5312	2.0394
Cm-244 Capture	3.26601E+10	**14.4697**	0.0757	0.3669	0.3819	1.7977
Cm-245 Capture	2.81558E+09	**12.1820**	0.0652	0.3756	0.3849	1.8493
Fe (n,el)	1.41214E+09	**2.7838**	0.0950	0.3979	0.4007	1.1027
Na-23 (n,el)	1.55294E+09	**2.8903**	0.1006	0.4145	0.4181	1.1587
End of Cycle Masses						
EOC U-235 Mass (kg, 1/3 core)	1.9941E+00	**0.0611**	*0.0068*	*0.0101*	*0.0102*	*0.0264*
EOC U-238 Mass (kg, 1/3 core)	1.2944E+03	**0.0101**	*0.0011*	*0.0024*	*0.0025*	*0.0059*
EOC NP237 Mass (kg, 1/3 core)	5.9906E+00	**0.0969**	*0.0243*	*0.0270*	*0.0272*	*0.0459*
EOC PU238 Mass (kg, 1/3 core)	9.9789E+00	**0.3575**	*0.0024*	*0.0091*	*0.0143*	*0.0500*
EOC PU239 Mass (kg, 1/3 core)	1.6923E+02	**0.0753**	*0.0029*	*0.0114*	*0.0119*	*0.0462*
EOC PU240 Mass (kg, 1/3 core)	1.0233E+02	**0.1024**	*0.0039*	*0.0108*	*0.0110*	*0.0272*
EOC PU241 Mass (kg, 1/3 core)	1.3555E+01	**0.8082**	*0.0032*	*0.0187*	*0.0290*	*0.1159*
EOC PU242 Mass (kg, 1/3 core)	2.0207E+01	**0.1803**	*0.0012*	*0.0035*	*0.0055*	*0.0180*
EOC AM241 Mass (kg, 1/3 core)	1.3043E+01	**0.1339**	*0.0019*	*0.0087*	*0.0089*	*0.0414*
EOC AM242 Mass (kg, 1/3 core)	9.3048E-01	**0.8624**	*0.0039*	*0.0229*	*0.0324*	*0.1479*
EOC AM243 Mass (kg, 1/3 core)	6.5145E+00	**0.4022**	*0.0025*	*0.0103*	*0.0121*	*0.0446*
EOC CM242 Mass (kg, 1/3 core)	3.8436E-01	**2.1191**	*0.0255*	*0.1351*	*0.1368*	*0.6885*
EOC CM244 Mass (kg, 1/3 core)	3.0155E+00	**0.5141**	*0.0037*	*0.0196*	*0.0237*	*0.0712*
EOC CM245 Mass (kg, 1/3 core)	7.1012E-01	**1.7686**	*0.0044*	*0.0186*	*0.0236*	*0.1184*
Discharge Masses						
DIS U-235 Mass (kg, 1/3 core)	9.5694E-02	**7.3322**	*0.4816*	*1.1765*	*1.3545*	*1.8829*
DIS U-238 Mass (kg, 1/3 core)	8.1533E+01	**10.0496**	*0.7801*	*1.9277*	*2.1127*	*2.7249*
DIS NP237 Mass (kg, 1/3 core)	2.7183E-01	**73.4646**	*5.8761*	*14.9542*	*17.4563*	*22.2340*
DIS PU238 Mass (kg, 1/3 core)	1.3071E+00	**21.4872**	*2.8704*	*7.0326*	*7.2009*	*8.4022*
DIS PU239 Mass (kg, 1/3 core)	1.3642E+01	**16.8644**	*1.1033*	*2.8151*	*3.3276*	*4.5881*
DIS PU240 Mass (kg, 1/3 core)	1.2759E+01	**31.8332**	*2.2790*	*5.7181*	*6.5082*	*8.5705*
DIS PU241 Mass (kg, 1/3 core)	2.1243E+00	**35.1597**	*2.1887*	*5.7750*	*6.2526*	*8.2797*
DIS PU242 Mass (kg, 1/3 core)	3.0327E+00	**80.3409**	*5.2948*	*13.0165*	*14.8469*	*20.1272*
DIS AM241 Mass (kg, 1/3 core)	1.3990E+00	**44.2526**	*3.4762*	*8.7763*	*9.3773*	*12.3051*
DIS AM242 Mass (kg, 1/3 core)	1.1967E-01	**48.9414**	*3.6562*	*9.2969*	*10.2766*	*13.6536*
DIS AM243 Mass (kg, 1/3 core)	9.9116E-01	**99.3120**	*6.5449*	*15.9564*	*18.4942*	*24.9326*
DIS CM242 Mass (kg, 1/3 core)	6.0048E-02	**38.2103**	*2.6794*	*6.8516*	*7.3956*	*9.5896*
DIS CM244 Mass (kg, 1/3 core)	7.1269E-01	**118.1987**	*7.5732*	*18.5815*	*21.8197*	*29.4483*
DIS CM245 Mass (kg, 1/3 core)	2.1995E-01	**140.3874**	*8.9041*	*21.8791*	*25.8998*	*35.1021*

Table D.21: Posteriori uncertainties for ABTR-SU adapted to select ZPPR variations.

Parameter	A Priori	ZPPR_1_3	ZPPR_2_3	ZPPR_3_5	ZPPR_4_1	ZPPR_6_2	ZPPR_3_1
Average Reaction Rates							
U-235 Capture	**1.5221**	0.2730	0.2843	0.2741	0.2561	0.2531	0.2755
Np-237 Capture	**3.0851**	0.5489	0.6469	0.6193	0.6238	0.5225	0.5809
Pu-238 Capture	**11.8061**	0.8345	0.8072	0.7903	0.6804	0.7561	0.8224
Pu-239 Capture	**4.6378**	0.7763	0.7843	0.7784	0.6797	0.7024	0.7701
Pu-240 Capture	**10.9878**	0.4776	0.4778	0.4603	0.4114	0.4219	0.4774
Pu-241 Capture	**10.8240**	0.7538	0.7756	0.7472	0.6241	0.6541	0.7391
Pu-242 Capture	**19.7742**	1.2485	1.2203	1.2110	1.1200	1.1741	1.2368
Am-241 Capture	**4.7001**	0.5103	0.5324	0.5512	0.4266	0.4479	0.5242
Am-242m Capture	**14.2233**	2.1190	2.1751	2.1941	2.1084	2.0369	2.1139
Am-243 Capture	**5.1920**	1.6868	1.9725	1.9241	1.9532	1.6476	1.7707
Cm-242 Capture	**15.6376**	0.8703	1.0782	0.8605	1.1401	1.1599	0.8627
Cm-244 Capture	**14.0488**	1.5662	2.3437	2.3177	2.1429	1.4460	1.7923
Cm-245 Capture	**12.3336**	1.8567	2.6546	2.7038	2.3502	1.6760	2.1302
Fe (n,el)	**3.1362**	0.5574	0.5652	0.5605	0.5450	0.5412	0.5515
Na-23 (n,el)	**3.2893**	0.6218	0.6369	0.6278	0.6237	0.6118	0.6099
End of Cycle Masses							
EOC U-234 Mass	**0.3596**	0.3553	0.3553	0.3553	0.3553	0.3553	0.3553
EOC U-235 Mass	**0.0524**	0.0091	0.0096	0.0093	0.0088	0.0085	0.0092
EOC U-236 Mass	**0.2421**	0.1166	0.1163	0.1175	0.1143	0.1147	0.1193
EOC U-238 Mass	**0.0100**	0.0024	0.0025	0.0025	0.0024	0.0023	0.0024
EOC NP237 Mass	**0.1893**	0.1044	0.1051	0.1048	0.1047	0.1041	0.1043
EOC PU236 Mass	**2.4712**	2.3231	2.3233	2.3231	2.3229	2.3229	2.3229
EOC PU238 Mass	**0.5148**	0.0884	0.0895	0.0905	0.0843	0.0840	0.0910
EOC PU239 Mass	**0.0580**	0.0085	0.0094	0.0092	0.0086	0.0076	0.0088
EOC PU240 Mass	**0.2461**	0.0277	0.0276	0.0276	0.0234	0.0246	0.0275
EOC PU241 Mass	**1.0211**	0.0753	0.0756	0.0754	0.0636	0.0655	0.0754
EOC PU242 Mass	**0.2957**	0.0185	0.0189	0.0180	0.0150	0.0158	0.0182
EOC AM241 Mass	**0.1766**	0.0229	0.0225	0.0236	0.0180	0.0202	0.0231
EOC AM242 Mass	**1.4299**	0.2099	0.2706	0.2653	0.2470	0.1935	0.2295
EOC AM243 Mass	**0.8554**	0.0623	0.0671	0.0642	0.0615	0.0576	0.0637
EOC CM242 Mass	**2.2253**	0.3452	0.3382	0.3531	0.2808	0.3104	0.3471
EOC CM243 Mass	**2.9256**	2.9084	2.9084	2.9084	2.9082	2.9082	2.9084
EOC CM244 Mass	**0.7652**	0.1669	0.1992	0.1930	0.1969	0.1637	0.1775
EOC CM245 Mass	**3.1718**	0.2680	0.4122	0.4068	0.3754	0.2458	0.3116
EOC CM246 Mass	**1.0307**	0.1517	0.2196	0.2234	0.1943	0.1367	0.1749

Table D.22: Posteriori uncertainties for ABTR-SU adapted to ZPPR_5_3.

Parameter	Nominal	A Priori	ZPPR_5_3
Average Reaction Rates			
U-235 Capture	1.360695E+10	**1.5221**	0.2758
Np-237 Capture	1.154149E+11	**3.0851**	0.5638
Pu-238 Capture	2.837378E+10	**11.8061**	0.8019
Pu-239 Capture	1.028754E+12	**4.6378**	0.7969
Pu-240 Capture	3.131250E+11	**10.9878**	0.4492
Pu-241 Capture	5.724197E+10	**10.8240**	0.7914
Pu-242 Capture	3.823686E+10	**19.7742**	1.2348
Am-241 Capture	1.532693E+11	**4.7001**	0.5580
Am-242m Capture	7.669852E+08	**14.2233**	2.2246
Am-243 Capture	2.276872E+10	**5.1920**	1.7294
Cm-242 Capture	7.234716E+08	**15.6376**	0.9961
Cm-244 Capture	4.033729E+09	**14.0488**	1.6538
Cm-245 Capture	1.443770E+08	**12.3336**	1.9579
Fe (n,el)	1.646494E+09	**3.1362**	0.5885
Na-23 (n,el)	1.577207E+09	**3.2893**	0.6568
End of Cycle Masses			
EOC U-234 Mass (kg, 1/3 core)	7.589920E-03	**0.3596**	0.3553
EOC U-235 Mass (kg, 1/3 core)	1.669750E+00	**0.0524**	0.0092
EOC U-236 Mass (kg, 1/3 core)	1.139810E-01	**0.2421**	0.1205
EOC U-238 Mass (kg, 1/3 core)	1.081980E+03	**0.0100**	0.0025
EOC NP237 Mass (kg, 1/3 core)	1.249740E+00	**0.1893**	0.1050
EOC PU236 Mass (kg, 1/3 core)	8.622900E-06	**2.4712**	2.3236
EOC PU238 Mass (kg, 1/3 core)	5.872250E-01	**0.5148**	0.0893
EOC PU239 Mass (kg, 1/3 core)	2.125080E+02	**0.0580**	0.0091
EOC PU240 Mass (kg, 1/3 core)	2.781380E+01	**0.2461**	0.0269
EOC PU241 Mass (kg, 1/3 core)	3.026360E+00	**1.0211**	0.0726
EOC PU242 Mass (kg, 1/3 core)	1.378460E+00	**0.2957**	0.0183
EOC AM241 Mass (kg, 1/3 core)	1.328540E+00	**0.1766**	0.0253
EOC AM242 Mass (kg, 1/3 core)	3.925810E-02	**1.4299**	0.2248
EOC AM243 Mass (kg, 1/3 core)	2.610410E-01	**0.8554**	0.0617
EOC CM242 Mass (kg, 1/3 core)	4.811490E-02	**2.2253**	0.3757
EOC CM243 Mass (kg, 1/3 core)	1.371040E-03	**2.9256**	2.9085
EOC CM244 Mass (kg, 1/3 core)	6.665970E-02	**0.7652**	0.1701
EOC CM245 Mass (kg, 1/3 core)	6.212820E-03	**3.1718**	0.2840
EOC CM246 Mass (kg, 1/3 core)	4.296680E-04	**1.0307**	0.1603